

# 第 52 回 フラーレン・ナノチューブ・グラフェン 総合シンポジウム

The 52<sup>nd</sup> Fullerenes–Nanotubes–Graphene General Symposium



## 講演要旨集

## Abstracts

2017年2月28日(火) ~ 3日(金)

東京大学 伊藤国際学術研究センター

The University of Tokyo, ITO INTERNATIONAL RESEARCH CENTER

**主催** フラーレン・ナノチューブ・グラフェン学会

The Fullerenes, Nanotubes and Graphene Research Society

**共催**・**後援**

日本化学会 The Chemical Society of Japan

JST 戦略的国際共同研究プロジェクト IRENA

IRENA Project by JST-EC DG RTD, SICORP

東京大学 CIAiS Consortium for Innovation of Advanced Integrated Science (UTokyo)

東京大学 GMSI Graduate Program for Mechanical Systems Innovation (UTokyo)

東京大学大学院工学系研究科 School of Engineering, The University of Tokyo

**協賛**

日本物理学会 The Physical Society of Japan

応用物理学会 The Japan Society of Applied Physics

高分子学会 The Society of Polymer Science, Japan

電気化学会 The Electrochemical Society of Japan

# エイジングケアの最高峰 “フラーレン”

## 【特徴】

- ・抗酸化力はビタミンCの250倍以上
- ・多くの活性酸素を満遍なく除去し、その効果は長時間続く
- ・発見者はノーベル化学賞を受賞
- ・著名研究者との共同研究による豊富なエビデンス

## 水溶性フラーレン：ラジカルスポンジ



表示名称：フラーレン、PVP、BG、水

- 強くて持続性のある抗酸化力
- あらゆる製品へ容易に配合可能
- 採用実績「No.1！」



## 油溶性フラーレン：リポフラーレン



表示名称：フラーレン、スクワラン

- 強くて持続性のある抗酸化力
- 植物性スクワラン使用
- 「オイルリッチな製品」に最適



## パウダー状フラーレン：ヴェールフラーレン



表示名称：フラーレン、シリカ

- 肌の外側で抗酸化力を発揮
- フラーレンの「美容効果」がある粉末原料
- メイクアップ・スキンケアパウダー製品等を差別化



## リポソーム化用フラーレン：モイストフラーレン



表示名称：フラーレン、水添レシチン、フィトステロールズ、BG

- 抗酸化力に「保湿と浸透性」をプラス
- 肌なじみの良いテクスチャー
- オリジナルカプセル処方で差別化



お問い合わせ先：

ビタミンC60バイオリサーチ株式会社

<http://www.vc60.com/>

〒103-0028 東京都中央区八重洲1-3-19 辰沼建物9F

TEL: 03-3517-3251 FAX: 03-3517-3260

E-mail: info@vc60.com

# Abstract of The 52<sup>nd</sup> Fullerenes-Nanotubes-Graphene General Symposium

Sponsored by : The Fullerenes, Nanotubes and Graphene Research Society

Co-Sponsored by : The Chemical Society of Japan  
IRENA Project by JST-EC DG RTD, SICORP  
Consortium for Innovation of Advanced Integrated Science(UTokyo)  
Graduate Program for Mechanical Systems Innovation(UTokyo)  
School of Engineering, The University of Tokyo

Supported by : The Physical Society of Japan  
The Japan Society of Applied Physics  
The Society of Polymer Science, Japan  
The Electrochemical Society of Japan

Date : February 28<sup>th</sup>(Tue.) – March 3<sup>rd</sup>(Fri.), 2017

Place : The University of Tokyo, ITO INTERNATIONAL RESEARCH CENTER  
7-3-1 Hongo, Bunkyo-ku, Tokyo 113-8656

Presentation Time : Special Lecture (25 min presentation + 5min discussion)  
General Lecture (10 min presentation + 5min discussion)  
Poster Preview (1 min presentation without discussion)

---

## 第 52 回 フラーレン・ナノチューブ・グラフェン 総合シンポジウム 講演要旨集

主催 : フラーレン・ナノチューブ・グラフェン学会

共催・後援 : 日本化学会  
JST 戦略的国際共同研究プロジェクト IRENA  
東京大学 CIAiS  
東京大学 GMSI  
東京大学大学院工学系研究科

協賛 : 日本物理学会、応用物理学会、高分子学会、電気化学会

日時 : 平成 29 年 2 月 28 日(火)～3 月 3 日(金)

場所 : 東京大学 伊藤国際学術研究センター 伊藤謝恩ホール  
〒113-8656 東京都文京区本郷 7-3-1

発表時間 : 特別講演 (発表 25 分 + 質疑応答 5 分)  
一般講演 (発表 10 分 + 質疑応答 5 分)  
ポスタープレビュー (発表 1 分・質疑応答 なし)

## 展示団体御芳名 (五十音順、敬称略)

アイクストロン(株)  
IOP英国物理学会出版局  
QuantumWise Japan(株)  
埼玉県庁 産業労働部 先端産業課  
(株)島津製作所  
(株)シンキー  
(株)セントラル科学貿易  
東京ダイレック(株)  
ナノフォトン(株)  
(株)ニューメタルスエンドケミカルスコーポレーション  
日立工機(株)  
ブルカー・エイエックスエス(株)  
(株)堀場製作所  
(株)名城ナノカーボン

## 広告掲載団体御芳名 (五十音順、敬称略)

アイクストロン(株)  
エクセルソフト(株)  
(株)コロナ社  
埼玉県庁 産業労働部 先端産業課  
シグマ アルドリッチ ジャパン(同)  
(株)セントラル科学貿易  
ソーラボジャパン(株)

## Contents

Time Table	• • • • •	i
Chairperson	• • • • •	iii
Program	Japanese • • • • •	iv
	English • • • • •	xix
Abstracts	Special Lecture • • • • •	1
	General Lecture • • • • •	11
	Poster Preview • • • • •	43
Author Index	• • • • •	171

## 目次

早見表	• • • • •	i
座長一覧	• • • • •	iii
プログラム	和文 • • • • •	iv
	英文 • • • • •	xix
講演予稿	特別講演 • • • • •	1
	一般講演 • • • • •	11
	ポスター発表 • • • • •	43
発表索引	• • • • •	171

# プログラム早見表

3月1日 (水)	
	受付開始 8:30～ 講演開始 9:45～
9:45	特別講演 (篠原 久典) 9:45-10:15
10:15	特別講演 (Esko I. Kauppinen) 10:15-10:45
10:45	休憩 10:45-11:00
11:00	一般講演 4件 (ナノチューブの生成と精製・ ナノチューブの物性・グラフェンの 物性) 11:00-12:00
12:00	昼食 (幹事会) 12:00-13:15
13:15	特別講演 (Christophe Bichara) 13:15-13:45
13:45	特別講演 (松本 和彦) 13:45-14:15
14:15	一般講演 3件 (グラフェンの物性・グラ フェンの応用) 14:15-15:00
15:00	ポスタープレビュー (1P-1 ~ 1P-42) 15:00-16:00
16:00	ポスターセッション (多目的スペース) 16:00-17:45
17:45	休憩 17:45-18:00
18:00	チュートリアル 講師: 篠原久典 名古屋大学 (伊藤謝恩ホール) 18:00-19:30

19:30

2月28日 (火)	
第8回ナノカーボン実用化推進研究会 (伊藤謝恩ホール)	
第6回ナノカーボンバイオシンポジウム (3階中教室)	

3月2日 (木)	
	受付開始 8:30～ 講演開始 9:00～
9:00	特別講演 (Yan Li) 9:00-9:30
9:30	一般講演 4件 (ナノチューブの生成と精製・ ナノチューブの物性) 9:30-10:30
10:30	休憩 10:30-10:45
10:45	特別講演 (Shyamal Kumar Saha) 10:45-11:15
11:15	一般講演 3件 (原子層) 11:15-12:00
12:00	昼食 12:00-13:15
13:15	授賞式 13:15-14:00
14:00	ポスタープレビュー (2P-1 ~ 2P-43) 14:00-15:00
15:00	ポスターセッション (多目的スペース) 15:00-16:45
16:45	特別講演 (野田 優) 16:45-17:15
17:15	一般講演 7件 (フラーレンの応用・金属 内包フラーレン・フラーレン ・ ナノ炭素粒子・その他) 17:15-19:00
19:00	懇親会 (多目的スペース) 19:00-20:45

20:45

3月3日 (金)	
	受付開始 8:30～ 講演開始 9:00～
9:00	特別講演 (河野 淳一郎) 9:00-9:30
9:30	一般講演 4件 (ナノチューブの物性) 9:30-10:30
10:30	休憩 10:30-10:45
10:45	特別講演 (Kaihui Liu) 10:45-11:15
11:15	一般講演 3件 (ナノチューブの物性・ナノ チューブの応用) 11:15-12:00
12:00	昼食 12:00-13:15
13:15	ポスタープレビュー (3P-1 ~ 3P-42) 13:15-14:15
14:15	ポスターセッション (多目的スペース) 14:15-16:00
16:00	特別講演 (Erik Einarsson) 16:00-16:30
16:30	一般講演 4件 (グラフェン生成・ グラフェンの応用) 16:30-17:30

17:30

講演会場 伊藤謝恩ホール  
特別講演 発表25分・質疑5分  
一般講演 発表10分・質疑5分  
ポスタープレビュー 発表1分・質疑なし

# Time table

March 1 (Wed.)	
	Registration begins at 8:30 Lectures begin at 9:45
9:45	Special Lecture (Hisanori Shinohara) 9:45–10:15
10:15	Special Lecture (Esko I. Kauppinen) 10:15–10:45
10:45	Coffee Break 10:45–11:00
11:00	General Lectures [4] (Formation and purification of nanotubes • Properties of nanotubes • Properties of graphene) 11:00–12:00
12:00	Lunch (Administrative meeting) 12:00–13:15
13:15	Special Lecture (Christophe Bichara) 13:15–13:45
13:45	Special Lecture (Kazuhiko Matsumoto) 13:45–14:15
14:15	General Lectures [3] (Properties of graphene • Applications of graphene) 14:15–15:00
15:00	Poster Preview ( 1P–1 through 1P–42 ) 15:00–16:00
16:00	Poster Session ( Event Space ) 16:00–17:45
17:45	Coffee Break 17:45–18:00
18:00	Tutorial Lecturer : Hisanori Shinohara Nagoya University ( Ito Hall ) 18:00–19:30

19:30

February 28 (Tue.)	
The 8 <sup>th</sup> NanoCarbon Application Forum ( Ito Hall )	

February 28 (Tue.)	
The 6 <sup>th</sup> NanoCarbon–Bio Symposium ( 3F Seminar Room )	

March 2 (Thu.)	
	Registration begins at 8:30 Lectures begin at 9:00
9:00	Special Lecture (Yan Li) 9:00–9:30
9:30	General Lectures [4] (Formation and purification of nanotubes • Properties of nanotubes) 9:30–10:30
10:30	Coffee Break 10:30–10:45
10:45	Special Lecture (Shyamal K Saha) 10:45–11:15
11:15	General Lectures [3] (Atomic Layers) 11:15–12:00
12:00	Lunch 12:00–13:15
13:15	Award Ceremony 13:15–14:00
14:00	Poster Preview ( 2P–1 through 2P–43 ) 14:00–15:00
15:00	Poster Session ( Event Space ) 15:00–16:45
16:45	Special Lecture (Suguru Noda) 16:45–17:15
17:15	General Lectures [7] (Applications of fullerenes • Endohedral metallofullerenes • Fullerenes • Carbon nanoparticles • Other topics ) 17:15–19:00
19:00	Banquet ( Event Space ) 19:00–20:45

20:45

March 3 (Fri.)	
	Registration begins at 8:30 Lectures begin at 9:00
9:00	Special Lecture (Junichiro Kono) 9:00–9:30
9:30	General Lectures [4] (Properties of nanotubes) 9:30–10:30
10:30	Coffee Break 10:30–10:45
10:45	Special Lecture (Kaihui Liu) 10:45–11:15
11:15	General Lectures [3] (Properties of nanotubes • Applications of nanotubes) 11:15–12:00
12:00	Lunch 12:00–13:15
13:15	Poster Preview ( 3P–1 through 3P–42 ) 13:15–14:15
14:15	Poster Session ( Event Space ) 14:15–16:00
16:00	Special Lecture (Erik Einarsson) 16:00–16:30
16:30	General Lectures [4] (Graphene synthesis • Applications of graphene) 16:30–17:30

17:30

Place : Ito Hall

Special Lecture : 25 min (Presentation) + 5 min (Discussion)

General Lecture : 10 min (Presentation) + 5 min (Discussion)

Poster Preview : 1 min (Presentation)

## 座長一覧 (Chairpersons)

3月1日 (水)

(敬称略)

セッション	時 間	座 長
特別講演 (篠原 久典)	9:45 ~ 10:15	丸山 茂夫
特別講演 (Esko I. Kauppinen)	10:15 ~ 10:45	篠原 久典
一般講演	11:00 ~ 12:00	北浦 良
特別講演 (Christophe Bichara)	13:15 ~ 13:45	丸山 茂夫
特別講演 (松本 和彦)	13:45 ~ 14:15	長汐 晃輔
一般講演	14:15 ~ 15:00	長汐 晃輔
ポスタープレビュー	15:00 ~ 16:00	杉目 恒志 大町 遼
チュートリアル (篠原 久典)	18:00 ~ 19:30	丸山 茂夫

3月2日 (木)

セッション	時 間	座 長
特別講演 (Yan Li)	9:00 ~ 9:30	野田 優
一般講演	9:30 ~ 10:30	野田 優
特別講演 (Shyamal Kumar Saha)	10:45 ~ 11:15	斎藤 晋
一般講演	11:15 ~ 12:00	高井 和之
ポスタープレビュー	14:00 ~ 15:00	桜井 俊介 長谷川 馨
特別講演 (野田 優)	16:45 ~ 17:15	吾郷 浩樹
一般講演	17:15 ~ 17:30	吾郷 浩樹
	17:30 ~ 19:00	松尾 豊

3月3日 (金)

セッション	時 間	座 長
特別講演 (河野 淳一郎)	9:00 ~ 9:30	加藤 雄一郎
一般講演	9:30 ~ 10:30	松田 一成
特別講演 (Kaihui Liu)	10:45 ~ 11:15	Yan Li
一般講演	11:15 ~ 12:00	宮内 雄平
ポスタープレビュー	13:15 ~ 14:15	蓬田 陽平 井ノ上 泰輝
特別講演 (Erik Einarsson)	16:00 ~ 16:30	千足 昇平
一般講演	16:30 ~ 17:30	大野 雄高

3月1日(水)

特別講演 発表 25分 ・ 質疑応答 5分  
一般講演 発表 10分 ・ 質疑応答 5分  
ポスタープレビュー 発表 1分 ・ 質疑応答 なし

特別講演 ( 9:45-10:15 )

- 1S-1 Putting  $sp^3$ -diamondoids into carbon nanotubes 1  
\* 篠原 久典

特別講演 ( 10:15-10:45 )

- 1S-2 Direct dry deposition of SWNTs by thermophoresis 2  
\* Esko I. Kauppinen, Patrik Laiho, Kimmo Mustonen, Shigeo Maruyama, Yutaka Ohno

>>>>>>> 休憩 ( 10:45-11:00 ) <<<<<<<<

一般講演 ( 11:00-12:00 )

ナノチューブの生成と精製 ・ ナノチューブの物性 ・ グラフェンの物性

- 1-1 Fabrication of multiple transistors from semiconducting single-walled carbon nanotube arrays after water-assisted burning of metallic tubes 11  
\* 大塚 慶吾, 井ノ上 泰輝, 千足 昇平, 丸山 茂夫
- 1-2 2層カーボンナノチューブにおける非対称な電荷蓄積 12  
\* 古地 健人, 岡田 晋
- 1-3 Enhancement of Raman scattering from monolayer graphene by photonic crystal nanocavities 13  
\* Issei Kimura, Masahiro Yoshida, Masaki Sota, Hidenori Machiya, Taiki Inoue, Shohei Chiashi, Shigeo Maruyama, Yuichiro K. Kato
- 1-4 二次元炭化水素ネットワークの磁性 14  
\* 反町 純也, 岡田 晋

>>>>>>> 昼食 ( 12:00-13:15 ) <<<<<<<<

特別講演 ( 13:15-13:45 )

- 1S-3 Growth modes and chiral selectivity of Single Wall Carbon Nanotubes 3  
\* Christophe Bichara

特別講演 ( 13:45-14:15 )

- 1S-4 糖鎖修飾グラフェンを用いた高感度ウイルス検出 4  
\* 松本 和彦

一般講演 ( 14:15-15:00 )

グラフェンの物性 ・ グラフェンの応用

- 1-5 Opening a Gap in Graphene Field Effect Devices with Periodic Uniaxial Strain 15  
\* 友利 ひかり, 平出 璃音可, 大塚 洋一, 渡辺 賢司, 谷口 尚, 神田 晶申

## 3月1日(水)

1-6 Gas Adsorption Effects on Stabilities and Electronic Properties of Graphene Bilayers 16  
\* Yoshitaka Fujimoto, Susumu Saito

1-7 Edge Roughness Analysis for Developing GNR-based FET 17  
\* Kengo Takashima, Takahiro Yamamoto

### ポスタープレビュー (15:00-16:00)

### ポスターセッション (16:00-17:45) (☆) 若手奨励賞候補

#### 金属内包フラーレン

1P-1 Photochemical Addition of Siliranes to  $\text{Sc}_3\text{N}@I_h\text{-C}_{80}$ : Interconversion of the [6,6]- and [5,6]-Adducts 43  
\* 杉浦 健, 宮部 恭輔, 加固 昌寛, 安井 正憲, 山田 道夫, 前田 優, Jingdong Guo, 永瀬 茂, 赤坂 健

1P-2 Conclusive Characterization of  $\text{Li}@C_{60}$  by X-ray Structure Analysis 44  
\* Hiroshi Ueno, Shinobu Aoyagi, Naohiko Ikuma, Hiroshi Okada, Kei Ohkubo, Tatsuhisa Kato, Shunichi Fukuzumi, Yutaka Matsuo, Ken Kokubo

#### ナノチューブの物性

1P-3 Diameter and defect density dependence of intermediate frequency Raman mode of single-walled carbon nanotubes 45  
\* 稲葉 工, 小鍋 哲, 本間 芳和

1P-4 Spectral tuning of optical coupling between air-mode nanobeam cavities and individual carbon nanotubes 46  
☆ \* Hidenori Machiya, Takushi Uda, Akihiro Ishii, Yuichiro K. Kato

1P-5 Tuning of Photo-thermoelectric effect of Metallic and Semiconducting Single wall carbon nanotube thin films by electrolyte gating 47  
\* 中村 昌稔, 一ノ瀬 遥太, 河合 英輝, 蓬田 陽平, 柳 和宏

1P-6 単層カーボンナノチューブの蛍光特性: フォトン再吸収効果 48  
\* 魏 小均, 都築 真由美, 蓬田 陽平, 王 国偉, 平野 篤, 藤井 俊治郎, 田中 丈士, 片浦 弘道

1P-7 カーボンナノポットの表面状態-KFM観察- 49  
\* 横井 裕之, 池田 晃三, 畠山 一翔, 鯉沼 陸央

1P-8 界面活性剤溶液中でのSWCNTの分散安定性に対するアニオンの効果 50  
\* 平野 篤, Gao Weilu, He Xiaowei, 河野 淳一郎

#### ナノチューブの応用

1P-9 Paper-based carbon nanotube field effect transistor by photolithography 51  
\* Jong Mok Shin, Do Hyun Kim, InYeob Na, Ho-Kyun Jnag, Jun Hee Choi, Se Jeong Park, Gyu-Tae Kim

1P-10 Doping effect of electrolyte droplet on carbon nanotube thin film 52  
☆ \* Tomohiro Yasunishi, Shigeru Kishimoto, Yutaka Ohno

## 3月1日(水)

1P-11	メルトブレンドによるCNT/Polyethylene複合材料の開発 * 小野寺 厚, Sami Ristimäki, 関戸 大	53
1P-12	Defluorination-Assisted Synthesis of Nitrogen-Doped Single-Walled Carbon Nanotubes and Their Catalytic Activity of Oxygen Reduction Reaction for Polymer Electrolyte Fuel Cells * Koji Yokoyama, Shun Yokoyama, Yoshinori Sato, Masashi Yamamoto, Tetsuo Nishida, Kenichi Motomiya, Hiromichi Ohta, Hideyuki Takahashi, Kazuyuki Tohji, Yoshinori Sato	54
☆		
1P-13	Film fabrication of Semiconducting Single-Wall Carbon Nanotubes by Aqueous-Two Phase System and Thin Film Transistor Applications * Haruka Omachi, Tomohiko Komuro, Jun Hirotsu, Yutaka Ohno, Hisanori Shinohara	55
<b>ナノチューブの生成と精製</b>		
1P-14	Growth of Horizontally Aligned Chirality-Specific Single-Walled Carbon Nanotubes * Feng Yang, Yan Li	56
1P-15	高濃度エチレン原料からのサブミリメートル長カーボンナノチューブの高収率流動層合成 * 蜂谷 宗一郎, 陳 忠明, 川端 孝祐, 長谷川 馨, 大沢 利男, 野田 優	57
☆		
1P-16	電界誘起層形成法を用いた大量連続金属型・半導体型CNT分離 * 二瓶 史行, 佐々木 美紗子, 桑原 有紀, 斎藤 毅, 遠藤 浩幸	58
1P-17	Development of gels for high-efficiency metal/ semiconductor separation of SWCNTs * Guowei Wang, Xiaojun Wei, Atsushi Hirano, Takeshi Tanaka, Hiromichi Kataura	59
☆		
1P-18	Purity Analysis and Purification of Double-walled Carbon Nanotubes * Kenshi Miyaura, Hidekazu Nishino, Shirou Honda	60
<b>内包ナノチューブ</b>		
1P-19	An experimental and theoretical study on the scanning spectroscopy of europium nanowires encapsulated in carbon nanotubes * Terunobu Nakanishi, Ryo Kitaura, Takazumi Kawai, Susumu Okada, Shoji Yoshida, Osamu Takeuchi, Hidemi Shigekawa, Hisanori Shinohara	61
☆		
1P-20	単層カーボンナノチューブに内包されたヨウ化セシウムの電子状態および固体NMRパラメーターのDFT計算 * 横倉 瑛太, 片岡 洋右, 緒方 啓典	62
<b>グラフェン生成</b>		
1P-21	Au-Ni触媒CVDによる高い均一性を有する多層グラフェン成長に関する研究 * 上田 悠貴, 山田 純平, 藤原 亨介, 山本 大地, 丸山 隆浩, 成塚 重弥	63
1P-22	一酸化炭素からのグラフェンの熱力学的制御合成 * 永井 款也, 長谷川 馨, 野田 優	64
☆		
<b>グラフェンの応用</b>		
1P-23	Fe及びCaをインターカレートした2層グラフェンの作製と電気特性 * 倉金 夏己, 星野 峻, 櫻井 亮太, 山岸 多門, 永田 知子, 岩田 展幸, 山本 寛	65

## 3月1日 (水)

1P-24	Functional group dependence of Spin magnetism of Graphene oxide * 田嶋 健太郎, 井坂 琢也, 山科 智貴, 松尾 吉晃, 高井 和之	66
1P-25	Highly efficient, mechanically durable perovskite solar cells with graphene electrodes * Jungjin Yoon, Namyoung Ahn, Mansoo Choi	67
1P-26	溶液分散した酸化グラフェン単一片の還元反応のトワイライト蛍光顕微鏡による追跡 * 佐藤 光, 佐野 正人	68
1P-27	Production and characterization of graphene quantum dots derived from SWNTs and graphite * 森田 博暉, 菅井 俊樹	69
<b>グラフェンの物性</b>		
1P-28	BNドープグラフェンのエネルギー論と電子状態 * 澤畑 恒来, 丸山 実那, 岡田 晋	70
1P-29	Charge transfer dynamics at graphene/SiC interface studied by time-resolved soft X-ray photoemission spectroscopy ☆ * 染谷 隆史, 吹留 博一, 山本 達, 遠藤 則史, 松田 巖	71
1P-30	顕微ラマン分光を使ったグラフェンのひずみ方位の簡単な決定法 * 中村 和史, 友利 ひかり, 神田 晶申	72
1P-31	グラフェンナリボンの力学特性 * 米山 和文, 山中 綾香, 岡田 晋	73
1P-32	Introduction of spin-orbit interaction into graphene by various methods * T. Nanba, T. Tamura, Y. Katagiri, C. Ohata, Pierre Seneor, J. Haruyama	74
1P-33	Influences of Graphene Structure on Electrochemical Interactions in LiBF <sub>4</sub> Organic Electrolyte Solution * 鈴木 大輔, 高井 和之	75
<b>原子層</b>		
1P-34	Detection of photo current arising from atom-thin MoS <sub>2</sub> Schottky junction fabricated by electron beam irradiation * Yuto Katagiri, C. Ohata, Y. Inoue, S. Maruyama, T. Nakamura, S. Katamoto, A. Ishi, M. Hasegawa, G. Fioli, S. Roche, J. Haruyama	76
1P-35	マイルド酸素プラズマ処理による架橋型2層WSe <sub>2</sub> デバイスのコンタクト抵抗改善機構 ☆ * 永井 黎人, 金子 俊郎, 加藤 俊顕	77
1P-36	Optical spectroscopy on monolayer transition metal dichalcogenides immersed in an aqueous solution * Wenjin Zhang, Yusuke Hasegawa, Kazunari Matsuda, Yuhei Miyauchi	78
1P-37	グラフェンと遷移金属ダイカルコゲナイドにおけるヘリシティ選択的な1次共鳴ラマンスペクトル ☆ * 辰巳 由樹, 齋藤 理一郎	79

## 3月1日(水)

- 1P-38 C<sub>60</sub>が吸着したグラフェンのエネルギー論と電子状態 80  
\* ソーシアー アレキサンダー大和, 丸山 実那, 岡田 晋

### バイオ

- 1P-39 カーボンナノチューブのマウス組織中アップコンバージョン発光スペクトル 81  
\* 奥平 早紀, 飯泉 陽子, 湯田坂 雅子, 岡崎 俊也, 松田 一成, 宮内 雄平

### その他

- 1P-40 Electrical properties of defective hexagonal boron nitride nanosheet 82  
\* Ho-Kyun Jang, Jun Hee Choi, Kook Jin Lee, Do-Hyun Kim, Gyu Tae Kim
- 1P-41 Modification of Electrical Properties in MoS<sub>2</sub> by Using Catalytic Oxidation 83  
\* Jun Hee Choi, Ho-Kyun Jang, Jun Eon Jin, Jong Mok Shin, Do-Hyun Kim, Gyu-Tae Kim
- 1P-42 Hidden symmetries in one-dimensional photonic crystals 84  
\* M. Shoufie Ukhtary, Haihao Liu, Riichiro Saito

>>>>>>> 休憩 ( 17:45-18:00 ) <<<<<<<<

### チュートリアル ( 18:00-19:30 )

- ナノカーボンが創るナノ空間の創製と探索  
\* 篠原 久典

3月2日(木)

特別講演 発表 25分 ・ 質疑応答 5分  
一般講演 発表 10分 ・ 質疑応答 5分  
ポスタープレビュー 発表 1分 ・ 質疑応答 なし

特別講演 ( 9:00-9:30 )

- 2S-5 Catalyst design for controlled growth of single-walled carbon nanotubes 5  
\* Yan Li

一般講演 ( 9:30-10:30 )

ナノチューブの生成と精製 ・ ナノチューブの物性

- 2-1 酸化マグネシウム触媒下地層のアニール処理による単層カーボンナノチューブフォレスト  
合成効率の大幅な向上 18  
\* 辻 享志, 畠 賢治, フタバドン, 桜井 俊介
- 2-2 交流インピーダンス法によるCNTスラリーの分散状態評価 19  
\* 渡邊 敬之, 小橋 和文, 森本 崇宏, 岡崎 俊也
- 2-3 垂直配向CNT成長用の鉄触媒粒子形成における貴金属元素添加効果 20  
\* 桜井 俊介, 畠 賢治, フタバドン
- 2-4 ロックインサーモグラフィーを用いたCNTネットワーク構造の可視化 21  
\* 森本 崇宏, 阿多 誠介, 山田 健郎, 岡崎 俊也

>>>>>>> 休憩 ( 10:30-10:45 ) <<<<<<<<

特別講演 ( 10:45-11:15 )

- 2S-6 Functionalized 2D materials for sensing applications 6  
\* Shyamal K Saha, Diptiman Dinda

一般講演 ( 11:15-12:00 )

原子層

- 2-5 Scanning Electrochemical Cell Microscopy for Visualization of Local Electrochemical  
Activities on Graphene/Graphite 22  
\* 熊谷 明哉, 三浦 千穂, 岡田 健, 寒川 誠二, 珠玖 仁, 高橋 康史, 末永 智一
- 2-6 Out-of-Plane Strain Generation of Monolayer MoS<sub>2</sub> and MoSe<sub>2</sub> Formed a Moiré  
Superstructure on the Au(111) Surface 23  
Ryosuke Takahashi, Ryo Osaka, Yasumitsu Miyata, Susumu Okada, Yuhei Hayamizu,  
\* Satoshi Yasuda, Kei Murakoshi
- 2-7 Magnetic tunnel junction built from intercalated transition metal dichalcogenide ferromagnets  
with different magnetic anisotropy 24  
\* 山崎 雄司, 守谷 頼, 荒井 美穂, 増渕 覚, 卞 舜生, 為ヶ井 強, 上野 啓司,  
町田 友樹

3月2日(木)

>>>>>>> 昼食 (12:00-13:15) <<<<<<<<

大澤賞・飯島賞・若手奨励賞の授賞式 (13:15-14:00)

ポスターレビュー (14:00-15:00)

ポスターセッション (15:00-16:45) (☆) 若手奨励賞候補

フラーレンの化学

- 2P-1 計算化学的手法による活性化フラーレンの電子特性と反応性の評価 85  
\* 伊熊 直彦, 小久保 研, 大島 巧
- 2P-2 Pd触媒を用いたフラーレンの位置選択的変換反応と構造 86  
☆ \* 橋川 祥史, 村田 理尚, 若宮 淳志, 村田 靖次郎
- 2P-3 リチウムイオン内包フルオレノ[60]フラーレンの合成 87  
\* 松尾 豊, 岡田 洋史, 上野 裕

フラーレンの応用

- 2P-4 フラーレン二重膜をテンプレートとしたポリマー集合体のナノスケール形態制御 88  
\* 原野 幸治, ゴルゴル リカルドミングチ, 中村 栄一
- 2P-5 電子線照射によるフラーレン薄膜の金属的重合化 89  
\* 上野山 寛人, 田中 悠, 山之内 真悟, 落合 勇一, 青木 伸之
- 2P-6 Synthesis of CdS-Mn-[C<sub>60</sub>]Fullerene Nanocomposites and Their Photocatalytic Activities for Degradation of Organic Dyes 90  
\* Jeong Won Ko, Jiulong Li, Weon Bae Ko
- 2P-7 Studies on the Aggregated Structures and Crystallinities of Bulk Heterojunction Films Constituting Organic Solar Cells 91  
\* 河野 紗希, 緒方 啓典

金属内包フラーレン

- 2P-8 Production and Characterization of Hetero-dimetallofullerene: GdY@C<sub>80</sub>(I<sub>h</sub>) 92  
\* 三谷 拓示, 中島 なつみ, 山口 貴久, 古川 貢, 加藤 立久, 菊地 耕一, 阿知波 洋次, 兒玉 健
- 2P-9 La@C<sub>60</sub>(CF<sub>3</sub>)<sub>5</sub>の単離と構造解析 93  
☆ \* 西野 眞希子, 青柳 忍, 大町 遼, 中川 綾乃, 北浦 良, 篠原 久典
- 2P-10 Photoreactions of Cyclic Organosilanes with Trimetallic Nitride Template Endohedral Metallofullerenes 94  
\* 深澤 新平, 杉浦 健, 宮部 恭輔, 加固 昌寛, 赤坂 健

フラーレン

- 2P-11 1次元SIMEF鎖のエネルギー論と電子状態 95  
\* 古谷 匠, 岡田 晋

## 3月2日(木)

2P-12	Absolute yield of fullerene formed by graphite laser ablation at medium-high ambient temperatures * Haruka Suzuki, Yuki Taguchi, Takeshi Kodama, Yohji Achiba, Haruo Shiromaru	96
2P-13	Energetics and electronic properties of fullerenes consisting of fused pentagonal rings * 岡田 晋	97
<b>ナノチューブの物性</b>		
2P-14	Macroscopic aligned single-walled carbon nanotubes achieved with vacuum filtration * 張 浩, 項 榮, 井ノ上 泰輝, 千足 昇平, 丸山 茂夫	98
2P-15	Selective phonon mode generations in single wall carbon nanotubes and graphene nanoribbons ☆ * Ahmad R. T. Nugraha, Eddwi H. Hasdeo, Riichiro Saito	99
2P-16	Electrically conductive multi-walled boron nitride nanotubes by catalytic etching * Do-Hyun Kim, Ho-Kyun Jang, Min-Seok Kim, Sung-Dae Kim, Dong-Jin Lee, Gyu Tae Kim	100
<b>ナノチューブの応用</b>		
2P-17	Artificial muscle using single wall carbon nanotube bundles ☆ * グエン タン フン, アフマド リドワン トレスナ ヌグラハ, 齋藤 理一郎	101
2P-18	Electrochemical Properties of Nitrogen-Doped Vertically Aligned Multi-Walled Carbon Nanotubes Prepared by Defluorination * Rei Nonomura, Takashi Itoh, Yoshinori Sato, Masashi Yamamoto, Tetsuo Nishida, Kenichi Motomiya, Kazuyuki Tohji, Yoshinori Sato	102
2P-19	基板上CNT合成と集合形態制御、電子エミッタ応用 ☆ * 北川 紗映, 杉目 恒志, 野田 優	103
<b>ナノチューブの生成と精製</b>		
2P-20	Analysis of Pt catalyst for SWNT growth by In-situ XANES * 熊倉 誠, 桐林 星光, 才田 隆広, 成塚 重弥, 丸山 隆浩	104
2P-21	Time-dependent selective synthesis and growth mechanism of single-walled carbon nanotubes from sputtered W-Co catalyst ☆ * Hua An, Rong Xiang, Akihito Kumamoto, Taiki Inoue, Shohei Chiashi, Yuichi Ikuhara, Shigeo Maruyama	105
2P-22	Extraction of High-Purity Single-Chirality Single-Wall Carbon Nanotubes by Precise Tuning of pH using CO <sub>2</sub> Bubbling * 一ノ瀬 遥太, 枝 淳子, 真庭 豊, 蓬田 陽平, 柳 和宏	106
2P-23	単層カーボンナノチューブ成長過程に対する磁場効果とその機構の検討 ☆ * 高嶋 泰正, 浜崎 亜富, 内村 仁, 尾関 寿美男	107
2P-24	Chemical reaction analysis of Fe-Co and Co-Cu clusters with ethanol by FT-ICR mass spectrometer * 水谷 健, 佐藤 仁紀, 箕輪 絃弥, 山田 涼平, 井ノ上 泰輝, 千足 昇平, 丸山 茂夫	108

## 3月2日(木)

### グラフェンの物性

- 2P-25 端の水酸化によるグラフェンリボンへの自由電子注入 109  
\* 平 麗実, 山中 綾香, 岡田 晋
- 2P-26 電場によるNドープグラフェンの電子構造制御 110  
\* 松原 愛帆, 岡田 晋
- 2P-27 Electronic structures of graphene exposed to electrolyte solution 111  
\* *Mari Ohfuchi*
- 2P-28 エッジ状態スピンとフェロセニウムイオンスピン間の磁氣的相互作用 112  
\* *Akira Suzuki, Kazuyuki Takai*
- 2P-29 過熱還元された酸化グラフェンの電気伝導特性 113  
\* 石田 拓也, 仁科 勇太, 青木 伸之
- 2P-30 グラフェンへの分子吸着による電荷移動における水分子の影響 114  
梅原 隆, \* 高井 和之

### 原子層

- 2P-31 二次元積層系のための均一な多層h-BNの大面积成長 115  
☆ \* 仲村渠 翔, 河原 憲治, 内田 勇氣, 山崎 重人, 光原 昌寿, 吾郷 浩樹
- 2P-32 2次元材料によるレーザー水分解の高効率化II 116  
\* 宮本 良之, *Hong Zhang, Xinlu Cheng, Angel Rubio*
- 2P-33 Photoluminescence and photocurrent properties of monolayer WSe<sub>2</sub> FETs fabricated by dry-transfer process 117  
☆ \* 王 曉凡, 張 文金, モハメッド ヌル バイズラ, 譚 徳志, リム ホンエン, 宮内 雄平, 松田 一成
- 2P-34 Piezoelectric properties of 3R bulk transition metal dichalcogenides 118  
\* 小鍋 哲, 山本 貴博
- 2P-35 Molecular beam epitaxy growth of molybdenum diselenide atomic layers on hexagonal boron nitride substrates 119  
☆ \* *Takuto Tokuda, Takato Hotta, Kenji Watanabe, Takashi Taniguchi, Hisanori Shinohara, Ryo Kitaura*

### ナノ炭素粒子

- 2P-36 隕石ナノダイヤモンドと爆轟法ナノダイヤモンドは同一物質 120  
\* 大澤 映二, バーナード アマンダ, 田中 利彦, 深谷 正義
- 2P-37 窒素ドープカーボンナノバルーンの合成 121  
\* 高橋 良太, 針谷 達, 滝川 浩史, 須田 善行

### その他

- 2P-38 界面活性剤を用いたゾルゲル法で作製した試料からの酸化鉄ナノチューブの分離と  
キャラクタリゼーション 122  
田中 佑佳, \* 坂東 俊治

## 3月2日(木)

2P-39	多段トラップ気相移動度測定装置の開発とナノ物質の分離 * 菅井 俊樹, 椎野 恭平, 星野 裕大, 寺田 夏樹, 浜野 裕太, 森田 博暉, 陣内 涼太	123
2P-40	トリプチセン誘導体の力学特性 * 秋葉 実樹, 岡田 晋	124
2P-41	メタン熱触媒分解による炭素触媒の活性低下メカニズムの調査 * 西井 春樹, 梅田 良人, 濱口 裕昭, 鈴木 正史, 針谷 達, 滝川 浩史, 須田 善行	125
2P-42	直接メタノール型燃料電池用触媒の触媒活性に対するPtRu合金化率の効果 * 川崎 航平, 大廣 達郎, 針谷 達, 滝川 浩史, 植 仁志, 須田 善行	126
2P-43	集束イオンビーム加工装置を用いたカーボンナノコイルの微細加工 * 高橋 宗浩, 針谷 達, 滝川 浩文, 植 仁志, 須田 善行	127

### 特別講演 (16:45-17:15)

2S-7	カーボンナノチューブの合成・機能化とエネルギーデバイス応用 * 野田 優	7
------	---	---

### 一般講演 (17:15-19:00)

#### フラーレンの応用・金属内包フラーレン・フラーレン・ナノ炭素粒子・その他

2-8	メタノインデンフラーレンを用いたペロブスカイト太陽電池における開放電圧の向上 * 松尾 豊	25
2-9	Electronic Structures and Stability of Metal Encapsulated C <sub>80</sub> fullerenes: Ab initio DFT study * Archana Velloth, Yutaka Imamura, Takeshi Kodama, Masahiko Hada	26
2-10	Searching for the unprecedented endohedral metallofullerenes by applying the separation method for those stable only in an anion form * 中島 なつみ, 三谷 拓示, 山口 貴久, 古川 貢, 加藤 立久, 菊地 耕一, 阿知波 洋次, 兒玉 健	27
2-11	C <sub>60</sub> フラーレンに内包されたLi <sup>+</sup> イオンの運動 * 鈴木 晴, 石田 美咲, 山下 将嗣, 大谷 知行, 河地 和彦, 笠間 泰彦, 権 垠相	28
2-12	Geometric and electronic structures of polymerized C <sub>40</sub> fullerene * Mina Maruyama, Susumu Okada	29
2-13	炭化水素ガス流中のレーザー誘起ブレイクダウンによるポリイン生成 田口 裕貴, 遠藤 瞳, 兒玉 健, 若林 知成, 阿知波 洋次, * 城丸 春夫, Wales Benji, Sanderson Joseph	30
2-14	爆轟法ナノダイヤモンドにおける基本粒子の内核 * 田中 利彦, 深谷 真芳, バーナード アマンダ, 大澤 映二	31

### 懇親会 (19:00-20:45)

3月3日（金）

特別講演 発表 25分 ・ 質疑応答 5分  
一般講演 発表 10分 ・ 質疑応答 5分  
ポスタープレビュー 発表 1分 ・ 質疑応答 なし

特別講演（9:00-9:30）

- 3S-8 Strong Light-Matter Coupling in (6,5) Carbon Nanotubes 8  
\* Junichiro Kono, Weilu Gao, Kankan Cong, Xinwei Li, G. Timothy Noe II, Huaping Liu,  
Takeshi Tanaka, Hiromichi Kataura

一般講演（9:30-10:30）

ナノチューブの物性

- 3-1 Optical bistability in carbon nanotubes 32  
\* Takushi Uda, Akihiro Ishii, Yuichiro K. Kato
- 3-2 Single photon generation through exciton-exciton annihilation in air-suspended carbon nanotubes 33  
\* Akihiro Ishii, Takushi Uda, Yuichiro K. Kato
- 3-3 Raman Spectroscopy of Individual Single-Walled Carbon Nanotubes 34  
\* Juan Yang, Daqi Zhang, Yan Li
- 3-4 酸化単層カーボンナノチューブの修飾率に依存する競争的な脱離と分解反応 35  
\* 前田 優, 曾根 絵理香, 西野 朱音, 天谷 優里, Wang Wei-Wei, 山田 道夫,  
鈴木 光明, 松井 淳, 三ツ石 方也, 岡崎 俊也, 永瀬 茂

>>>>>>> 休憩（10:30-10:45）<<<<<<<<

特別講演（10:45-11:15）

- 3S-9 Optical Spectroscopy of Individual Carbon Nanotubes with Defined Atomic Structure 9  
\* Kaihui Liu

一般講演（11:15-12:00）

ナノチューブの物性 ・ ナノチューブの応用

- 3-5 多層カーボンナノチューブ電子源を搭載したナノ分解能FE-SEMとX線顕微鏡の開発 36  
\* 入田 賢, 山崎 慎太郎, 勝山 翔太, 中原 仁, 安坂 幸師, 齋藤 弥八, 村田 英一,  
大野 輝昭
- 3-6 Cold exciton electroluminescence from air-suspended carbon nanotube split-gate devices 37  
Noriyuki Higashide, \* Masahiro Yoshida, Takushi Uda, Akihiro Ishii, Yuichiro K. Kato
- 3-7 ペロブスカイト太陽電池におけるコストおよび安定性の問題解決へ向けたオールカーボンアプローチ 38  
\* 田 日, Namyoun Ahn, Jungjin Yoon, Esko Kauppinen, Mansoo Choi, 松尾 豊,  
丸山 茂夫

## 3月3日 (金)

>>>>>>> 昼食 ( 12:00-13:15 ) <<<<<<<<

ポスタープレビュー ( 13:15-14:15 )

ポスターセッション ( 14:15-16:00 ) (☆) 若手奨励賞候補

金属内包フラーレン

3P-1 Attempt to produce dimetallofullerenes containing Yb 128  
\* 小林 和博, 三谷 拓示, 中島 なつみ, 菊地 耕一, 阿知波 洋次, 兒玉 健

3P-2 Spectroscopic studies of  $\text{La}_2@C_{78}$  anion 129  
\* 西本 真也, 小林 和博, 平山 貴晟, 三谷 拓示, 中島 なつみ, 山口 貴久, 古川 貢, 加藤 立久, 菊地 耕一, 阿知波 洋次, 兒玉 健

ナノチューブの物性

3P-3 ディスク式遠心沈降法によるナノ材料の分散状態の評価 130  
\* Naoko Tajima, Takahiro Morimoto, Yuichi Kato, Kazufumi Kobashi, Takeo Yamada, Toshiya Okazaki

3P-4 Unified analysis of quantum and classical transport properties on metallic carbon nanotubes 131  
☆ \* Keisuke Ishizeki, Kenji Sasaoka, Satoru Konabe, Satofumi Souma, Takahiro Yamamoto

3P-5 High Temperature Surface Enhanced Raman Scattering of Single-Walled Carbon Nanotubes 132  
\* Ming Liu, Keigo Otsuka, Rong Xiang, Taiki Inoue, Shohei Chiashi, Shigeo Maruyama

3P-6 Fabrication and photoluminescence characterization of carbon nanotube dual-gate devices 133  
\* Akihiro Sasabe, Takushi Uda, Masahiro Yoshida, Akihiro Ishii, Yuichiro K. Kato

3P-7 Optical Measurement of Single-Walled Carbon Nanotubes Using Rayleigh Scattering Spectroscopy 134  
\* 大河内 健史, 大沢 徹, 古川 頼誉, 大鋸本 達郎, 鎌倉 駿, 井ノ上 泰輝, 千足 昇平, 丸山 茂夫

ナノチューブの応用

3P-8 熱界面材料に向けた銅箔上のカーボンナノチューブの垂直配向成長と構造制御 135  
\* 小林 峻司, 長谷川 馨, 杉目 恒志, 大堀 真直, 塩見 淳一郎, 周 暁松, 二瓶 瑞久, 野田 優

3P-9 Selective detection of neurotransmitters by adsorption voltammetry with carbon nanotube film 136  
\* Takuya Ushiyama, Shigeru Kishimoto, Yutaka Ohno

3P-10 Time-dependent change of the semiconducting-CNT ink evaluated from the performance of CNT-TFTs 137  
\* 桑原 有紀, 佐々木 扶紗子, 二瓶 史行, 斎藤 毅

3P-11 Lamination of Vertically Aligned Single-Walled Carbon Nanotube Forests on Perovskite Solar Cells via Membrane Filter Transfer Method 138  
☆ \* Seungju Seo, IL Jeon, Takahiro Sakaguchi, Taiki Inoue, Rong Xiang, Shohei Chiashi, Yutaka Matsuo, Shigeo Maruyama

## 3月3日 (金)

3P-12	Yields of carbon nanotube integrated circuits on flexible plastic film * Jun Hirotani, Shigeru Kishimoto, Yutaka Ohno	139
3P-13 ☆	Modeling of carbon nanotube thin-film transistor on flexible plastic film * 鹿嶋 大雅, 松浦 智紀, 廣谷 潤, 岸本 茂, 大野 雄高	140
3P-14	Improved Efficiency and Stability of Perovskite Solar Cells with Single-Walled Carbon Nanotube Electrodes * Takahiro Sakaguchi, Jeon Il, Hiroki Suko, Taiki Inoue, Rong Xiang, Shohei Chiashi, Esko I. Kauppinen, Nam-Gyu Park, Yutaka Matsuo, Shigeo Maruyama	141
<b>ナノチューブの生成と精製</b>		
3P-15	2液相法とラマン分光を利用した金属/半導体単層カーボンナノチューブの比の評価 裏谷 研人, 金澤 尚宜, * 鈴木 信三	142
3P-16 ☆	ハロゲンガスによる多様なカーボンナノチューブからの触媒金属の除去 * 浜田 航綺, 杉目 恒志, 野田 優	143
3P-17	Controllable growth of single-walled carbon nanotubes in quality and uniformity by extended alcohol catalytic chemical vapor deposition * Bo Hou, Cheng Wu, Yuko Izumi, Takahiro Morimoto, Toshiya Okazaki, Taiki Inoue, Shohei Chiashi, Rong Xiang, Shigeo Maruyama	144
3P-18	W-Co触媒を用いた構造制御合成 * Shinnosuke Ohyama, Shun Yamamoto, Hua An, Feng Yang, Taiki Inoue, Rong Xiang, Shohei Chiashi, Yan Li, Shigeo Maruyama	145
3P-19	Growth of Semiconducting (14,4) Carbon Nanotubes using W-Co Salts as Catalyst Precursor * Xiulan Zhao, Feng Yang, Yan Li	146
3P-20	Single-Walled Carbon Nanotube Growth from Bimetallic Catalyst by Molecular Dynamics Simulations * 吉川 亮, 鶴飼 浩行, 高木 勇海, 千足 昇平, 丸山 茂夫	147
<b>内包ナノチューブ</b>		
3P-21 ☆	Template Synthesis of $\pi$ -Conjugated Nanomaterials using Inner Space of Carbon Nanotubes * Yasuhiro Kinno, Haruka Omachi, Ryo Kitaura, Hisanori Shinohara	148
3P-22	第一原理計算によるカーボンナノチューブに内包されたカルコゲンの電子状態評価 * 佐藤 豊, 横倉 瑛太, 片岡 洋右, 緒方 啓典	149
<b>ナノホーン</b>		
3P-23	リポポリサッカライド処理をしたマクロフェージに対するカーボンナノホーンの影響 * 中村 真紀, 黒岩 輝代子, 飯島 澄男, 湯田坂 雅子	150
3P-24	A study of Preparation Conditions of Carbon Nanobrush * Ryota Yuge, Fumiyuki Nihey, Kiyohiko Toyama, Masako Yudasaka	151

## 3月3日 (金)

### グラフェン生成

- 3P-25 Analysis of Initial Formation Process of Graphene on SiC(0001) Surfaces Based on the First-Principles Molecular Dynamics 152  
☆ \* *Fumihiko Imoto, Jun-Ichi Iwata, Mauro Boero, Atsushi Oshiyama*
- 3P-26 Growth of Single-Crystal Single-Layer and Bi-Layer Graphene Using Alcohol Catalytic CVD 153  
\* *Masaki Sota, Kotaro Kashiwa, Naomasa Ueda, Keigo Otsuka, Taiki Inoue, Rong Xiang, Shohei Chiashi, Shigeo Maruyama*

### グラフェンの応用

- 3P-27 太陽電池応用に向けたグラフェン電極上の高配向CuInS<sub>2</sub>薄膜 154  
\* *石川 亮佑, 大矢 智也, 山田 凶南, 野本 隆宏, 坪井 望*
- 3P-28 Controlled fabrication of graphene liquid cells 155  
\* *Yoshimasa Michiya, Tomohiro Yasunishi, Yutaka Ohno, Hisanori Shinohara, Ryo Kitaura*
- 3P-29 酸化アミンカップリング反応における酸化グラフェンの反応性の要因 156  
\* *井坂 琢也, 田嶋 健太郎, 山科 智貴, 高井 和之*
- 3P-30 CVD成長した大面積二層グラフェンへのMoCl<sub>5</sub>のインターカレーションと透明導電膜応用 157  
\* *木下 博貴, 河原 憲治, 寺尾 友里, Il Jeon, 丸山 実那, 松本 里香, 岡田 晋, 松尾 豊, 吾郷 浩樹*

### グラフェンの物性

- 3P-31 グラフェン端への酸素吸着のエネルギー論 158  
\* *安間 愛莉, 山中 綾香, 岡田 晋*
- 3P-32 Band unfolding study on Fermi-level-velocity reduction induced by Dirac cone interaction in twisted bilayer graphene 159  
☆ \* *西 紘史, 松下 雄一郎, 押山 淳*
- 3P-33 グラフェン端形成過程のエネルギー論 160  
\* *山中 綾香, 岡田 晋*
- 3P-34 Electronic structure of edge functionalized graphene under an external electric field 161  
\* *Yanlin Gao, Susumu Okada*
- 3P-35 Brillouin zone topology and band structure of four-dimensional diamond 162  
*Yuichi Kato, \* Masanori Yamanaka*
- 3P-36 単原子空孔を有する二層グラフェンの電導特性 163  
\* *岸本 健, 岡田 晋*

### 原子層

- 3P-37 Tuning of local optical properties of MoS<sub>2</sub> monolayer and its structural control using electric-field-effect scanning near-field optical microscopy techniques 164  
☆ \* *野崎 純司, 福村 武蔵, 青木 孝晶, 真庭 豊, 蓬田 陽平, 柳 和宏*

## 3月3日 (金)

- 3P-38 Optical properties of superacid-treated MoS<sub>2</sub> 165  
\* 林 宏恩, モハメッド ヌル バイズラ, 宮内 雄平, 松田 一成
- 3P-39 原子層物質ヘテロ積層構造における層間エキシトンの緩和過程 166  
☆ \* 岡田 光博, 暮石 宥介, 長谷川 勇介, *Kutana Alex*, 渡邊 賢司, 谷口 尚,  
宮内 雄平, 松田 一成, 篠原 久典, 北浦 良
- 3P-40 Transition of crystal structure and electrical property of MoTe<sub>2</sub> crystal by laser irradiation 167  
\* *Kota Kamiya, Tomoki Yamanaka, Masahiro Matsunaga, Ayaka Higuchi, Yuichi Ochiai,*  
*Michio Kida, Jonathan P. Bird, Nobuyuki Aoki*

### ナノ炭素粒子

- 3P-41 爆轟法ナノダイヤモンドのレーザー脱離イオン化質量スペクトル 168  
\* 深谷 真芳, 田中 利彦, バーナード アマンダ, 大澤 映二
- 3P-42 窒素ガス中衝突反応によるナノ粒子上でのアミノ酸合成 169  
\* 三重野 哲, 大河内 一輝, 関口 俊介, 長谷川 直

### 特別講演 (16:00-16:30)

- 3S-10 Localized growth of transition metal dichalcogenides on patterned graphene 10  
\* *Erik Einarsson, Fei Lu, Arka Karmakar, Simran Shahi*

### 一般講演 (16:30-17:30)

#### グラフェン生成・グラフェンの応用

- 3-8 Fabrication and characterization of IrO<sub>2</sub> / nano-carbon catalysts 39  
\* 原 正則, *Badam Rajashekar, Kanishka De Silva, Hsin-Hui Huang, 吉村 雅満*
- 3-9 Bottom-up approach for edge-functionalized graphene nanoribbons 40  
\* *Hideyuki Jippo, Junichi Yamaguchi, Shintaro Sato, Hironobu Hayashi, Hiroko Yamada,*  
*Mari Ohfuchi*
- 3-10 CoCu触媒を用いた単層グラフェンの低温成長 41  
\* 杉目 恒志, *Lorenzo D'Arsié, Robert Weatherup, Santiago Esconjauregui,*  
*Guofang Zhong, Xingyi Wu, John Robertson*
- 3-11 2層グラフェンを用いた熱的に安定なSERS基板の作製 42  
\* 鈴木 誠也, 吉村 雅満

March 1st, Wed.

Special Lecture: 25min (Presentation) + 5min (Discussion)

General Lecture: 10min (Presentation) + 5min (Discussion)

Poster Preview: 1min (Presentation)

**Special Lecture ( 9:45–10:15 )**

- 1S-1 Putting  $sp^3$ -diamondoids into carbon nanotubes 1  
\* *Hisanori Shinohara*

**Special Lecture ( 10:15–10:45 )**

- 1S-2 Direct dry deposition of SWNTs by thermophoresis 2  
\* *Esko I. Kauppinen, Patrik Laiho, Kimmo Mustonen, Shigeo Maruyama, Yutaka Ohno*

>>>>>>> Coffee Break ( 10:45–11:00 ) <<<<<<<<

**General Lecture ( 11:00–12:00 )**

**Formation and purification of nanotubes ▪ Properties of nanotubes**

▪ **Properties of graphene**

- 1-1 Fabrication of multiple transistors from semiconducting single-walled carbon nanotube arrays after water-assisted burning of metallic tubes 11  
\* *Keigo Otsuka, Taiki Inoue, Shohei Chiashi, Shigeo Maruyama*
- 1-2 Asymmetric carrier accumulation in double-walled carbon nanotube under an electric field 12  
\* *Taketo Kochi, Susumu Okada*
- 1-3 Enhancement of Raman scattering from monolayer graphene by photonic crystal nanocavities 13  
\* *Issei Kimura, Masahiro Yoshida, Masaki Sota, Hidenori Machiya, Taiki Inoue, Shohei Chiashi, Shigeo Maruyama, Yuichiro K. Kato*
- 1-4 Magnetic properties of two-dimensional hydrocarbon networks 14  
\* *Jun-ya Sorimachi, Susumu Okada*

>>>>>>> Lunch Time ( 12:00–13:15 ) <<<<<<<<

**Special Lecture ( 13:15–13:45 )**

- 1S-3 Growth modes and chiral selectivity of Single Wall Carbon Nanotubes 3  
\* *Christophe Bichara*

March 1st, Wed.

**Special Lecture ( 13:45–14:15 )**

- 1S-4 Sugar Chain Modified Graphene FET for Detection of Virus 4  
\* *Kazuhiko Matsumoto*

**General Lecture ( 14:15–15:00 )**

**Properties of graphene · Applications of graphene**

- 1-5 Opening a Gap in Graphene Field Effect Devices with Periodic Uniaxial Strain 15  
\* *Hikari Tomori, Rineka Hiraide, Youiti Ootuka, Kenji Watanabe, Takashi Taniguchi, Akinobu Kanda*
- 1-6 Gas Adsorption Effects on Stabilities and Electronic Properties of Graphene Bilayers 16  
\* *Yoshitaka Fujimoto, Susumu Saito*
- 1-7 Edge Roughness Analysis for Developing GNR-based FET 17  
\* *Kengo Takashima, Takahiro Yamamoto*

**Poster Preview ( 15:00–16:00 )**

**Poster Session ( 16:00–17:45 ) (★)Candidates for the Young Scientist Poster Award**

**Endohedral metallofullerenes**

- 1P-1 Photochemical Addition of Siliranes to  $\text{Sc}_3\text{N}@I_h\text{-C}_{80}$ : Interconversion of the [6,6]- and [5,6]-Adducts 43  
\* *Takeshi Sugiura, Kyosuke Miyabe, Masahiro Kako, Masanori Yasui, Michio Yamada, Yutaka Maeda, Jingdong Guo, Shigeru Nagase, Takeshi Akasaka*
- 1P-2 Conclusive Characterization of  $\text{Li}@C_{60}$  by X-ray Structure Analysis 44  
\* *Hiroshi Ueno, Shinobu Aoyagi, Naohiko Ikuma, Hiroshi Okada, Kei Ohkubo, Tatsuhisa Kato, Shunichi Fukuzumi, Yutaka Matsuo, Ken Kokubo*

**Properties of nanotubes**

- 1P-3 Diameter and defect density dependence of intermediate frequency Raman mode of single-walled carbon nanotubes 45  
\* *Takumi Inaba, Satoru Konabe, Yoshikazu Homma*
- 1P-4 Spectral tuning of optical coupling between air-mode nanobeam cavities and individual carbon nanotubes 46  
★ \* *Hidenori Machiya, Takushi Uda, Akihiro Ishii, Yuichiro K. Kato*
- 1P-5 Tuning of Photo-thermoelectric effect of Metallic and Semiconducting Single wall carbon nanotube thin films by electrolyte gating 47  
\* *Masatoshi Nakamura, Yota Ichinose, Hideki Kawai, Yohei Yomogida, Kazuhiro Yanagi*

**March 1st, Wed.**

1P-6	Photoluminescence Characteristic of Single-Wall Carbon Nanotubes: Photon Reabsorption Effect <i>* Xiaojun Wei, Mayumi Tsuzuki, Yohei Yomogida, Guowei Wang, Atsushi Hirano, Shunjiro Fujii, Takeshi Tanaka, Hiromichi Kataura</i>	48
1P-7	Surface state of carbon nanopot -KFM study- <i>* Hiroyuki Yokoi, Kozo Ikeda, Kazuto Hatakeyama, Michio Koinuma</i>	49
1P-8	Anion effects on colloidal stability of surfactant-dispersed SWCNTs <i>* Atsushi Hirano, Weilu Gao, Xiaowei He, Junichiro Kono</i>	50
<b>Applications of nanotubes</b>		
1P-9	Paper-based carbon nanotube field effect transistor by photolithography <i>* Jong Mok Shin, Do Hyun Kim, InYeob Na, Ho-Kyun Jnag, Jun Hee Choi, Se Jeong Park, Gyu-Tae Kim</i>	51
1P-10	Doping effect of electrolyte droplet on carbon nanotube thin film ☆ <i>* Tomohiro Yasunishi, Shigeru Kishimoto, Yutaka Ohno</i>	52
1P-11	Development of CNT/Polyethylene Composites via Melt Blending <i>* Atsushi Onodera, Sami Ristimäki, Masaru Sekido</i>	53
1P-12	Defluorination-Assisted Synthesis of Nitrogen-Doped Single-Walled Carbon Nanotubes and Their Catalytic Activity of Oxygen Reduction Reaction for Polymer Electrolyte Fuel Cells ☆ <i>* Koji Yokoyama, Shun Yokoyama, Yoshinori Sato, Masashi Yamamoto, Tetsuo Nishida, Kenichi Motomiya, Hiromichi Ohta, Hideyuki Takahashi, Kazuyuki Tohji, Yoshinori Sato</i>	54
1P-13	Film fabrication of Semiconducting Single-Wall Carbon Nanotubes by Aqueous-Two Phase System and Thin Film Transistor Applications <i>* Haruka Omachi, Tomohiko Komuro, Jun Hirotsu, Yutaka Ohno, Hisanori Shinohara</i>	55
<b>Formation and purification of nanotubes</b>		
1P-14	Growth of Horizontally Aligned Chirality-Specific Single-Walled Carbon Nanotubes <i>* Feng Yang, Yan Li</i>	56
1P-15	Fluidized-bed synthesis of sub-millimeter-long carbon nanotubes at high yield from concentrated ethylene source ☆ <i>* Soichiro Hachiya, Zhongming Chen, Kosuke Kawabata, Kei Hasegawa, Toshio Osawa, Suguru Noda</i>	57

**March 1st, Wed.**

1P-16	Large-scale continuous separation of metallic / semiconducting carbon nanotubes by electric-field-induced layer formation method * <i>Fumiyuki Nihey, Fusako Sasaki, Yuki Kuwahara, Takeshi Saito, Hiroyuki Endoh</i>	58
1P-17	Development of gels for high-efficiency metal/ semiconductor separation of SWCNTs ☆ * <i>Guowei Wang, Xiaojun Wei, Atsushi Hirano, Takeshi Tanaka, Hiromichi Kataura</i>	59
1P-18	Purity Analysis and Purification of Double-walled Carbon Nanotubes * <i>Kenshi Miyaura, Hidekazu Nishino, Shirou Honda</i>	60
<b>Endohedral nanotubes</b>		
1P-19	An experimental and theoretical study on the scanning spectroscopy of europium nanowires encapsulated in carbon nanotubes ☆ * <i>Terunobu Nakanishi, Ryo Kitaura, Takazumi Kawai, Susumu Okada, Shoji Yoshida, Osamu Takeuchi, Hidemi Shigekawa, Hisanori Shinohara</i>	61
1P-20	DFT calculations of electronic states and solid state NMR parameters in Cesium Iodide encapsulated single-walled carbon nanotubes * <i>Eita Yokokura, Yosuke Kataoka, Hironori Ogata</i>	62
<b>Graphene synthesis</b>		
1P-21	Study of Au-Ni catalytic CVD of uniform multilayer graphene * <i>Yuki Ueda, Jumpei Yamada, Kyosuke Fujiwara, Daichi Yamamoto, Takahiro Maruyama, Shigeya Naritsuka</i>	63
1P-22	Thermodynamically Controlled Synthesis of Graphene from Carbon Monoxide ☆ * <i>Yukuya Nagai, Kei Hasegawa, Suguru Noda</i>	64
<b>Applications of graphene</b>		
1P-23	Fabrication and Electric Properties of Fe and Ca intercalated Bilayer Graphenes * <i>Natsuki Kuragane, Ryo Hoshino, Ryota Sakurai, Tamon Yamagishi, Tomoko Nagata, Nobuyuki Iwata, Hiroshi Yamamoto</i>	65
1P-24	Functional group dependence of Spin magnetism of Graphene oxide * <i>Kentaro Tajima, Takuya Isaka, Tomoki Yamashina, Yoshiaki Matsuo, Kazuyuki Takai</i>	66
1P-25	Highly efficient, mechanically durable perovskite solar cells with graphene electrodes * <i>Jungjin Yoon, Namyoun Ahn, Mansoo Choi</i>	67
1P-26	Reduction reaction of a single graphene oxide sheet in solution as probed by twilight fluorescence microscopy * <i>Hikaru Sato, Masahito Sano</i>	68

March 1st, Wed.

1P-27	Production and characterization of graphene quantum dots derived from SWNTs and graphite * Hiroki Morita, Toshiki Sugai	69
<b>Properties of graphene</b>		
1P-28	Energetics and electronic structure of B <sub>3</sub> N <sub>3</sub> -doped graphene * Hisaki Sawahata, Mina Maruyama, Susumu Okada	70
1P-29	Charge transfer dynamics at graphene/SiC interface studied by time-resolved soft X-ray photoemission spectroscopy ☆ * Takashi Someya, Hirokazu Fukidome, Susumu Yamamoto, Norifumi Endo, Iwao Matsuda	71
1P-30	Simplified estimation of crystallographic orientation of strained graphene by micro-Raman spectroscopy * Kazushi Nakamura, Hikari Tomori, Akinobu Kanda	72
1P-31	Mechanical properties of graphene nanoribbons * Kazufumi Yoneyama, Ayaka Yamanaka, Susumu Okada	73
1P-32	Introduction of spin-orbit interaction into graphene by various methods * T. Nanba, T. Tamura, Y. Katagiri, C. Ohata, Pierre Seneor, J. Haruyama	74
1P-33	Influences of Graphene Structure on Electrochemical Interactions in LiBF <sub>4</sub> Organic Electrolyte Solution * Daisuke Suzuki, Kazuyuki Takai	75
<b>Atomic Layers</b>		
1P-34	Detection of photo current arising from atom-thin MoS <sub>2</sub> Schottky junction fabricated by electron beam irradiation * Yuto Katagiri, C. Ohata, Y. Inoue, S. Maruyama, T. Nakamura, S. Katamoto, A. Ishi, M. Hasegawa, G. Fioli, S. Roche, J. Haruyama	76
1P-35	Mechanism of contact-resistance improvement in suspended device of bi-layer WSe <sub>2</sub> by mild oxygen plasma treatment ☆ * Reito Nagai, Toshiro Kaneko, Toshiaki Kato	77
1P-36	Optical spectroscopy on monolayer transition metal dichalcogenides immersed in an aqueous solution * Wenjin Zhang, Yusuke Hasegawa, Kazunari Matsuda, Yuhei Miyauchi	78

March 1st, Wed.

1P-37	Helicity-resolved first order resonant Raman spectra of graphene and transition metal dichalcogenides	79
☆	* <i>Yuki Tatsumi, Riichiro Saito</i>	
1P-38	Energetics and electronic properties of C <sub>60</sub> adsorbed on graphene	80
	* <i>Yamato Alexander Saucier, Mina Maruyama, Susumu Okada</i>	
<b>Bio</b>		
1P-39	Upconversion photoluminescence spectra of carbon nanotubes in mice tissues	81
	* <i>Saki Okudaira, Yoko Iizumi, Masako Yudasaka, Toshiya Okazaki, Kazunari Matuda, Yuhei Miyauchi</i>	
<b>Other topics</b>		
1P-40	Electrical properties of defective hexagonal boron nitride nanosheet	82
	* <i>Ho-Kyun Jang, Jun Hee Choi, Kook Jin Lee, Do-Hyun Kim, Gyu Tae Kim</i>	
1P-41	Modification of Electrical Properties in MoS <sub>2</sub> by Using Catalytic Oxidation	83
	* <i>Jun Hee Choi, Ho-Kyun Jang, Jun Eon Jin, Jong Mok Shin, Do-Hyun Kim, Gyu-Tae Kim</i>	
1P-42	Hidden symmetries in one-dimensional photonic crystals	84
	* <i>M. Shoufie Ukhtary, Haihao Liu, Riichiro Saito</i>	

>>>>>>> Coffee Break ( 17:45–18:00 ) <<<<<<<<

**Tutorial ( 18:00–19:30 )**

Exploring the Nano-space Made in Nanocarbon

\* *Hisanori Shinohara*

March 2nd, Thu.

**Special Lecture: 25min (Presentation) + 5min (Discussion)**

**General Lecture: 10min (Presentation) + 5min (Discussion)**

**Poster Preview: 1min (Presentation)**

**Special Lecture ( 9:00–9:30 )**

- 2S-5 Catalyst design for controlled growth of single-walled carbon nanotubes 5  
\* *Yan Li*

**General Lecture ( 9:30–10:30 )**

**Formation and purification of nanotubes ▪ Properties of nanotubes**

- 2-1 Drastically improved efficiency of single wall carbon nanotube forest synthesis 18  
on a MgO catalyst underlayer by a simple annealing process  
\* *Takashi Tsuji, Kenji Hata, Don Futaba, Shunsuke Sakurai*
- 2-2 A study of dispersion states of CNTs in slurry by AC impedance method 19  
\* *Takayuki Watanabe, Kazufumi Kobashi, Takahiro Morimoto, Toshiya Okazaki*
- 2-3 The effect of noble metals on the formation of iron catalyst nanoparticle for the 20  
synthesis of vertically-aligned carbon nanotubes  
\* *Shunsuke Sakurai, Kenji Hata, Don Futaba*
- 2-4 Lock-in thermography technique for visualization of CNT network structures 21  
\* *Takahiro Morimoto, Seisuke Ata, Takeo Yamada, Toshiya Okazaki*

>>>>>>> **Coffee Break ( 10:30–10:45 )** <<<<<<<<

**Special Lecture ( 10:45–11:15 )**

- 2S-6 Functionalized 2D materials for sensing applications 6  
\* *Shyamal K Saha, Diptiman Dinda*

**General Lecture ( 11:15–12:00 )**

**Atomic Layers**

- 2-5 Scanning Electrochemical Cell Microscopy for Visualization of Local 22  
Electrochemical Activities on Graphene/Graphite  
\* *Akichika Kumatani, Chiho Miura, Takeru Okada, Seiji Samukawa, Hitoshi Shiku, Yasufumi Takahashi, Tomokazu Matsue*

**March 2nd, Thu.**

2-6	Out-of-Plane Strain Generation of Monolayer MoS <sub>2</sub> and MoSe <sub>2</sub> Formed a Moiré Superstructure on the Au(111) Surface <i>Ryosuke Takahashi, Ryo Osaka, Yasumitsu Miyata, Susumu Okada, Yuhei Hayamizu, * Satoshi Yasuda, Kei Murakoshi</i>	23
2-7	Magnetic tunnel junction built from intercalated transition metal dichalcogenide ferromagnets with different magnetic anisotropy <i>* Yuji Yamasaki, Rai Moriya, Miho Arai, Satoru Masubuchi, Sunseng Pyon, Tsuyoshi Tamegai, Keiji Ueno, Tomoki Machida</i>	24

>>>>>>> Lunch Time ( 12:00–13:15 ) <<<<<<<<

**Awards Ceremony ( 13:15–14:00 )**

**Poster Preview ( 14:00–15:00 )**

**Poster Session ( 15:00–16:45 ) (★) Candidates for the Young Scientist Poster Award**

**Chemistry of fullerenes**

2P-1	Theoretical estimation for the electronic property and reactivity of activated fullerenes <i>* Naohiko Ikuma, Ken Kokubo, Takumi Oshima</i>	85
2P-2	Palladium-Catalyzed Functionalization of C <sub>60</sub> Derivatives: Regioselectivity and Structures <i>★ * Yoshifumi Hashikawa, Michihisa Murata, Atsushi Wakamiya, Murata Yasujiro</i>	86
2P-3	Synthesis of Lithium-ion-encapsulated Fluoreno[60]fullerenes <i>* Yutaka Matsuo, Hiroshi Okada, Hiroshi Ueno</i>	87

**Applications of fullerenes**

2P-4	Nanoscale Control of Polymer Assembly on Fullerene Bilayer Membranes <i>* Koji Harano, Ricardo M. Gorgoll, Eiichi Nakamura</i>	88
2P-5	Metallic Polymerization of C <sub>60</sub> Thin Film by Electron-Beam Irradiation <i>* Hiroto Uenoyama, Yu Tanaka, Shingo Yamanouchi, Yuichi Ochiai, Nobuyuki Aoki</i>	89
2P-6	Synthesis of CdS-Mn-[C <sub>60</sub> ]Fullerene Nanocomposites and Their Photocatalytic Activities for Degradation of Organic Dyes <i>* Jeong Won Ko, Jiulong Li, Weon Bae Ko</i>	90

March 2nd, Thu.

2P-7	Studies on the Aggregated Structures and Crystallinities of Bulk Heterojunction Films Constituting Organic Solar Cells * <i>Saki Kawano, Hironori Ogata</i>	91
<b>Endohedral metallofullerenes</b>		
2P-8	Production and Characterization of Hetero-dimetallofullerene: GdY@C <sub>80</sub> (I <sub>h</sub> ) * <i>Takuji Mitani, Natsumi Nakatori, Takahisa Yamaguchi, Ko Furukawa, Tatsuhisa Kato, Koichi Kikuchi, Yohji Achiba, Takeshi Kodama</i>	92
2P-9	Isolation and structural analysis of La@C <sub>60</sub> (CF <sub>3</sub> ) <sub>5</sub> ☆ * <i>Makiko Nishino, Shinobu Aoyagi, Haruka Omachi, Zhiyong Wang, Ayano Nakagawa, Ryo Kitaura, Hisanori Shinohara</i>	93
2P-10	Photoreactions of Cyclic Organosilanes with Trimetallic Nitride Template Endohedral Metallofullerenes * <i>Shinpei Fukazawa, Takeshi Sugiura, Kyosuke Miyabe, Masahiro Kako, Takeshi Akasaka</i>	94
<b>Fullerenes</b>		
2P-11	Energetics and electronic structure of SIMEF chains * <i>Sho Furutani, Susumu Okada</i>	95
2P-12	Absolute yield of fullerene formed by graphite laser ablation at medium-high ambient temperatures * <i>Haruka Suzuki, Yuki Taguchi, Takeshi Kodama, Yohji Achiba, Haruo Shiromaru</i>	96
2P-13	Energetics and electronic properties of fullerenes consisting of fused pentagonal rings * <i>Susumu Okada</i>	97
<b>Properties of nanotubes</b>		
2P-14	Macroscopic aligned single-walled carbon nanotubes achieved with vacuum filtration * <i>Zhang Hao, Rong Xiang, Taiki Inoue, Shohei Chiashi, Shigeo Maruyama</i>	98
2P-15	Selective phonon mode generations in single wall carbon nanotubes and graphene nanoribbons ☆ * <i>Ahmad R. T. Nugraha, Eddwi H. Hasdeo, Riichiro Saito</i>	99
2P-16	Electrically conductive multi-walled boron nitride nanotubes by catalytic etching * <i>Do-Hyun Kim, Ho-Kyun Jang, Min-Seok Kim, Sung-Dae Kim, Dong-Jin Lee, Gyu Tae Kim</i>	100

March 2nd, Thu.

**Applications of nanotubes**

- 2P-17 Artificial muscle using single wall carbon nanotube bundles 101  
☆ \* *Nguyen Tuan Hung, Ahmad Ridwan Tresna Nugraha, Riichiro Saito*
- 2P-18 Electrochemical Properties of Nitrogen-Doped Vertically Aligned Multi-Walled Carbon Nanotubes Prepared by Defluorination 102  
\* *Rei Nonomura, Takashi Itoh, Yoshinori Sato, Masashi Yamamoto, Tetsuo Nishida, Kenichi Motomiya, Kazuyuki Tohji, Yoshinori Sato*
- 2P-19 Synthesis and morphology control of carbon nanotubes on substrate for electron emitter application 103  
☆ \* *Sae Kitagawa, Hisashi Sugime, Suguru Noda*

**Formation and purification of nanotubes**

- 2P-20 Analysis of Pt catalyst for SWNT growth by In-situ XANES 104  
\* *Makoto Kumakura, Hoshimitsu Kiribayashi, Takahiro Saida, Shigeya Naritsuka, Takahiro Maruyama*
- 2P-21 Time-dependent selective synthesis and growth mechanism of single-walled carbon nanotubes from sputtered W-Co catalyst 105  
☆ \* *Hua An, Rong Xiang, Akihito Kumamoto, Taiki Inoue, Shohei Chiashi, Yuichi Ikuhara, Shigeo Maruyama*
- 2P-22 Extraction of High-Purity Single-Chirality Single-Wall Carbon Nanotubes by Precise Tuning of pH using CO<sub>2</sub> Bubbling 106  
\* *Yota Ichinose, Junko Eda, Yutaka Maniwa, Yohei Yomogida, Kazuhiro Yanagi*
- 2P-23 Magnetic field effects on the growth process of SWCNTs and examination of its mechanism 107  
☆ \* *Yasumasa Takashima, Atom Hamasaki, Jin Uchimura, Sumio Ozeki*
- 2P-24 Chemical reaction analysis of Fe-Co and Co-Cu clusters with ethanol by FT-ICR mass spectrometer 108  
\* *Ken Mizutani, Yoshinori Sato, Hiroya Minowa, Ryohei Yamada, Taiki Inoue, Shohei Chiashi, Shigeo Maruyama*

**Properties of graphene**

- 2P-25 Carrier injection in nearly free electron states of graphene nanoribbons by edge hydroxylation 109  
\* *Remi Taira, Ayaka Yamanaka, Susumu Okada*
- 2P-26 Fermi level tuning of N-doped graphene by an external electric field 110  
\* *Manaho Matsubara, Susumu Okada*

## March 2nd, Thu.

2P-27	Electronic structures of graphene exposed to electrolyte solution * <i>Mari Ohfuchi</i>	111
2P-28	Magnetic interactions between Edge-state spins and Ferrocenium ion spins * <i>Akira Suzuki, Kazuyuki Takai</i>	112
2P-29	Electrical properties of reduced graphene oxide by thermal annealing * <i>Takuya Ishida, Yuta Nishina, Nobuyuki Aoki</i>	113
2P-30	Influence of Water Molecules on Molecular Adsorption induced Charge Transfer in Graphene <i>Takashi Umehara, * Kazuyuki Takai</i>	114

### Atomic Layers

2P-31	Growth of large-area and uniform multilayer hexagonal boron nitride as an ideal 2D insulator * <i>Sho Nakandakari, Kenji Kawahara, Yuki Uchida, Shigeto Yamasaki, Masatoshi Mitsuhashi, Hiroki Ago</i>	115
☆		
2P-32	Enhancement of laser-induced water decomposition by 2D sheets studied by first-principles simulations II * <i>Yoshiyuki Miyamoto, Hong Zhang, Xinlu Cheng, Angel Rubio</i>	116
2P-33	Photoluminescence and photocurrent properties of monolayer WSe <sub>2</sub> FETs fabricated by dry-transfer process * <i>Xiaofan Wang, Wenjin Zhang, Nur Baizura Mohamed, Dezhi Tan, Hong En Lim, Yuhei Miyauchi, Kazunari Matsuda</i>	117
☆		
2P-34	Piezoelectric properties of 3R bulk transition metal dichalcogenides * <i>Satoru Konabe, Takahiro Yamamoto</i>	118
2P-35	Molecular beam epitaxy growth of molybdenum diselenide atomic layers on hexagonal boron nitride substrates * <i>Takuto Tokuda, Takato Hotta, Kenji Watanabe, Takashi Taniguchi, Hisanori Shinohara, Ryo Kitaura</i>	119
☆		

### Carbon nanoparticles

2P-36	Meteorite- and detonation-nanodiamonds are the same substances * <i>Eiji Osawa, Amanda Barnard, Toshihiko Tanaka, Masayoshi Fukaya</i>	120
2P-37	Synthesis of N-doped carbon nanoballoons with nitrogen plasma * <i>Ryota Takahashi, Toru Harigai, Hirofumi Takikawa, Yoshiyuki Suda</i>	121

March 2nd, Thu.

**Other topics**

- 2P-38 Separation of iron oxide nanotubes from the products prepared by surfactant assisted sol-gel method and characterization 122  
*Yuka Tanaka, \* Shunji Bandow*
- 2P-39 Development of Multi-stage Ion Trap Ion Mobility Measurement System and Separation of Nano Materials 123  
*\* Toshiki Sugai, Kyohei Shiino, Yuudai Hoshino, Natsuki Terada, Yuuta Hamano, Hiroki Morita, Ryota Jinnouchi*
- 2P-40 Mechanical properties of nano-rotors: Energetics of triptycene derivatives 124  
*\* Miki Akiba, Susumu Okada*
- 2P-41 Study of deactivation mechanism of carbon catalyst by thermo-catalytic decomposition of methane 125  
*\* Haruki Nishii, Yoshito Umeda, Hiroaki Hamaguchi, Masashi Suzuki, Toru Harigai, Hirofumi Takikawa, Yoshiyuki Suda*
- 2P-42 Effect of PtRu alloying on catalytic activity of catalysts for direct methanol fuel cells 126  
*\* Kohei Kawasaki, Tatsuo Ohiro, Toru Harigai, Hirofumi Takikawa, Hitoshi Ue, Yoshiyuki Suda*
- 2P-43 Microfabrication of carbon nanocoil using Focused Ion Beam 127  
*\* Munehito Takahashi, Toru Harigai, Hirofumi Takikawa, Hitoshi Ue, Yoshiyuki Suda*

**Special Lecture ( 16:45-17:15 )**

- 2S-7 Production and functionalization of carbon nanotubes for energy devices 7  
*\* Suguru Noda*

**General Lecture ( 17:15-19:00 )**

**Applications of fullerenes** ▪ **Endohedral metallofullerenes** ▪ **Fullerenes**  
▪ **Carbon nanoparticles** ▪ **Other topics**

- 2-8 Improvement of Open-circuit Voltage in Perovskite Solar Cells by Using Methano-Indene-Fullerene (MIF) 25  
*\* Yutaka Matsuo*
- 2-9 Electronic Structures and Stability of Metal Encapsulated C<sub>80</sub> fullerenes: Ab initio DFT study 26  
*\* Archana Velloth, Yutaka Imamura, Takeshi Kodama, Masahiko Hada*

**March 2nd, Thu.**

2-10	Searching for the unprecedented endohedral metallofullerenes by applying the separation method for those stable only in an anion form <i>* Natsumi Nakatori, Takuji Mitani, Takahisa Yamaguchi, Ko Furukawa, Tatsuhisa Kato, Koichi Kikuchi, Yohji Achiba, Takeshi Kodama</i>	27
2-11	Dynamics of Li <sup>+</sup> ions encapsulated in C <sub>60</sub> fullerene at low temperature <i>* Hal Suzuki, Misaki Ishida, Masatsugu Yamashita, Chiko Otani, Kazuhiko Kawachi, Yasuhiko Kasama, Eunsang Kwon</i>	28
2-12	Geometric and electronic structures of polymerized C <sub>40</sub> fullerene <i>* Mina Maruyama, Susumu Okada</i>	29
2-13	Polyynes formation by laser induced breakdown in hydrocarbon gas flow <i>Yuki Taguchi, Hitomi Endo, Takeshi Kodama, Tomonari Wakabayashi, Yohji Achiba, * Haruo Shiromaru, Benji Wales, Joseph Sanderson</i>	30
2-14	Inner Core in the Elementary Particles of Detonation Nanodiamond <i>* Toshihiko Tanaka, Masayoshi Fukaya, Amanda Barnard, Eiji Osawa</i>	31

**Banquet ( 19:00–20:45 )**

March 3rd, Fri.

Special Lecture: 25min (Presentation) + 5min (Discussion)

General Lecture: 10min (Presentation) + 5min (Discussion)

Poster Preview: 1min (Presentation)

**Special Lecture ( 9:00–9:30 )**

- 3S-8 Strong Light-Matter Coupling in (6,5) Carbon Nanotubes 8  
\* Junichiro Kono, Weilu Gao, Kankan Cong, Xinwei Li, G. Timothy Noe II,  
Huaping Liu, Takeshi Tanaka, Hiromichi Kataura

**General Lecture ( 9:30–10:30 )**

**Properties of nanotubes**

- 3-1 Optical bistability in carbon nanotubes 32  
\* Takushi Uda, Akihiro Ishii, Yuichiro K. Kato
- 3-2 Single photon generation through exciton-exciton annihilation in air-suspended carbon nanotubes 33  
\* Akihiro Ishii, Takushi Uda, Yuichiro K. Kato
- 3-3 Raman Spectroscopy of Individual Single-Walled Carbon Nanotubes 34  
\* Juan Yang, Daqi Zhang, Yan Li
- 3-4 Competitive elimination and decomposition reaction of oxidized single-walled carbon nanotubes depending on the degree of functionalization 35  
\* Yutaka Maeda, Erika Sone, Akane Nishino, Yuri Amagai, Wei-Wei Wang,  
Michio Yamada, Mitsuaki Suzuki, Jun Matsui, Masaya Mitsuichi, Toshiya Okazaki,  
Shigeru Nagase

>>>>>>> Coffee Break ( 10:30–10:45 ) <<<<<<<<

**Special Lecture ( 10:45–11:15 )**

- 3S-9 Optical Spectroscopy of Individual Carbon Nanotubes with Defined Atomic Structure 9  
\* Kaihui Liu

**General Lecture ( 11:15–12:00 )**

**Properties of nanotubes ▪ Applications of nanotubes**

- 3-5 Development of Nano-Resolution Desktop FE-SEM and X-ray microscope with Multi-Walled Carbon Nanotube Electron Source 36  
\* Masaru Irita, Shintarou Yamazaki, Shota Katsuyama, Hitoshi Nakahara,  
Koji Asaka, Yahachi Saito, Hidekazu Murata, Teruaki Ohno

**March 3rd, Fri.**

- 3-6 Cold exciton electroluminescence from air-suspended carbon nanotube split-gate devices 37  
*Noriyuki Higashide, \* Masahiro Yoshida, Takushi Uda, Akihiro Ishii, Yuichiro K. Kato*
- 3-7 The Solution to Stability and Cost in Perovskite Solar Cells by All-Carbon Approach 38  
*\* Il Jeon, Namyoung Ahn, Jungjin Yoon, Esko Kauppinen, Mansoo Choi, Yutaka Matsuo, Shigeo Maruyama*

>>>>>>> Lunch Time ( 12:00-13:15 ) <<<<<<<<

**Poster Preview ( 13:15-14:15 )**

**Poster Session ( 14:15-16:00 ) (★)Candidates for the Young Scientist Poster Award**

**Endohedral metallofullerenes**

- 3P-1 Attempt to produce dimetallofullerenes containing Yb 128  
*\* Kazuhiro Kobayashi, Takuji Mitani, Natsumi Nakatori, Koichi Kikuchi, Yohji Achiba, Takeshi Kodama*
- 3P-2 Spectroscopic studies of La<sub>2</sub>@C<sub>78</sub> anion 129  
*\* Shinya Nishimoto, Kazuhiro Kobayashi, Takaaki Hirayama, Takuji Mitani, Natsumi Nakatori, Takahisa Yamaguchi, Ko Furukawa, Tatsuhisa Kato, Koichi Kikuchi, Yohji Achiba, Takeshi Kodama*

**Properties of nanotubes**

- 3P-3 Evaluation of dispersion states of nanomaterials by disc centrifuge sedimentation technique 130  
*\* Naoko Tajima, Takahiro Morimoto, Yuichi Kato, Kazufumi Kobashi, Takeo Yamada, Toshiya Okazaki*
- 3P-4 Unified analysis of quantum and classical transport properties on metallic carbon nanotubes 131  
*\* Keisuke Ishizeki, Kenji Sasaoka, Satoru Konabe, Satofumi Souma, Takahiro Yamamoto*
- ★
- 3P-5 High Temperature Surface Enhanced Raman Scattering of Single-Walled Carbon Nanotubes 132  
*\* Ming Liu, Keigo Otsuka, Rong Xiang, Taiki Inoue, Shohei Chiashi, Shigeo Maruyama*

March 3rd, Fri.

3P-6	Fabrication and photoluminescence characterization of carbon nanotube dual-gate devices <i>* Akihiro Sasabe, Takushi Uda, Masahiro Yoshida, Akihiro Ishii, Yuichiro K. Kato</i>	133
3P-7	Optical Measurement of Single-Walled Carbon Nanotubes Using Rayleigh Scattering Spectroscopy <i>* Takeshi Okochi, Toru Osawa, Yoritaka Furukawa, Tatsuro Ogamoto, Shun Kamakura, Taiki Inoue, Shohei Chiashi, Shigeo Maruyama</i>	134
<b>Applications of nanotubes</b>		
3P-8	Synthesis and structure control of vertically-aligned carbon nanotubes on Cu foils for thermal interface materials <i>* Shunji Kobayashi, Kei Hasegawa, Hisashi Sugime, Masanao Obori, Junichiro Shiomi, Xiaosong Zhou, Mizuhisa Nihei, Suguru Noda</i>	135
3P-9	Selective detection of neurotransmitters by adsorption voltammetry with carbon nanotube film <i>* Takuya Ushiyama, Shigeru Kishimoto, Yutaka Ohno</i>	136
3P-10	Time-dependent change of the semiconducting-CNT ink evaluated from the performance of CNT-TFTs <i>* Yuki Kuwahara, Fusako Sasaki, Fumiyuki Nihey, Takeshi Saito</i>	137
3P-11	Lamination of Vertically Aligned Single-Walled Carbon Nanotube Forests on Perovskite Solar Cells via Membrane Filter Transfer Method <i>* Seungju Seo, IL Jeon, Takahiro Sakaguchi, Taiki Inoue, Rong Xiang, Shohei Chiashi, Yutaka Matsuo, Shigeo Maruyama</i>	138
☆		
3P-12	Yields of carbon nanotube integrated circuits on flexible plastic film <i>* Jun Hirotani, Shigeru Kishimoto, Yutaka Ohno</i>	139
3P-13	Modeling of carbon nanotube thin-film transistor on flexible plastic film <i>* Taiga Kashima, Tomoki Matsuura, Jun Hirotani, Shigeru Kishimoto, Yutaka Ohno</i>	140
☆		
3P-14	Improved Efficiency and Stability of Perovskite Solar Cells with Single-Walled Carbon Nanotube Electrodes <i>* Takahiro Sakaguchi, Jeon Il, Hiroki Suko, Taiki Inoue, Rong Xiang, Shohei Chiashi, Esko I. Kauppinen, Nam-Gyu Park, Yutaka Matsuo, Shigeo Maruyama</i>	141

March 3rd, Fri.

**Formation and purification of nanotubes**

- 3P-15 Evaluation of the ratio of metal/semiconductive SWNTs by utilizing ATP technique and Raman spectroscopy 142  
*Kento Uratani, Naoki Kanazawa, \* Shinzo Suzuki*
- 3P-16 Removing catalyst metals from various carbon nanotubes by halogen gas 143  
☆ *\* Koki Hamada, Hisashi Sugime, Suguru Noda*
- 3P-17 Controllable growth of single-walled carbon nanotubes in quality and uniformity by extended alcohol catalytic chemical vapor deposition 144  
*\* Bo Hou, Cheng Wu, Yuko Iizumi, Takahiro Morimoto, Toshiya Okazaki, Taiki Inoue, Shohei Chiashi, Rong Xiang, Shigeo Maruyama*
- 3P-18 Synthesis and Characterization of SWNTs Using W-Co Catalyst 145  
*\* Shinnosuke Ohyama, Shun Yamamoto, Hua An, Feng Yang, Taiki Inoue, Rong Xiang, Shohei Chiashi, Yan Li, Shigeo Maruyama*
- 3P-19 Growth of Semiconducting (14,4) Carbon Nanotubes using W-Co Salts as Catalyst Precursor 146  
*\* Xiulan Zhao, Feng Yang, Yan Li*
- 3P-20 Single-Walled Carbon Nanotube Growth from Bimetallic Catalyst by Molecular Dynamics Simulations 147  
*\* Ryo Yoshikawa, Hiroyuki Ukai, Yukai Takagi, Shohei Chiashi, Shigeo Maruyama*

**Endohedral nanotubes**

- 3P-21 Template Synthesis of  $\pi$ -Conjugated Nanomaterials using Inner Space of Carbon Nanotubes 148  
☆ *\* Yasuhiro Kinno, Haruka Omachi, Ryo Kitaura, Hisanori Shinohara*
- 3P-22 Electronic states of chalcogen encapsulated in single-walled carbon nanotubes studied by First-principles DFT calculations( II ) 149  
*\* Yutaka Sato, Eita Yokokura, Yousuke Kataoka, Hironori Ogata*

**Nanohorns**

- 3P-23 Effect of carbon nanohorns on lipopolysaccharide-induced RAW264.7 macrophage cells 150  
*\* Maki Nakamura, Kiyoko Kuroiwa, Sumio Iijima, Masako Yudasaka*
- 3P-24 A study of Preparation Conditions of Carbon Nanobrush 151  
*\* Ryota Yuge, Fumiyuki Nihey, Kiyohiko Toyama, Masako Yudasaka*

March 3rd, Fri.

### Graphene synthesis

- 3P-25 Analysis of Initial Formation Process of Graphene on SiC(0001) Surfaces Based on the First-Principles Molecular Dynamics 152  
☆ \* *Fumihiko Imoto, Jun-Ichi Iwata, Mauro Boero, Atsushi Oshiyama*
- 3P-26 Growth of Single-Crystal Single-Layer and Bi-Layer Graphene Using Alcohol Catalytic CVD 153  
\* *Masaki Sota, Kotaro Kashiwa, Naomasa Ueda, Keigo Otsuka, Taiki Inoue, Rong Xiang, Shohei Chiashi, Shigeo Maruyama*

### Applications of graphene

- 3P-27 Highly Oriented CuInS<sub>2</sub> Thin-Films on Graphene Electrodes for Solar Cells Applications 154  
\* *Ryousuke Ishikawa, Tomoya Oya, Tonan Yamada, Takahito Nomoto, Nozomu Tsuboi*
- 3P-28 Controlled fabrication of graphene liquid cells 155  
\* *Yoshimasa Michiya, Tomohiro Yasunishi, Yutaka Ohno, Hisanori Shinohara, Ryo Kitaura*
- 3P-29 Factors for reactivity of GO regarding oxidative amine coupling reaction 156  
\* *Takuya Isaka, Kentaro Tajima, Tomoki Yamashina, Kazuyuki Takai*
- 3P-30 Highly conductive and transparent large-area bilayer graphene realized by MoCl<sub>5</sub> intercalation 157  
\* *Hiroki Kinoshita, Kenji Kawahara, Yuri Terao, Il Jeon, Mina Maruyama, Rika Matsumoto, Susumu Okada, Yutaka Matsuo, Hiroki Ago*

### Properties of graphene

- 3P-31 Energetics of edge oxidization of graphene nanoribbons with clean edges 158  
\* *Airi Yasuma, Ayaka Yamanaka, Susumu Okada*
- 3P-32 Band unfolding study on Fermi-level-velocity reduction induced by Dirac cone interaction in twisted bilayer graphene 159  
☆ \* *Hirofumi Nishi, Yu-ichiro Matsushita, Atsushi Oshiyama*
- 3P-33 Energetics of Edge Formation Processes of Graphene 160  
\* *Ayaka Yamanaka, Susumu Okada*
- 3P-34 Electronic structure of edge functionalized graphene under an external electric field 161  
\* *Yanlin Gao, Susumu Okada*

**March 3rd, Fri.**

3P-35 Brillouin zone topology and band structure of four-dimensional diamond 162  
*Yuichi Kato, \* Masanori Yamanaka*

3P-36 Transport property of bilayer graphene with monovacancy 163  
*\* Ken Kishimoto, Susumu Okada*

**Atomic Layers**

3P-37 Tuning of local optical properties of MoS<sub>2</sub> monolayer and its structural control using 164  
electric-field-effect scanning near-field optical microscopy techniques  
*\* Junji Nozaki, Musashi Fukumura, Takaaki Aoki, Yutaka Maniwa,  
☆ Yohei Yomogida, Kazuhiro Yanagi*

3P-38 Optical properties of superacid-treated MoS<sub>2</sub> 165  
*\* Hong En Lim, Nur Baizura Mohamed, Yuhei Miyauchi, Kazunari Matsuda*

3P-39 Relaxation Mechanism of Interlayer Excitons in 2D van der Waals Heterostructures 166  
*\* Mitsuhiro Okada, Yusuke Kureishi, Yusuke Hasegawa, Alex Kutana,  
☆ Kenji Watanabe, Takashi Taniguchi, Yuhei Miyauchi, Kazunari Matsuda,  
Hisanori Shinohara, Ryo Kitaura*

3P-40 Transition of crystal structure and electrical property of MoTe<sub>2</sub> crystal 167  
by laser irradiation  
*\* Kota Kamiya, Tomoki Yamanaka, Masahiro Matsunaga, Ayaka Higuchi,  
Yuichi Ochiai, Michio Kida, Jonathan P. Bird, Nobuyuki Aoki*

**Carbon nanoparticles**

3P-41 The LDI spectra of Detonation Nanodiamonds 168  
*\* Masayoshi Fukaya, Toshihiko Tanaka, Amanda Barnard, Eiji Osawa*

3P-42 Impact synthesis of amino acids on carbon nano-particles in nitrogen gas 169  
*\* Tetsu Mieno, Kazuki Okochi, Syunsuke Sekiguchi, Sunao Hasegawa*

**Special Lecture ( 16:00–16:30 )**

3S-10 Localized growth of transition metal dichalcogenides on patterned graphene 10  
*\* Erik Einarsson, Fei Lu, Arka Karmakar, Simran Shahi*

**General Lecture ( 16:30–17:30 )**

**Graphene synthesis ▪ Applications of graphene**

3-8 Fabrication and characterization of IrO<sub>2</sub> / nano-carbon catalysts 39  
*\* Masanori Hara, Badam Rajashekar, Kanishka De Silva, Hsin-Hui Huang,  
Masamichi Yoshimura*

**March 3rd, Fri.**

- 3-9 Bottom-up approach for edge-functionalized graphene nanoribbons 40  
*\* Hideyuki Jippo, Junichi Yamaguchi, Shintaro Sato, Hironobu Hayashi, Hiroko Yamada, Mari Ohfuchi*
- 3-10 Low temperature growth of fully covered single layer graphene using CoCu catalyst 41  
*\* Hisashi Sugime, Lorenzo D'Arsié, Robert Weatherup, Santiago Esconjauregui, Guofang Zhong, Xingyi Wu, John Robertson*
- 3-11 Fabrication of a thermally stable SERS substrate using bilayer graphene 42  
*\* Seiya Suzuki, Masamichi Yoshimura*

特別講演  
**Special Lecture**

**1S – 1 ~ 1S – 4**

**2S – 5 ~ 2S – 7**

**3S – 8 ~ 3S – 10**

## Putting $sp^3$ -Diamondoids into Carbon Nanotubes

Hisanori Shinohara

*Department of Chemistry & Institute for Advanced Research,  
Nagoya University,  
Nagoya 464-8602, Japan*

By putting atoms, molecules, and, even, nanowires of various kind into carbon nanotubes (CNT), one can easily and drastically alter the electronic structures, electron transport and magnetic properties of CNTs, in which charge transfers between encapsulates and CNTs may oftentimes play crucial roles [1]. In some cases, novel one-dimensional (1D) nanowires can be fabricated within carbon nanotubes which are not possible to produce in the conventional bulk conditions [2-5].

A similar thing can be achieved when bilayer graphene is used for “sandwiching” atoms and molecules to fabricate unique nano-materials as well as to observe novel phenomena, but in two dimensional (2D) fashion [6,7].

In this talk, I will discuss some unique and novel properties of 1D and 2D nano-space and its application to syntheses of new materials prepared by nanotubes and bilayer graphene, respectively.

### References:

- [1] L.H.G.Tizei et al. *Phys.Rev.Lett.* 114, 197602 (2015).
- [2] H.E.Lim et al. *ACS Nano*, 9, 5034 (2015).
- [3] H.E.Lim et al. *Nature Commun.* 4, 2548 (2013).
- [4] R.Nakanishi et al. *Sci.Rep.*3, 1385 (2013).
- [5] Y.Nakanishi et al. *Angew.Chem.Int.Ed.* 54, 10802 (2015).
- [6] Y.Sasaki et al. *Appl.Phys.Express*, 5, 065103 (2012).
- [7] Y.Sasaki et al. *Chem.Phys.Lett.* 650, 107 (2016).

Corresponding Author: H.Shinohara

Tel: +81-52-789-2482, Fax: +81-52-747-6442

E-mail: noris@nagoya-u.jp

## Direct dry deposition of SWNTs by thermophoresis

Patrik Laiho<sup>a</sup>, Kimmo Mustonen<sup>a,b</sup>, Shigeo Maruyama<sup>c</sup>, Yutaka Ohno<sup>d</sup> and Esko I. Kauppinen<sup>a</sup>

*<sup>a</sup> Department of Applied Physics, Aalto University School of Science,  
P.O. Box 15100, FI-00076 Aalto, Finland*

*<sup>b</sup> Physics of Nanostructured Materials, Faculty of Physics, University of Vienna,  
Boltzmanngasse 5, A-1090 Vienna, Austria*

*<sup>c</sup> Department of Mechanical Engineering, The University of Tokyo,  
Bunkyo-ku, Tokyo 113-8656, Japan*

*<sup>d</sup> EcoTopia Science Institute, Nagoya University, Furo-cho, Chikusa-ku,  
Nagoya 464-8603, Japan*

We have developed the dry and continuous thermophoretic deposition of pristine, individual single-walled carbon nanotubes grown using a floating-catalyst CVD process. Based on aerosol loss measurements, the thermophoretic terminal velocity of SWCNTs is much lower i.e. approximately only one third of the usual free molecular regime prediction and shows a weak dependence on the nanotube diameter. Scanning electron microscopy and atomic force microscopy of the deposited samples indicate that pristine, as-synthesized SWCNTs with controllable densities, ranging from individual, separated nanotubes to multilayer thin films, can be deposited on practically any flat substrate with high efficiencies close to unity. Depending on the lateral flow inside the precipitator, the angular distribution of the deposited SWCNTs can be changed from uniform to non-uniform. As a demonstration of the applicability of our technique, we have used thermophoretic deposition to fabricate carbon nanotube thin film transistors with uniform electrical properties and a high, over 99,5% yield and high field effect electrical mobility exceeding 400 cm<sup>2</sup>/Vs while simultaneously having a  $I_{ON}/I_{OFF}$  in excess of 10<sup>6</sup>.

e-mail: [esko.kauppinen@aalto.fi](mailto:esko.kauppinen@aalto.fi)

## Growth modes and chiral selectivity of SWNTs

**Christophe Bichara**

*CINaM, Aix-Marseille University and CNRS  
bichara@cinam.univ-mrs.fr*

Significant progress has been made recently in the synthesis of single wall carbon nanotube (SWNT) by catalytic chemical vapor deposition (CCVD), along with a rise of commercially viable applications. A property selective synthesis seems still elusive, though, because of specific issues. High synthesis temperatures, nanometric sizes and a large number of correlated growth parameters make the experimental investigation of the growth mechanisms specially challenging. Theoretical approaches are not easier, but I will show here that dedicated computer simulations, including tight binding models [1], as well as DFT based calculations can provide a useful insight. Different aspects have been investigated.

It starts with the complex stability pattern of atomic carbon dissolved in subsurface layers of crystalline Ni, that depends on the presence of a graphene layer on top of it [2]. For catalyst nanoparticles below 3 nm, relevant for the CCVD growth, the presence of carbon dissolved in the surface layers induces a gradual melting at temperatures well below the melting temperature of pure nanoparticles of the same size. Calculated size dependent phase diagrams for Ni-C nanoparticles [3] indicate that faceted crystalline nanoparticles are unlikely to be observed in this size range under growth conditions.

This raises the question of the role of the carbon dissolved in the catalyst during growth that is shown to have a strong influence on the wetting properties of the metal-SWNT interface [4]. Through careful Transmission Electron Microscopy observations [5], so called tangential and perpendicular growth modes were identified. Computer simulations were used to analyze these growth modes at the atomic scale, demonstrating that tangential mode corresponds to a weak carbon supply and slow growth, while perpendicular one is observed when the carbon fraction in the nanoparticle is larger [6]. Growth experiments designed to tune the carbon fraction in the nanoparticle by changing the carbon feedstock (CO and CH<sub>4</sub>) confirm this analysis. Finally the role of different contributions to the stability and dynamics of the nanotube/nanoparticle interface on the possibility of a chiral selectivity will be discussed.

### References

- [1] Amara, H. *et al.* Phys. Rev. B **79**, 014109 (2009).
- [2] Weatherup, R. S. *et al.* J. Am. Chem. Soc., **136**, 13698–13708 (2014).
- [3] Magnin, Y. *et al.* Phys. Rev. Lett., 205502, 1–5 (2015).
- [4] Diarra, M. *et al.* Phys. Rev. Lett., 109, 185501 (2012).
- [5] Fiawoo, M.-F. C. *et al.* Phys. Rev. Lett., 108, 195503 (2012).
- [6] He, M. *et al.* Carbon, **113**, 231-6 (2017).

## Sugar Chain Modified Graphene FET for Detection of Virus

Kazuhiko Matsumoto

*Institute of Scientific & Industrial Research, Osaka University, Osaka 567-0047, Japan*

We formed a bio-platform by modified the surface of graphene FET with the sugar chain, which emulates a biological surface of human cell, and have succeeded in detecting electrically the human & bird influenza virus selectively, and also the dissociation process of virus from the sugar chain.

In order to selectively detect the influenza virus, two types of the graphene FET, one is modified by the human type sugar chain, the other is modified by the birds sugar chain, are prepared as shown in Fig.1. For the purpose of the safety, the pseud influenza virus, such as Lectin was used.

Figure 2 shows the selective detection of the pseud human influenza virus. SSA is the Lectin for the pseud human influenza virus, the MAM for the pseud bird influenza virus, and BSA is completely non target protein. In Fig.2, the pseud human influenza virus can be selectively caught by the human-type sugar chain and modified the current of the graphene FET, that means the selective detection of the pseud human influenza virus.

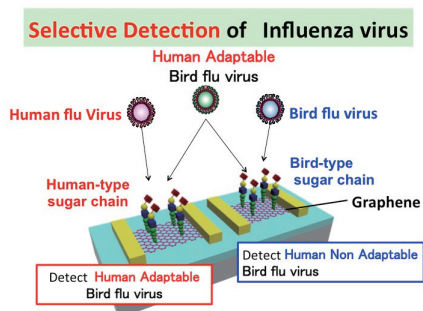


Fig.1, Schematics of SG(Sugar Chain)- functionalized graphene FET for the selective detection of Influenza Virus.

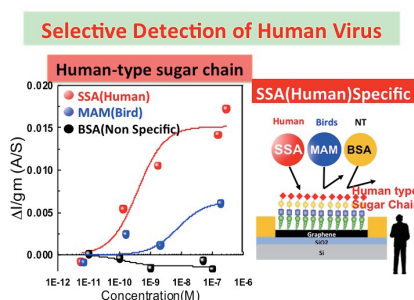


Fig.2, Selective detection of pseud Human flu virus (Lectin) by Human sugar chain modified graphene FET.

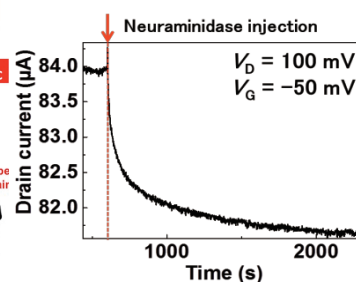


Fig. 3, Time course of the neuraminidase reaction monitored by the graphene FET.

When virus released from the cell to another cell and continues the infection, neuraminidase of the virus tip dissolves the sialic acid of the sugar chain where the hemagglutinin is attached. There was no approach to the physical measurement of the status of this dissociation process until now.

We introduced the neuraminidase to the system of sugar chain modified graphene FET. The neuraminidase dissolves sialic acid, and the negative charge of the carboxyl group of the sialic acid is removed. Then, the induced positive charge in the graphene channel by this negative charge is decreased, and we have first succeeded in observing the decrease of the drain current by this reaction as shown in Fig.3. This is the first time result that captures the dissociation process of virus by the neuraminidase from sugar chain by electrical method.

Corresponding Author: K. Matsumoto

Tel: +81-6-6879-8410, Fax: +81-6-6879-8414,

E-mail: [k-matsumoto@sanken.osaka-u.ac.jp](mailto:k-matsumoto@sanken.osaka-u.ac.jp)

## Catalyst design for controlled growth of single-walled carbon nanotubes

○Yan Li

*College of Chemistry and Molecular Engineering, Peking University, Beijing 100871, China*

Single-walled carbon nanotubes (SWNTs) have shown great potentials in various applications attribute to their unique structure-dependent properties. Therefore the controlled preparation of chemically and structurally pristine SWNTs is a crucial issue for their advanced applications (e.g. nanoelectronics) and has been a great challenge in more than two decades. The composition and morphology of the catalyst nanoparticles and the property of the catalyst supports were widely reported to affect the structure of SWNTs produced. In this talk, I will discuss the strategy in catalyst design for the structural controlled growth of SWNTs.

- [1] F. Yang *et al.* *Acc. Chem. Res.* **49**, 606-615 (2016).
- [2] F. Yang *et al.* *Nature* **510**, 522-524 (2014).
- [3] F. Yang *et al.* *J. Am. Chem. Soc.* **137**, 8688-8691 (2015).
- [4] X. Qin *et al.* *Nano Lett.* **14**, 512-517 (2014).
- [5] Y. Li *et al.*, *Adv. Mater* **22**, ,1508-1515 (2010).

Corresponding Author: Y. Li  
Tel & Fax: +86-10-6275-6773  
E-mail: yanli@pku.edu.cn

## Functionalized 2D materials for sensing applications

Diptiman Dinda and Shyamal K Saha

*Department of Materials Science, Indian Association for the Cultivation of Science, Jadavpur,  
Kolkata 700032, India*

It is needless to mention that graphene is an excellent electronic material, however, its optical property is very poor due to zero band gap. In this presentation, I would like to focus how optical property could be generated in graphene using functionalization technique. Graphene oxide is functionalized by organic moieties to develop superior optical property with intense photoluminescence behavior. Exploiting large surface area of graphene, hazardous heavy metals viz. Cr, Hg, As etc. are adsorbed on the surface of functionalized graphene oxide, which has potential application in water purification. This attachment of heavy metal ions on functionalized graphene oxide surface will be supported by photoluminescence quenching technique. Finally, using photoluminescence quenching technique, selective detection of nitroexplosives will also be discussed.

### **Ref:**

1. Emerging Photoluminescence in azo-pyridine intercalated graphene oxide layers. Abhisek Gupta and Shyamal K. Saha; **Nanoscale**, 2012, 4, 6562
2. Removal of toxic Cr(VI) by UV-active functionalized graphene oxide for water purification, Diptiman Dinda, Abhisek Gupta and Shyamal K. Saha  
**J. Mater. Chem. A**, 2013, 1, 11221
3. Highly Selective Detection of Trinitrophenol by Luminescent Functionalized Reduced Graphene Oxide through FRET Mechanism. Diptiman Dinda, Abhisek Gupta, Bikash Kumar Shaw, Suparna Sadhu, and S. K. Saha; **ACS Appl. Mater. Interfaces**, 2014, 6 (13), 10722.
4. Thymine Functionalized Graphene Oxide for Fluorescence “Turn-off-on” Sensing of Hg<sup>2+</sup> and I<sup>-</sup> in Aqueous Medium. Diptiman Dinda, Bikash Kumar Shaw, and Shyamal Kumar Saha. **ACS applied materials & interfaces**. 2015,27, 14743-14749

### **Corresponding Author:**

Shyamal K Saha; Email: [cnsks@iacs.res.in](mailto:cnsks@iacs.res.in)

## Production and functionalization of carbon nanotubes for energy devices

○Suguru Noda

*Department of Applied Chemistry, Waseda University, Tokyo 169-8555, Japan*

To efficiently use renewable energy at larger scale and support society, energy devices should be produced at lower cost using abundant chemical elements. Carbon nanotubes (CNTs), which are composed of carbon, are attractive due to their properties including high specific surface area, fairly high electric conductivity, lightness, flexibility, thermal/chemical stability, and good compatibility with solution processing. We focus on their use as passive electrode materials in combination with various active materials in energy devices.

Transparent conductive films (TCFs) are an attractive target, which need 5–10 mg CNTs per 1 m<sup>2</sup> and thus are cost effective. But such small amount of CNTs need to carry sufficient current. We proposed repetitive dispersion-centrifugation process to overcome the quality-quantity trade-off and realized >90% conversion of CNTs into TCFs of 80% transmittance and 50 Ω/sq resistance with HNO<sub>3</sub> doping [1]. We used such solution-processed CNT-TCFs to fabricate CNT-Si heterojunction solar cells and realized ~10% photoconversion efficiency with flat n-Si wafer with HNO<sub>3</sub> doping and with textured n-Si wafer without doping (Fig. 1) [2]. This technology will be combined with our large-grain Si films fabricated rapidly in 1 min by vapor deposition [3] toward low-cost, stable, and flexible CNT-Si solar cells.

Battery/capacitor electrodes are also an attractive target in which carbon black and carbon nanofibers have been used as conductive fillers. Small-diameter CNTs show unique self-supporting nature, and we are trying to replace heavy 2D metal foils with light-weight 3D CNT sponges for current collectors. We use long CNTs by fluidized bed [4] for CNT sponges. Electrodes of activated carbon particles captured in 10 wt% few-wall CNTs realized capacity ×3 of pure single-wall CNTs [5], and worked with metal contact on only their edge [6]. Electrodeposition of MnO<sub>2</sub> nanoparticles in CNT papers realized practically thick pseudocapacitive electrodes [7]. 1 wt% CNTs realized self-supporting LiCoO<sub>2</sub> cathodes and graphite anodes, which minimized the use of metal foils in lithium ion batteries (Fig. 2) [8]. CNT-sponge based S cathodes and Si anodes will also be presented.

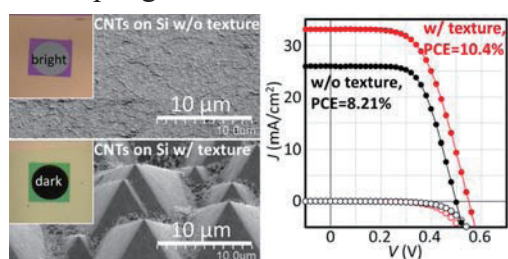


Fig. 1. CNT-Si solar cells [2].



Fig. 2. CNT-sponge-based lithium ion battery [8].

- [1] H. Shiraie, et al., Carbon 91, 20 (2015).
- [2] E. Muramoto, et al., RSC Adv. 6, 93575 (2016).
- [3] Y. Yamasaki, et al., CrystEngComm 18, 3404 (2016).
- [4] Z. Chen, et al., Carbon 80, 339 (2014).
- [5] R. Quintero, et al., RSC Adv. 5, 16101 (2015).
- [6] R. Quintero, et al., RSC Adv. 4, 8230 (2014).
- [7] M. Narubayashi, et al., RSC Adv. 6, 41496 (2016).
- [8] K. Hasegawa and S. Noda, J. Power Sources 321, 155 (2016).

Corresponding Author: S. Noda Tel&Fax: +81-3-5286-2769, E-mail: noda@waseda.jp

## Strong Light-Matter Coupling in (6,5) Carbon Nanotubes

Weilu Gao,<sup>1</sup> Kankan Cong,<sup>1</sup> Xinwei Li,<sup>1</sup> G. Timothy Noe II,<sup>1</sup> Huaping Liu,<sup>2</sup> Takeshi Tanaka,<sup>2</sup> Hiromichi Kataura,<sup>2</sup> and Junichiro Kono<sup>1</sup>

<sup>1</sup>*Department of Electrical and Computer Engineering, Rice University, Houston, TX, U.S.A.*

<sup>2</sup>*Nanomaterials Research Institute, National Institute of Advanced Industrial Science and Technology, Tsukuba, Ibaraki, Japan*

Strong resonant coupling between light and interband transitions in semiconductors leads to the formation of hybridized excitations, i.e., exciton-polaritons, which exhibit a rich variety of coherent many-body phenomena. In single-wall carbon nanotubes (SWCNTs), the large oscillator strength of excitons is expected to lead to extremely large light-matter coupling strengths. Moreover, the one-dimensional nature of excitons in SWCNTs provides a versatile platform for tunable light-matter coupling via polarization control.

Recent progress on large-scale separation of high-purity SWCNTs [1] and macroscopically aligned chirality-enriched SWCNT films [2] paves the way for such research. First, we studied a high-purity (6,5) SWCNT suspension, prepared through gel chromatography, utilizing pump-probe spectroscopy in free space. Upon resonant optical pumping with the  $E_{11}$  excitonic transition, within the laser pulse duration the  $E_{11}$  absorption peak splits into Rabi doublets; see Figs. 1(a)-1(c). Furthermore, a macroscopically aligned (6,5) film, prepared through vacuum filtration, was sandwiched between a pair of metals forming a Fabry-Perot microcavity. By adjusting the angle between the incident light polarization and the nanotube alignment direction, the Rabi splitting can be widely and continuously tuned from  $\sim 170$  meV (parallel, Fig. 1(d)) to zero (perpendicular, Fig. 1(e)), as shown in Fig. 1(f).

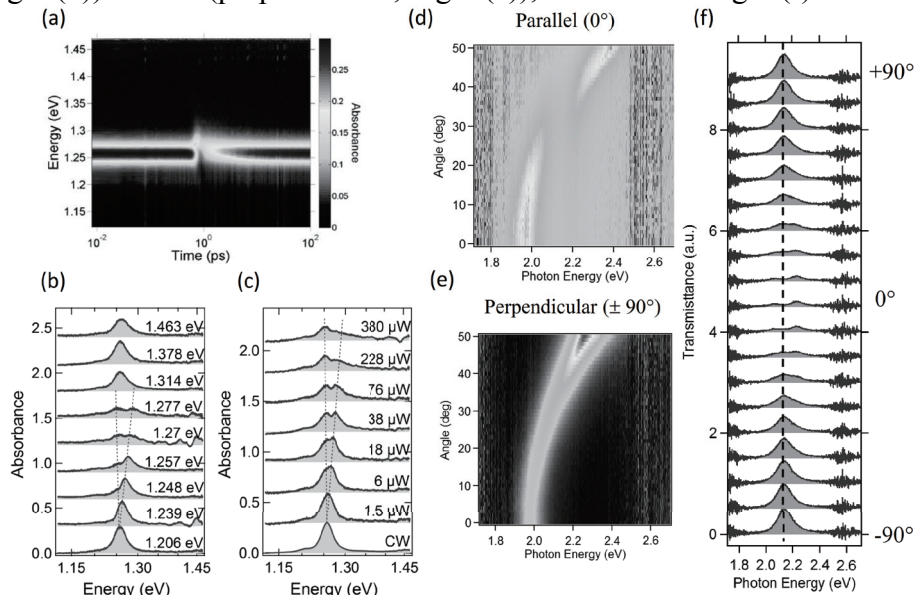


Fig.1 Strong light-matter coupling in (6,5) suspension (a)-(c) and macroscopically aligned film (d)-(f).

1. H. Liu, D. Nishide, T. Tanaka, and H. Kataura, *Nat. Comm.* **2**, 309 (2011)
2. X. He *et al.*, *Nat. Nanotechnol.* **11**, 633 (2016)

Corresponding Author: J. Kono

Tel: +1-713-348-2209, Fax: +1-713-348-3091

E-mail: [kono@rice.edu](mailto:kono@rice.edu)

## Optical Spectroscopy of Individual Carbon Nanotubes with Defined Atomic Structure

Kaihui Liu

*School of Physics, Peking University, Beijing 100871, China*

When the characteristic length of a material shrink to 1 nm scale, many distinct physical phenomena, such as quantum confinement, enhanced many-body interactions, strong van der Waals inter-material couplings and ultrafast charge separation, will appear. To investigate the related fascinating low-dimensional physics, we need a tool to quantitatively link the atomic structures to the physical properties of these very small nano-materials. In this talk, I will introduce our recently developed in-situ TEM + high-sensitive ultrafast nanooptics technique [1,2], which combines capability of structural characterization in TEM and property characterization in nanooptics on the same individual nano-materials. Several examples of using this technique to study the 1D carbon nanotube system will be demonstrated [3,4].

- [1] Kaihui Liu, Xuedong Bai\*, Enge Wang\*, and et al, “Chirality-Dependent Transport Properties of Double-Walled Nanotubes Measured in Situ on Their Field-Effect Transistors”, **J. Am. Chem. Soc.** 2009, 131, 62.
- [2] Kaihui Liu, Feng Wang\* and et al., “High-throughput Optical Imaging and Spectroscopy of Individual Carbon Nanotubes in Devices”, *Nature Nanotechnology* **2013**, 8, 917-922.
- [3] Kaihui Liu, Steven G. Louie, Enge Wang\*, Feng Wang\* and et al. “An atlas of carbon nanotube optical transitions”, *Nature Nanotechnology* **2012**, 7, 325-329.
- [4] Kaihui Liu, Enge Wang, Feng Wang\* and et al., “Van der Waals-Coupled Electronic States in Incommensurate Double-walled Carbon Nanotubes”, *Nature Physics* **2014**, 10, 737-742.

Corresponding Author: Kaihui Liu

Tel: +86-10-6276-6013,

E-mail: khliu@pku.edu.cn

## Localized growth of transition metal dichalcogenides on patterned graphene

Fei Lu<sup>1</sup>, Arka Karmakar<sup>1</sup>, Simran Shahi<sup>1</sup>, Erik Einarsson<sup>1,2</sup>

<sup>1</sup>Department of Electrical Engineering, University at Buffalo, Buffalo, NY USA

<sup>2</sup>Department of Materials Design and Innovation, University at Buffalo, Buffalo, NY USA

As we deepen our understanding of two-dimensional (2D) materials, there is an increasing shift in focus from individual materials to 2D heterostructures. The vastly different properties and atomically sharp interfaces give rise to unique properties [1]. The result depends on the combination of materials chosen, with graphene, hexagonal boron nitride, and transition metal dichalcogenides being the most common. Although various heterostructures have been studied and several devices demonstrated, they are almost always fabricated by picking and placing exfoliated materials. The ability to grow these materials in place is expected to considerably facilitate and accelerate this area of research.

Here we report the localized growth of transition metal dichalcogenides on patterned graphene using chemical vapor deposition (CVD). We initially grew graphene on copper foil using methane as a precursor.

After growth, we transferred the graphene onto a SiO<sub>2</sub>/Si wafer using a commercially available copolymer in addition to poly(methyl methacrylate) (PMMA) [2], and then patterned the graphene using conventional photolithography and oxygen plasma. We found that if we used the SiO<sub>2</sub>/Si wafer and patterned graphene as a substrate, MoS<sub>2</sub> growth is limited to the graphene areas. This was confirmed using Raman spectroscopy, with mapped areas shown in Fig. 1. When growing WS<sub>2</sub> instead of MoS<sub>2</sub>, the crystallinity is improved but the coverage is less, presumably due to poorly optimized growth conditions.

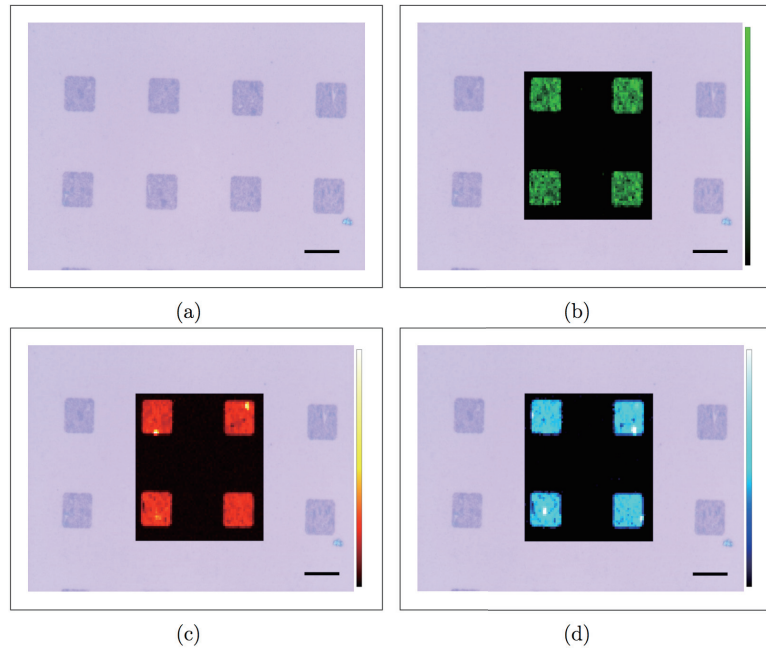


Fig. 1 (a) Optical micrograph of MoS<sub>2</sub> grown on patterned graphene. (b) Overlaid Raman map of MoS<sub>2</sub> peaks, integrating signal from 370 cm<sup>-1</sup> to 420 cm<sup>-1</sup>. (c) Overlaid Raman map of graphene G-peak and (d) 2D peak intensity. Scale bars are 20 μm.

[1] A.C. Ferrari, F. Bonaccorso, V. Fal'ko, K.S. Novosev *et al.*, *Nanoscale* **7** (2015) 4598.

[2] A. Karmakar, M.A. Philip, E. Einarsson, *Carbon* (under review).

Corresponding Author: E. Einarsson

Tel: +1-716-645-5089,

E-mail: erikeina@buffalo.edu

一般講演  
**General Lecture**

**1-1 ~ 1-7**

**2-1 ~ 2-14**

**3-1 ~ 3-11**

## Fabrication of multiple transistors from semiconducting single-walled carbon nanotube arrays after water-assisted burning of metallic tubes

○Keigo Otsuka<sup>1</sup>, Taiki Inoue<sup>1</sup>, Shohei Chiashi<sup>1</sup>, Shigeo Maruyama<sup>1,2</sup>

<sup>1</sup> Department of Mechanical Engineering, The University of Tokyo, Tokyo 113-8656, Japan

<sup>2</sup> Energy NanoEngineering Lab., National Institute of Advanced Industrial Science and Technology (AIST), 305-8564, Japan

Single-walled carbon nanotubes (SWNTs) have attracted attention as a material for high-performance field-effect transistor (FET) channels. Densely-packed arrays of aligned semiconducting (s-) SWNTs are an ideal structure for the application. Selective removal of metallic (m-) SWNTs after lattice-oriented growth on single-crystal substrates has been studied intensively to obtain this structure. We have been working on an extended method of electrical breakdown [1], by which m-SWNTs are selectively removed in much longer length with the assistance of polymer coating and water vapor [2]. However, one-way burning from initial breakdown position hindered full-length removal of m-SWNTs and thus reproducible fabrication of multiple FETs with high on/off ratio. Here, we report that reproducible full-length removal of m-SWNTs was achieved by re-burning from site-controlled nanogaps. In addition, multiple FETs was fabricated on the resultant long s-SWNT arrays, which showed advantages of this method over conventional electrical breakdown in fabrication of both short-channel FETs and scaled-up integrated devices at the same time.

Horizontally aligned SWNTs were grown on r-cut quartz substrates by the alcohol chemical vapor deposition method, and then were transferred on Si substrates with oxide layer (100 nm). Long-channel (~10 μm) FET structures were fabricated by patterning Au electrodes. As shown in Fig. 1a, nanogaps in m-SWNTs were created near the lower side of electrodes (white arrows) by the electrical breakdown method [1] using temporally placed intermediate electrodes. Broken m-SWNTs on the upper side were re-burned almost in full length by further voltage application with polymer coating and water vapor exposure [2,3] (Fig. 1b). Multiple FETs fabricated from the resultant s-SWNT arrays showed high on/off ratio (Fig. 1c,d), which indicates the possibility of highly integrated FET fabrication by this strategy.

[1] P. G. Collins *et al.*, *Science* **292**, 706 (2001).

[2] K. Otsuka *et al.*, The 49th FNTG general symposium, 3P-16 (2015)

[3] K. Otsuka *et al.*, *Nanoscale* **8**, 16363 (2016).

Corresponding Author: S. Maruyama

Tel: +81-3-5841-6421, Fax: +81-3-5841-6983,

E-mail: maruyama@photon.t.u-tokyo.ac.jp

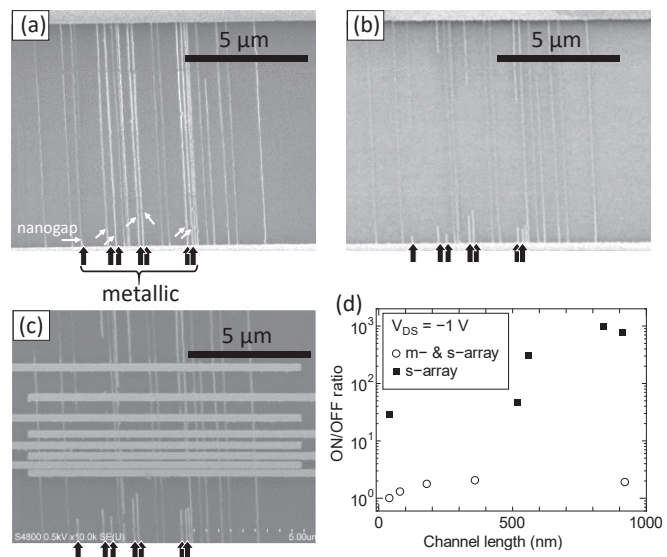


Fig.1 Fabrication procedures of multiple FETs after m-SWNT removal. Identical SWNT array (a) after gap formation, (b) after full-length removal of m-SWNTs, and (c) after the patterning of source and drain electrodes with small separation. (d) On/off ratio of FETs versus channel length.

## Asymmetric carrier accumulation in double-walled carbon nanotube under an electric field

○Taketo Kochi and Susumu Okada

*University of Tsukuba, 1-1-1 Tennodai, Tsukuba, Ibaraki, 305-8571 Japan*

Carbon nanotubes (CNTs) are attracting much attention because of their unique geometric and electronic structure. Due to such unique properties, CNTs act as a conductive channel of the field effect transistor (FET). In the FET, CNTs intrinsically form the hybrid structures with other CNT and foreign materials, which affect the carrier accumulation by the gate electric field. Indeed, our previous calculation showed that the distribution of the accumulated carrier in the CNT thin films strongly depends on the CNT and carrier species, leading to the unusual induced electric field between CNTs [1]. In this work, we aim to elucidate the carrier accumulation in double-walled CNT (DWCNTs) in FET structure by the external electric field, using the density functional theory combined with the effective screening medium method. In this work, we consider the  $(7,0)@(16,0)$  and  $(8,0)@(17,0)$  as the representative DWCNTs. As shown in Fig. 1, the distribution of accumulated carrier is sensitive to the carrier species. For the hole doping, injected hole is primary distributed on the outer CNT, while the carriers are absent on the inner CNT. In contrast, for the electron doping, the accumulated electron is distributed both on outer and inner CNTs, owing to their complex electronic structure around the energy gap.

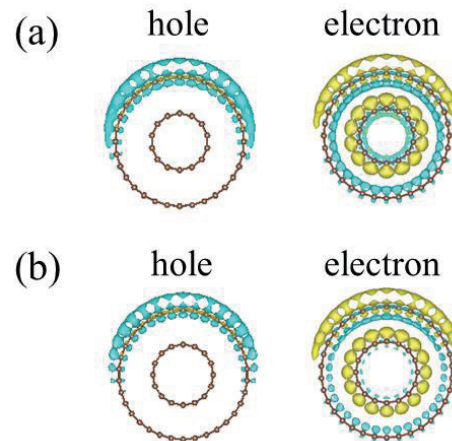


Fig. 1. Isosurfaces of the accumulated carriers in (a)  $(7,0)@(16,0)$  and (b)  $(8,0)@(17,0)$  nanotubes. In each panel, hole and electron denote the injection of holes and electrons, respectively. Yellow and blue isosurfaces indicate regions where electrons and holes increase, respectively, under the electric field.

[1]T. Kochi and S.Okada, Appl. Phys. Express **9**, 085103(2016).

Corresponding Author: T. Kochi

Tel: +81-29-853-5600(ext.; 8233) , E-mail: tkochi@comas.frsc.tsukuba.ac.jp

## Enhancement of Raman scattering from monolayer graphene by photonic crystal nanocavities

○I. Kimura<sup>1,2</sup>, M. Yoshida<sup>1,3</sup>, M. Sota<sup>4</sup>, H. Machiya<sup>1,2</sup>, T. Inoue<sup>4</sup>, S. Chiashi<sup>4</sup>, S. Maruyama<sup>4</sup>,  
Y. K. Kato<sup>1,3</sup>

<sup>1</sup> *Nanoscale Quantum Photonics Laboratory, RIKEN, Saitama 351-0198, Japan*

<sup>2</sup> *Department of Electrical Engineering, The University of Tokyo, Tokyo 113-8656, Japan*

<sup>3</sup> *Quantum Optoelectronics Research Team, RIKEN Center for Advanced Photonics, Saitama 351-0198, Japan*

<sup>4</sup> *Department of Mechanical Engineering, The University of Tokyo, Tokyo 113-8656, Japan*

Monolayer graphene is an atomically thin two-dimensional material that shows strong Raman scattering, while photonic crystal nanocavities with small mode volumes allow for efficient optical coupling at the nanoscale [1]. Here we demonstrate resonant enhancement of graphene Raman G' band by coupling to photonic crystal cavity modes. Hexagonal-lattice photonic crystal L3 cavities are fabricated from silicon-on-insulator substrates [2, 3], and monolayer graphene sheets grown by chemical vapor deposition are transferred onto the nanocavities. Excitation wavelength dependence of Raman spectra show that the Raman intensity is enhanced when the G' peak is in resonance with the cavity mode. By performing imaging measurements, we confirm that such an enhancement is only observed at the cavity position.

Work supported by JSPS KAKENHI Grant Numbers JP16K13613, JP25107002 and MEXT (Photon Frontier Network Program, Nanotechnology Platform).

[1] X. Gan, K. F. Mak, Y. Gao, Y. You, F. Hatami, J. Hone, T. F. Heinz, and D. Englund, *Nano Lett.* **12**, 5626 (2012).

[2] R. Watahiki, T. Shimada, P. Zhao, S. Chiashi, S. Iwamoto, Y. Arakawa, S. Maruyama, and Y. K. Kato, *Appl. Phys. Lett.* **101**, 141124 (2012).

[3] X. Liu, T. Shimada, R. Miura, S. Iwamoto, Y. Arakawa, and Y. K. Kato, *Phys. Rev. Applied* **3**, 014006 (2015).

Corresponding Author: Y. K. Kato

Tel: +81-48-462-1111 (ext. 3432)

E-mail: [yuichiro.kato@riken.jp](mailto:yuichiro.kato@riken.jp)

## Magnetic properties of two-dimensional hydrocarbon networks

○Jun-ya Sorimachi, Susumu Okada

*Graduate school of Pure and Applied Sciences, University of Tsukuba, Tsukuba  
305-8571, Japan*

Electronic and magnetic properties of hydrocarbon materials are sensitive to their  $\pi$  electron network. By assembling the appropriate hydrocarbon molecules as constituent units for two-dimensional covalent networks, we can tailor the electronic structure of the resultant network from a semiconductor to metal. For instance, the hexagonal network consisting of phenalenyl and phenyl, which are alternately arranged in hexagonal manner, has both Dirac cones and Kagome bands at and near the Fermi level, respectively, leading to the magnetic ordering which depends on the carrier concentration [1]. Although  $sp^3$  C atoms intrinsically terminate the  $\pi$  electron network of hydrocarbon materials, they allow us to design further variation of hydrocarbon covalent networks, of which electronic properties are absent in all  $sp^2$  C network materials. In the present work, we theoretically design the novel hydrocarbon covalent network comprising  $sp^2$  and  $sp^3$  C atoms as possible candidates for magnetic hydrocarbon materials with Kagome flat bands, using the density functional theory with generalized gradient approximation. As for the constituent blocks of the network, we consider the propellane and iptycene molecules consisting of  $sp^2$  and  $sp^3$  C atoms (Fig. 1). Because both molecules have  $C_3$  symmetry with respect to their molecular axis, they can form honeycomb networks containing  $sp^2$  and  $sp^3$  C atoms.

Our calculations show that these two-dimensional hydrocarbon network possess Kagome band at or near the Fermi level of which energy and width are sensitive to the network topology of  $sp^2$  C networks (polyacene structure) bridging  $sp^3$  atoms. The networks with propelanes exhibit spin polarization with various long-range ordering as their metastable spin configurations, owing to the partially filled Kagome flat band.

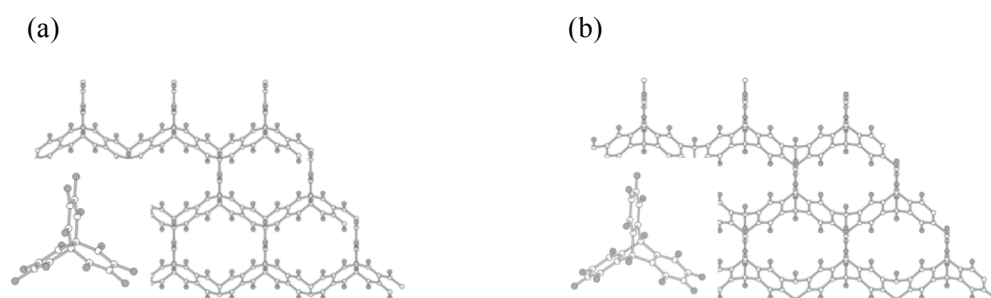


Fig. 1: Geometric structures of (a) propellane and (b) iptycene derived networks.

### Reference

[1] M. Maruyama, N. T. Cuong, S. Okada, *Carbon* **109**, 755 (2016).

Corresponding Author: J. Sorimachi

Tel: +81-29-853-5921,

E-mail: jsorimachi@comas.frsc.tsukuba.ac.jp

## Opening a Gap in Graphene Field Effect Devices with Periodic Uniaxial Strain

○Hikari Tomori<sup>1,2</sup>, Rineka Hiraide<sup>1</sup>, Youiti Ootuka<sup>1</sup>, Kenji Watanabe<sup>3</sup>, Takashi Taniguchi<sup>3</sup>, Akinobu Kanda<sup>1</sup>

<sup>1</sup>*Division of Physics and TIMS, University of Tsukuba, Tsukuba, 305-0006, Japan*

<sup>2</sup>*PRESTO-JST, Kawaguchi, 332-0012 Japan*

<sup>3</sup>*National Institute for Materials Science (NIMS), Tsukuba, 305-0047, Japan*

Due to high mobility, graphene is a promising candidate for electronic materials. However, for successful application of graphene to switching devices, gap formation is indispensable. In this study, we explore the gap formation in graphene based on strain engineering [1, 2].

For the periodic uniaxial strain, a band gap has been observed only in scanning tunnel spectroscopy, while it has not been confirmed in actual field effect devices [3]. This missing gap is presumably due to the relaxation of strain in device fabrication processes. Here, we develop a novel device fabrication method which makes graphene largely strained even after the formation of electrical contacts. In this method, a graphene film is placed on a periodic array of resist HSQ bars. The introduction of strain was confirmed with micro-Raman spectroscopy. The back gate voltage dependence of the conductance in the strained graphene exhibited remarkable difference from the conventional V-shaped curve observed in graphene placed on SiO<sub>2</sub>. The minimum conductance showed thermal activation behavior at high temperatures (> 100 K). From the Arrhenius plot, the band gap was estimated to be 2.4 meV (Fig. 1). Besides, the current-voltage characteristics became nonlinear around the origin. The high resistance region extended within +/- 2 meV at the gate voltage corresponding to the minimum conductance. This value agreed well with the band gap estimated from the temperature dependence. These observations confirm the formation of the band gap in our strained graphene. We expect that optimization of the device structure extends the gap and improves device performance.

[1] F. Guinea et al, Nat. Phys. **6**, 30 (2010)

[2] V.M. Pereira and A. H. Neto, Phys. Rev. Lett. **103**, 046801 (2009).

[3] J. K. Lee et al., Nano Lett. **13**, 3494 (2013).

Corresponding Author: H. Tomori

Tel: +81-29-853-4345,

Fax: +81-29-853-4345,

E-mail: tomori@lt.px.tsukuba.ac.jp

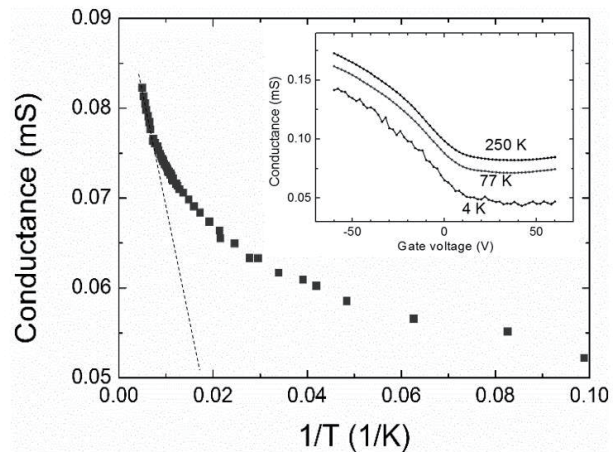


Fig.1 Arrhenius plot of minimum conductance. (insert) Gate voltage dependence of conductance at 250 K, 77 K and 4K.

## Gas Adsorption Effects on Stabilities and Electronic Properties of Graphene Bilayers

○Yoshitaka Fujimoto<sup>1</sup> and Susumu Saito<sup>1,2,3</sup>

<sup>1</sup>*Department of Physics, Tokyo Institute of Technology, Tokyo 152-8551, Japan*

<sup>2</sup>*International Research Center for Nanoscience and Quantum Physics, Tokyo Institute of Technology, Tokyo 152-8551, Japan*

<sup>3</sup>*Materials Research Center for Element Strategy, Tokyo Institute of Technology, Kanagawa 226-8503, Japan*

Ever since the successful exfoliation of graphene from multilayer graphite, graphene has received much interest from the viewpoints of fundamental physics and relevant applications in nanoelectronics because it shows various unique properties. Specifically, due to its extremely high carrier mobility, graphene still is a potential device material for next-generation nanoelectronics.

One of the effective ways to control the electronic properties of graphene is to dope with heteroatoms. Furthermore, substitutionally doped graphene can often enhance its chemical reactivity. Thus, doped graphene is also a good candidate for promising sensor applications because of the high carrier mobility as well as the high sensitivity.

In this talk, we report polluting or toxic gas adsorption effects on the stabilities and the electronic properties of graphene bilayers doped with boron and nitrogen atoms based on our first principles density functional study [1, 2]. We show that NO and NO<sub>2</sub> molecules can bind on B-doped bilayer graphene with chemical bonds. Furthermore, we also show that the adsorptions of NO and NO<sub>2</sub> molecules on the B-doped bilayer graphene can lead to charge transfers between gas molecules and graphene layers (Fig. 1). We also discuss the possibilities for these doped graphene layers to be applied to gas sensors.

[1] Y. Fujimoto and S. Saito, *Surf. Sci.* **634** (2015) 57.

[2] Y. Fujimoto and S. Saito, *Chem. Phys.* **478** (2016) 55.

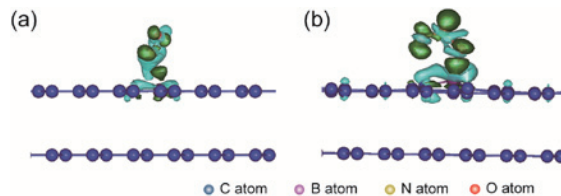


Fig. 1 Side views of charge transfers between B-doped bilayer graphene and gas molecules: (a) NO and (b) NO<sub>2</sub> molecules (Ref. [2]).

Corresponding Author: Yoshitaka Fujimoto

TEL: +81-3-5734-2368, FAX: +81-3-5734-2368, E-mail: [fujimoto@stat.phys.titech.ac.jp](mailto:fujimoto@stat.phys.titech.ac.jp)

## Edge Roughness Analysis for Developing GNR-based FET

○Kengo Takashima<sup>1</sup>, Takahiro Yamamoto<sup>1,2</sup>

<sup>1</sup> Department of Engineering, Tokyo University of Science, Tokyo 125-8585, Japan

<sup>2</sup> Department of Liberal Arts, Tokyo University of Science, Tokyo 125-8585, Japan

Graphene is expected to be a channel material of field effect transistors (FETs) because of its high carrier mobility. However, no band gap of the graphene is a serious problem for its FET application. One possible way to overcome the gap-opening problem is to process it in the form of a nanometer width ribbon, referred as graphene nanoribbons (GNRs). They have been successfully applied to FETs with high on-off ratio. We recently reported that resistance of GNR increase dramatically with edge disorder[1][2]. However, the edge roughness effect on the GNR-FET properties have not been clarified yet.

In this study, we have investigated the coherent electronic transport in edge-disordered armchair GNR FETs (ED-AGNR-FETs) using the nonequilibrium Green's function method combined with a tight-binding model[3]. In our simulation model, the edge vacancy is modeled by adding or removing pairs of carbon atoms at the edges (Fig. 1). We calculated drain current( $I_d$ ) versus gate voltage( $V_g$ ) characters of ED-AGNR-FETs by changing the roughness concentration  $P$  from 0% to 30% and the ribbon-width from 2.21nm (Fig. 2). We confirmed that a variance of on current( $\Delta I_{on}$ ) is independent of  $I_{on}$  and  $\Delta I_{on}$  is constant (universal conductance fluctuation), where  $P$  is under 10 %. On the other hand, when  $P$  exceed 10 %,  $\Delta I_{on}$  and variance of subthreshold become large drastically. This result provides a guideline for developing GNR-based FETs.

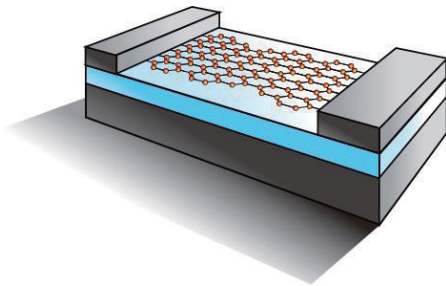


Fig. 1 Edge-disordered AGNR-FET

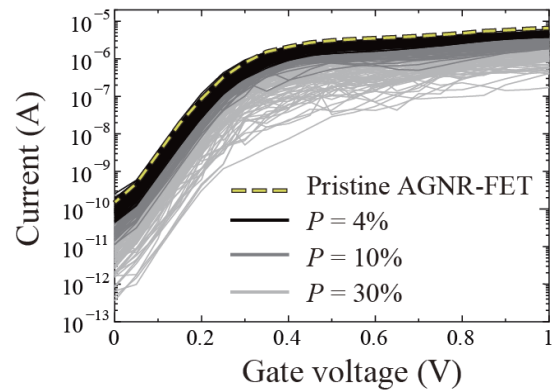


Fig. 2  $I_d$ - $V_g$  curves of edge-disordered AGNR-FETs

### References:

- [1] K. Takashima and T. Yamamoto, APL., **104**, 093105 (2014).
- [2] K. Takashima, S. Konabe and T. Yamamoto, JAP., **119**, 024301 (2016).
- [3] P. Koskinen and V. Mäkinen, Computational Materials Science, **47**, 237 (2009)

**Corresponding Author: T. Yamamoto**

E-mail: [takahiro@rs.tus.ac.jp](mailto:takahiro@rs.tus.ac.jp)

## **Drastically improved efficiency of single wall carbon nanotube forest synthesis on a MgO catalyst underlayer by a simple annealing process**

○Takashi Tsuji, Kenji Hata, Don N. Futaba, Shunsuke Sakurai

*CNT-Application Research Center, National Institute of Advanced Industrial Science and Technology (AIST), Tsukuba, Ibaraki 305-8565, Japan*

One of the important factors to synthesize single wall carbon nanotube (SWCNT) forest is the catalyst underlayer to support catalyst nanoparticle array. Up to date, alumina is the only choice to grow millimeter-scale SWCNT forest and reports on the use of other catalyst underlayer such as silica ( $\text{SiO}_2$ ), magnesia ( $\text{MgO}$ ) and zirconia ( $\text{ZrO}_2$ ) have shown difficulty in achieving high efficiency (e.g.  $> 100 \mu\text{m}$ ). This difficulty comes from the instability of iron (Fe) catalyst on these catalyst underlayers. For example, as we reported in the 50th FNTG conference [1], growth lifetime of CNTs from Fe catalyst supported on a sputtered MgO layer was much shorter than sputtered  $\text{Al}_2\text{O}_3$  layer, which was due to strong subsurface diffusion of Fe catalyst into the underlayer.

We recently demonstrated the drastic increase in the efficiency of SWCNT forest synthesis on a sputtered MgO catalyst underlayer by a simple pretreatment process. By annealing the as-sputtered MgO layer in the air ( $750^\circ\text{C}$ , 20 min) before the deposition of Fe catalyst layer, the height of CNT forest synthesized by water assisted chemical vapor deposition (10 min) increased about 5000% from 0.02 mm to 1.2 mm [2]. High percentage of SWCNTs in the forest (95%) was verified by transmission electron microscopy (TEM) observation. Furthermore, the growth lifetime of the SWCNT forest characterized by the *in-situ* height measurement was on par with those grown on  $\text{Al}_2\text{O}_3$ . Such high growth efficiency can be explained by the improved nanoparticle stability. Analyses by X-ray diffraction, X-ray photoelectron spectroscopy, and atomic force microscopy suggest that the underlayer treatment increased crystallinity of the MgO underlayer, that suppressed Fe subsurface diffusion into underlayer and retained the Fe metallic state. In this presentation, the effect of the annealing treatment temperature on the yield and structures (diameter, wall number) of CNT forest is also discussed. This presentation is based on results obtained from a project commissioned by the New Energy and Industrial Technology Development Organization (NEDO).

[1] T. Tsuji *et al.* Abstracts of the 50th Fullerene-Nanotubes-Graphene General Symposium (2015).

[2] T. Tsuji *et al.* *J. Am. Chem. Soc.* **138**, 16608 (2016).

Corresponding Author: S. Sakurai

Tel: +81-29-861-4654, Fax: +81-29-861-4851,

E-mail: shunsuke-sakurai@aist.go.jp

## A study of dispersion states of CNTs in slurry by AC impedance method

○Takayuki Watanabe<sup>1</sup>, Kazufumi Kobashi<sup>1,2</sup>, Takahiro Morimoto<sup>1,2</sup>, Toshiya Okazaki<sup>1,2</sup>

<sup>1</sup> *Technology Research Association for Single Wall Carbon Nanotubes (TASC), Tsukuba, 305-8565, Japan*

<sup>2</sup> *CNT Application Research Center, National Institute of Advanced Industrial Science and Technology (AIST), Tsukuba, 305-8565, Japan*

We report CNT-type and density dependences of the electrical properties of the surfactant-free CNT-dispersed organic solvents. CNT slurry/paste without surfactant is one of the measure forms in industrial application because it's easy to handle compared to the powder form. However, only few studies have been reported about the states of CNTs in the produced slurries despite of its industrial importance. To develop the effective evaluation method, AC impedance behaviors of several CNT slurries are systematically investigated.

Figure 1(a) shows CNT weight density dependence of conductivity of the CNT slurries measured by conventional impedance measurement setup (Fig. 1(b)). The CNT types we used here are super-growth-, e-DIPS- and VGCF-CNTs. They showed significant conductivity increases above threshold values of CNT weight density, which is well known as percolation behavior. All three slurries showed different threshold values and slope magnitude. These values seem to be affected by each type of CNTs, but they don't simply depend on individual CNT property, for example, the length. This is probably because property of CNT slurry strongly depends not only on isolated CNT properties, but also on degree of aggregation, distribution of particle sizes and so on. The relationship between the dispersion states of CNTs in each slurry and the AC impedance behaviors will be discussed in detail.

This study is based on results obtained from a project commissioned by the New Energy and Industrial Technology Development Organization (NEDO)

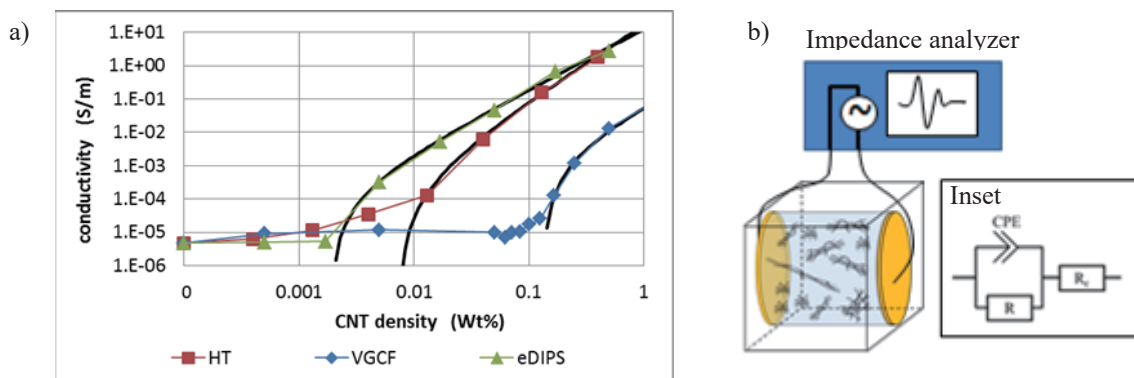


Fig.1 a) CNT weight density dependence of CNT slurry conductivity. b) Schematic image of measurement setup. An expected equivalent circuit model of CNT slurry is shown in the inset.

Corresponding Author: Toshiya Okazaki

E-mail: toshi.okazaki@aist.go.jp

## The effect of noble metals on the formation of iron catalyst nanoparticle for the synthesis of vertically-aligned carbon nanotubes

○Shunsuke Sakurai, Kenji Hata, Don N. Futaba

*CNT-Application Research Center, National Institute of Advanced Industrial Science and Technology (AIST), Tsukuba, Ibaraki 305-8565, Japan*

A highly dense assembly of metal iron nanoparticle formed on the substrate is frequently utilized as the catalyst for the synthesis of carbon nanotubes (CNTs) forest (i.e. vertically aligned CNTs) using chemical vapor deposition (CVD) method [1]. Commonly, such an assembly of catalyst nanoparticle is prepared by annealing the thin film of iron compounds in the reductive ambient (e.g. hydrogen) [2]. The importance of annealing in hydrogen is also demonstrated by the wide range modulation of single-walled CNT diameter in the forest by the parametric change in the annealing conditions [3].

Although the importance of reductive gases are widely recognized, we further investigated the preparation method of catalyst nanoparticle assembly, since most of the reductive gases are explosive and/or toxic. Here, we demonstrated that even without any reductive gases, the synthesis of CNT forest can be enabled by adding noble metals (such as iridium and ruthenium) into the iron catalyst film. First, aqueous solutions including iron chloride, citrate acid, polymer agents, and chloride of noble metals are coated on the alumina layer sputtered on silicon wafer to prepare catalyst substrates. Next, obtained substrates are annealed in helium ambient (750 °C, 6 min), and then acetylene is introduced in the furnace with addition of water vapor for 10 min. Although the height of CNT forest is shorter than 10 μm when only iron chloride is used, forests taller than 300 μm were successfully synthesized by adding iridium and ruthenium chlorides. The formation of catalyst nanoparticle by annealing in helium is suggested by the atomic force microscopy (AFM) images (Figure 1). The mechanism for the formation of catalyst nanoparticle without reductive gases triggered by noble metals are also discussed in the presentation.

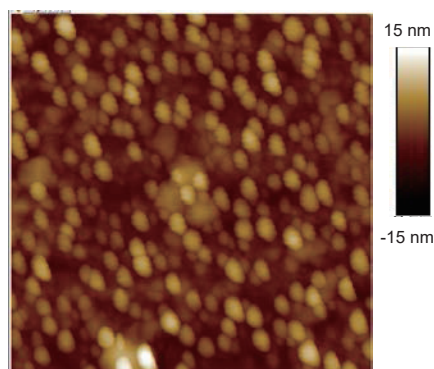


Figure 1. AFM image of catalyst particle obtained after annealing iron/iridium film in helium ambient (500 nm × 500 nm).

[1] K. Hata, D. N. Futaba, K. Mizuno, T. Namai, M. Yumura, S. Iijima *Science* **306**, 1362 (2004).

[2] S. Sakurai, H. Nishino, D. N. Futaba, S. Yasuda, T. Yamada, A. Maigne, Y. Matsuo, E. Nakamura, M. Yumura, and K. Hata *J. Am. Chem. Soc.* **134**, 2148 (2012).

[3] S. Sakurai, M. Inaguma, D. N. Futaba, M. Yumura, K. Hata *Small* **9**(21), 3584 (2013).

Corresponding Author: S. Sakurai

Tel: +81-29-861-6205, Fax: +81-29-861-4851,

E-mail: shunsuke-sakurai@aist.go.jp

## Lock-in thermography technique for visualization of CNT network structures

<sup>o</sup>Takahiro Morimoto<sup>1,2</sup>, Seisuke Ata<sup>1,2</sup>, Takeo Yamada<sup>1,2</sup> and Toshiya Okazaki<sup>1,2</sup>  
<sup>1</sup>*CNT-Application Research Center, National Institute of Advanced Industrial Science and  
 Technology, Tsukuba 305-8565, Japan*

<sup>2</sup>Technology Research Association for Single Wall Carbon Nanotubes (TASC), Japan

The randomly networked carbon nanotubes are important structures for various functional materials and devices. The bulk properties of these materials are understood by formalization of the percolation theory. In this theory, however, it is difficult to accurately expect the bulk properties depending on various experimental conditions. For more efficient material and device developments, the analysis method for the inside structures is strongly demanded as real space and short time measurement method.

In this time, we will present the new analysis method for these randomly networked systems. In many cases, the CNTs added to base materials are connected to each other inside materials. These network structures contribute to improve the electrical, thermal and physical properties of bulk properties. In the case of CNTs, these randomly network structures have conductivity after percolation threshold concentrations.

Figure.1 shows the schematic images of suggested method. The ac bias voltages (< 100 Hz) are applied to the materials contained CNTs. In that time, the infrared is radiated from the sample surface including both Joule heating and background heat storage. For the separation of these components, the lock-in technique is applied for thermal images.

Figure.2 shows the effect of the lock-in process at same sample and same conditions. In the conventional method (integrated thermal image), the detail structures are completely smeared out by the background heat storage of the base materials as shown in Fig.2 (a). In the case of lock-in thermal image, on the other hand, the current paths on the conductive network structures are clearly visualized depending on the local resistance and current distributions as shown in Fig. 2 (b). In the presentation, we will show the results on various materials and processes. We will also discuss the mechanism of heating structures related to bulk properties.

This paper is based on results obtained from a project commissioned by NEDO.

[1] T. Morimoto *et al.*, in preparation.

Corresponding Author: Takahiro Morimoto

Tel: +81-29-861-3804, Fax: +81-29-861-6241,

E-mail: t-morimoto@aist.go.jp

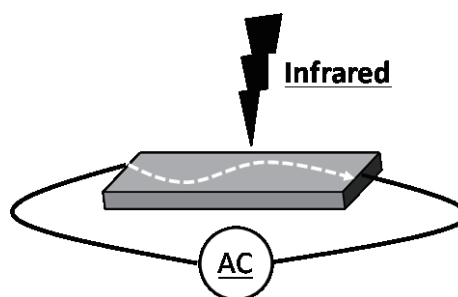


Fig.1 The schematic image of lock-in thermography.

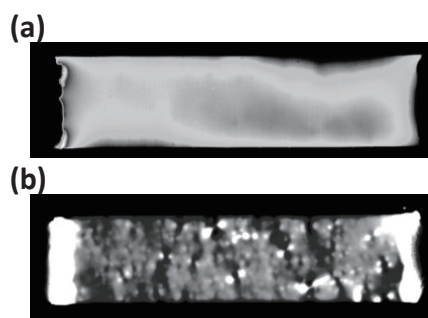


Fig.2 (a) non-lock-in image. (b) lock-in image.

## Scanning Electrochemical Cell Microscopy for Visualization of Local Electrochemical Activities on Graphene/Graphite

○Akichika Kumatani <sup>1</sup>, Chiho Miura <sup>1</sup>, Takeru Okada <sup>2</sup>, Seiji Samukawa <sup>2,3</sup>, Hitoshi Shiku <sup>1</sup>, Yasufumi Takahashi <sup>4,5</sup> Tomokazu Matsue <sup>1,3</sup>

<sup>1</sup> Tohoku University, Sendai 980-8579, Japan

<sup>2</sup> Institute of Fluid Science, Tohoku University, Sendai 980-8577, Japan

<sup>3</sup> Advanced Institute for Materials Research, Tohoku University, Sendai 980-8577, Japan

<sup>4</sup> Kanazawa University, Kanazawa 920-1192, Japan

<sup>5</sup> JST PRESTO, Saitama 332-0012, Japan

Towards the establishment of low-carbon emission society, one urgent issue is to standardize a highly efficient electrochemical device to store unused energy for secondary batteries or to generate hydrogen evolution for energy source of fuel cells. Two-dimensional layered materials such as graphene have shown great performance for those applications. It is already known that a careful control of their edge structures, defects or functionalization on the surface are a key to enhance their performance. In general, their unique properties are evaluated by indirect methods such as electrochemical analysis in bulk or probing techniques for electronic conductivities. It is therefore necessary to develop an electrochemical analytical technique in nanometer for classification of the factors at the desired location.

In this study, we introduce a scanning electrochemical cell microscopy with a single-barrel nanopipette filled with electrolyte and a reference electrode (nanoSECCM) in Fig. 1 (a) for direct visualization of local electrochemical activities under sub-micrometer scale [1]. 5 mM hexaammineruthenium chloride and 25 mM KCl in phosphate buffer or deionized water was prepared for an electrolyte. Then, the electrolyte was filled in nano-pipettes (100 nm or 1 μm in a diameter) with Ag/AgCl reference electrode for inducing redox reaction of ruthenium ion on the sample surface. The nanoSECCM was applied to graphite or cleaved graphene on silicon substrates. Once the pipette was in proximity of the sample surface, a meniscus was created as an electrochemical cell. Through the cell, local electrochemical activities was analyzed at a confined area. Also, by scanning the pipette on the sample surface, both electrochemical activities and topography simultaneously were obtained as shown in Fig 1 (b). Consequently, high activities at the edges of graphene/graphite were visualized.

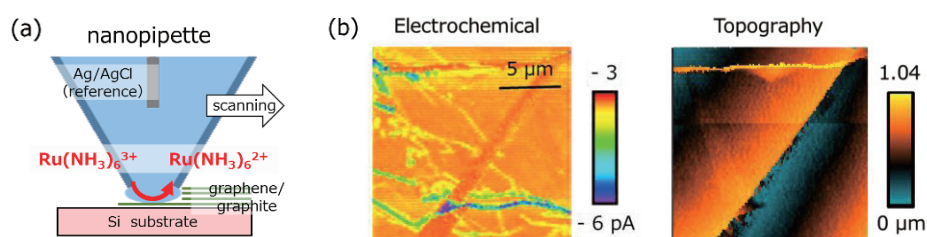


Fig.1 (a) a schematic of nanoSECCM, (b) nanoSECCM images of graphite/graphene surface on the substrate: Left electrochemical activities and topography.

[1] Y. Takahashi, A. Kumatani *et al.* Nat. Comm. **5**:6450 (2014).

Corresponding Author: Akichika Kumatani, Tomokazu Matsue

Tel: +81-22-795-7281, Fax: +81-22-795-6167,

E-mail: kumatani@bioinfo.che.tohoku.ac.jp, matsue@bioinfo.che.tohoku.ac.jp

## Out-of-Plane Strain Generation of Monolayer MoS<sub>2</sub> and MoSe<sub>2</sub> Formed a Moiré Superstructure on the Au(111) Surface

R. Takahashi<sup>1</sup>, R. Osaka<sup>1</sup>, Y. Miyata<sup>2</sup>, S. Okada<sup>3</sup>, Y. Hayamizu<sup>4</sup>,  
○S. Yasuda<sup>1</sup>, K. Murakoshi<sup>1</sup>

<sup>1</sup>Department of Chemistry, Hokkaido University, Sapporo, 060-0810, Japan

<sup>2</sup>Department of Physics, Tokyo Metropolitan University, Hachioji, 192-0397, Japan

<sup>3</sup>Graduate School of Pure and Applied Science, University of Tsukuba, Tsukuba, Ibaraki 305-8571, Japan

<sup>4</sup>Department of Organic and Polymeric Materials, Tokyo Institute of Technology, Ookayama, 152-8552, Japan

Contact of transition metal dichalcogenides (TMDCs) with a metal surface is essential for fabricating and designing electronic devices. It generates strain in the TMDCs and consequently may affect phonons and electrons in the TMDCs. Therefore detailed understanding of the mechanism of the strain generation is important for fully comprehend the phonon and electronic modulation effects. In this study, we grow MoS<sub>2</sub> and MoSe<sub>2</sub> monolayers on Au surface by chemical vapor deposition and investigated the influence of the metal contact upon the structure and electronic properties. Raman spectroscopy revealed that the contact with a crystalline Au(111) surface gives rise to only out-of-plane strain in both MoS<sub>2</sub> and MoSe<sub>2</sub> layers, whereas no strain generation is observed on polycrystalline Au or SiO<sub>2</sub>/Si surfaces. STM analysis provided information regarding consequent specific adsorption sites between lower S (Se) atoms in the S-Mo-S (Se-Mo-Se) structure and Au atoms via unique moiré superstructure formation for MoS<sub>2</sub> and MoSe<sub>2</sub> layers on Au(111) (Fig. 1). This observation indicates that the adsorption sites of the Au(111) surface strongly interact with lower S (Se) atoms in MoS<sub>2</sub> or MoSe<sub>2</sub> layers, giving rise to local out-of-plane strain in the layers. The finding would serve as complementary information for profound understanding of the modulation effect of phonons and electronic structure by TMDC-metal contact.

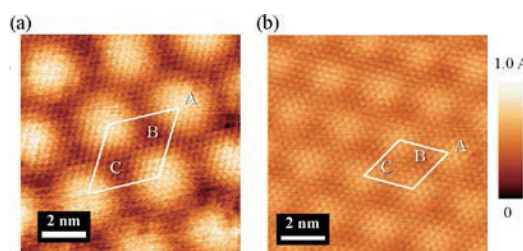


Fig. 1 STM images of (a) MoS<sub>2</sub>/Au(111) ( $V_s = +0.2$  V and  $I_t = 1$  nA) and (b) MoSe<sub>2</sub>/Au(111) ( $V_s = +0.3$  V and  $I_t = 1$  nA).

Corresponding Author: S. Yasuda

TEL & FAX: +81-(0)11-706-4811

E-mail: satoshi-yasuda@sci.hokudai.ac.jp

## Magnetic tunnel junction built from intercalated transition metal dichalcogenide ferromagnets with different magnetic anisotropy

○Yuji Yamasaki<sup>1</sup>, Rai Moriya<sup>1</sup>, Miho Arai<sup>1</sup>, Satoru Masubuchi<sup>1</sup>, Sunseng Pyon<sup>2</sup>,  
Tsuyoshi Tamegai<sup>2</sup>, Keiji Ueno<sup>3</sup>, and Tomoki Machida<sup>1,4</sup>

<sup>1</sup> *Institute of Industrial Science, The University of Tokyo, Tokyo 153-8505, Japan*

<sup>2</sup> *Department of Applied Physics, The University of Tokyo, Tokyo 113-8656, Japan*

<sup>3</sup> *Department of Chemistry, Saitama University, Saitama 338-8570, Japan*

<sup>4</sup> *CREST-JST, Saitama 332-0012, Japan*

Ferromagnetic two-dimensional (2D) materials have received considerable attention for constructing spintronic devices with all-2D-material heterostructures. Previously, we revealed mechanical exfoliation of the Fe-intercalated 2H-TaS<sub>2</sub>, Fe<sub>1/4</sub>TaS<sub>2</sub>, and construction of magnetic tunnel junction from two different flakes of Fe<sub>1/4</sub>TaS<sub>2</sub> [1]. So far Fe<sub>x</sub>TaS<sub>2</sub> is the only material that is experimentally verified as an exfoliatable metallic ferromagnet. Demonstration of other exfoliatable ferromagnets is in demand. Here, we investigate mechanical exfoliation of other intercalated transition metal dichalcogenide Cr<sub>1/3</sub>TaS<sub>2</sub>. Anisotropic magnetoresistance measurement reveals that exfoliated Cr<sub>1/3</sub>TaS<sub>2</sub> exhibits ferromagnetic ordering below ~110 K and its easy axis is along in-plane direction, in contrast to Fe<sub>1/4</sub>TaS<sub>2</sub> whose easy axis is along out-of-plane.

Further, we constructed heterojunction between Cr<sub>1/3</sub>TaS<sub>2</sub> and Fe<sub>1/4</sub>TaS<sub>2</sub> by using exfoliation and dry transfer method (Figs. 1 and 2). Due to the native oxidation of intercalated materials, Ta<sub>2</sub>O<sub>5</sub> tunnel barrier is formed at the heterojunction; thus device exhibits Fe<sub>1/4</sub>TaS<sub>2</sub>/Ta<sub>2</sub>O<sub>5</sub>/Cr<sub>1/3</sub>TaS<sub>2</sub> structure. The fabricated junction showed clear signature of tunnel magnetoresistance (TMR) effect (Fig. 3) [2]. We obtained maximum TMR ratio of 13% in Fe<sub>1/4</sub>TaS<sub>2</sub>/Ta<sub>2</sub>O<sub>5</sub>/Cr<sub>1/3</sub>TaS<sub>2</sub> junction and this value was significantly higher than the previous report on Fe<sub>1/4</sub>TaS<sub>2</sub>/Ta<sub>2</sub>O<sub>5</sub>/Fe<sub>1/4</sub>TaS<sub>2</sub> [1]; revealing larger tunnel spin polarization by using Cr<sub>1/3</sub>TaS<sub>2</sub>. These findings demonstrate possibilities to use magnetic atom intercalated transition metal dichalcogenide materials in the field of 2D material spintronics.

[1] M. Arai *et al.* Appl. Phys. Lett. **107**, 103107 (2015). [2] Y. Yamasaki *et al.* (submitted).

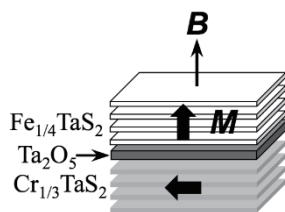


Fig.1 An illustration of Fe<sub>1/4</sub>TaS<sub>2</sub>/Cr<sub>1/3</sub>TaS<sub>2</sub> junction. Magnetization easy axis directions are indicated by arrows.

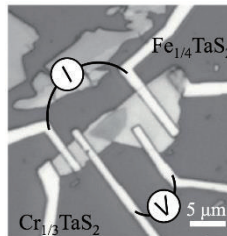


Fig.2 A micrograph of the device.

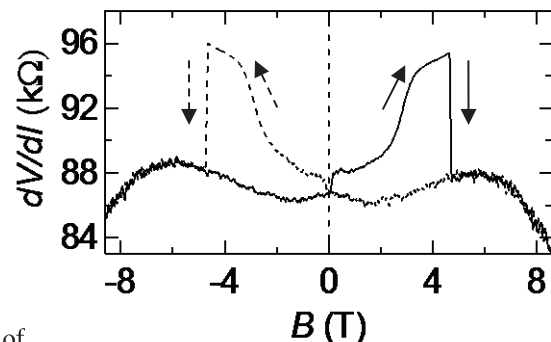


Fig.3 Magnetoresistance data obtained from Fe<sub>1/4</sub>TaS<sub>2</sub>/Cr<sub>1/3</sub>TaS<sub>2</sub> junction at 8 K.

Corresponding Author: Y. Yamasaki

Tel: +81-3-5452-6158, Fax: +81-3-5452-6157, E-mail:yu-yama@iis.u-tokyo.ac.jp

## Improvement of Open-circuit Voltage in Perovskite Solar Cells by Using Methano-Indene-Fullerene (MIF)

○Yutaka Matsuo<sup>1,2,3</sup>

<sup>1</sup>Hefei National Laboratory for Physical Sciences at the Microscale, University of Science and Technology of China, Hefei, Anhui 230026, China

<sup>2</sup>Department of Mechanical Engineering, School of Engineering, The University of Tokyo, Bunkyo-ku, Tokyo 113-8656, Japan

<sup>3</sup>Department of Chemistry, Northeast Normal University, Changchun, Jilin 130024, China

Methano-indene-fullerene (MIF,  $C_{60}(CH_2)Ind$ ) has been used in polymer/fullerene organic solar cells<sup>[1]</sup> and small-molecule organic solar cells<sup>[2]</sup> to have high open-circuit voltage ( $V_{OC}$ ). Methano and indeno addends reduces the  $\pi$ -conjugation of fullerene for a higher lying LUMO level, giving high  $V_{OC}$  values  $>1.0$  V without any significant loss in short-circuit current density ( $J_{SC}$ ) and fill factor (FF) due to the small volume of the indeno group that can provide short fullerene–fullerene contact distance for high electron mobility.

In this presentation, we will discuss the use of MIF in the inverted planar NiO-diethanolamine/ $CH_3NH_3PbI_3$ /fullerene p–i–n solar cells.<sup>[3]</sup> Compared the using PCBM,  $V_{OC}$  increased to 1.13 V because of the energy loss at the interface between perovskite and fullerene layers.

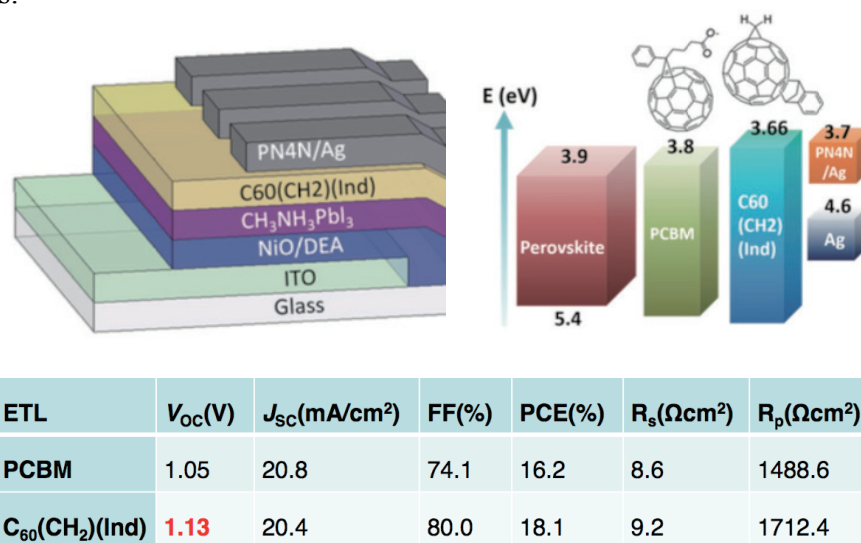


**Figure.** Device structure, energy diagram, and device performance of perovskite solar cells using methano-indene-fullerene.

### References

[1] Y. Matsuo, J. Kawai, H. Inada, T. Nakagawa, H. Ota, S. Otsubo, E. Nakamura, *Adv. Mater.* **2013**, *25*, 6266–6269.

[2] J. W. Ryan, Y. Matsuo, *Sci. Rep.* **2015**, *5*, 8319.

[1] Q. Xue, Y. Bai, M. Liu, R. Xia, Z. Hu, Z. Chen, X.-F. Jiang, F. Huang, S. Yang, Y. Matsuo, H.-L. Yip, Y. Cao, *Adv. Energy Mater.* **2017**, 1602333

Corresponding Author: Y. Matsuo

Tel: +81-3-5841-0978, E-mail: matsuo@ustc.edu.cn; matsuo@photon.t.u-tokyo.ac.jp

## Electronic Structures and Stability of Metal Encapsulated C<sub>80</sub> fullerenes: Ab initio DFT study

○Archana Velloth<sup>1</sup>, Yutaka Imamura<sup>1</sup>, Takeshi Kodama<sup>1</sup>, Masahiko Hada<sup>1</sup>

<sup>1</sup> Department of Chemistry, Tokyo Metropolitan University, Hachioji-shi 192-0397, Japan

Endohedral metallofullerenes are novel derivatives of fullerenes which find potential applications ranging from nanomemory devices to biomedical field.<sup>[1]</sup> Here, an extensive study of the structural and electronic properties on a series of neutral and anionic species of endohedral dimetallofullerenes<sup>[2]</sup> (di-EMFs) based on DFT and ab-initio computational calculations has been performed. Initially, we considered different configurations of M<sub>2</sub>@C<sub>80</sub> (M= Sc, Y, La, Gd and Lu) followed by examining the ground state of these di-EMFs. In the studied di-EMFs, except La<sub>2</sub>@C<sub>80</sub>, all other di-EMFs prefer to exist in the higher spin state as a ground state. The di-EMFs with a higher spin ground state were found to be kinetically unstable due to the unpaired spin distribution over the C<sub>80</sub> cage. Recently, the isolation of anion species of Y<sub>2</sub>@C<sub>80</sub><sup>[3]</sup> and Gd<sub>2</sub>@C<sub>80</sub><sup>[4]</sup> were reported. In order to find more stable species, further we analysed the anions of these di-EMFs. Then, we were able to find that the confinement of the unpaired electron inside the carbon cage enhanced the stability of anions of di-EMFs. Additionally, to gain more insight to the excited state, we have also investigated absorption spectra for the [M<sub>2</sub>@C<sub>80</sub>]<sup>-</sup> using time-dependent density functional theory (TDDFT) method. Finally, we have also examined a series of M<sub>1</sub>M<sub>2</sub>@C<sub>80</sub> hetero-di-EMFs incorporating different lanthanides like LaLn@C<sub>80</sub> (Ln= Ce to Gd) and yielded interesting results where Gd based analogues exhibits a higher stability.

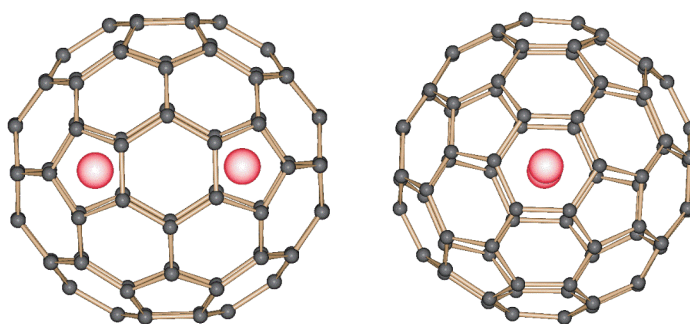


Fig 1. Optimized structure of M<sub>2</sub>@C<sub>80</sub>

[1] a) S. Yannoni et al. *Nature*, **366**, 123 (1993). b) H. Shinohara et al. *J. Am. Chem. Soc.*, **125**, 4391 (2003).

[2] a) A.A. Popov et al. *Chem. Rev.*, **113**, 5989 (2013). b) H. Shinohara, *Rep. Prog. Phys.*, **63**, 843 (2000).

[3] N. Nakatori, et al. *The 49<sup>th</sup> Fullerenes-Nanotubes-Graphene General Symposium* 46 (2015).

[4] T. Mitani, et al. *The 50<sup>th</sup> Fullerenes-Nanotubes-Graphene General Symposium* 95 (2016).

Corresponding Author: M. Hada

Tel: + 81-42-677-2554, Fax: + 81-42-677-2525

E-mail: hada@tmu.ac.jp

## Searching for the unprecedented endohedral metallofullerenes by applying the separation method for those stable only in an anion form

○Natsumi Nakatori<sup>1</sup>, Takuji Mitani<sup>1</sup>, Takahisa Yamaguchi<sup>2</sup>, Ko Furukawa<sup>3</sup>,  
Tatsuhisa Kato<sup>2,4</sup>, Koichi Kikuchi<sup>1</sup>, Yohji Achiba<sup>1</sup>, Takeshi Kodama<sup>1</sup>

<sup>1</sup>Department of Chemistry, Tokyo Metropolitan University, Hachioji 192-0397, Japan

<sup>2</sup>Graduate School of Human and Environmental Studies, Kyoto University, Kyoto 606-8501,  
Japan

<sup>3</sup>Center for Instrumental Analysis, Niigata University, Niigata 950-2181, Japan

<sup>4</sup>Institute for Liberal Arts and Sciences, Kyoto University, Kyoto 606-8501, Japan

In dimetallofullerenes, it has been well known only La, Ce, and Pr are encapsulated in the C<sub>80</sub>(I<sub>h</sub>) cage, and Y, Sc, Lu, and other metals are encapsulated in other cages such as C<sub>82</sub> and C<sub>84</sub>. So, until very recently, M<sub>2</sub>@C<sub>80</sub>(I<sub>h</sub>) (M≠La, Ce, Pr) has been thought to be one of the “hidden” metallofullerenes. However, for M=Y, we have succeeded in the isolation and characterization of Y<sub>2</sub>@C<sub>80</sub>(I<sub>h</sub>) using the method combining the ion-pair chromatography (IPC) with the extraction by a mixed solvent of triethylamine and acetone [1]. This new technique opened the door for investigating more generally the “hidden” metallofullerenes those are unstable in a neutral form but stable in an anion form. In this study, we apply the method to explore the unprecedented metallofullerenes encapsulating Sc or Lu.

Sc or Lu-metallofullerenes were produced and extracted by the almost identical method previously reported [1]. Separation was accomplished by the multi-stage IPC. The first-stage IPC chromatograms of Y, Sc, and Lu-metallofullerenes are shown in Fig.1, and the portions of the dimetallofullerenes are indicated. The elution behaviors are rather different depending on metals. For Sc-metallofullerenes, Sc<sub>2</sub>C<sub>76</sub> and Sc<sub>2</sub>C<sub>78</sub> eluted in the same time. Therefore, Sc<sub>2</sub>C<sub>78</sub> would be not Sc<sub>2</sub>@C<sub>78</sub> but Sc<sub>2</sub>C<sub>2</sub>@C<sub>76</sub>. Moreover, Sc<sub>2</sub>C<sub>80</sub> was isolated, but its absorption spectrum was a little bit different from other M<sub>2</sub>@C<sub>80</sub>(I<sub>h</sub>), then, we couldn't assign Sc<sub>2</sub>C<sub>80</sub> is Sc<sub>2</sub>@C<sub>80</sub>(I<sub>h</sub>). For Lu-metallofullerenes, Lu<sub>2</sub>C<sub>78</sub> and Lu<sub>2</sub>C<sub>80</sub> showed the same elution behavior. Then, like Sc<sub>2</sub>C<sub>78</sub>, Lu<sub>2</sub>C<sub>80</sub> should be not Lu<sub>2</sub>@C<sub>80</sub> but Lu<sub>2</sub>C<sub>2</sub>@C<sub>78</sub>. Lu<sub>2</sub>@C<sub>80</sub>(I<sub>h</sub>) was not obtained in our experiment.

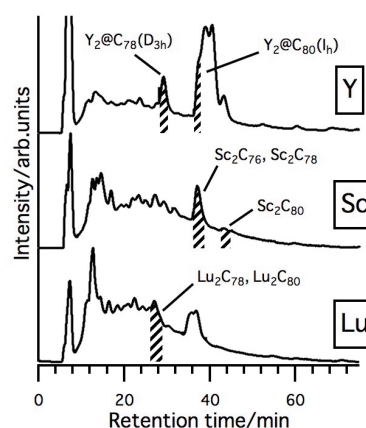


**Fig.1** IPC chromatograms of Y, Sc, Lu-metallofullerenes.

[1] N. Nakatori, et al. *The 49<sup>th</sup> Fullerenes-Nanotubes-Graphene General Symposium 46* (2015).

Corresponding Author: Takeshi Kodama

Tel:+81-42-677-2530, Fax:+81-42-677-2525

E-mail: kodama-takeshi@tmu.ac.jp

## Dynamics of Li<sup>+</sup> ions encapsulated in C<sub>60</sub> fullerene at low temperature

○Hal Suzuki<sup>1</sup>, Misaki Ishida<sup>2</sup>, Masatsugu Yamashita<sup>2</sup>, Chiko Otani<sup>2</sup>,  
Kazuhiko Kawachi<sup>3</sup>, Yasuhiko Kasama<sup>3</sup>, Eunsang Kwon<sup>4</sup>

<sup>1</sup> Graduate School of Science, Osaka University, Toyonaka, Japan

<sup>2</sup> RIKEN, Center for Advanced Photonics, Sendai, Japan

<sup>3</sup> Idea International Inc., Sendai, Japan

<sup>4</sup> Graduate School of Science, Tohoku University, Sendai, Japan

Endohedral fullerenes show potentially useful properties such as a single molecular switch or as a qubit in a quantum computer. These compounds are unique in that the encapsulated atoms and C<sub>60</sub> are not chemically bonded with each other, so that the atoms can move freely in the cage. The dynamics of encapsulated atoms is, therefore, expected to show quantum features at low temperature. In this work, we have investigated the dynamics of Li<sup>+</sup> ions encapsulated in C<sub>60</sub> cage in [Li<sup>+</sup>@C<sub>60</sub>](PF<sub>6</sub><sup>-</sup>) crystal by terahertz absorption spectroscopy (0.5 – 9.0 THz) between 10 K and 300 K.<sup>[1]</sup>

The THz spectrum at 300 K shows two peaks; a broad peak at ~1.2 THz and a sharp one at 2.3 THz. The former one was assigned to the rotational band of Li<sup>+</sup> ion in the carbon cage, and the latter one was assigned to the lattice vibration of [Li<sup>+</sup>@C<sub>60</sub>](PF<sub>6</sub><sup>-</sup>) crystal. The features of the rotational band were successfully explained by a free rotation model of Li<sup>+</sup> ion with radius of ~1.5 Å. This interpretation is consistent with the preceding crystallographic study, where the Li<sup>+</sup> ion was found to delocalized on a spherical shell with radius of ~1.5 Å in the C<sub>60</sub> cage.<sup>[2]</sup> It is interesting that the dynamics of the Li<sup>+</sup> ion was explained not by the librational and hopping model but by the free rotation model, indicating that the height of the rotational potential barriers are comparable to the zero point energy of Li<sup>+</sup> ions.

The spectrum dramatically changes at low temperature: As the temperature is lowered from 300 K to 120 K, the rotational band of Li<sup>+</sup> ion shifts to lower frequency, and it starts disappearing below 120 K. In addition, a new peak appears at 2.2 THz below 120 K. It is indicated that Li<sup>+</sup> ion does not rotate at low temperature, but librates with frequency at 2.2 THz.

Combining these results with the preceding crystallographic results, which revealed that the Li<sup>+</sup> ion localizes into two positions below 100 K, we have proposed an energy scheme of the rotational dynamics for the Li<sup>+</sup> ions (Fig. 1). In this scheme, a librational level lies beneath free rotational levels by 2.2 THz. The temperature dependences of the spectral peak intensities at ~1.2 THz and 2.2 THz were successfully explained by this model.

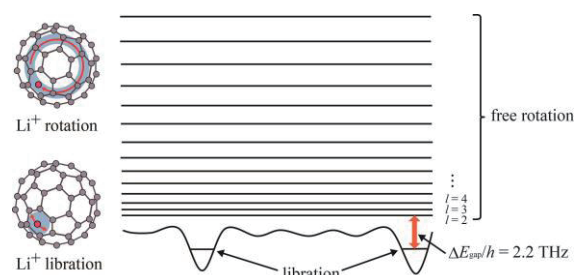


Fig. 1 A schematic energy diagram proposed to explain the spectral results.

[1] H. Suzuki *et al.* Phys. Chem. Chem. Phys., **18**, 31384 (2016).

[2] S. Aoyagi, *et al.* Angew. Chem., Int. Ed., **51**, 3377 (2012).

Corresponding Author: H. Suzuki

Tel: +81-6-6850-5526, Fax: +81-6-6850-5526,

E-mail: h\_suzuki@chem.sci.osaka-u.ac.jp

## Geometric and electronic structures of polymerized C<sub>40</sub> fullerene

○Mina Maruyama, Susumu Okada

*Graduate School of Pure and Applied Sciences, University of Tsukuba, Tsukuba 305-8577, Japan*

Moderate chemical reactivity of fullerenes arising from their hollow-cage structure allows them atom-like constituent units of nanocarbon network materials by forming intermolecular covalent bonds. For instance, C<sub>60</sub> can form various polymeric forms, in which C<sub>60</sub> is connected to its neighboring molecules via [2+2] cycloaddition or other covalent bonding, resulting in their electronic structures from a metal to a semiconductor depending on the local atomic structures. Small fullerenes are expected to inherently possess polymerized structures because of their higher chemical reactivity than that of the conventional fullerenes larger than C<sub>60</sub>. Among such small fullerene, C<sub>40</sub> with *T<sub>d</sub>* symmetry and an acorn shape is an interesting fullerene in its polymeric phase, because it contains four acpentalene (three pentagonal rings sharing their edges) being expected to result in remarkable chemical reactivity and spin polarization. In this work, we aim to investigate geometric and electronic structures of C<sub>40</sub> polymers in which C<sub>40</sub> is covalently connected in two-dimensional honeycomb network, using the density functional theory with generalized gradient approximation.

Figure 1 shows optimized structures of C<sub>40</sub> polymers with parallel and antiparallel intermolecular arrangements under the optimum lattice constant of 13.5 nm. In polymeric structures, C<sub>40</sub> is connected to its three adjacent molecules via cycloaddition covalent bonds. Total energies of C<sub>40</sub> polymers with parallel and antiparallel arrangements are 0.596 and 0.597 eV/atom with respect to that of graphene. Although C<sub>40</sub> polymers with antiparallel and parallel arrangements are semiconductors with direct band gap of 0.08 and 0.05 eV at M point, respectively, C<sub>40</sub> polymers possess spin polarization around the apex of acorn owing to the narrow bandwidth and small band gap. Furthermore, C<sub>40</sub> polymer sheet possesses dipole moment normal to the polymeric layer owing to their asymmetric molecular shape. Thus, the network is an all carbon two-dimensional material exhibiting both magnetic and electric polarities.

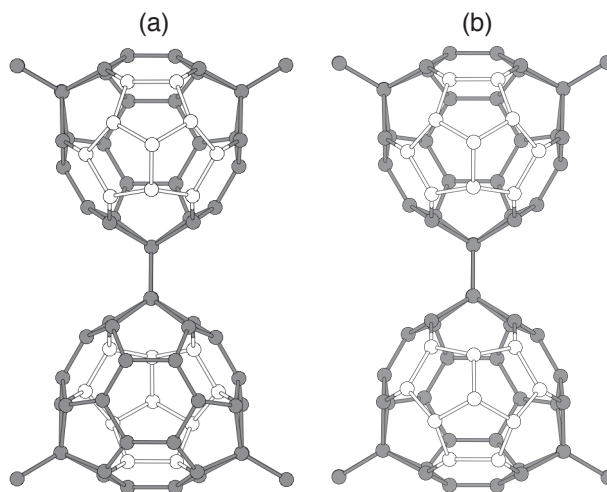


Figure 1: Optimized structures of C<sub>40</sub> polymer with (a) antiparallel and (b) parallel intermolecular arrangements.

Corresponding Author: M. Maruyama  
 Tel: +81-29-853-5921, Fax: +81-29-853-5924,  
 E-mail: mmaruyama@comas.frsc.tsukuba.ac.jp

## Polyynes formation by laser induced breakdown in hydrocarbon gas flow

Yuki Taguchi<sup>1</sup>, Hitomi Endo<sup>1</sup>, Takeshi Kodama<sup>1</sup>, Tomonari Wakabayashi<sup>2</sup>, Yohji Achiba<sup>1</sup>,  
○Haruo Shiromaru<sup>1</sup>, Benji Wales<sup>3</sup>, Joseph H. Sanderson<sup>3</sup>

<sup>1</sup> Department of Chemistry, Tokyo Metropolitan University, Tokyo 192-0397, Japan

<sup>2</sup> Department of Chemistry, Kindai University, Osaka, 577-8502, Japan

<sup>3</sup> Department of Physics and Astronomy, University of Waterloo, Canada

Nowadays polyynes have been easily synthesized by laser ablation of graphite in an organic solvent, or its vapor, in which hydrogen termination of chain-form carbon clusters is considered to be the main pathway [1-3]. At the 50<sup>th</sup> FNTG symposium, we reported that polyynes were efficiently produced also by laser-induced breakdown (LIB) in argon-diluted propane gas flow, in which bottom-up formation process, namely chain growth from carbon-rich fragments, is most likely the main pathway [4]. In the present study we employed various hydrocarbon molecules as starting materials and found that the efficiency of the polyynes-forming reactions are highly target-dependent [5].

Flowing gases of hydrocarbon molecules seeded in Ar were irradiated by tightly focused ns and fs laser, and the products were captured in hexane solution. In the case of ns laser irradiation, short polyynes up to C<sub>10</sub>H<sub>2</sub> were produced efficiently from all the hydrocarbons (propane, hexane, octane, benzene, toluene). The yields vary significantly among the products from different target molecules, extending beyond the effects of difference in the vapor pressures. Among them, LIB in benzene gives polyynes most efficiently. As shown in Fig.1, polyynes up to C<sub>12</sub>H<sub>2</sub> is clearly identified, while the longest polyynes identified for other starting materials is C<sub>10</sub>H<sub>2</sub>. The visible emission spectrum of the focused spot is shown in Fig. 2, where emission of C<sub>2</sub> fragment is observed, indicating deep fragmentation takes place. In the case of fs laser irradiation of hexane, polyynes were produced efficiently much more than the ns-laser case, whereas for the toluene target, polyynes were not produced. Such a variation in the polyynes yield suggests there would be more suitable molecules for formation of polyynes, or any other carbon-rich materials, by gas-phase laser irradiation method.

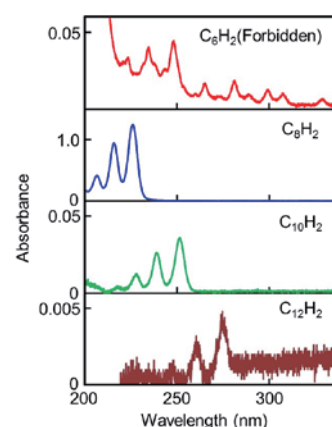


Fig.1 UV absorption spectra of the solution prepared by ns-LIB in benzene, separated by HPLC.

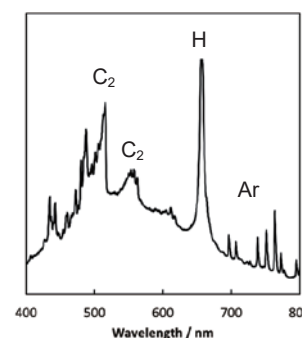


Fig.2 Emission spectrum of the ns(1064 nm)-LIB in benzene.

[1] M. Tsuji et al., *Chem. Phys. Lett.* 355, 101 (2002).

[2] Y. Taguchi et al, *Carbon* 94, 124 (2015).

[3] T. Wakabayashi et al., *Carbon* 50, 47 (2012).

[4] Y. Taguchi et al., *50<sup>th</sup> FNTG*, 87 (2016).

[5] Y. Taguchi et al, *Carbon*, in press.

Corresponding Author: H. Shiromaru,

Tel: +81-46-677-1111, Fax: +81-42-677-2533,

E-mail: shiromaru-haruo@tmu.ac.jp

## Inner Core in the Elementary Particles of Detonation Nanodiamond

○Toshihiko Tanaka<sup>1</sup>, Masayoshi Fukaya<sup>1</sup>, Amanda S. Barnard<sup>2</sup> and Eiji Ōsawa<sup>3</sup>

<sup>1</sup>Department of Chemistry and Biochemistry, National Institute of Technology, Fukushima College, 30 Aza-nagao, Tairakamiarakawa, Iwaki, Fukushima, 970-8034, Japan

<sup>2</sup>CSIRO Materials Science and Engineering, 343 Royal Parade, Parkville, Victoria 3052, Australia

<sup>3</sup>NanoCarbon Research Institute Ltd., Asama Research Extension Centre, Faculty of Textile Science and Technology, Shinshu University 3-15-1 Tokita, Ueda, Nagano, 386-8567 Japan

Elementary particles of detonation nanodiamond (PPDND) could be the 4th novel nanocarbon following fullerenes, nanotubes, and graphenes. PPDND is known to be strongly polarized due to the core-shell structure [1]. Details of the internal structure have been revealed by density functional theory (DFT) calculations, consisting of a shell of  $sp^2$  carbons and doubly layered core of  $sp^{2+x}$  and  $sp^3$  carbons [2]. However, its experimental confirmation has been delayed due to technical difficulties in isolating analytical samples. Elaborate attrition milling of the agglutinates of detonation nanodiamonds recently produced aqueous solution of single-nano sized PPDNDs in high purity [1].

We report herein that the inner core of PPDND is a cubic diamond containing nearly 1000  $sp^3$  carbon atoms based on laser desorption/ionization mass spectra (LDI MS). Korepanov *et al.* confirmed the size by 3D-phonon confinement analysis of Raman spectra [3]. The positive ion mass peak of  $\sim 12$  k Da ( $\sim C_{1000}$ ) was first reported two years ago [4]. Little change of the peak from a linear to a reflector mode shows the significant stability of the peak [Fig.1], thus convincing us that it is the inner core of  $\sim C_{1000}$ . We think that the peak is generated from the PPDND crystals that can be precipitated at drying only from the well-dispersed solution of PPDNDs. We need a higher laser power to generate the inner core peak from the crystal, showing that it should be significantly decomposed into an emerged inner core, thermally and photochemically. Such a stable fragment furthermore should be the cubic diamond ion that corresponds to be one of the energy-minimized model structures simulated by a DFT calculation.

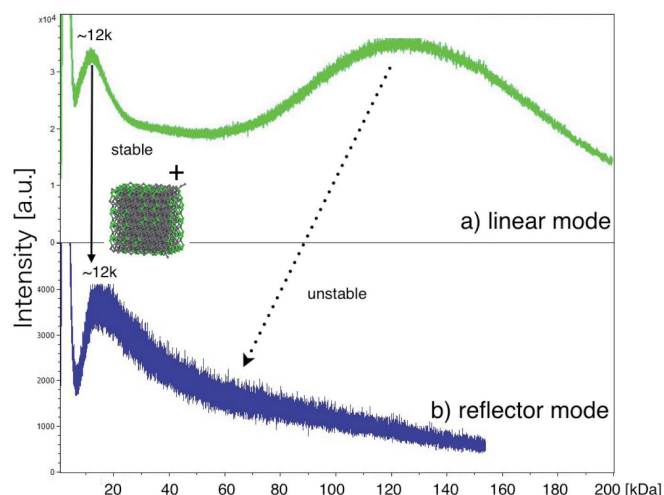


**Fig.1** LDI MS of the detonation nanodiamonds deposited from the aqueous solution of dispersible PPDNDs.

[1] E. Osawa, D. Ho, H. Huang, M. V. Korobov, N. N. Rozhkova; *Diam. Rel. Mat.* 18, 904 (2009).

[2] A. S. Barnard, E. Osawa; *Nanoscale* 6, 1188 (2014).

[3] V. I. Korepanov, H. Witek, H. Okajima, E. Osawa, and H. Hamaguchi; *J. Chem. Phys.* 140, 41107 (2014).

[4] T. Tanaka, R. Yamanoi, E. Osawa; *48<sup>th</sup> FNTG*, Abstract Book, No. 19 (2015).

Corresponding Author: Toshihiko Tanaka/Tel: +81-246-46-0810/E-mail: [tanaka@fukushima-nct.ac.jp](mailto:tanaka@fukushima-nct.ac.jp)

## Optical bistability in carbon nanotubes

○T. Uda<sup>1,2</sup>, A. Ishii<sup>1,3</sup>, Y. K. Kato<sup>1,4</sup>

<sup>1</sup> *Nanoscale Quantum Photonics Laboratory, RIKEN, Saitama 351-0198, Japan*

<sup>2</sup> *Department of Applied Physics, The University of Tokyo, Tokyo 113-8656, Japan*

<sup>3</sup> *Department of Electrical Engineering, The University of Tokyo, Tokyo 113-8656, Japan*

<sup>4</sup> *Quantum Optoelectronics Research Team, RIKEN center for Advanced Photonics, Saitama 351-0198, Japan*

Optical bistability refers to situations with two stable optical outputs for the same optical input, and it has been studied for applications involving all-optical switching and optical memories. Here we report on the observation of optical bistability in individual carbon nanotubes (Fig. 1). Excitation power dependence of photoluminescence (PL) spectra taken with various energy detunings reveals that the bistability occurs due to simultaneous shifts of absorption and emission resonances. We also demonstrate reversible and reproducible optical switching (Fig. 2), and perform time resolved measurements to obtain time scales of the operation. Our results open up new pathways for utilizing carbon nanotubes as an all-optical-switching medium at the nanoscale.

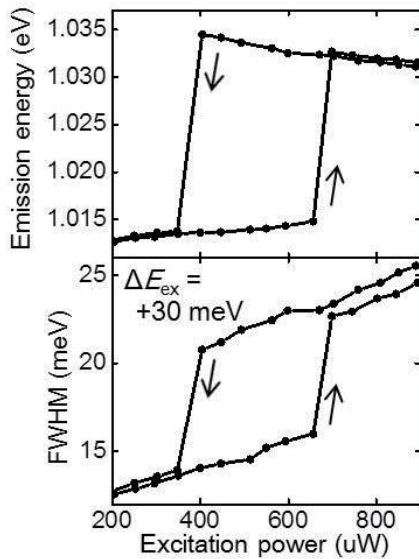


Fig.1 Excitation power dependence of PL energy and linewidth

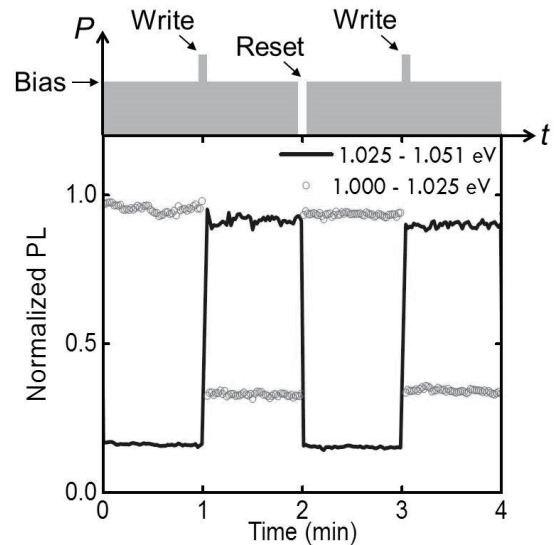


Fig. 2 All-optical switching of PL

Work supported by JSPS (KAKENHI JP26610080, JP16H05962), Canon Foundation, and MEXT (Photon Frontier Network Program, Nanotechnology Platform). T.U. is supported by ALPS, and A.I. is supported by MERIT and JSPS Research Fellowship.

Corresponding Author: Yuichiro K. Kato

Tel: +81-48-462-1111 (ext. 3432)

E-mail: [yuichiro.kato@riken.jp](mailto:yuichiro.kato@riken.jp)

## Single photon generation through exciton-exciton annihilation in air-suspended carbon nanotubes

○Akihiro Ishii<sup>1,2</sup>, Takushi Uda<sup>1,3</sup>, Yuichiro K. Kato<sup>1,4</sup>

<sup>1</sup> *Nanoscale Quantum Photonics Laboratory, RIKEN, Saitama 351-0198, Japan*

<sup>2</sup> *Department of Electrical Engineering, The University of Tokyo, Tokyo 113-8656, Japan*

<sup>3</sup> *Department of Applied Physics, The University of Tokyo, Tokyo 113-8656, Japan*

<sup>4</sup> *Quantum Optoelectronics Research Team, RIKEN center for Advanced Photonics, Saitama 351-0198, Japan*

Carbon nanotubes have great potential for single photon sources as they have stable exciton states even at room temperature and their emission wavelengths cover the telecommunication bands. In recent years, single photon emission from carbon nanotubes has been achieved by creating localized states of excitons. In contrast to such an approach, here we utilize mobile excitons and show that single photons can be generated in air-suspended carbon nanotubes, where exciton diffusion length is as long as several hundred nanometers and exciton-exciton annihilation is efficient [1]. We perform photoluminescence microscopy on as-grown air-suspended carbon nanotubes in order to determine their chirality and suspended length. Photon correlation measurements are performed on nanotube emission at room temperature using a Hanbury-Brown-Twiss setup with InGaAs/InP single photon detectors. We observe antibunching with a clear excitation power dependence, where we obtain  $g^{(2)}(0)$  value less than 0.5 at low excitation powers (Fig. 1), indicating single photon generation. We show such  $g^{(2)}(0)$  data with different chiralities and suspended lengths, and the effects of exciton diffusion on single photon generation processes are discussed.

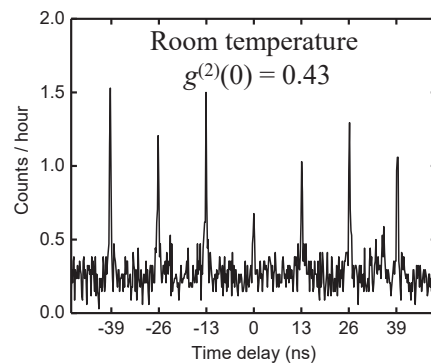


Fig.1 Photon correlation of an individual (9,7) carbon nanotube measured at room temperature.

Work supported by KAKENHI (JP26610080, JP16H05962), The Canon Foundation, and MEXT (Photon Frontier Network Program, Nanotechnology Platform). A.I. is supported by MERIT and JSPS Research Fellowship, and T.U. is supported by ALPS.

[1] A. Ishii, M. Yoshida, Y. K. Kato, Phys. Rev. B 91, 125427 (2015).

Corresponding Author: Yuichiro K. Kato

Tel: +81-48-462-1111 (ext. 3432)

E-mail: [yuichiro.kato@riken.jp](mailto:yuichiro.kato@riken.jp)

## Raman Spectroscopy of Individual Single-Walled Carbon Nanotubes

○Juan Yang, Daqi Zhang, Yan Li

*College of Chemistry and Molecular Engineering, Peking University, Beijing 100871, China*

Single-walled carbon nanotubes (SWNTs) have been one of the most intensively studied materials since the discovery in 1993 [1]. Among all the characterization methods of SWNTs, Raman spectroscopy is widely recognized as a versatile tool that can achieve the most information with the maximum simplicity. To explicitly explore the intrinsic structures and properties of SWNTs, we study Raman spectra of individual SWNTs at the single-tube level to minimize the ambiguities caused by the assortment of different tube species.

1. Single chirality enriched individual SWNTs on standard silicon substrates have been realized recently [2] and are a promising candidate for the next generation of electronic and photoelectronic devices. We provide a convenient and nondestructive method based on Raman spectroscopy to make  $(n,m)$  assignments and quantification for such samples. We establish a relation of  $\omega_{\text{RBM}} = 235.9/d_t + 5.5$ . We develop a counting-based quantification method calibrated by the tube density and laser resonance window [3].

2. We observe multiple electronic Raman scattering (ERS) features in individual metallic SWNTs (M-SWNTs) [4]. These features provide direct measurements on the excitonic transition energies ( $M_{ii}^+$  and  $M_{ii}^-$ ) using a commercialized Raman spectrometer with several laser lines.  $M_{ii}$ 's can be determined with an extremely small uncertainty of  $\pm 1$  meV for a single measurement, and of  $\pm 10$  meV when environmental effects are taken into account. We study the environmental effects including bundling, substrate, and laser heating on the Raman features. We observe a constant  $M_{ii}$  splitting value that is insensitive to environmental changes, and thus use this value as a universal criteria for assignments in various environments [5].

3. We decorate gold nanoparticles (AuNPs) onto individual SWNTs to enhance the weak Raman signals via the surface enhanced Raman scattering (SERS) effect. Enormous Raman enhancements, up to 33000 times of the original Raman intensity, is achieved. Such enormous enhancement are attributed to the polyhedral shape of the AuNPs and the narrow spacing between the AuNPs, and more importantly, to the fact that SWNTs are located exactly at the “hot spots” produced by AuNPs.

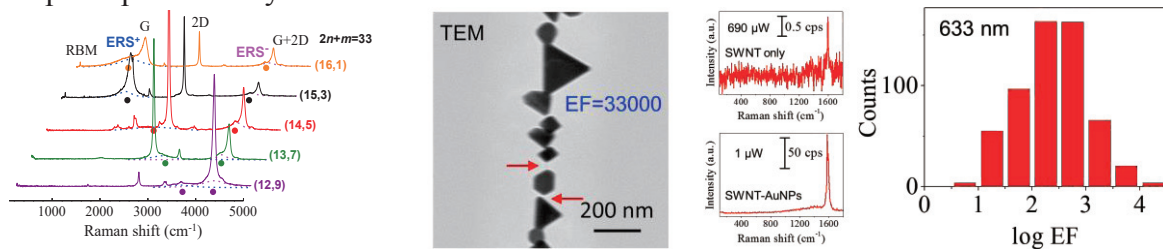


Fig. 1 ERS spectra of the  $2n+m=33$  family. Fig. 2 TEM image and Raman enhancement of SWNT-AuNPs.

- [1] S. Iijima and T. Ichihashi, *Nature* **363**, 603 (1993).  
 [2] F. Yang, X. Wang, D. Zhang, *et al.* *Nature* **510**, 522 (2014).  
 [3] D. Zhang, J. Yang\*, F. Yang, *et al.* *Nanoscale* **7**, 10719 (2015).  
 [4] D. Zhang, J. Yang\*, E. H. Hasdeo, *et al.* *Phys. Rev. B* **93**, 245428 (2016).  
 [5] D. Zhang, J. Yang\*, M. Li, *et al.* *ACS Nano*. **10**, 10789 (2016)

Corresponding Author: J. Yang

Tel: +86-10-62755357

E-mail: [yang\\_juan@pku.edu.cn](mailto:yang_juan@pku.edu.cn)

## Competitive elimination and decomposition reaction of oxidized single-walled carbon nanotubes depending on the degree of functionalization

○Yutaka Maeda<sup>1</sup>, Erika Sone<sup>1</sup>, Akane Nishino<sup>1</sup>, Yuri Amagai<sup>1</sup>, Wei-Wei Wang<sup>2</sup>, Michio Yamada<sup>1</sup>, Mitsuaki Suzuki<sup>1</sup>, Jun Matsui<sup>3</sup>, Masaya Mitsuishi<sup>4</sup>, Toshiya Okazaki<sup>5</sup>, Shigeru Nagase<sup>2</sup>

<sup>1</sup> *Department of Chemistry, Tokyo Gakugei University, Tokyo 184-8501, Japan*

<sup>2</sup> *Fukui Institute for Fundamental Chemistry, Kyoto University, Kyoto 606-8103, Japan*

<sup>3</sup> *Department of Material and Biological Chemistry, Yamagata University, Yamagata 990-8560, Japan*

<sup>4</sup> *Institute of Multidisciplinary Research for Advanced Materials (IMRAM), Tohoku University, Sendai 980-8577, Japan*

<sup>5</sup> *CNT-Application Research Center, National Institute of Advanced Industrial Science and Technology (AIST), Tsukuba 305-8565, Japan*

Epoxide is a useful functional group owing to its high reactivity. At this point, Barron et al reported reversible epoxidation of SWNTs.<sup>[1]</sup> Furthermore, chemical reactions of the epoxidized SWNTs with nucleophiles were also studied by Fusco et al.<sup>[2]</sup> In 2010, Weisman et al. reported that photoreaction of SWNTs with ozone resulted in new, bright, and red shifted photoluminescence (PL).<sup>[3]</sup> It is worthwhile to increase NIR PL efficiency for practical applications of SWNTs such as bioprobe, biosensor, and so on. It is important to control functionalization degree of SWNTs because it is strongly influenced on their electronic and optical properties including the efficiency of the newly generated NIR PL. Therefore, we focus our attention on the control of functionalization degree of alkylated SWNTs and their NIR PL efficiency by thermal elimination reaction.<sup>[4,5]</sup> In this context, we here present the thermal elimination and decomposition reaction of the oxidized SWNTs depending on their functionalization degrees.<sup>[6]</sup>

Oxidized SWNTs (SWNTs-O) were prepared by photoreaction of SWNTs in the presence of disulfide and oxygen.<sup>[7]</sup> The functionalization degrees of SWNTs-O were controlled by the photo irradiation time. Decrease of the characteristic absorption peaks and that of the RBM and G bands with increase of the D bands upon photo-irradiation indicated the progress of the sidewall oxidation. The characteristic peaks recovered by the thermal treatment under the nitrogen flow when the degree of functionalization was low. In contrast, the characteristic peaks did not recover except for the D bands by the thermal treatment when the degree of functionalization was high. Considering the results of XPS analysis, it is suggested that elimination reaction proceeded predominantly when the degree of oxidation was low, but decomposition reaction competed as the degree of oxidation increased. We also studied a possible pathway for the decomposition of oxidized SWNTs using density functional calculations.

[1] D. Ogrin *et al. J. Am. Chem. Soc.* **128**, 11322 (2006). [2] C. Annese *et al. Eur. J. Org. Chem.* 1666 (2014). [3] S. Ghosh *et al. Science* **330**, 1656 (2010). [4] Y. Maeda *et al. J. Am. Chem. Soc.* **134**, 18101 (2012). [5] Y. Maeda *et al. Chem. Commun.* **51**, 13462 (2015). [6] Y. Maeda *et al. Chem. Eur. J.* **22**, 15373 (2016). [7] Y. Maeda *et al. J. Am. Chem. Soc.* **135**, 6356 (2013).

Corresponding Author: Y. Maeda

Tel: +81-42-329-7512, Fax: +81-42-329-7512,

E-mail: ymaeda@u-gakugei.ac.jp

## Development of Nano-Resolution Desktop FE-SEM and X-ray microscope with Multi-Walled Carbon Nanotube Electron Source

○Masaru Irita<sup>1,2</sup>, Shintarou Yamazaki<sup>1</sup>, Shota Katsuyama<sup>1</sup>, Hitoshi Nakahara<sup>1</sup>, Koji Asaka<sup>1</sup>, Yahachi Saito<sup>1</sup>, Hidekazu Murata<sup>3</sup>, Teruaki Ohno<sup>4</sup>

<sup>1</sup> Department of Quantum Engineering, Nagoya Univ., Nagoya 464-8603, Japan

<sup>2</sup> Venture Business Laboratory, Nagoya Univ., Nagoya 464-8603, Japan

<sup>3</sup> Department of Electric and Electronic Engineering, Meijo Univ., Nagoya 468-8502, Japan

<sup>4</sup> Technex Lab Co., Tokyo 194-0044, Japan

Field emission (FE) from carbon nanotube (CNT) have been studied over 25 years [1]. Multi-walled CNT (MWNT) have exhibited high brightness  $10^9 \sim 10^{10}$  A/(cm<sup>2</sup>•sr) as an electron source for FE - scanning electron microscope (SEM) [2]. Furthermore, the FE current is stable even under a poor vacuum condition  $10^{-6} \sim 10^{-7}$  Pa without ion pump [3]. In the scene of an archaeological site excavation, the mobile microscope is necessary to investigate. In this work, we developed a desktop FE-SEM and X-ray microscope (XRM) with a single isolated MWNT electron source, and its spacial-resolution was investigated.

MWNT electron source and Butler electrostatic lens were installed in a gun chamber with an ICF-114 flange, and the chamber was evacuated with a turbo pump down to  $10^{-7}$  Pa. The SEM image was acquired using focused beam current 61.1 pA at Butler voltage  $V_{\text{but}} = 1.5$  kV and accelerating voltage  $V_{\text{acc}} \sim 15$  kV as shown in Fig. 1 (a). The observed sample is Au-Pd coated Polystyrene latex sphere (PLS) with 200 or 500 nm in diameter. Fig. 1 (c) shows the line profile between substrate and PLS. The spatial resolution, which was

estimated from the width at 80-20% of a fitting profile across the SEM image, was 9 nm, suggesting that the beam diameter was approximately 9 nm. A projection-type XRM based on the CNT-FE-SEM also was constructed with an Au target for the X-ray source. The XRM image was acquired by 30-min exposure at  $V_{\text{but}} = 1.5$  kV and  $V_{\text{acc}} \sim 17$  kV as shown in Fig. 1 (b). The observed sample is 400-mesh Au. Fig. 1 (d) shows the line profile between hole and bar. The spatial resolution was 200 nm. These results demonstrate nano-resolution desktop microscope with the MWNT electron source.

[1] Y. Saito et al., Nature, 389, 554–555, (1997).

[2] H. Nakahara et al., Appl. Surf. Sci. 256, 1214–1217, (2009).

[3] H. Nakahara et al., e-J. Surf. Sci. Nanotech. 9, 400-403, (2011).

E-mail: [masaru.irit@surf.nuqe.nagoya-u.ac.jp](mailto:masaru.irit@surf.nuqe.nagoya-u.ac.jp)

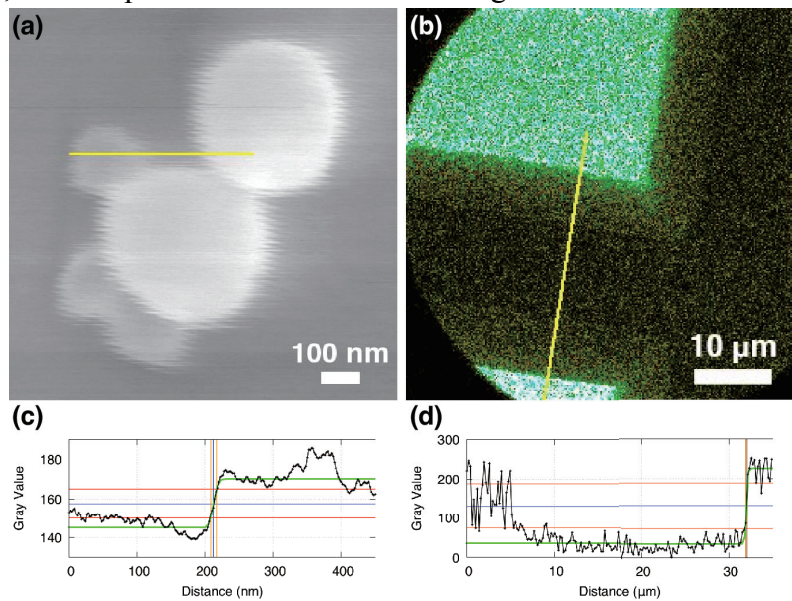


**Fig. 1** (a) SEM image of Au-Pd coated PLS. (b) XRM image of Au mesh. (c), (d) Line profiles of the SEM (a) and XRM (b) images obtained at lines indicated in respective images.

## Cold exciton electroluminescence from air-suspended carbon nanotube split-gate devices

Noriyuki Higashide<sup>1</sup>, ○Masahiro Yoshida<sup>2,3</sup>, Takushi Uda<sup>2,4</sup>, Akihiro Ishii<sup>1,2</sup>,  
Yuichiro K. Kato<sup>2,3</sup>

<sup>1</sup> *Department of Electrical Engineering, The University of Tokyo, Tokyo 113-8656, Japan*

<sup>2</sup> *Nanoscale Quantum Photonics Laboratory, RIKEN, Saitama 351-0198, Japan*

<sup>3</sup> *Quantum Optoelectronics Research Team, RIKEN center for Advanced Photonics, Saitama  
351-0198, Japan*

<sup>4</sup> *Department of Applied Physics, The University of Tokyo, Tokyo 113-8656, Japan*

Electroluminescence from individual carbon nanotubes within split-gate devices are investigated. The devices are fabricated from silicon-on-insulator substrates [1], and the top silicon layer is used as gates for electrostatic carrier doping [2]. By characterizing the nanotubes with photoluminescence spectroscopy, chirality is identified and electroluminescence peaks are assigned. We observe electroluminescence linewidth comparable to photoluminescence, indicating negligible heating and state-mixing effects. Split-gate and bias voltage dependences are consistent with emission from an electrostatically formed *pn*-junction.

Work supported by JSPS (KAKENHI JP16H05962, JP26610080), MEXT (Photon Frontier Network Program, Nanotechnology Platform), Canon Foundation, and Asahi Glass Foundation. A.I. is supported by MERIT and JSPS Research Fellowship, and T.U. is supported by ALPS.

[1] M. Jiang, Y. Kumamoto, A. Ishii, M. Yoshida, T. Shimada, Y. K. Kato, [Nature Commun. 6, 6335 \(2015\)](#).

[2] S. Yasukochi, T. Murai, S. Moritsubo, T. Shimada, S. Chiashi, S. Maruyama, Y. K. Kato, [Phys. Rev. B 84, 121409\(R\) \(2011\)](#).

Corresponding Author: Yuichiro K. Kato

Tel: +81-48-462-1111 (ext. 3432)

E-mail: [yuichiro.kato@riken.jp](mailto:yuichiro.kato@riken.jp)

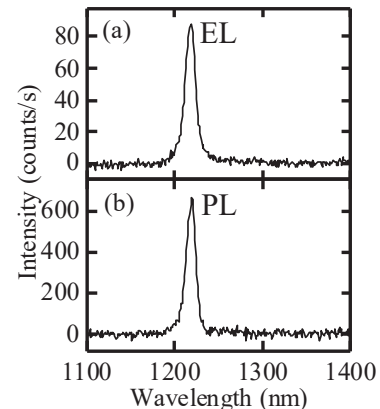


Fig. 1(a-b) EL and PL spectra, respectively. An individual (10,5) nanotube is measured in N<sub>2</sub> atmosphere at room temperature.

## The Solution to Stability and Cost in Perovskite Solar Cells by All-Carbon Approach

○ Il Jeon<sup>1</sup>, Namyoungh Ahn<sup>2</sup>, Jungjin Yoon<sup>2</sup>, Esko I. Kauppinen<sup>3</sup>, Mansoo Choi<sup>1</sup>, Yutaka Matsuo<sup>1,4</sup>, Shigeo Maruyama<sup>1,5</sup>

<sup>1</sup>Department of Mechanical Engineering, The University of Tokyo, Tokyo 113-8656, Japan

<sup>2</sup>Department of Mechanical and Aerospace Engineering, Seoul National University, Seoul 08826, South Korea

<sup>3</sup>Department of Applied Physics, Aalto University School of Science, FI-00076 Aalto, Finland

<sup>4</sup>Hefei National Laboratory for Physical Sciences at Microscale, University of Science and Technology of China, Anhui 230026, China

<sup>5</sup>National Institute of Advanced Industrial Science and Technology, Ibaraki 305-8564, Japan

Since Miyasaka and colleagues adopted perovskite semiconductors into photovoltaic devices, and Park and colleagues realized solidified lead halide perovskite, perovskite solar cells (PSCs) have received much attention on account of high power conversion efficiency (PCE) and other advantages of organic solar cells. Their reported PCEs have soared rapidly in the last five years, and now some certified efficiencies exceed 20%. However, there remains several shortcomings, prominently high-cost and stability that need to be addressed.

Here, we report PSCs in which the lead halide perovskite layer is sandwiched by C<sub>60</sub> and single-walled carbon nanotubes (SWCNTs) as the solution to both stability and cost (Fig. 1). Such all-carbon approach enabled low-cost fabrication by removing metal electrodes. The new device structure not only allowed room temperature process, but also long-term stability by preventing vapor penetration and charge trapping. Air-processed PSCs with a configuration of ITO/C<sub>60</sub>/CH<sub>3</sub>NH<sub>3</sub>PbI<sub>3</sub>/SWCNT were tested in the stability and cost perspectives by adding three mainstream hole-transporting materials (HTMs), namely, 2,2',7,7'-tetrakis(N,N-di-p-methoxyphenylamino)-9,9'-spirobifluorene, poly[bis(4-phenyl)(2,4,6-trimethylphenyl)amine], and poly(3-hexylthiophene-2,5-diyl) (P3HT) (Fig. 2).

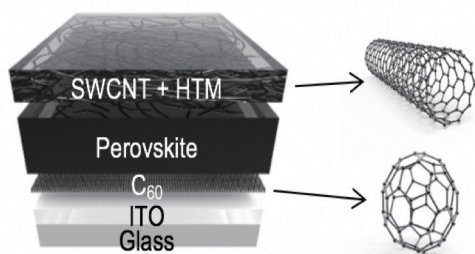


**Fig.1** Device Schematics

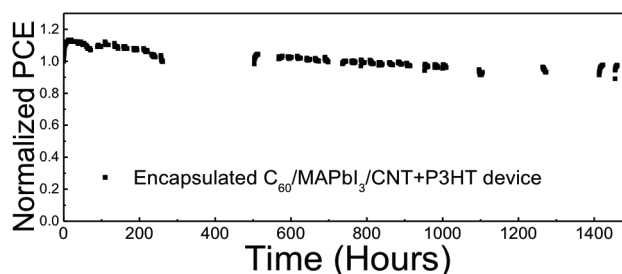


**Fig.2** Stability data under constant one sun illumination in ambience

Corresponding Author: S. Maruyama

Tel: +81-3-5841-6421, Fax: +81-3-5841-6421,

E-mail: maruyama@photon.t.u-tokyo.ac.jp

## Fabrication and characterization of IrO<sub>2</sub> / nano-carbon catalysts

○Masanori Hara, Badam Rajashekar, Kanishka De Silva, Hsin-Hui Huang,  
Masamichi Yoshimura

*Toyota Technological Institute, Nagoya 468-8511, Japan*

### 1. Introduction

In recent years, environmental issues, such as global warming and depletion of fossil fuels, have become important topic for progress toward sustainable societies. In terms of energy storage, conversion of renewable energies to hydrogen via water electrolysis has attracted attention. However, in water electrolysis systems, activity, durability, and cost of catalysts are insufficient for practical application due to high over-potential and low kinetics of electrode reactions, especially, oxygen evolution reaction (OER) on the anode [1-3]. In this study, we have prepared novel nanoparticle catalysts of iridium oxide (IrO<sub>2</sub>), which is one of the most active catalysts for OER, supported on nano-carbon materials, graphene and carbon nanotube (CNT), with high stability and conductivity. Electrochemical properties of the IrO<sub>2</sub>-graphene and IrO<sub>2</sub>-CNT catalysts were examined in sulfuric acid solution.

### 2. Experimental

The IrO<sub>2</sub>-graphene (or reduced graphene oxide, rGO) and IrO<sub>2</sub>-CNT catalysts were synthesized by hydrothermal method. In brief, required amount of H<sub>2</sub>IrCl<sub>6</sub> complex and GO or oxidized CNT (CNT-COOH) were dispersed in ethanol/water mixture and the mixture was heated at 80 °C for 6 h and then heated at 150 °C in hydrothermal autoclave for 4 h. The IrO<sub>2</sub>-rGO and IrO<sub>2</sub>-CNT catalysts were characterized by XRD, TEM, EDX, XPS and electrochemical methods, LSV and RDE.

### 3. Results and discussion

Figs. 1 show TEM images of the IrO<sub>2</sub>-rGO and IrO<sub>2</sub>-CNT catalysts. The IrO<sub>2</sub> nanoparticles were dispersed on the substrates surface and an average particle size of IrO<sub>2</sub> on both the substrates was ca. 1.5 nm. Electrochemical measurement of the IrO<sub>2</sub>-rGO and IrO<sub>2</sub>-CNT catalysts reveals high

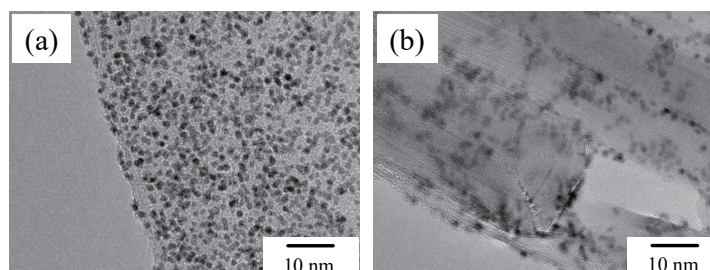


Fig. 1 TEM images of (a) IrO<sub>2</sub>-rGO and (b) IrO<sub>2</sub>-CNT.

activity of both the catalysts for OER; onset potential is ca. 1.43 V vs. RHE and mass activity at 1.60 V is ca. 380 A g<sup>-1</sup>. In addition, both the catalysts showed very high durability for 1000 potential cycling between 1.2 – 1.65 V with 20% and 9% reduction in the current density, respectively. The overvoltage of the IrO<sub>2</sub> / nano-carbon catalysts is 70 mV lower than that of conventional catalysts. The present results suggest that the IrO<sub>2</sub> / nano-carbon catalysts with high activity and durability is promising anode for polymer electrolyte water electrolyzer.

[1] M. Carmo, D. L. Fritz, J. Mergel, D. Stolten, *Int. J. Hydrogen Energy* 38 (2013) 4901.

[2] E. Antolini, *ACS Catal.* 4 (2014), 4, 1426.

[3] J. Cheng, H. Zhang, H. Ma, H. Zhong, Y. Zou, *Electrochim. Acta* 55 (2010) 1855.

Corresponding Author: M. Hara

Tel: +81-52-809-1850, Fax: +81-52-809-1851,

E-mail: haram@toyota-ti.ac.jp

## Bottom-up approach for edge-functionalized graphene nanoribbons

○Hideyuki Jippo<sup>1</sup>, Junichi Yamaguchi<sup>1</sup>, Shintaro Sato<sup>1</sup>, Hironobu Hayashi<sup>2</sup>, Hiroko Yamada<sup>2</sup>,  
Mari Ohfuchi<sup>1</sup>

<sup>1</sup> *Advanced System Research & Development Unit, Fujitsu Limited, 10-1  
Morinosato-Wakamiya, Atsugi, Kanagawa 243-0197, Japan*

<sup>2</sup> *Graduate School of Materials Science, Nara Institute of Science and Technology (NAIST),  
8916-5, Takayama-cho, Ikoma, Nara 630-0192, Japan*

To realize graphene-based electronics, it is important to modulate the electronic properties of graphene nanoribbons (GNRs), which can be realized by, for instance, chemical modification of the edges. A bottom-up synthesis [1] is one of the promising approaches for obtaining edge-functionalized GNRs. In this study, we have attempted edge-fluorination of GNRs using the bottom-up approach.

Figure 1 shows an expected reaction scheme from precursor molecules of HFH-DBTA to HFH-7AGNRs. However, our scanning tunneling microscopy and X-ray photoelectron spectroscopy measurements indicate that the GNRs fabricated on Au(111) surface have no fluorinated edges and that the defluorination occurred during the cyclodehydrogenation process from the polyanthrylenes to the GNRs.

We calculated activation energies using the nudged elastic band method based on density functional theory to reveal the mechanism of the dissociation of the strong C-F bond. We have found that the activation energy of the direct F desorption from the polyanthrylenes or the GNRs to the metal surface is over 200 kJ/mol; however the activation energies are approximately 80 kJ/mol and 40 kJ/mol for the reactions of I0→I1 and I1→I2 (Fig. 2), respectively. The dissociation of the C-F bond can proceed along the reaction from I0 to I2 via I1 states during the cyclodehydrogenation process.

These results suggest that it is important to design precursors considering the structural transformation during the reaction process for synthesizing edge-functionalized GNRs.

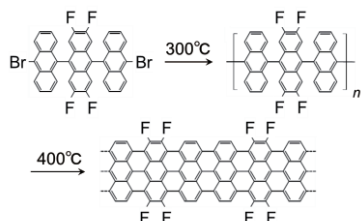


Fig. 1: Reaction scheme from precursors of HFH-DBTA to HFH-7AGNR.

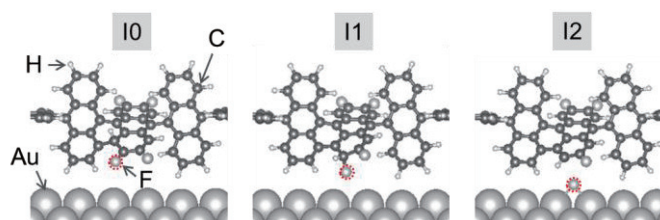


Fig. 2: Optimized geometries of the intermediate states of I0, I1, and I2 along the C-F dissociation path.

This work was partly supported by JST, CREST.

[1] J. Cai *et al.*, Nature 466, 470 (2010).

Corresponding Author: H. Jippo, Tel: +81-46-250-8843, E-mail: jippo.hideyuki@jp.fujitsu.com

## Low temperature growth of fully covered single layer graphene using CoCu catalyst

○Hisashi Sugime<sup>1,2</sup>, Lorenzo D'Arsiè<sup>2</sup>, Robert S. Weatherup<sup>2</sup>, Santiago Esconjauregui<sup>2</sup>, Guofang Zhong<sup>2</sup>, Xingyi Wu<sup>2</sup>, John Robertson<sup>2</sup>

<sup>1</sup> Waseda Institute for Advanced Study, Waseda University, Tokyo 169-8050, Japan

<sup>2</sup> Department of Engineering, University of Cambridge, Cambridge CB3 0FA, UK

Chemical vapour deposition (CVD) has emerged as the most scalable technique to grow large area graphene for industrial applications, and improving the growth method for high quality single layer graphene (SLG) is required. Lowering the growth temperature is a key requirement especially when the graphene is grown directly on devices. Cu is the most commonly used catalyst to grow SLG [1], able to produce complete coverage SLG with the average grain size in the millimetre-scale [2]. Although its low carbon solubility plays an important role for the growth of uniform SLG, the low catalytic activity makes it necessary to use high growth temperature, typically  $\sim 1000^\circ\text{C}$ . On the other hand, Ni or Co are well known catalysts for the low temperature growth of carbon nanotubes due to their high catalytic activity [3]. They are supposed to be applied for the low temperature graphene growth, however the higher carbon solubility of Ni or Co compared to Cu promotes multilayer graphene growth [4].

Here we investigate the growth of SLG on bimetallic CoCu alloy catalyst films. The growth outcome is found to vary significantly as the Cu concentration is changed. At  $700 - 750^\circ\text{C}$ , the addition of  $\sim 1$  at% Cu to Co leads to uniform SLG growth and suppresses the multilayer formation, typically observed using pure Co. X-ray photoemission spectroscopy (XPS) shows Co and Cu form an alloy at high temperatures, which has a drastically lower carbon solubility, as determined by the calculated Co-Cu-C ternary phase diagram. By Raman characterisation, we observe CoCu-catalysed graphene presents high quality and spatial uniformity across large catalyst surface. The fully covered single layer graphene shows hole mobilities as high as  $\sim 1,100 \text{ cm}^2 \text{ V}^{-1} \text{ s}^{-1}$  in ambient conditions, suggesting bimetallic catalysts may pave the way to produce graphene with tailored properties [5].

[1] X.S. Li, et al., *Science* **324**, 1312 (2009).

[2] X.Y. Wu, et al., *Sci. Rep.* **6**, 21152 (2016).

[3] J. Robertson, et al., *Jpn. J. Appl. Phys.* **51**, 01AH01 (2012).

[4] Q. Yu, et al., *Appl. Phys. Lett.* **93**, 113103 (2008).

[5] H. Sugime et al., *in preparation*.

Corresponding Author: H. Sugime

Tel: +81-3-5286-2769

E-mail: sugime@aoni.waseda.jp

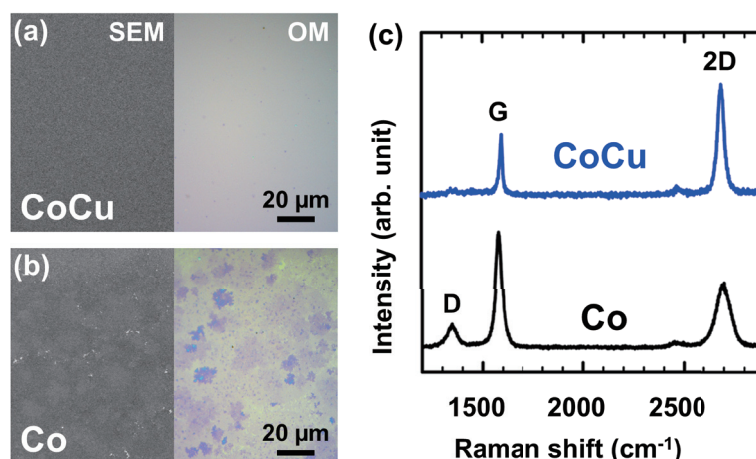


Fig. 1: SEM and OM images of fully covered graphene grown on (a) CoCu (Cu: 6 nm on Co: 500 nm) and (b) Co (500 nm) catalyst. (c) Representative Raman spectra of the samples shown in (a) and (b). The scale bars in OM images (a, b) are common for SEM images.

## Fabrication of a thermally stable SERS substrate using bilayer graphene

○Seiya Suzuki, Masamichi Yoshimura

*Graduate School of Engineering, Toyota Technological Institute, Nagoya 468-8511, Japan*

Surface enhanced Raman scattering (SERS) technique is a novel method to highly sense molecular and lattice vibrations. Although nanostructured silver (Ag) surface provides the most intense SER signals [1], Ag is not chemically stable compared to gold which is another representative element for SERS. Graphene has very high chemical and thermal stability. We previously demonstrated that a graphene coated Ag nanoparticles show SERS with tolerance for strong acids (hydrogen chloride) [2]. Here, we report that bilayer graphene (BLG) can serve high thermal stability to nanostructured Ag surface for SERS.

A 10 nm thick Ag thin film was deposited on a quartz substrate by vacuum evaporation. Graphene, which consists of mainly single layer and partially bilayer, was grown by atmospheric pressure chemical vapor deposition on a Cu foil [3], and was transferred onto the Ag/quartz substrate with a polymethyl methacrylate (PMMA) supporting layer. The PMMA was removed by immersing in an organic mixture (acetone, methyl isobutyl ketone, and isopropyl alcohol) and heating in air at 350 °C. To examine thermal durability of the graphene coated Ag on quartz (graphene/Ag/quartz), the sample was heated at 800 °C in vacuum (<2 Pa). Subsequently, rhodamine 6G (R6G) was loaded by dropping and drying of 20  $\mu$ L solution (50 nM). Raman spectra were obtained using a 532 nm laser after each step of sample preparation (removal of PMMA, heating at 800 °C, and R6G deposition).

Figure 1(a) shows an optical microscope image of the graphene/Ag/quartz after heating at 800 °C in vacuum. The hexagonal BLG domain showed bright contrast. Enhancements of Raman peaks of graphene (D, G, and G' peaks) were only observed in the BLG domain but not in single layer (SLG) region, and D peak was appeared in the entire graphene after the heating. These indicate that the Ag underneath BLG was remained, while the other Ag was evaporated by the heating through defects in the top layer (Fig. 1(b)).

Figure 1(c) shows Raman spectra from different sample. The BLG/Ag/quartz shows very large Raman peaks of graphene and the observed enhancement factor of G' peak is  $\sim 43$ . The R6G/BLG/Ag shows strong Raman peaks of R6G (indicated by arrows in Fig. 1(c)) implying that the BLG/Ag/quartz has SERS ability after high temperature heating (800 °C) in vacuum.

[1] K. Kneipp *et al.*, “Surface-Enhanced Raman Scattering”, Springer (2006).

[2] S. Suzuki and M. Yoshimura, “Graphene coated silver substrate for SERS with acid tolerance”, FNTG51 (2016).

[3] S. Suzuki *et al.*, e-J. Surf. Sci. Nanotech. **13**, 404 (2015).

Corresponding Author: Seiya Suzuki

Tel: +81-52-809-1852, E-mail: seiya09417@gmail.com

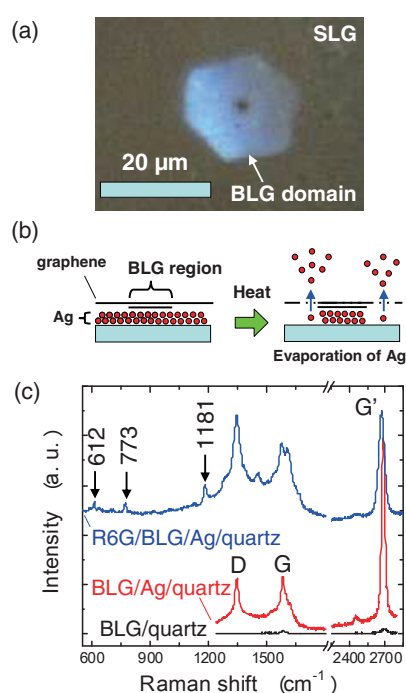


Fig. 1. (a) Optical microscope image of the graphene/Ag/quartz after the heating. (b) Schematic model of evaporation of Ag by heating. (c) Raman spectra of BLG/quartz, BLG/Ag/quartz, and R6G/BLG/Ag/quartz.

ポスター発表  
**Poster Preview**

**1P-1 ~ 1P-42**

**2P-1 ~ 2P-43**

**3P-1 ~ 3P-42**

## Photochemical Addition of Siliranes to $\text{Sc}_3\text{N}@I_h\text{-C}_{80}$ : Interconversion of the [6,6]- and [5,6]-Adducts

○Takeshi Sugiura<sup>1</sup>, Kyosuke Miyabe<sup>1</sup>, Masahiro Kako<sup>\*,1</sup>, Masanori Yasui<sup>1</sup>,  
 Michio Yamada<sup>2</sup>, Yutaka Maeda<sup>2</sup>, Jingdong Guo<sup>3</sup>,  
 Shigeru Nagase<sup>3</sup>, Takeshi Akasaka<sup>2,4,5</sup>

<sup>1</sup>Department of Engineering Science, The University of Electro-Communications, Chofu, Tokyo 182-8585, Japan

<sup>2</sup>Department of Chemistry, Tokyo Gakugei University, Tokyo 184-8501, Japan

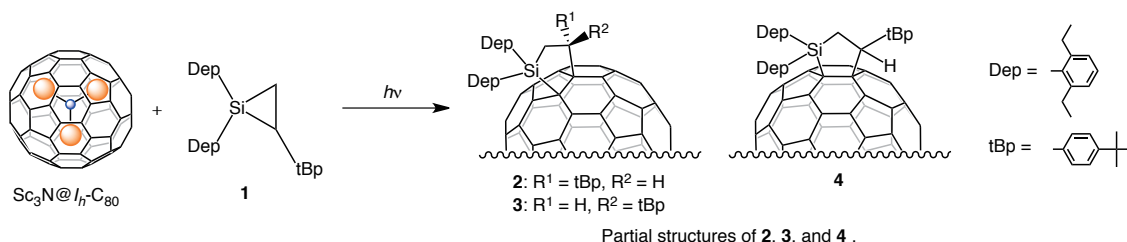
<sup>3</sup>Fukui Institute for Fundamental Chemistry, Kyoto University, Kyoto 606-8103, Japan

<sup>4</sup>Life Science Center of Tsukuba Advanced Research Alliance, University of Tsukuba, Tsukuba, Ibaraki 305-8577, Japan

<sup>5</sup>Foundation for Advancement of International Science, Ibaraki 305-0821, Japan

Functionalization of endohedral metallofullerenes (EMFs) has been explored extensively to broaden their range of potential applications in biochemistry, nanomaterial science, and molecular electronics. Among the many functionalizing reactions, 1,3-dipolar cycloaddition of azomethine ylides has been frequently employed as a versatile method to afford the corresponding pyrrolidino derivatives [1]. For example, the addition of azomethine ylides to  $\text{Sc}_3\text{N}@I_h\text{-C}_{80}$  affords the corresponding [5,6]- and [6,6]-adducts. Several mechanistic studies indicated that the reactions of azomethine ylides initially produce the [6,6]-adducts, which subsequently isomerize to the thermodynamically stable [5,6]-adducts. As these reactions are generally conducted in heated or refluxed solutions, the substantial [6,6] to [5,6] isomerization of adducts should occur during the addition of azomethine ylides. To the best of our knowledge, the example of the isolation of [6,6]-pyrrolidino- $\text{Sc}_3\text{N}@I_h\text{-C}_{80}$  has been limited to the synthesis using *N*-tritylazomethine ylide [2]. Meanwhile, we reported the preliminary results of the photochemical carbosilylation of  $\text{Sc}_3\text{N}@I_h\text{-C}_{80}$  [3]. We now report the details of the photoreaction of  $\text{Sc}_3\text{N}@I_h\text{-C}_{80}$  with silirane **1**, which afforded the corresponding [5,6]-adducts **2**, **3**, and the [6,6]-adduct **4**. Furthermore, the interconversion of **2**, **3**, and **4** took place at 100 °C. The relative stabilities of these adducts are consistent with the result obtained by the density functional theory calculations.

### Scheme 1.



[1] M. Prato *et al.* *J. Am. Chem. Soc.* **115**, 9798–9799 (1993).

[2] H. C. Dorn *et al.* *J. Am. Chem. Soc.* **128**, 6486–6492 (2006).

[3] M. Kako *et al.* *Phosphorus, Sulfur, and Silicon and the Related Elements.* **191**, 201–206 (2016).

Corresponding Author: Masahiro Kako Tel: +81-42-442-5570 E-mail: [kako@e-one.uec.ac.jp](mailto:kako@e-one.uec.ac.jp)

## Conclusive Characterization of Li@C<sub>60</sub> by X-ray Structure Analysis

○Hiroshi Ueno<sup>1</sup>, Shinobu Aoyagi<sup>2</sup>, Naohiko Ikuma<sup>3</sup>, Hiroshi Okada<sup>4</sup>, Kei Ohkubo<sup>5</sup>,  
Tatsuhisa Kato<sup>6</sup>, Shunichi Fukuzumi<sup>7,8</sup>, Yutaka Matsuo<sup>1,4,9</sup>, Ken Kokubo<sup>3</sup>

<sup>1</sup>Department of Chemistry, Northeast Normal University, Changchun, Jilin 130024, China

<sup>2</sup>Department of Information and Basic Science, Nagoya City University, Mizuho-ku, Nagoya 467-8501, Japan

<sup>3</sup>Division of Applied Chemistry, Graduate School of Engineering, Osaka University, Suita, Osaka 565-0871, Japan

<sup>4</sup>Department of Mechanical Engineering, The University of Tokyo, Tokyo 113-8656, Japan

<sup>5</sup>Division of Innovative Research for Drug Design Institute of Academic Initiatives, Osaka University, Suita, Osaka 565-0871, Japan

<sup>6</sup>Department of Interdisciplinary Environment, Graduate School of Human and Environment Studies, Kyoto University, Sakyo-ku, Kyoto 606-8501, Japan

<sup>7</sup>Department of Chemistry and Nanoscience, Ewha Womans University, Seoul 120750, Korea

<sup>8</sup>Faculty of Science and Engineering, Meijo University, and SENTAN, Japan Science and Technology (JST), Nagoya, Aichi 468-0073, Japan

<sup>9</sup>Hefei National Laboratory for Physical Sciences at Microscale, University of Science and Technology of China, Hefei, Anhui 230026, China

Endohedral metallofullerenes (EMFs) are one of the best studied materials for the past 30 years. Among all EMFs, C<sub>60</sub>-based EMFs are attracted special attention owing to its highly symmetrical structure and expected unique electronic properties. Due to the difficulty of their isolation and the lack of the structural evidences especially by the X-ray structure analysis, however, the studies on metallo[60]fullerenes are much stagnant. Although previously we have succeeded the isolation of Li@C<sub>60</sub>,<sup>[1]</sup> the X-ray structure analysis has been never achieved yet.

The Li@C<sub>60</sub> was synthesized by the electrochemical reduction of cationic Li<sup>+</sup>@C<sub>60</sub>.<sup>[2-4]</sup> The appropriate single crystal for X-ray structure analysis was obtained by the electrochemical reaction in the presence of NiOEP. As shown in Fig. 1, dimerized structure which could be formed by the coupling of spin centers of Li@C<sub>60</sub>s were determined. This is the first report of C<sub>60</sub>-based EMF characterized by X-ray structure analysis. The details will be discussed on the presentation.

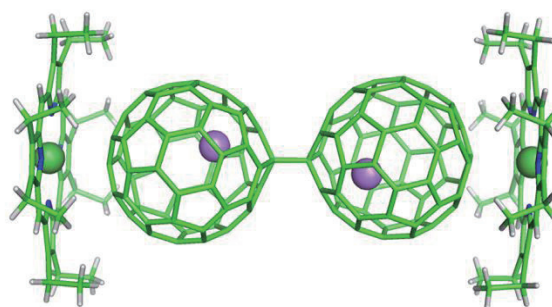


Fig. 1. Crystal structure of Li@C<sub>60</sub>-NiOEP co-crystal measured at 100 K.

[1] H. Ueno *et al.*, *The 46<sup>th</sup> FNTG general symposium* (2014) 3P-3.

[2] S. Aoyagi *et al.*, *Nature Chem.* **2010**, 2, 678.

[3] H. Ueno *et al.*, *Chem. Commun.* **2013**, 49, 7376.

[4] H. Ueno *et al.*, *Chem. Sci.* **2016**, 7, 5770.

Corresponding Author: H. Ueno and Y. Matsuo

Tel: +81-3-5841-0978, E-mail:ueno@photon.t.u-tokyo.ac.jp; matsuo@photon.t.u-tokyo.ac.jp

## Diameter and defect density dependence of intermediate frequency Raman mode of single-walled carbon nanotubes

○Takumi Inaba<sup>1</sup>, Satoru Konabe<sup>2</sup>, and Yoshikazu Homma<sup>1,2</sup>

<sup>1</sup> *Department of Physics, Tokyo University of Science, Kagurazaka 1-3, Shinjuku Tokyo 162-8601, Japan*

<sup>2</sup> *Research Institute of Science and Technology, Tokyo University of Science, Niijuku 6-3-1, Katsushika Tokyo 125-8585, Japan*

Raman spectroscopy provides fruitful information of lattice structures. For the Raman spectroscopy of SWCNTs, not only graphene originated Raman modes but also nanotube exclusive modes such as the radial breathing mode and G<sup>-</sup> mode can be observed. Besides those peaks including the D mode that originates from finite momentum phonon, Raman emission peaks exist in the range of intermediate frequency (IFM, 300-1000 cm<sup>-1</sup>), which were not fully analyzed with single molecule spectroscopy level. Here, the results of Raman spectroscopy for singly suspended SWCNTs are shown in order to discuss Raman emission in the IFM range.

In our experiments, individual SWCNTs suspended between micropillars were used. After the synthesizing suspended SWCNTs, Photoluminescence (PL) excitation map was acquired so that bundled effects were excluded. SWCNTs with relatively intense PL emission showed detailed Raman emission in IFM range (Fig.1). The Raman emission peak energy in the range of 1.50-1.55 eV showed chirality dependence indicating the signature of nanotube exclusive phonon mode. Furthermore, the intensity of this Raman emission increased as an increase in optical defect density.

Corresponding Author: T. Inaba

Tel: +81-3-5228-8244

E-mail: takumi.inaba.63@rs.tus.ac.jp

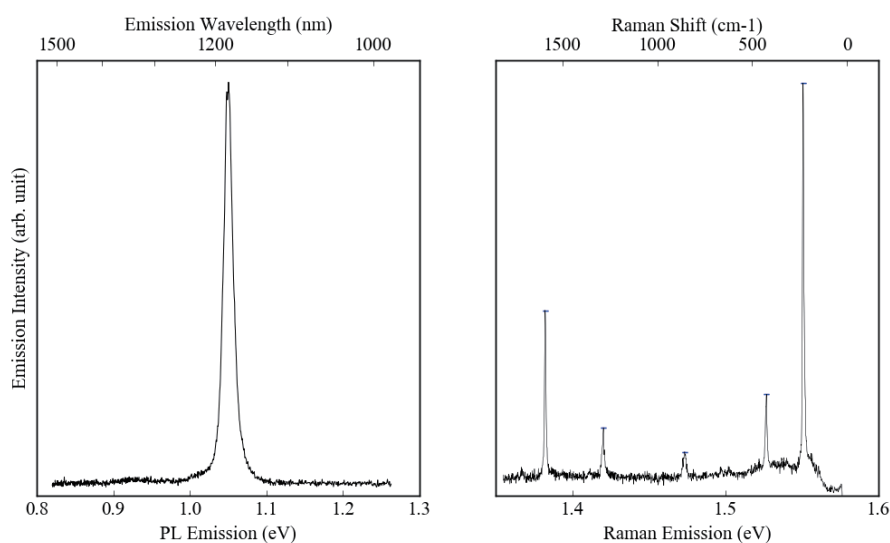


Figure 1. Photoluminescence (Left) and Raman (Right) simultaneous spectroscopy for a (11,3) nanotube with relatively intense PL emission.

## Spectral tuning of optical coupling between air-mode nanobeam cavities and individual carbon nanotubes

○Hidenori Machiya<sup>1,2</sup>, Takushi Uda<sup>1,3</sup>, Akihiro Ishii<sup>1,2</sup>, Yuichiro K. Kato<sup>1,4</sup>

<sup>1</sup> *Nanoscale Quantum Photonics Laboratory, RIKEN, Saitama 351-0198, Japan*

<sup>2</sup> *Department of Electrical Engineering, The University of Tokyo, Tokyo 113-8656, Japan*

<sup>3</sup> *Department of Applied Physics, The University of Tokyo, Tokyo 113-8656, Japan*

<sup>4</sup> *Quantum Optoelectronics Research Team, RIKEN center for Advanced Photonics, Saitama 351-0198, Japan*

Air-mode nanobeam cavities allow for high efficiency coupling to air-suspended carbon nanotubes due to their unique mode profile that has large electric fields in air [1]. Here we utilize heating-induced energy shift of carbon nanotube emission [2] to investigate the cavity quantum electrodynamics effects. In particular, we use laser-induced heating which causes a large blue-shift of the nanotube photoluminescence as the excitation power is increased. Combined with a slight red-shift of the cavity mode at high powers, detuning of nanotube emission from the cavity can be controlled. We estimate the spontaneous emission coupling factor  $\beta$  at different spectral overlaps and find an increase of  $\beta$  factor at small detunings, which is consistent with Purcell enhancement of nanotube emission.

Work supported by JSPS (KAKENHI JP26610080, JP16K13613), Asahi Glass Foundation, Canon Foundation, and MEXT (Photon Frontier Network Program, Nanotechnology Platform).

[1] R. Miura, S. Imamura, R. Ohta, A. Ishii, X. Liu, T. Shimada, S. Iwamoto, Y. Arakawa, and Y. K. Kato, *Nature Commun.* **5**, 5580 (2014).

[2] P. Finnie, Y. Homma, and J. Lefebvre, *Phys. Rev. Lett.* **94**, 247401 (2005).

Corresponding Author: Yuichiro K. Kato

Tel: +81-48-462-1111 (ext. 3432)

E-mail: [yuichiro.kato@riken.jp](mailto:yuichiro.kato@riken.jp)

## Tuning of Photo-thermoelectric effect of Metallic and Semiconducting Single wall carbon nanotube thin films by electrolyte gating

○Masatoshi Nakamura<sup>1</sup>, Yota Ichinose<sup>1</sup>, Hideki Kawai<sup>1</sup>, Yohei Yomogida<sup>1</sup>, Kazuhiro Yanagi<sup>1</sup>

<sup>1</sup> Department of Tokyo Metropolitan University, Tokyo 192-0397, Japan

Photo-thermoelectric (PTE) process is a process that can generate photo-voltage through thermoelectric properties of materials. In this processes, increase of electron temperature caused by absorption of light can be converted to the electricity through thermoelectric properties of materials. In the field of nano-carbon materials, because of their small heat capacity, this process has often been observed, for example photo-voltage generations from PTE effects have been reported in carbon nanotubes, graphene, transition-metal di-chalcogenides and so on. Especially, in the case of carbon nanotubes, they can absorb THz light energy because of the presence of their longitudinal surface plasmon modes, thus, PTE process attracts a lot of interest for applications toward THz light detection devices. The PTE processes strongly depend on the thermoelectric performance of SWCNTs, and previously we have succeeded to tune the thermoelectric properties of SWCNT using electrolyte gating techniques.[1] Here we tuned the PTE performance of SWCNTs using electrolyte gating techniques. Figure 1 indicates the generated PTE voltages of metallic and semiconducting SWCNTs with diameter of 1.4 nm as a function of shift of reference voltage ( $V_r$ ). As show here, the PTE voltages of metallic SWCNTs increased as the increase of the amount of injected carriers in both electron and hole regions. It has been considered that the metallic SWCNTs are useless for PTE devices because of their small Seebeck coefficient. However, the observation indicates the PTE voltage can be enhanced by carrier injections. We found that high-carrier injections induced large Seebeck coefficient and then large PTE voltages. The fact suggests the breaking of the thermoelectric trade-off, in which increase of conductivity induces decrease of Seebeck coefficient.

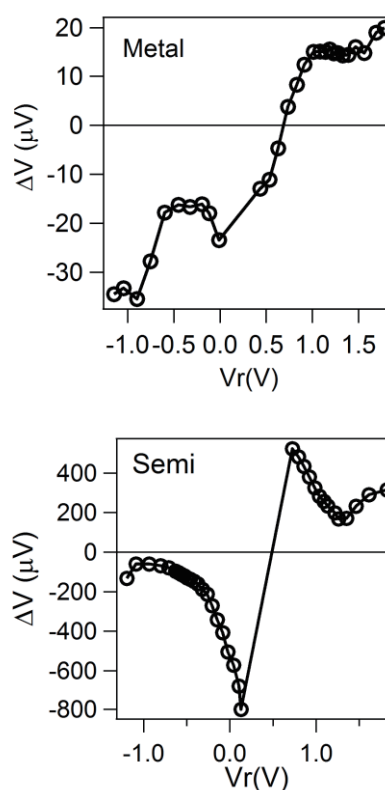


Fig1. Relationships between photovoltage and reference voltage of Metal, Semi

References: [1] Yanagi et al, *Nano Lett.* 14, 6437-6442 (2014), Oshima et al, *APL* 107, 043106 (2015)

Corresponding Author: K. Yanagi

Tel: +81-42-677-2493, E-mail: yanagi-kazuhiro@tmu.ac.jp

## Photoluminescence Characteristic of Single-Wall Carbon Nanotubes: Photon Reabsorption Effect

○Xiaojun Wei<sup>1</sup>, Mayumi Tsuzuki<sup>1</sup>, Yohei Yomogida<sup>2</sup>, Guowei Wang<sup>1</sup>, Atsushi Hirano<sup>1</sup>,  
Shunjiro Fujii<sup>1</sup>, Takeshi Tanaka<sup>1</sup>, and Hiromichi Kataura<sup>1</sup>

<sup>1</sup> *Nanomaterials Research Institute, National Institute of Advanced Industrial Science and Technology (AIST), Tsukuba, Ibaraki 305-8565, Japan*

<sup>2</sup> *Department of Physics, Tokyo Metropolitan University, Tokyo 192-0397, Japan*

Semiconducting single-wall carbon nanotubes (SWCNTs) exhibit  $(n,m)$ -specific near-infrared  $E_{11}$  photoluminescence (PL) via  $E_{22}$  excitation. By assigning this pair of  $E_{11}$  and  $E_{22}$  wavelengths, we can identify individual  $(n,m)$  species contained in the examined samples. In PL measurement, the PL intensity is also important to deduce the abundance of specific  $(n,m)$  species in the as-grown mixture or  $(n,m)$ -sorted sample. It is important to note that the experimentally measured PL intensity does not correspond to the true intensity due to photon reabsorption effect [1]. The detailed analysis of the PL characteristic induced by photon reabsorption is very significant for quantitatively evaluating the abundance of specific  $(n,m)$  species.

In this study,  $(n,m)$ -sorted semiconducting SWCNTs suspended in 0.5% sodium cholate (SC) solution were prepared by gel chromatography. To modulate photon reabsorption, the SWCNT concentration of each  $(n,m)$  sample was gradually increased. We confirmed that the  $E_{11}$  absorbance increased linearly with increasing SWCNT concentration for all  $(n,m)$  SWCNTs, while the PL intensity exhibited a nonlinear change. Figure 1 shows the results of the PL intensity normalized by  $E_{22}$  absorbance for near-armchair (7,6) and zigzag (10,0) SWCNTs with the same  $2n+m$  value, as a function of each  $E_{11}$  absorbance (SWCNT concentration). After magnifying the intensities of (10,0) samples 5 times, the trend of the nonlinear change of (10,0) samples is consistent with that of (7,6). It suggests that (7,6) SWCNTs is 5 times the PL efficiency of (10,0). For both (7,6) and (10,0) SWCNTs, photon reabsorption probability was gradually increased with increasing SWCNT concentration, leading to this nonlinear intensity change. We also investigated the photon reabsorption induced PL characteristics of other  $(n,m)$  species and found that individual  $(n,m)$  SWCNTs have the same photon reabsorption characteristic, but their PL efficiencies are depending on  $(n,m)$  structures.

This work was supported by KAKENHI No. 25220602.

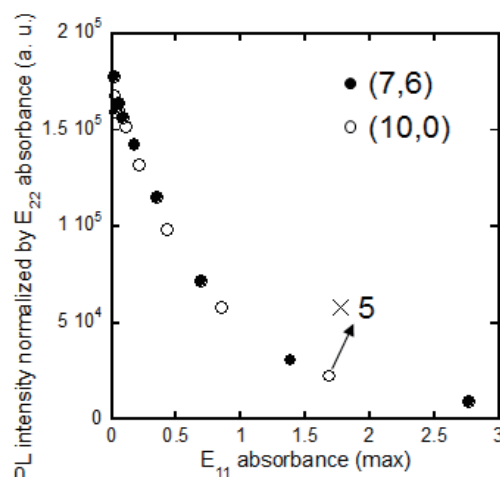


**Figure 1.** The plots of the PL intensity normalized by  $E_{22}$  absorbance for (7,6) (solid dots) and (10,0) (open dots) as a function of each  $E_{11}$  absorbance. All PL intensities of (10,0) were magnified 5 times for comparing that of (7,6).

[1] T. S. Ahn *et al.*, *Rev. Sci. Instrum.* **78**, 086105 (2007).

Corresponding Author: H. Kataura

Tel: +81-29-861-2551, Fax: +81-29-861-2786, E-mail: h-kataura@aist.go.jp

**Surface state of carbon nanopot –KFM study-**

○Hiroyuki Yokoi<sup>1</sup>, Kozo Ikeda<sup>2</sup>, Kazuto Hatakeyama<sup>1</sup>, Michio Koinuma<sup>1</sup>

<sup>1</sup> Faculty of Advanced Science and Technology, Kumamoto University, Kumamoto 860-8555, Japan

<sup>2</sup> Faculty of Engineering, y, Kumamoto University, Kumamoto 860-8555, Japan

Carbon nanopot, a novel material developed recently[1], is a pot-shaped material composed with multi-layered graphene sheets, and is produced in series to form fibers (nanopot fibers). The typical size of carbon nanopot is 20-40 in diameter and 100-200 nm in length. Its narrow and deep mesopore is closed on one end, which suggests that this material could be applied as nano-container.

It has been revealed through high-resolution TEM studies that carbon nanopot consists of several parts including a multi-wall CNT like part and a tapered part where graphene edges are exposed and distributed densely. Furthermore, an XPS study has suggested that those graphene edges may be terminated by hydroxyl groups. We expect that the surface states in the MWCNT-like part and those in the tapered part could be different. In this study, we employed a Kelvin force microscope (KFM) to investigate local surface states of carbon nanopot. We have obtained a result that the surface potential varies by about 7 mV between the ends of nanopot and the middle of the tapered part. We tentatively attribute this variation of the local potential to the difference of surface morphology, i.e. graphene wall-like surface or surface with densely exposed and OH-terminated graphene edges.

[1] H. Yokoi *et al.* J. Mater. Res., **31**, 117-126 (2016).

Corresponding Author: H. Yokoi

Tel: +81-96-342-3727, Fax: +81-96-342-3710,

E-mail: yokoihr@kumamoto-u.ac.jp

## Anion effects on colloidal stability of surfactant-dispersed SWCNTs

○Atsushi Hirano<sup>1</sup>, Weilu Gao<sup>2</sup>, Xiaowei He<sup>2</sup>, Junichiro Kono<sup>2,3,4</sup>

<sup>1</sup> *Nanomaterials Research Institute, National Institute of Advanced Industrial Science and Technology (AIST), Tsukuba, Ibaraki 305-8562, Japan*

<sup>2</sup> *Department of Electrical and Computer Engineering, Rice University, Houston, Texas 77005, USA*

<sup>3</sup> *Department of Physics and Astronomy, Rice University, Houston, Texas 77005, USA*

<sup>4</sup> *Department of Materials Science and NanoEngineering, Rice University, Houston, Texas 77005, USA*

The colloidal stability of surfactant-dispersed single-wall carbon nanotubes (SWCNTs) is reflected in microscopic physicochemical processes, such as SWCNT association, partitioning into a biphasic system, and adsorption propensities onto hydrogels. These processes can be controlled by the addition of salts due to the alteration of the colloidal stability. Previous studies clarified the effects of cations on the colloidal stability of the SWCNTs [1], whereas the effects of anions remain unclear. Here, we show the anion effects on the SWCNTs dispersed by sodium dodecyl sulfate (SDS) using sodium salts, such as NaCl and NaSCN.

We observed that Raman spectral intensity in the radial breathing mode of the SWCNTs tended to decrease with increasing salt concentration (Fig.1), even at concentrations less than 25 mM, which is consistent with the reported results concerning SWCNT association [2,3]. Importantly, the effect was stronger with NaSCN than with NaCl, which means NaSCN more readily causes the SWCNT association. We attribute this association to thermodynamic destabilization of SDS assemblies on the SWCNTs by the salts (Fig.2) [4], which was further confirmed through SWCNT separation experiments using a biphasic system and gel chromatography. These findings provide a basis for understanding the colloidal behavior of surfactant-dispersed SWCNTs and for developing the separation technology of SWCNTs.

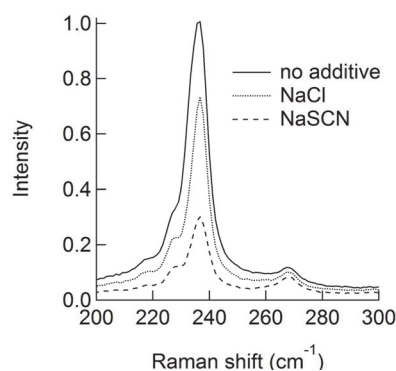


Fig.1 Raman spectra of the SDS-dispersed SWCNTs excited at 785 nm in 25 mM salt solutions.

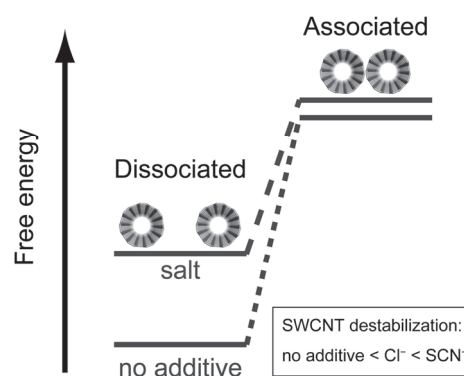


Fig.2 Schematic diagrams of the free energy of the SDS-dispersed SWCNTs in the salt solutions

- [1] S. Niyogi *et al.* *J. Am. Chem. Soc.* **131**, 1144 (2009).  
 [2] M.S. Strano *et al.* *J. Nanosci. Nanotechnol.* **3**, 81 (2003).  
 [3] D.A. Heller *et al.* *J. Phys. Chem. B* **108**, 6905 (2004).  
 [4] S. Ikeda *et al.* *J. Phys. Chem.* **85**, 106 (1981).

Corresponding Author: A. Hirano

Tel: +81-29-849-1064, Fax: +81-29-861-2786,

E-mail: hirano-a@aist.go.jp

## Paper-based carbon nanotube field effect transistor by photolithography

○Jong Mok Shin, Do Hyun Kim, InYeob Na, Ho-Kyun Jang, Jun Hee Choi, So Jeong Park,  
Gyu-Tae Kim

*School of Electrical Engineering, Korea University, Seoul 02841, South Korea*

Paper electronic devices are emerging as a new research topic in accordance with the increasing needs for eco-friendly materials.[1] Generally, the shadow mask[2] or ink-jet printing[3] method is used to pattern the metal contacts of the channel devices on a paper substrate, but it has a limit in reducing the pattern size. On the other hand, the photolithography method frequently used in the conventional substrates can be utilized for realizing the design beyond the bounds of the shadow mask process. In this work, the carbon nanotube field effect transistor was fabricated on the paper substrate through the photolithography process. To avoid wetting paper, the paper cups designed to contain water were used as the base substrates without any additional water-repellent treatment. However, it was difficult to deposit the liquid material including photoresist by spin coating method since the paper was hydrophobic. Thus, the argon plasma treatment was carried out on the paper to change the substrate from hydrophobic to hydrophilic. In the presentation, the device characteristics of carbon nanotube field effect-transistors on paper substrates will be shown.



Fig.1 Conventional paper cup

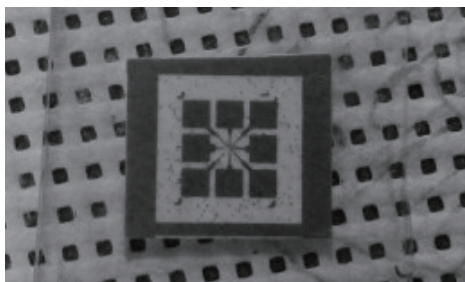


Fig.2 Paper based field effect transistor patterned by photolithography.

Beyond photolithography techniques, electron beam lithography techniques can also be applied to paper substrates. This will enable the fabrication of nano-sized electronic devices smaller than micro-sized devices on paper substrates. With these methods, the device will could be freely manufactured as it is processed on silicon substrates.

[1] D. Tobjork *et al.* Adv. Mater. **23**, 1935 (2011)

[2] Y. Li *et al.* Organic Electronics **13**, 815 (2012)

[3] X. Li *et al.* Collids and Surfaces B: Biointerfaces **76**, 564 (2010)

Corresponding Author: Jong Mok Shin

Tel: +82-10-2951-4530, Fax: +82-2-953-3780,

E-mail: jmshin89@korea.ac.kr

## Doping effect of electrolyte droplet on carbon nanotube thin film

○Tomohiro Yasunishi<sup>1</sup>, Shigeru Kishimoto<sup>1</sup>, and Yutaka Ohno<sup>1,2</sup>

<sup>1</sup> Graduate school of Engineering, Nagoya University, Nagoya 464-8603, Japan

<sup>2</sup> Institute of Materials and Systems for Sustainability, Nagoya University, Nagoya 464-8603, Japan

Energy harvesting from environment energy sources is emerging technology for driving sensor devices for IoT. Recently, the voltage generation of a few millivolts from the movement of electrolyte solution have been demonstrated by using graphene [1, 2] and carbon nanotubes (CNTs) [3]. Previously, we fabricated the generator using the single-walled CNT thin film on flexible substrate and proposed the simple model of voltage generation mechanism on the basis of their characteristics such as the dependences on concentration of electrolyte solution. In this work, we have investigated the doping effect of electrolyte solution on the CNT film by using Raman scattering spectroscopy.

Highly-conductive CNT thin films were formed on a quartz substrate by the dry transfer process based on the floating-catalyst chemical vapor deposition [4]. NaCl aqueous solution of 0.01 mol/l was used as the electrolyte. The Pt electrode was used as the counter electrode to apply the potential difference between the CNT film and electrolyte droplet (Fig. 1(a)). We measured Raman scattering spectroscopy through the quartz substrate at various potential differences. The line mapping measurement was carried out across the edge of electrolyte droplet.

When the counter electrode potential increased from 0V to 0.9 V, the G-peak shifted to smaller wave number in the region covered by the electrolyte solution as shown in Fig. 1(b). It is known that G-peak frequency depends on carrier density in the CNT film [5]. Even when the Pt electrode was electrically open, G-peak frequency shifted as much as the case under voltage of  $\sim 0.2$  V. This result shows the contact to the electrolyte solution has an doping effect on the CNT film.

[1] P. Dhiman *et al.*, Nano Lett. **11**, 3123, (2011).

[2] J. Yin *et al.*, Nat. Nanotechnol. **9**, 378, (2014).

[3] S. Ghosh *et al.*, Science **299**, 1042 (2003).

[4] A. Kaskela *et al.*, Nano Lett. **10**, 4349 (2010).

[5] J. C. Tsang *et al.*, Nature Nanotechnol. **2**, 725 (2007).

Corresponding Author: Y. Ohno

Phone & Fax: +81-52-789-5387,

E-mail: yohn@nagoya-u.jp

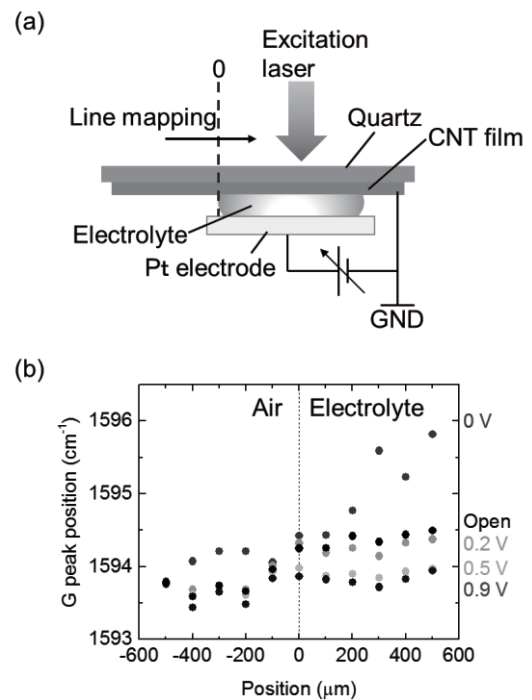


Fig. 1 (a) Schematic of measured device. (b) G-peak position versus position at various potential differences.

## Development of CNT/Polyethylene Composites *via* Melt Blending

○Atsushi Onodera<sup>1</sup>, Sami Ristimäki<sup>2</sup>, Masaru Sekido<sup>3</sup>

<sup>1</sup> *Advanced Course of Production System Engineering, National Institute of Technology, Sendai College, Natori 981-1239, Japan*

<sup>2</sup> *Machine Automation, Metropolia University of Applied Sciences, Finland*

<sup>3</sup> *Department of Materials Science and Engineering, National Institute of Technology, Sendai College, Natori 981-1239, Japan*

Resin composites are used as structural materials in airplanes, helicopters and so on. Adding CNTs to resin nanocomposites may increase various properties of resin composites, such as high tensile strength, high thermal conduction, and high electric conduction. Previously we have reported that tensile strength of MWNT/Nylon 6 (PA-6) prepared by simple melt-blending was increased [1]. In this work we have prepared CNT/Polyethylene (PE) and functionalized-CNT (f-CNT) /PE composite and studied the effect on tensile strength.

f-CNTs were prepared by using 1,3-dipolar cycloaddition reaction. The mixture of SWNT (0.5 g), sarcosine (1.5 g), and 3,4-dihydroxybenzaldehyde (1.5 g) in DMF were refluxed. After 3 days DMF was removed by rotary evaporator and remaining powder were washed by water and acetone to obtain f-SWNT (2.0 g). CNT/PE composites were prepared by melt blending at 220 °C for 10 minutes. Tensile strength of CNT/ PE composites were measured by tension tester (Dak System Inc., UTB9052-TT).

The result of tensile strength is shown in table 1. Tensile strength of SWNT/PE (entry 2 and 7), f-SWNT/PE (entry 3 and 8), MWNT/PE (entry 4 and 9), and f-MWNT/PE (entry 5 and 10) were compared with HDPE (entry 1) and LDPE (entry 6) and did not show the improvement as expected. However, f-SWNT/LDPE composite showed a slight improvement of tensile strength.

**Table 1.** The result of tensile strength.

entry	CNT	PE	tensile strength (MPa)	entry	CNT	PE	tensile strength (MPa)
1	Non	HD	27.2659 ± 1.2556	6	Non	LD	13.6884 ± 2.0841
2	SWNT	HD	25.6690 ± 1.3491	7	SWNT	LD	10.2684 ± 0.3321
3	f-SWNT	HD	25.4298 ± 0.6568	8	f-SWNT	LD	14.8636 ± 0.8021
4	MWNT	HD	25.6728 ± 1.4943	9	MWNT	LD	10.4611 ± 0.3560
5	f-MWNT	HD	26.0849 ± 1.1807	10	f-MWNT	LD	10.6018 ± 0.1663

[1] Yoshimi Muraoka *et al.* The 46th Fullerenes-Nanotubes-Graphene General Symposium, 3P-17(2014)

Corresponding Author: A. Onodera

Tel: +81-22-381-0329, Fax: +81-22-381-0329

E-mail: a1601008@sendai-nct.jp

## Defluorination-Assisted Synthesis of Nitrogen-Doped Single-Walled Carbon Nanotubes and Their Catalytic Activity of Oxygen Reduction Reaction for Polymer Electrolyte Fuel Cells

○Koji Yokoyama<sup>1</sup>, Shun Yokoyama<sup>1</sup>, Yoshinori Sato<sup>2</sup>, Masashi Yamamoto<sup>2</sup>, Tetsuo Nishida<sup>2</sup>, Kenichi Motomiya<sup>1</sup>, Hiromichi Ohta<sup>3</sup>, Hideyuki Takahashi<sup>1</sup>, Kazuyuki Tohji<sup>1</sup>, Yoshinori Sato<sup>1,4,\*</sup>

<sup>1</sup> Graduate School of Environmental Studies, Tohoku University, Sendai 980-8579, Japan

<sup>2</sup> Stella Chemifa Corporation, Osaka 595-0075, Japan

<sup>3</sup> Research Institute for Electronic Science, Hokkaido University, Sapporo 001-0020, Japan

<sup>4</sup> Institute for Biomedical Sciences, Interdisciplinary Cluster for Cutting Edge Research, Shinshu University, Matsumoto 390-8621, Japan

Nitrogen-doped single-walled carbon nanotubes (N-SWCNTs) are now focused on as excellent catalysts for oxygen reduction reaction (ORR) which can alternate for platinum-based catalysts<sup>[1]</sup>. In N-SWCNT catalysts, controlling structural factors such as nitrogen doping levels and the chemical states of doped nitrogen atoms (e.g. pyridinic-, pyrrolic-, and graphitic-types) is key to improving their ORR catalytic activities. However, in the existing methods for synthesizing N-CNTs based on “direct doping”, it is hard to control the above structural factors. Here, we report a new synthesis process for N-SWCNTs using defluorination-assisted “post-doping” approach<sup>[2]</sup>. Also, we evaluate the ORR catalytic activity of the prepared N-SWCNTs.

Highly crystalline SWCNTs (hc-SWCNTs) synthesized by an arc discharge method were fluorinated using a gas mixture of F<sub>2</sub> (20%) and N<sub>2</sub> (80%) at 250 °C for 4 h. The fluorinated SWCNTs were reacted with a gas mixture of NH<sub>3</sub> (1%) and N<sub>2</sub> (99%) at temperatures of 300–600 °C for 30 min. The nitrogen doping levels and chemical states of doped nitrogen atoms were characterized using X-ray photoelectron spectroscopy (XPS). Linear sweep voltammetry was performed to evaluate the ORR catalytic activity, using the RDE technique in 0.5 M H<sub>2</sub>SO<sub>4</sub>.

From the results of XPS analysis, their levels of nitrogen doping were estimated to be 1.38–3.04 at%, with enriched pyridinic- and pyrrolic-nitrogen species (Fig. 1). The onset potential value ( $E_{\text{onset}}$ ) and number of electrons transferred per oxygen molecule ( $n$ ) in ORR of the N-SWCNTs were +0.51 V and 3.31, while those of hc-SWCNTs were +0.16 V and 2.32, respectively (Fig. 2)<sup>[3]</sup>. These results clearly show that our defluorination-assisted post-nitrogen doping is more effective for introducing nitrogen atoms at high concentrations, and the prepared N-SWCNTs exhibit excellent ORR catalytic activity.

[1] D. Yu *et al.*, *J. Am. Chem. Soc.* **2010**, 132, 15127.

[2] K. Yokoyama *et al.*, *Carbon* **2015**, 94, 1052.

[3] K. Yokoyama *et al.*, *J. Mater. Chem. A* **2016**, 4, 9184.

\*Corresponding Author: Y. Sato

Tel & Fax: +81-22-795-3215, E-mail: yoshinori.sato.b5@tohoku.ac.jp

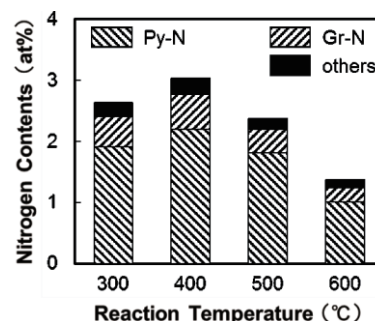


Fig. 1 Nitrogen contents and composition of the N-SWCNTs.

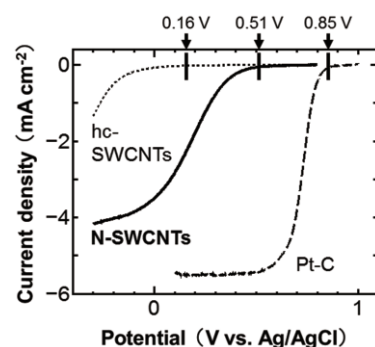


Fig. 2  $E_{\text{onset}}$  and  $n$  of hc-SWCNTs, N-SWCNTs, and Pt-C<sup>[3]</sup>.

## Film fabrication of Semiconducting Single-Wall Carbon Nanotubes by Aqueous-Two Phase System and Thin Film Transistor Applications

○Haruka Omachi,<sup>1</sup> Tomohiko Komuro,<sup>1</sup> Jun Hirotsu,<sup>2</sup> Yutaka Ohno,<sup>2,3</sup>  
and Hisanori Shinohara<sup>1\*</sup>

<sup>1</sup> Department of Chemistry & Institute for Advanced Research, Nagoya University, Nagoya 464-8602, Japan. <sup>2</sup> Graduate School of Engineering, Nagoya University, Nagoya, 464-8603, Japan, <sup>3</sup> Institute of Materials and Systems for sustainability, Nagoya University, Nagoya, 464-8603, Japan

Semiconducting single-wall carbon nanotubes (s-SWCNTs) are promising materials for electronic devices [1]. However, because the conventional as-grown carbon nanotubes contain ca. 30 % metallic (m-) SWCNTs, separation is required to obtain high purity s-SWCNTs. Recently, a rapid and single-step aqueous two-phase (ATP) extraction [2] of highly enriched s-SWCNTs is demonstrated. The extraction with the combination of polyethylene glycol and polysaccharide yielded >95% purity of s-SWCNTs from arc-discharge samples.

In this work, we report the s-SWCNTs thin films fabrication and thin film transistor (TFT) applications. With high-purity s-SWCNTs currently separated, we succeeded to fabricate the uniform films (Figure 1). An extra addition of dispersants prevented a self-aggregation of extracted s-SWCNTs. The performance of the fabricated devices was improved by the dry etching process (Figure 2).

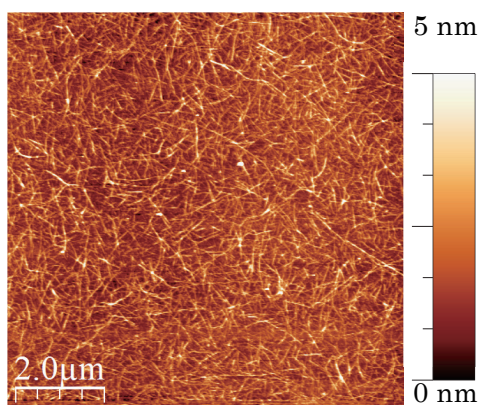


**Figure 1.** AFM image of extracted s-SWCNT film

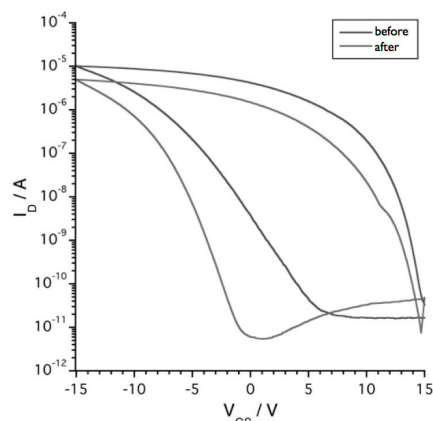


**Figure 2.** TFT device performances before and after the dry etching process

[1] D. Park *et al.*, *Appl. Phys. Lett.*, **82**, 2145 (2003)

[2] M. Zheng *et al.*, *J. Am. Chem. Soc.*, **135**, 6822 (2013)

Corresponding Author: Hisanori Shinohara

Tel: +81-52-789-2482, Fax: +81-52-747-6442

E-mail: noris@nagoya-u.jp

## Growth of Horizontally Aligned Chirality-Specific Single-Walled Carbon Nanotubes

○Feng Yang, Yan Li

*Beijing National Laboratory for Molecular Science, College of Chemistry and Molecular Engineering, Peking University, Beijing 100871, China*

High-performance and integrated circuits essentially require SWNT samples with well-aligned arrays of pure chirality [1]. Recently, employing tungsten-based intermetallic catalyst with high melting points and consequently are able to maintain their specific crystal structure during the chemical vapor deposition (CVD) process, which regulates the chirality of the grown SWNTs [2,3]. We have developed herein an approach for the growth of horizontally aligned chirality-specific SWNTs using uniform  $W_6Co_7$  nanoparticles as catalysts on the sapphire surface.

Using the uniform  $W_6Co_7$  nanoparticles as structural templated catalysts, we are able to grow the high abundance of the (18,7) SWNT arrays on the sapphire surface at the optimized growth condition. Our findings open up the possibility of the wafer-scale growth of aligned chirality-specific SWNTs by using uniform intermetallic nanoparticles as catalysts for practical nanoelectronics applications.

[1] A. D. Franklin. *Nature* **498**, 443 (2013).

[2] F. Yang, Y. Li *et al.* *Nature*. **510**, 522 (2014).

[3] F. Yang, Y. Li *et al.* *Acc. Chem. Res.* **49**, 606 (2016).

Corresponding Author: Yan Li

Tel: +86-10-6275-6773, Fax: +86-10-6275-6773,

E-mail: yanli@pku.edu.cn

## Fluidized-bed synthesis of sub-millimeter-long carbon nanotubes at high yield from concentrated ethylene source

°Soichio Hachiya, Zhongming Chen, Kosuke Kawabata,  
Kei Hasegawa, Toshio Osawa and Suguru Noda\*

*Department of Applied Chemistry, Waseda University, Tokyo 169-8555, Japan*

Fluidized-bed chemical vapor deposition (FBCVD) has realized mass production of carbon nanotubes (CNTs) [1] owing to the catalysts supported on powders which are filled in 3D in the reactor. Such CNTs, however, are entangled with catalyst powders. We previously reported submillimeter-long CNTs by FBCVD using 0.5-mm-sized alumina beads with flat surfaces, which enabled easy separation of CNTs ( $\geq 99$  wt%) from the beads [2–4]. Highly reactive  $C_2H_2$  was fed with  $H_2O$  at low concentrations and high flow rates. The process realized efficient conversion of  $C_2H_2$  at a carbon yield of 70% and residence time of  $\sim 0.3$  s, however, wasted a larger amount of the carrier gas than the carbon source gas.

We here report FBCVD synthesis of CNTs using less reactive  $C_2H_4$  and  $CO_2$  at higher concentration instead of  $C_2H_2$  and  $H_2O$  vapor to reduce the production cost by using cheaper carbon source and less carrier gas. We used smaller alumina beads (0.3 mm) for support to reduce the gas flow rate and increase the bead surface area so as to achieve high conversion of  $C_2H_4$ . Fe (1–5 nm)/Al (15 nm)/Fe (0.6 nm)/Al (15 nm) catalysts are deposited on the beads by sputtering. The catalyst is annealed by flowing 10 vol%  $H_2/N_2$  and then CNTs are synthesized by flowing 20 vol%  $C_2H_4/10$  vol%  $H_2/1$  vol%  $CO_2/N_2$  both by fluidized bed at 675–850 °C. The nominally 1 nm-thick Fe catalyst yielded single-wall CNTs at 204 mg/910 mg and 6.3 at%/28 at% using 10 g/30 g beads in 1 batch of 10 min at 850 °C (Fig. 1a,d). Whereas the nominally 5 nm-thick Fe thickness were deactivated 850 °C due to the tar formation. The catalyst worked efficiently at lower temperatures for longer period, yielding multi-wall CNTs at 244 mg/1025 mg and 2.5 at%/11 at% using 10 g/50 g beads in one batch of 30 min at 725 °C (Fig. 1a,b,c,e).

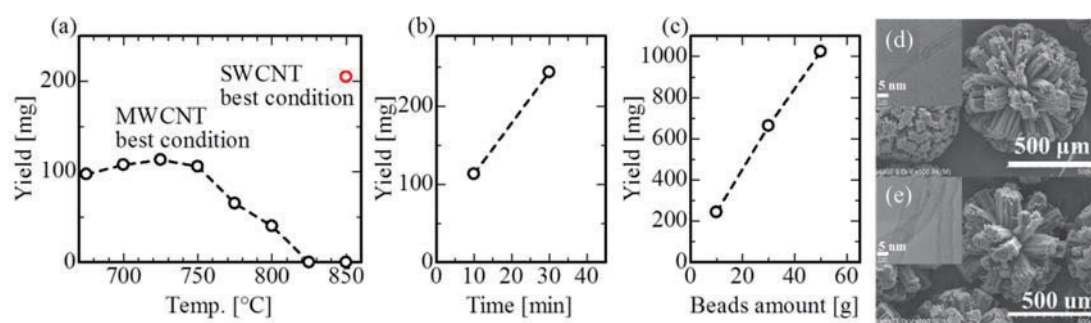


Fig. 1 Submillimeter-long CNTs by FBCVD. Yield vs (a) CVD temperature, (b) CVD time, and (c) beads amount. TEM and SEM images of (d) SWCNTs by the 1-nm-Fe catalyst and (e) MWCNTs by the 5-nm-Fe catalyst.

- [1] Q. Zhang, *et al.*, *ChemSusChem* 4, 864 (2011). [2] D.Y. Kim, *et al.*, *Carbon* 49, 1972 (2011).  
[3] D.Y. Kim, *et al.*, *Carbon* 50, 1538 (2012). [4] Z. Chen, *et al.*, *Carbon* 80, 1972 (2014).

Corresponding Author: S. Noda, Tel&Fax: +81-3-5286-2769, E-mail: noda@waseda.jp

## Large-scale continuous separation of metallic / semiconducting carbon nanotubes by electric-field-induced layer formation method

○Fumiyuki Nihey<sup>1,\*</sup>, Fusako Sasaki<sup>2</sup>, Yuki Kuwahara<sup>2,3</sup>, Takeshi Saito<sup>2,3</sup>, Hiroyuki Endoh<sup>1</sup>

<sup>1</sup> *IoT Devices Research Laboratories, NEC Corporation, Tsukuba 305-8501, Japan*

<sup>2</sup> *Technology Research Association for Single Wall Carbon Nanotubes, Tsukuba 305-8565*

<sup>3</sup> *National Institute of Advanced Industrial Science and Technology, Tsukuba 305-8565*

The electric-field-induced layer formation (ELF) method [1] is an electrophoretic method for separating metallic and semiconducting carbon nanotubes (CNTs) without the use of supporting media (such as gel). Electrophoresis is commonly conducted by batch processing; introducing the dispersion, applying electric-field, and then collecting separated fractions. In this case, the separation yield is limited by the separation-cell volume and the separation time (typically 0.1 L and 24 hours, respectively, in or ELF). Therefore, in order to obtain higher yield in the ELF separation, the enlargement of cell volume and the development of continuous processing are required. In this presentation, we report a large-scale and continuous process for separating metallic and semiconducting CNTs by free-flow electrophoresis based on the ELF method.

CNTs synthesized by eDIPS method [2] were dispersed in the aqueous solution of polyoxyethylene (100) stearyl ether (Brij S 100) for the free-flow electrophoresis experiments. We have designed and fabricated a narrow rectangular 5-liter-volume container with the several pairs of anodes and cathodes as a separation cell for free-flow electrophoresis. Here, on a side of the cell, multiple inlets are located to inject CNT dispersion and carrier solution during the application of electric-field. On the opposite side of the cell, multiple outlets are located to collect separated CNTs. By controlling the contents of CNT dispersion / carrier solution and the injection speed, it has been confirmed that the metallic and semiconducting CNTs has been successfully separated. The details will be discussed in the presentation.

**Acknowledgment:** This presentation is based on results obtained from a project subsidized by the New Energy and Industrial Technology Development Organization (NEDO).

**References:** [1] K. Ihara et al., J. Phys. Chem. C 115, 22827 (2011). [2] T. Saito et al., J. Nanosci. Nanotechnol. 8, 6153 (2008).

**\*Corresponding Author:** Tel: +81-29-856-1168, E-mail: nihey@cd.jp.nec.com

## Development of gels for high-efficiency metal/ semiconductor separation of SWCNTs

G. Wang, X. Wei, A. Hirano, T. Tanaka, and H. Kataura\*

*Nanomaterials Research Institute, National Institute of Advanced Industrial Science and Technology (AIST), Tsukuba, Ibaraki 305-8565, Japan*

Gel column chromatography method has shown a substantial potential for scalable metal/semiconductor (M/S) separation and further single-chirality separation of single-wall carbon nanotubes (SWCNTs) [1]. However, the role of the gel is not well known. Towards higher separation efficiency, more efforts should be made to clarify the role and to develop novel gels. Commercially available Sephacryl gel (GE Healthcare) has been often used for gel column chromatography. However, Sephacryl was not designed for SWCNT separation but was designed for size exclusion chromatography. There could be room for development of better performance for SWCNT separation.

In this study, as the first step of gel development, we have synthesized dextran-based gels containing different concentrations of allyl dextran as analogues of Sephacryl. Our research showed that more semiconducting (s-) SWCNTs adsorbed in the gels as the ratio of allyl dextran increased, indicating the increase of the adsorption site for s-SWCNTs. Surprisingly, our best gel adsorbed 15 times more s-HiPco SWCNTs (diameter,  $1.0\pm 0.3$  nm) than Sephacryl S-200 did. This means the new gel can separate 15 times more s-SWCNTs without changing column size. This enhancement in the separation efficiency can reduce the cost of industrial scale M/S separation of SWCNTs. Furthermore, all the synthesized gels showed chirality selectivity for the overloading of SWCNT, demonstrating a potential for the single-chirality separation.

[1] H. Liu et al. *Nat. Commun* **2**, 309 (2011).

Corresponding Author: H. Kataura

Tel: +81-29-861-2551, Fax: +81-29-861-2786,

E-mail: [h-kataura@aist.go.jp](mailto:h-kataura@aist.go.jp)

**Purity Analysis and Purification of  
Double-walled Carbon Nanotubes**

○Kenshi Miyaura, Hidekazu Nishino, Shirou Honda

*Chemicals Research Laboratories, Toray Industries, Inc., Nagoya 455-8502, Japan*

We have started development of the applied product for double-walled carbon nanotubes (DWCNTs) since 2001. The applied products of DWCNTs have been developed as transparent conductive film (TCF). The DWCNTs-TCF has very high conductivity, high stretching and durable bending. We are trying to apply for devices on which these features can be utilized. The DWCNT-TCFs have been commercialized as upper electrode of e-paper.

The high electric conductivity DWCNTs have been synthesized by chemical vapor deposition (CVD). DWCNTs have both merit of SWCNTs which have small diameter and high conductivity and MWCNTs which have high durability and productivity. In particular, DWCNTs can be purified in severe condition than SWCNTs. We have synthesized DWCNTs and studied many reaction parameters. Finally, we have succeeded development of high purity DWCNTs. The features of our DWCNTs are very small diameter (<2 nm), high DWCNT ratio (>90%) and high crystallinity (Raman G/D ratio is more than 80). In this presentation, we report the purity analysis techniques required when DWCNTs are purified.

This work is partially supported by the New Energy and Industrial Technology Development Organization (NEDO).

Corresponding Author: H. Nishino

Tel: +81-52-613-5276, Fax: +81-52-613-5283

E-mail: Hidekazu\_Nishino@nts.toray.co.jp

## An experimental and theoretical study on the scanning tunneling spectroscopy of europium nanowires encapsulated in carbon nanotubes

○Terunobu Nakanishi<sup>1</sup>, Ryo Kitaura<sup>1</sup>, Takazumi Kawai<sup>2</sup>, Susumu Okada<sup>3</sup>, Shoji Yoshida<sup>4</sup>,  
Osamu Takeuchi<sup>4</sup>, Hidemi Shigekawa<sup>4</sup>, and Hisanori Shinohara<sup>1</sup>

<sup>1</sup> *Department of Chemistry and Institute for Advanced Research, Nagoya University, Nagoya, 464-8602, Japan*

<sup>2</sup> *Smart Energy Research Laboratories, NEC Corporation, Tsukuba, 305-8501, Japan*

<sup>3</sup> *Graduate School of Pure and Applied Sciences, University of Tsukuba, Tsukuba, 305-8571, Japan*

<sup>4</sup> *Faculty of Pure and Applied Sciences, University of Tsukuba, Tsukuba, 305-8573, Japan*

Metal nanowires, whose diameter is typically one to several atoms, are one of the most ideal one-dimensional nanosystems, the preparation and characterization of these have been difficult because of their high reactivity towards air. Previously, we have found that ultrathin europium (Eu) nanowires can be synthesized in the interior space of carbon nanotubes (CNTs).<sup>[1-2]</sup> Here, the spatially-resolved electronic structure of a CNT encapsulating the Eu nanowire (EuNW@CNT) investigated with scanning tunneling spectroscopy (STS) reveal that an electronic state, which is absent in the corresponding pristine CNT, appears just below the first van-Hove singularity of the CNT. To identify the origin of this electronic state, we have calculated the electronic states of EuNW@CNTs by density functional theory using the generalized gradient approximation + U method.

Figure 1(a) presents a geometrically optimized structure of EuNW@CNT which is shown schematically along the tube axis. As shown in the figure, two rows of Eu atoms align at the middle of the interior space of the CNT. Atom- and spin-resolved density of states (DOS) shown in Fig. 1(b) clearly demonstrate that a peak arising from Eu-6s state exists at the gap region of CNT. The C-2p state also has a finite DOS at the energy where the Eu-6s state exists. This suggests that the Eu encapsulation can generate an additional peak in the STS spectra, which is consistent with the current observation.

[1] R.Kitaura *et al.* *Angew.Chem.Int.Ed.* **48**, 8298, (2009).

[2] R.Nakanishi *et al.* *Phys. Rev. B* **86**, 115445, (2012).

Corresponding Author: R. Kitaura and H. Shinohara

Tel: +81-52-789-2477, Fax: +81-52-747-6442,

E-mail: r.kitaura@nagoya-u.jp and noris@nagoya-u.jp

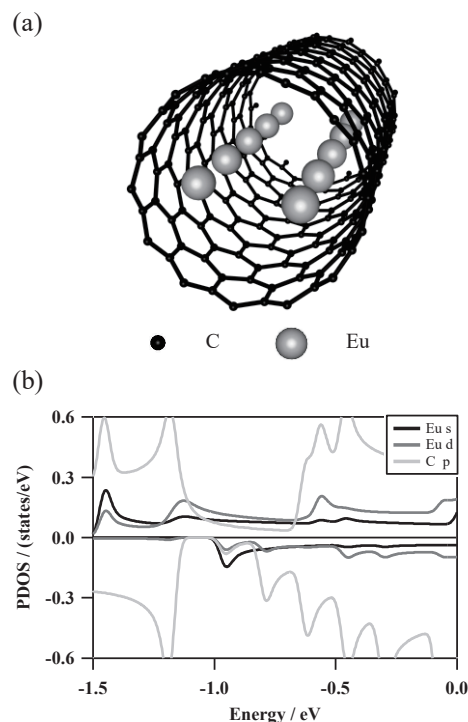


Fig. 1(a) Structure model of EuNW@CNTs. (b) Partial DOS. +y axis shows spin up states and -y spin down states.

## DFT calculations of electronic states and solid state NMR parameters in Cesium Iodide encapsulated single-walled carbon nanotubes

○Eita Yokokura<sup>1</sup>, Yosuke Kataoka<sup>1</sup> and Hironori Ogata<sup>1,2</sup>

<sup>1</sup> Graduate School of Engineering, Hosei University, Koganei, 184-8584, Japan

<sup>2</sup> Research Center for Micro-Nano Technology, Hosei University, Koganei, 184-0003, Japan

Single-walled carbon nanotubes (SWNTs) have a hollow space in the nanometer size that can be encapsulated various functional molecules. The confined molecular assemblies may exhibit unique low-dimensional structures and solid state properties that can not be realized in the bulk. Synthesis and structure of alkali halide encapsulated SWNTs have been reported [1-4]. In our previous studies, the systematic studies of tube diameter dependence, chirality dependence and temperature dependence on the local structures and electronic properties of alkali halides encapsulated in SWNTs were systematically investigated [5].

In this study, we calculated solid <sup>133</sup>Cs- or <sup>127</sup>I-NMR parameters (NMR chemical shift tensors and electric field gradient (EFG) tensors). All of the calculations were done by using a Open-Source computer code package PWscf and GIPAW in Quantum ESPRESSO. We used the pseudo potential methods.

Table 1. shows the chiral vector dependence of <sup>133</sup>Cs-NMR chemical shift tensors in CsI@SWNT. Figure 1 also shows the predicted <sup>133</sup>Cs-NMR spectrum in CsI@(10, 10)SWNT. Detailed results including another will be presented.

Table 1. NMR chemical shift and Electric field gradient (EFG) tensor in CsI@SWNT

Materials	$\delta_{iso}$ (ppm)	$\Delta\delta_{anis}=3/2(\delta_{33}-\delta_{iso})$ (ppm)
bulkCsI	0	0
CsI@(6, 6)SWNT	187.68	786.75
CsI@(8, 8)SWNT	50.41	591.75
CsI@(9, 9)SWNT	+90±5	119±5
CsI@(10, 10)SWNT	9.12	236.75

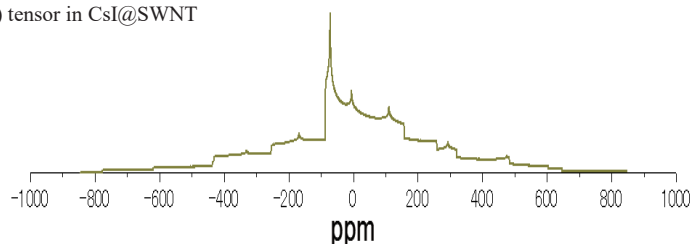


Fig.1 <sup>133</sup>Cs -NMR spectrum of CsI@(10,10)SWNT.

### References:

- [1] J. Sloan, M.C. Novotny, *Chem. Phys. Lett.*, **329** (2000)61.
- [2] M. Wilson, P.A. Madden, *J. Am. Chem. Soc.*, **123** (2001)2101.
- [3] ChiYung Yam, ChiChiu Ma, XiuJun Wang and GuanHua Chen . *Appl. Phys. Lett.* 85, 4484 (2004)
- [4] Ryosuke Senga, Hannu-Pekka Komsa, Zheng Liu, Kaori Hirose-Takai, Arkady V. Krasheninnikov and Kazu Suenaga, *Nature Materials*, 13(2014)1050.
- [5] Abstract of the 50<sup>rd</sup> Fullerenes-Nanotubes-Graphene General Symposium **2P25**.

Corresponding Author: H. Ogata Tel: +81-42-387-6229, Fax: +81-42-387-6229, E-mail: hogata@hosei.ac.jp

## Study of Au-Ni catalytic CVD of uniform multilayer graphene

○Yuki Ueda<sup>1</sup>, Jumpei Yamada<sup>1</sup>, Daichi Yamamoto<sup>1</sup>, Kyosuke Fujiwara<sup>1</sup>  
Takahiro Maruyama<sup>2</sup>, and Shigeya Naritsuka<sup>1</sup>

<sup>1</sup> *Department of Materials Science and Engineering, Meijo University  
Nagoya 468-8502, Japan*

<sup>2</sup> *Department of Applied Chemistry, Meijo University, Nagoya 468-8502, Japan*

Chemical vapor deposition (CVD) is conventionally used to grow a high-quality, single-layer graphene using a copper foil. However, a multilayer graphene is difficult to grow by the method because the growth is terminated by the covering of the catalyst by the grown layer. Though Ni is sometimes used as a catalyst to grow multilayer graphene, the uniformity of the grown layers is very bad. In this study, Au-Ni catalysis is used to grow high-quality multilayer graphene, whose alloy was reported to be useful to grow uniform few-layer graphene at very low temperature of 450°C [1].

Au and Ni layers were deposited on a c-plane sapphire substrate. The alloy composition of the catalyst can be controlled by the thickness ratio of these layers. Ethanol was supplied to the low-pressure CVD chamber as a source material with bubbled by H<sub>2</sub> carrier gas. The growth temperature and alloy compositions were systematically changed to optimize the growth conditions so as to obtain both uniform and high-quality multilayer graphene.

Figure 1 shows a surface optical microscope image of the sample grown on Au-Ni catalyst at 1150 °C. It shows a very uniform growth was performed though the grain boundaries of the catalyst is recognized in the figure. The Raman signal in Fig.2a shows the high-quality of the layer, and the transmittance spectra in Fig.2b demonstrates its thickness of about 9 monolayers. The addition of Au in the catalyst is thought to functionally decrease both the carbon solubility and the interaction between the catalyst and the grown layer [2], which helps the uniform growth of high-quality multilayer graphene.

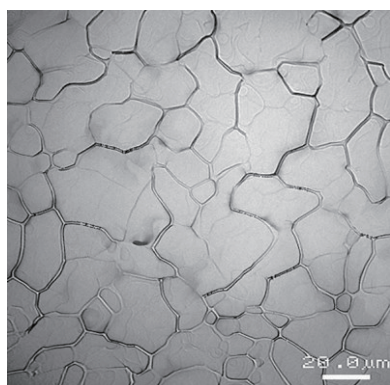


Fig.1 Surface image of sample grown using Au-Ni catalyst.

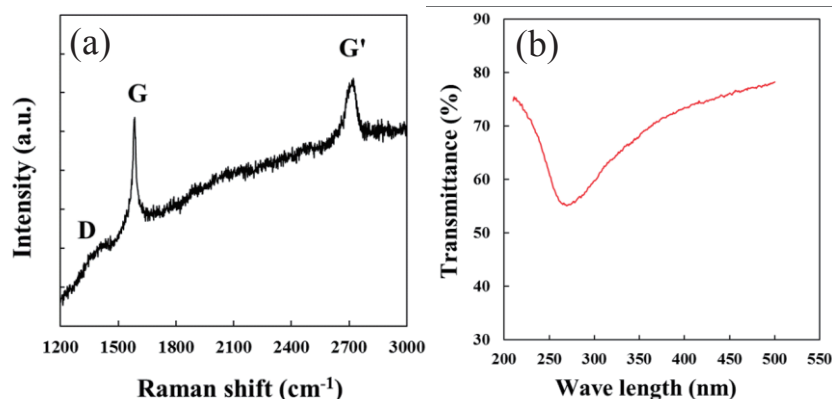


Fig.2 Raman signal (a) and its transmittance spectra (b) of multilayer graphene after transferred on sapphire substrate.

Acknowledgment: This work was supported in parts by JSPS KAKENHI Grant Numbers 2660089, 15H03558, 26105002, 25000011.

[1] R. S. Weatherup, B. C. Bayer, R. Blume, C. Ducati, C. Baetz, R. Schlogl, and S. Hofmann, *NANO Lett.*, 11 (2011) 4154.

[2] M. H. Kang, S. C. Jung, and J. W. Park, *Physic. Rev.*, 82 (2010) 085409.

Corresponding author: Y. Ueda Tel: +81-52-838-2387, E-mail: [153434003@ccalumni.meijo-u.ac.jp](mailto:153434003@ccalumni.meijo-u.ac.jp)

## Thermodynamically Controlled Synthesis of Graphene from Carbon Monoxide

○Yukuya Nagai<sup>1</sup>, Kei Hasegawa<sup>1</sup>, Suguru Noda<sup>1,\*</sup>

<sup>1</sup>Department of Applied Chemistry, Waseda University, Tokyo 169-8555, Japan

Chemical vapor deposition (CVD) has become the mainstream for the synthesis of graphene in which copper (Cu) having low carbon solubility is widely used as catalyst [1]. High temperatures closed to the melting point of Cu (1085 °C) are often applied to achieve better crystallinity and larger grains, and to prevent multilayer formation, CH<sub>4</sub> is widely used due to its less reactive nature.

Here we notice that carbon monoxide (CO) can also be a less reactive carbon source, which has been used for the synthesis of carbon nanotubes (CNTs) [2]. CO yields C through the disproportionation reaction ( $2\text{CO} \rightleftharpoons \text{C} + \text{CO}_2$ ). This reaction is thermodynamically favored at low temperatures, oppositely to the decomposition of CH<sub>4</sub> (Fig. 1). Thus CO needs be highly pressurized to mass-produce CNTs in the HiPco process [2]. However, low-pressure CO may be enough for the synthesis of graphene of 1–2 atomic layers on Cu.

We conduct H<sub>2</sub>-free ambient-pressure CVD for the synthesis of graphene from CO on Cu foils. We change partial pressure of CO (0.09 and 10 vol%), CVD temperature (600–1000 °C), and CVD time (30 and 60 min). We analyze obtained graphene on Cu foils by scanning electron microscope (SEM) and Raman scattering spectroscopy. As Fig. 2 shows, single-layer graphene (SLG) and bilayer graphene (BLG) with tens-micrometer grains are obtained at 800 °C. Graphene formation is thermodynamically favored but kinetically suppressed at low temperatures, resulting in graphene at high coverage and small grain size. Graphene formation process will be discussed in terms of both thermodynamics and kinetics.

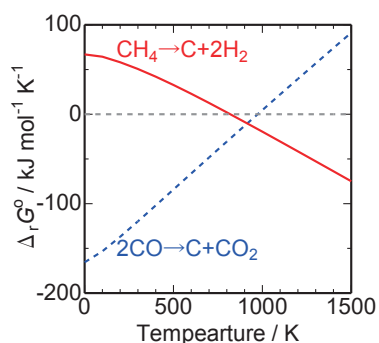


Fig. 1. Gibbs free energy of reaction: C from CH<sub>4</sub> vs CO.

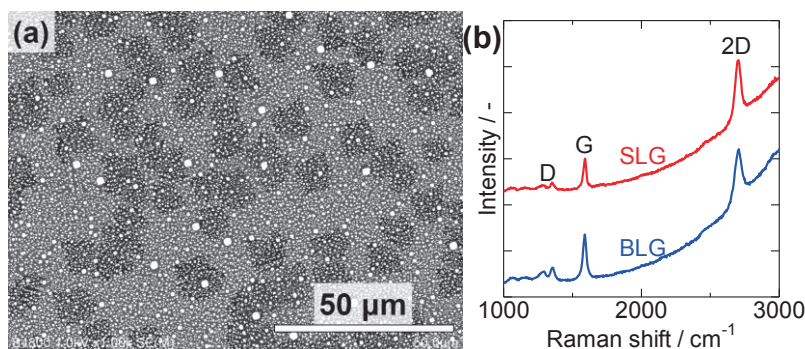


Fig. 2. Graphene formed from CO on Cu (10 vol%, 800 °C, 60 min). (a) SEM, (b) Raman.

[1] X. Li, et al., Science 324, 1312 (2009).

[2] P. Nikolaev et al., Chem. Phys. Lett. 313, 91 (1999).

Corresponding Author: S. Noda, Tel&Fax: +81-3-5286-2769, E-mail: noda@waseda.jp

## Fabrication and Electric Properties of Fe and Ca intercalated Bilayer Graphenes

○N. Kuragane, R. Hoshino, R. Sakurai, T. Yamagishi, T. Ngata, N. Iwata, H. Yamamoto

*College of Science & Technology, Nihon University, 7-24-1 Narashinodai, Funabashi-shi, Chiba 274-8501 japan*

In order to realize superconductivity at room temperature, we fabricate metal intercalated bilayer graphene, in which the electron-exciton coupling is expected to generate high temperature superconductivity [1]. In this study, we fabricated metal intercalated bilayer graphene with different metal and different concentration. The electric properties of iron- and calcium-intercalated bilayer graphenes are discussed.

The single-layered graphene sheet was synthesized on Cu foil by chemical vapor deposition (CVD) method. Graphene/Cu foil was dipped in  $\text{Fe}(\text{NO})_3$  and  $\text{CaCl}_2$  solution to etch the Cu foil and leave the Fe and Ca atoms on the graphene. Metal intercalated bilayer graphene was fabricated by transferring another graphene on the etched graphene/ $\text{SiO}_2/\text{Si}$ .

Fig. 1 shows the temperature dependence of a sheet resistance of the bilayer graphene detected by traditional four wire resistance measurement. Bilayer graphene of Fig.1(a) was fabricated using 0.06mol/L of  $\text{Fe}(\text{NO})_3$  solution. Sheet resistance of Fig.1(a) at room temperature is 30 k $\Omega$ /sq. The bilayer graphene showed semiconducting property. Bilayer graphene of Fig.1(b) was fabricated by 0.12mol/L of  $\text{Fe}(\text{NO})_3$  solution. Sheet resistance of Fig.1(b) at room temperature was 1300  $\Omega$ /sq. The bilayer graphene showed metallic property by increasing the amount of intercalated metal.

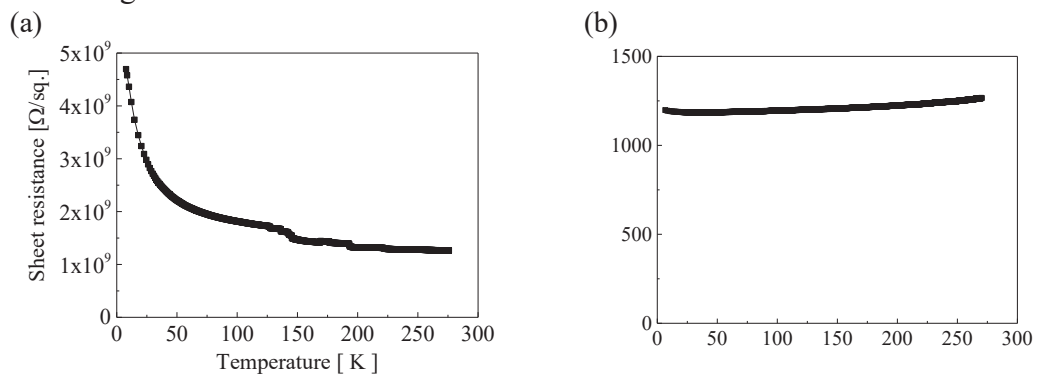


Fig. 1 Temperature dependence of the sheet resistance of the bilayer graphene Bilayer graphene

The electrical properties of the Ca intercalation of metal intercalated bilayer graphene will be discussed.

### References :

- [1] Jun Akimitsu, Parity. MARUZEN. **05**, 6-12 (2008).
- [2] Yan-Feng, Appl. Phys. Lett. **102**, 231906(2013).

Corresponding Author: N. Kuragane

Tel: : +81-47-469-5457 , E-mail: csna13035@g.nihon-u.ac.jp

## Functional group dependence of Spin magnetism of Graphene oxide

○Kentarō Tajima<sup>1</sup>, Takuya Isaka<sup>1</sup>, Tomoki Yamashina<sup>1</sup>, Yoshiaki Matsuo<sup>2</sup>, Kazuyuki Takai<sup>1,3</sup>

<sup>1</sup> Graduate School of Science and Engineering, Hosei University, Tokyo 184-8584 Japan

<sup>2</sup> Graduate School of Engineering, University of Hyogo, Hyogo 671-2201 Japan

<sup>3</sup> Department of Chemical Science and Technology, Hosei University, Tokyo 184-8584 Japan

Graphene oxide (GO) has different hydration / solvation properties according to the synthesis method [1]. However, there is little research on chemical structure and electronic properties of GO synthesized by different methods. In this study, we evaluated GOs synthesized by Brodie [2] (BGO) method and Hummers [3] (HGO) method in terms of chemical structure and spin magnetism.

FT-IR spectra were recorded by the FT/IR6600 (JASCO co.). XPS spectra were obtained using ESCA5600. The magnetic susceptibility was measured using a squid magnetometer (Quantum Design, MPMS-XL).

The FT-IR spectra of GO and graphite were shown in **Fig. 1**, where peaks for hydroxyl, carboxyl, epoxy and carbonyl groups [4] appear for GO in spite of absence of any peak for graphite. Interestingly, the peak around  $1224\text{ cm}^{-1}$  attributed to C-OH stretching for HGO is larger than that for BGO, while the peak around  $1050\text{ cm}^{-1}$  for C-O-C stretching is larger for BGO. Hydroxyl and epoxy groups are more likely to be introduced by Hummers and Brodie method, respectively. This is also supported by the C1s region of XPS spectra for BGO which exhibits the larger component for epoxy groups at  $286.6\text{ eV}$  than that for HGO, being consistent with the FTIR results. The magnetic susceptibility shows an order of magnitude larger localized spin concentration of HGO ( $N_s = 2 \times 10^{19}$ ) than that of BGO ( $N_s = 2 \times 10^{18}$ ) (**Fig. 2**). The difference in functional groups between HGO and BGO explains the larger spin magnetism for HGO. In the case of introduction of epoxy group, oxygen atom bonds to adjacent carbon atoms, remaining symmetry of A, B sub-lattice of graphene lattice. On the other hand, attaching hydroxyl group occurs randomly on carbon atoms of graphene and breaks symmetry of A, B-sublattice, resulting in the emergence of the localized states and the spin magnetism.

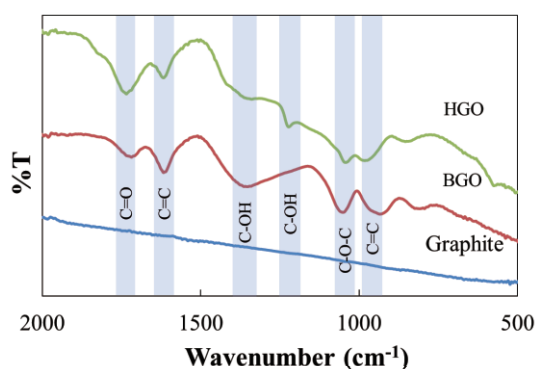


Fig.1 FT-IR spectrum of HGO and BGO

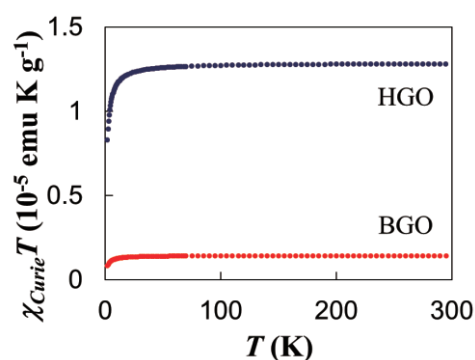


Fig.2 Temperature dependence of the magnetic susceptibility for HGO and BGO

[1] A. V. Talyzin *et al*, *Nanoscale*, **6**, 272, (2014) [2] T. Nakajima, Y. Matsuo, *Carbon*, **32**, 469-475 (1994) [3] D. C. Marcano *et al*, *ACS Nano*, **4**, 8, 4806-4814 (2010) [4] J. Guerrero-Contreras, F. Caballero-Briones, *Mater. Chem. Phys.*, **153**, 209 (2015).

Corresponding Author: K. Takai (takai@hosei.ac.jp)

## Highly efficient, mechanically durable perovskite solar cells with graphene electrodes

Jungjin Yoon<sup>1,2</sup>, Namyong Ahn<sup>1,2</sup>, and Mansoo Choi<sup>1,2</sup>

<sup>1</sup> Department of Mechanical Engineering, Seoul National University, Seoul 08826, Republic of Korea

<sup>2</sup> Global Frontier Center for Multiscale Energy Systems, Seoul National University, Seoul 08826, Republic of Korea

Organic-inorganic hybrid perovskites have unique properties such as high absorption coefficient, tunable bandgap, and ambipolar charge transport. Since Miyasaka's group reported their use as a photoactive material of solar cells in 2009 [1], the perovskite solar cells (PSCs) have been intensively researched by many research groups and their power conversion efficiency (PCE) reached even over 20% [2]. Usually, metal oxides such as TiO<sub>2</sub> and Al<sub>2</sub>O<sub>3</sub> have been adopted to general device architecture of PSCs, which require high process temperature over 450 °C and are not compatible with the low-cost manufacturing. As an alternative to the metal oxides, organic materials were exploited in PSCs, which enable low temperature and solution processes leading to low-cost production.

Taking advantages of these features, the PSCs have been demonstrated on flexible substrates, where indium tin oxide (ITO) on plastic substrates has been mostly used [3]. However, it was found that ITO generated cracks and induced fracture under bending condition due to its mechanical brittleness. Furthermore, the limited supplement of indium accelerates the development of alternative transparent electrodes. Considering their applications as flexible and portable devices, the transparent electrode material should cover following conditions: high optical transparency, mechanical robustness against bending, electrical conductivity, abundance of raw material, and lightweight. In this regard, graphene must be a promising candidate as an alternative transparent electrode in PSCs.

Here, we demonstrated highly efficient and mechanically durable perovskite solar cells with graphene electrodes. A few nanometers doping of MoO<sub>3</sub> layer on graphene lowered sheet resistance and work function of graphene. Besides, the MoO<sub>3</sub> layer made the graphene surface hydrophilic so that the reproducibility of device performance could be guaranteed. Furthermore, to verify the mechanical robustness of graphene electrode, we fabricated the PSCs with same architecture on plastic substrate and carried out bending cycle test. Under a bending radius of 4 mm, PCEs of ITO-based flexible PSCs were shown to < 30% of their initial values, which was attributed to cracks generated on the ITO surface. Whereas, the graphene-based PSCs maintained their PCEs by 85% even after 5000 bending cycles. Additionally, the graphene device maintained a PCE of 85% of its initial after 5000 cycles under bending radius of 2 mm.

[1] A. Kojima *et al.* J. Am. Chem. Soc., **131**, 6050-6051 (2009).|

[2] W. S. Yang *et al.* Science, **348**, 1234-1237 (2015).

[3] B. J. Kim *et al.* Energy Environ. Sci., **8**, 916 (2015).

Corresponding Author: Jungjin Yoon

Tel: +82-2-887-8626, Fax: +82-2-887-8762

E-mail: jyoona27@snu.ac.kr|

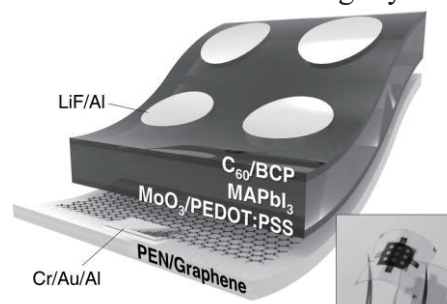


Figure 1. Schematic of perovskite solar cell with graphene electrode

## Reduction reaction of a single graphene oxide sheet in solution as probed by twilight fluorescence microscopy

○Hikaru Sato<sup>1</sup>, Masahito Sano<sup>2</sup>

<sup>1</sup> *Department of Polymer Science and Engineering, Yamagata University, 992-8510, Japan*

<sup>2</sup> *Department of Organic Materials Science, Yamagata University, 992-8510, Japan*

Graphene oxide (GO) is used widely in various applications because of excellent dispersibility, large surface areas, high catalytic activities, and photoluminescence properties. For electrical and mechanical applications, it is preferable to reduce GO so that graphene-like properties can be recovered. Presently, the reduction efficiency stays about 80% at best. One of the reasons for incomplete reduction is that the reaction is conducted using a mixture of GO sheets with various sizes, layers and degrees of oxidation. A small piece has a larger contribution from reactive edges. A layer that is hidden inside a multilayer sheet has less chance of collisions with reactant molecules. It is difficult to improve and optimize the reaction when the only available sample is a mixture of GO sheets with various parameters.

Recently, we have developed Twilight Fluorescence (TwiF) Microscopy that is capable of imaging each GO sheet dispersed in solution. A GO solution is mixed with a highly concentrated fluorescent dye. A small fluorescence change caused by GO-dye interactions gives enough contrast to image individual sheet floating in solution. Using TwiF microscopy, it may become possible to evaluate a reaction process at a single sheet level. In this study, we have examined whether a reaction can be followed as a change of image contrasts in real time.

The first requirement is to find a reducing agent that has no significant effect on dye yet reduces GO efficiently. A screening test using various compounds indicated that L-ascorbic acid satisfies the condition using rhodamine as a dye. NMP was chosen as a solvent, since we had observed previously that GO gives a bright image whereas an independently prepared reduced GO appears dark. NMP also dispersed reduced GO well. An extent of reaction was followed by quantifying the contrasts of several GO sheets with varying sizes appearing within a single imaging window.

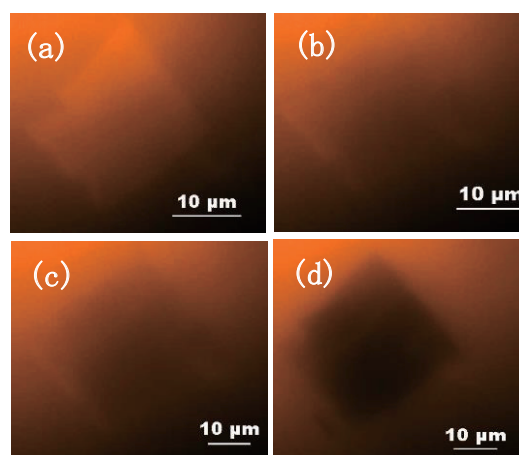


**Fig.1.** TwiF images of a GO sheet in the reacting solution, (a) 0, (b) 300, (c) 600, and (d) 2700 sec after initiation.

Corresponding Author: M. Sano

Tel: +81-238-26-3072,

E-mail: mass@yz.yamagata-u.ac.jp

## Production and characterization of graphene quantum dots derived from SWNTs and graphite.

○H. Morita and T. sugai

*Department of Chemistry, Toho University, Miyama 2-2-1, Funabashi 274-8510, Japan*

Graphene quantum dots (GQD) are nanometer-size graphene fragments derived from various carbonaceous materials. They are promising materials because of their unique fluorescent properties which should be independent of excitation like fluorescent molecules for the applications such as biomarkers. However, the emission wavelength of GQD depends on excitation wavelength.[1] Here we present production of GQD with molecule-like fluorescence by chemical oxidation from various carbon materials.

GQD was prepared from CoMoCAT-SWNTs (Sigma-Aldrich) and graphite powder (nacalai tesque) by oxidation in a mixture of concentrated  $\text{H}_2\text{SO}_4$  and  $\text{HNO}_3$ . The solution was mildly treated by a bath sonicator for tens of hours. The oxidized mixture was diluted with deionized water followed by centrifugation at 10000 rpm for 30 min to separate GQD. Collected supernatant containing GQD was neutralized with NaOH and re-crystallized to eliminate by-produced salt. The produced GQD was characterized by TEM, absorption, and fluorescence observation.

Fig.1 shows emission spectra of the GQD prepared from (a)SWNTs and (b)graphite. GQD from SWNTs shows the emissions at 410 and 520 nm independent of the excitation wavelength. Those molecular like emission may come from the mild preparation conditions utilized here compared to the conventional reflux in concentrated  $\text{H}_2\text{SO}_4$  and  $\text{HNO}_3$  at high-temperature.[2] On the other hand, GQD from graphite shows emissions similar to those derived from graphite reported previously[3] but much weaker than those derived from SWNTs. Those salient differences should come from the differences in the production processes.

[1] D. Pan, J. Zhang, Z. Li, M. Wu, *Adv. Mater.*, **22**, 734-738 (2010)

[2] R. Sekiya, Y. Uemura, H. Naito, K. Naka, & T. Haino, *Chem. Eur. J.*, **22**, 1-10 (2016).

[3] L. Lu, Y. Zhu, C. Shi, Y. T. Pei, *Carbon* **109**, 373-383 (2016).

Corresponding Author: T. Sugai. Tel: 047-472-4406, E-mail: sugai@chem.sci.toho-u.ac.jp

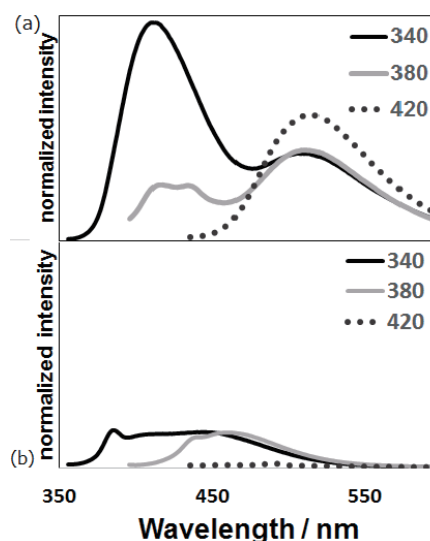


**Fig.1** Emission spectra of GQD derived from (a)SWNTs and (b)graphite.

## Energetics and electronic structure of $B_3N_3$ -doped graphene

○Hisaki Sawahata, Mina Maruyama, and Susumu Okada

*Graduate school of Pure and Applied Sciences, University of Tsukuba, Tsukuba  
305-8571, Japan*

Electronic structures of porous  $sp^2$  carbon networks strongly depend on their network topology and an arrangement of the pores, making them a semiconductor or metal. In addition to pores, interfaces with other two-dimensional materials also modulate the electronic structure of graphene depending on the interface shape and constituents. These facts open a question whether the energetics and electronic structure of porous graphene is further tunable by filling pores with nanoflakes of other two-dimensional materials. Among various two-dimensional materials, BN is an appropriate counterpart of the fillers. Thus, in this work, we aim to investigate the energetics and electronic structure of BN-doped graphene in which  $B_3N_3$  (borazine unit) is triangularly embedded, using the density functional theory with the generalized gradient approximation.

Figure 1 shows the total energy of  $B_3N_3$ -doped graphene as a function of the spacing between adjacent  $B_3N_3$ . The total energy is found to be inversely proportional the  $B_3N_3$  spacing. Furthermore, the energy also depends on the network topology of the graphene domain. The heterosheet with full-benzenoid graphene domain is more stable than the other sheets. Network topology of the graphene domain also affects the electronic structures of  $B_3N_3$ -doped graphene. Figure 2 shows the band gap energy of the heterosheet as a function of the spacing between  $B_3N_3$ , indicating that the all sheets are semiconductors with finite energy gap irrespective to the arrangements of  $B_3N_3$  in graphene. The gap also monotonically decreases with increasing the  $B_3N_3$  spacing. The heterosheet with full-benzenoid graphene domain has a direct gap at the  $\Gamma$  point, while the other heterosheets have direct gap at K point. Calculated band gap in full-benzenoid sheets is narrower than that in non-benzenoid sheets with the almost the same  $B_3N_3$  spacing.

Corresponding author: H. Sawahata  
TEL: +81-29-853-5921, FAX: +81-29-853-5924  
E-mail: [hsawahata@comas.frsc.tsukuba.ac.jp](mailto:hsawahata@comas.frsc.tsukuba.ac.jp)

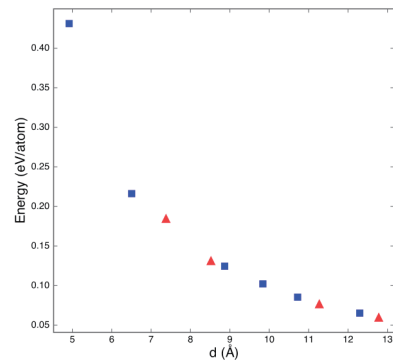


Fig. 1, Total energy of BNC heterosheets as a function of the lattice parameter.

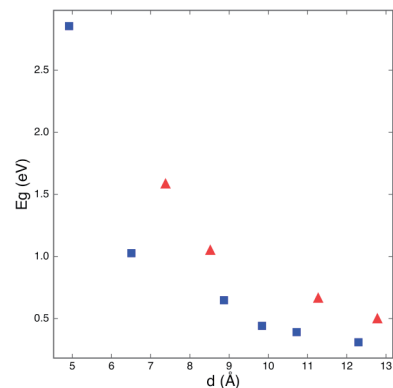


Fig. 2, Band gap of BNC heterosheets as a function of the lattice parameter.

## Charge transfer dynamics at graphene/SiC interface studied by time-resolved soft X-ray photoemission spectroscopy

○T. Someya<sup>1</sup>, H. Fukidome<sup>2</sup>, S. Yamamoto<sup>1</sup>, N. Endo<sup>2</sup>, I. Matsuda<sup>1</sup>

<sup>1</sup> Institute for Solid State Physics, The University of Tokyo, Kashiwa 277-8581, Japan

<sup>2</sup> Research Institute of Electrical Communication, Tohoku University, Sendai 980-8577, Japan

Graphene, a two-dimensional carbon crystal with a gas of massless Dirac fermions, has promise as a material that is useful in photonic and electronic devices. For these applications, epitaxial growth of graphene by thermal decomposition of a silicon carbide (SiC) is one of the suited fabrication methods as it can directly produce graphene sheet on a semiconducting substrate. However it has been known that graphene/SiC interface have negative effects on electrical properties of graphene, such as carrier mobility, and therefore unrevealing the charge transfer at the interface is essential for the device applications.

In this study, we observed surface photovoltage (SPV) effect at the graphene/SiC interface by using time-resolved X-ray photoemission spectroscopy and succeeded in uncovering the role of interface state to the charge transfer dynamics at the interface.

Figure 1 shows the relaxation dynamics of the SPV observed as the transient shifts of the C1s core level spectra. For comparison, we prepared two types of graphene samples which have different interface properties; graphene on SiC(0001) Si-terminated surface and graphene on SiC(000 $\bar{1}$ ) C-terminated surface. On the C-terminated face, carriers survived until 100 ns while on the Si-terminated face, carrier relaxed within 10 ns. These relaxation processes are successfully understood by phenomenological thermionic emission model of the Schottky diode.

In the poster session, we will discuss the origin of the carrier lifetime on different graphene/SiC interfaces.

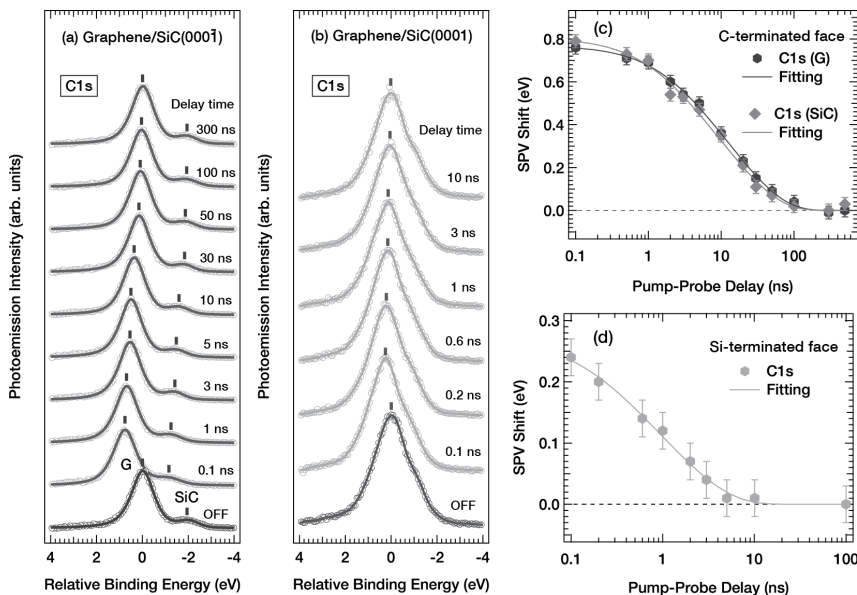


Figure 1. (a, b) Time-resolved C1s core level spectra of graphene on SiC(0001) and SiC(000 $\bar{1}$ ).

(c, d) Relaxation of surface photovoltage on C-face and Si-face graphene, respectively.

Probe light : 740 eV  
Pump light : 3.0 eV  
(350  $\mu\text{J}/\text{cm}^2$ )  
Temperature : 300 K.

Corresponding Author: I. Matsuda

Tel: +81-4-7136-3402, Fax: +81-4-7136-3402,  
E-mail: imatsuda@issp.u-tokyo.ac.jp

## Simplified estimation of crystallographic orientation of strained graphene by micro-Raman spectroscopy

○Kazushi Nakamura<sup>1</sup>, Hikari Tomori<sup>1,2</sup>, Akinobu Kanda<sup>1</sup>

<sup>1</sup> Division of Physics and TIMS, University of Tsukuba, Tsukuba 305-8571, Japan

<sup>2</sup> PRESTO, Japan Science and Technology Agency, Kawaguchi 332-0012, Japan

Strain engineering is a promising but unexplored method of modulating electron transport in graphene. Graphene has a peculiar property that lattice strain produces a vector potential exerted only on conduction electrons[1]. The resulting spatially varying pseudo magnetic field can be used, for example, to induce a transport gap in graphene.[2] Here, it is noted that the magnitude of the pseudo magnetic field strongly depends on the crystallographic orientation of strain. Thus, for the further understanding of the strain related phenomena, determination of the crystallographic orientation of strain is indispensable.

So far, the crystallographic orientation of strain has been estimated by using the polarized Raman spectroscopy.[3] Under uniaxial strain, the Raman G band splits into two subbands (G+ and G-), which have different polarization dependence. The polarization dependence of the G+ (G-) amplitude together with the orientation of the polarizer gives the crystallographic orientation of strain. However, when a commercial micro-Raman spectroscopy system is used, it is not easy to accurately determine the orientation of the polarizer inserted in the system, the error of which is directly connected to the error of the strain orientation. Here, we propose a simple method by which one can determine the strain orientation regardless of the accuracy of the polarizer orientation.

Our method of estimating the strain orientation is based on a recent theory telling that by uniaxial strain the Raman 2D band splits into three subbands with different polarization dependence[4]. From the comparison of the polarization dependence of G and 2D bands, one can derive the strain orientation and the polarizer orientation simultaneously. An example is shown in Fig. 1. Here, we induced uniaxial strain in exfoliated graphene by placing parallel resist bars between graphene and the substrate. Due to small strain, neither G nor 2D band splits, but the peak frequency of each band exhibits periodic modulation as a function of the rotation angle of the sample,  $\theta_r$ , from which we estimated the strain orientation with respect to the zigzag direction to be 50.3 degree. The details will be explained in the presentation.

[1] H. Suzuura and T. Ando, Phys. Rev. B **65**, 235412 (2002).

[2] V.M. Pereira and A.H.C. Neto, Phys. Rev. Lett. **103**, 046801 (2009).

[3] M. Huang *et al.*, Proc. Natl. Acad. Sci. **106**, 7304 (2009).

[4] V.N. Popov and P. Lambin, Carbon **54**, 86 (2013).

Corresponding Author: A. Kanda

Tel: +81-29-853-5081, Fax: +81-29-853-4345,

E-mail: kanda@lt.px.tsukuba.ac.jp

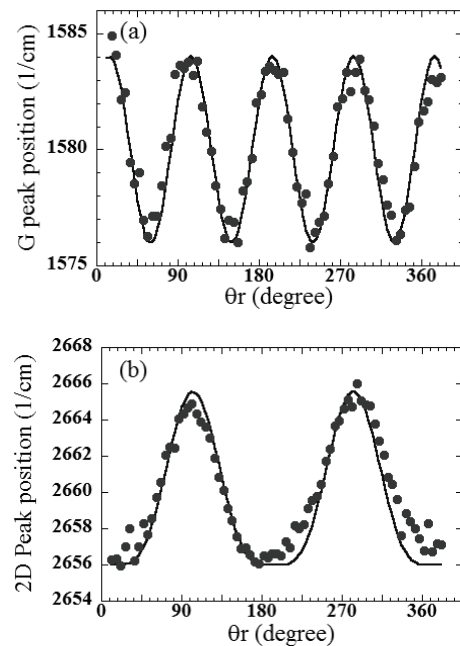


Fig. 1: Peak positions of (a) G and (b) 2D bands as a function of the the rotation angle of the sample.

## Mechanical properties of graphene nanoribbons

Kazufumi Yoneyama, Ayaka Yamanaka, and Susumu Okada

*Graduate school of Pure and Applied Sciences, University of Tsukuba, Tsukuba  
305-8571, Japan*

Graphene exhibits remarkable mechanical strength of which Young's modulus is up to TPa, allowing it a promising material for designing novel mechanical and electromechanical devices. For the practical application of graphene in these devices, it is mandatory to precisely control their size and geometry. Nanoscale graphene flakes and ribbons are attracting much attention because of their potential application for the nanoscale mechanical devices. Experimental and theoretical works have elucidated electronic structure and energetics of graphene nanoribbons. However, a little is known for microscopic mechanical aspects of graphene nanoribbons. Thus, in this work, we aim to elucidate mechanical properties of graphene nanoribbons in terms of their edge atomic arrangements, using the density functional theory with the generalized gradient approximation and pseudopotential procedure.

Figure 1 shows the geometric structure of graphene nanoribbon with hydrogenated edges studied here. In this work, we focus on the graphene nanoribbons, of which edge angles are 0 (armchair), 16, and 30 (zigzag) degrees, to elucidate whether the edge shape affects the mechanical properties of these graphene nanoribbons. Calculated Young's modulus is

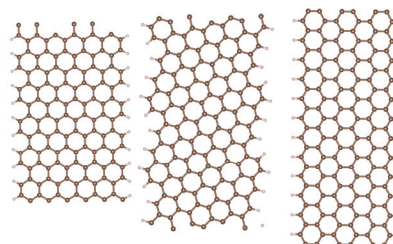


Fig. 1, Geometric structures of graphene nanoribbons with edge angles of 0, 16, and 30 degree.

124, 114, and 131 GPa for the ribbons with armchair (0 deg.), chiral (16 deg.), and zigzag (30 deg.) shapes, respectively, indicating that the mechanical properties are sensitive to their edge shapes. We apply the uniaxial tensile strain on these ribbons to elucidate an initial process of the mechanical fracture in these ribbons. In the ribbon with the edge angle of 16 degree, the fracture is started at the boundary between zigzag and armchair edges, where the charge density on the chemical bond is slightly lower than the other edges.

Corresponding Author: K. Yoneyama

TEL/FAX: +81-29-853-5921/+81-29-853-5924

E-mail: kyoneyama@comas.frsc.tsukuba.ac.jp

## Introduction of spin-orbit interaction into graphene by various methods

T. Nanba, T. Tamura, Y. Katagiri, C. Ohata, Pierre Seneor<sup>1</sup>, J. Haruyama  
*Faculty of Sciences and Engineering, Aoyama Gakuin University, 5-10-1 Fuchinobe,  
 Sagamihara, Kanagawa252-5258, Japan*  
<sup>1</sup>CRNS/Thales

Introduction of spin-orbit interaction into graphene is highly important and interesting for two-dimensional topological insulator with small mass and voltage-controlled spintronic devices. Nevertheless, experimental reports are few, although there are many theories. Basically, the following two different methods exist for it; (1) Rashba-type SOI introduced by destructing out-of-plane symmetry by attaching extremely small amount of hydrogen (H) or fuluoro atoms to graphene surface and (2) Proximity SOI realized by large-mass particles (e.g., Au, Ag, Cu) placed on graphene. Previously, we carried out (1) following [1] and reported possibility that internal magnetic field unique to graphene SOI tends to suppress dephasing of electro spin waves in weak interaction[2,3]. However, precise control of H atom amount and its estimation was difficult. Here, we demonstrate (2) in the present poster.

Graphene has been fabricated on SiO<sub>2</sub>/Si substrate following mechanical exfoliation method of HOPG by scotch tape. In order to effectively detect SOI, spin Hall Effect (SHE), and its distance dependence, Hall pattern shown in Fig.1 has been designed. Au and Ag particles are placed on this pattern SHE has been investigated as non-local resistance ( $R_{NL}$ ) peaks for back-gate voltage ( $V_{bg}$ ) change. Figure 2 shows the result. Indeed, large  $R_{NL}$  peaks are observed for them. Because they cannot be observed in graphene without metal particles and also Larmor spin precession has been detected for the  $R_{NL}$  peaks, they are attributed to SOI and SHE. More details are presented in poster.

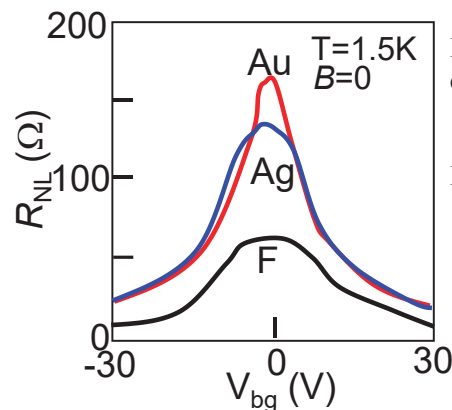
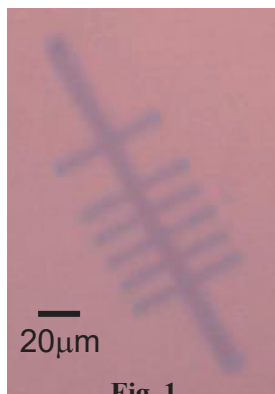


Fig.1: Graphene Hall pattern for detection of SOI and AHE

Fig. 2: Non-local resistance observed in Fig.1-pattern with Au and Ag particles

- [1] J. Balakrishnan, et al., *Nature Commun.* DOI: 10.1038 /ncomm5748 (2014).  
 [2] T. Kato, T. Nakamura, S. Katsumoto, J. Haruyama *et al.*,  
*J. Royal Society of Chemistry Advances* **6**, 67586 (2016).  
 [3] T. Nakamura, J. Haruyama, S. Katsumoto, *J. Phys. Soc. Japan* **85**, 105002 (2016)

Corresponding Author: J. Haruyama  
 Tel: +81-42-759-6256, E-mail: J-haru@ee.aoyama.ac.jp

## Influences of Graphene Structure on Electrochemical Interactions in LiBF<sub>4</sub> Organic Electrolyte Solution

○Daisuke Suzuki<sup>1</sup>, Kazuyuki Takai<sup>1,2</sup>

<sup>1</sup> Graduate School of Science and Engineering, Hosei University, Tokyo 184-8584, Japan

<sup>2</sup> Department of Chemical Science and Technology, Hosei University, Tokyo 184-8584, Japan

Phenomena at the interface between carbon electrode and electrolyte are crucial for the performance of energy storage devices; such as ion storage, degradation mechanism, and Solid Electrolyte Interphase (SEI) formation. However these are still unclear in the case of actual carbon electrode materials due to its complex structure. In this study, the influence of the structure of graphene as a model material for carbon electrodes was investigated in terms of electrochemical interaction at the interface between graphene and organic electrolyte.

Electrochemical potential dependence of conductivity was measured for mechanically exfoliated graphene and epitaxial graphene (EG), where the graphene channel and Pt wire in the electrolyte (1 M LiBF<sub>4</sub> in EC: DMC (1:1 v/v %)) were applied as working and counter electrodes, respectively. Raman spectra and XPS were measured by LabRAM HR and ESCA5600, respectively.

Increment of electrochemical current below -2 V becomes suppressed after cycles of electrochemical gate sweeping (**Fig.1**), attributed to SEI formation by the reaction between graphene and EC/DMC [1] [2]. In the case of EG, the intensity ratio of Raman G' to G bands increases after cycles of sweeping. This indicates an increment of the number of layers of graphene by Li intercalation between buffer layer of graphene and SiC substrate. This is supported by XPS, where the larger take-off angle is, the larger intensity of Li spectrum is (**Fig.2**). In addition, both peaks for graphene and SiC shifted to the higher energy side after applying electrochemical potential, indicating an oxidation reaction at the interface between graphene and SiC substrate. The presence of the substrate significantly affects phenomena at the interface between electrolyte and graphene.

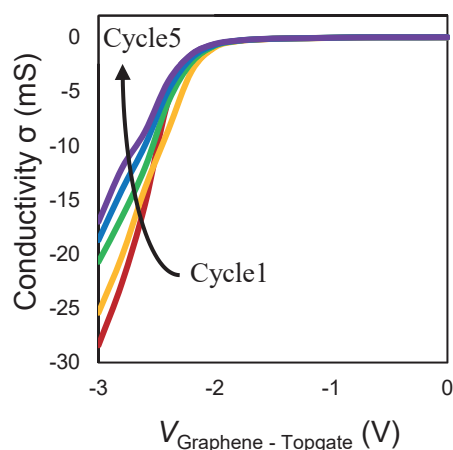


**Fig.1** Gate voltage dependence of Conductivity in FET with LiBF<sub>4</sub> organic electrolyte solution

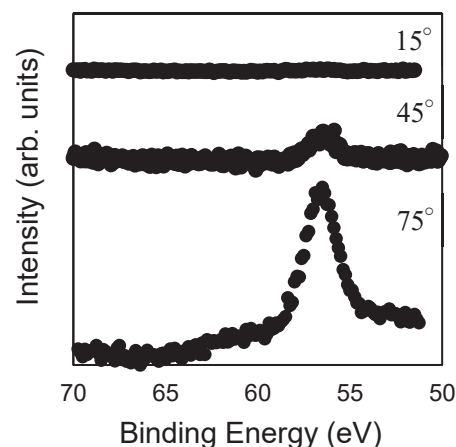


**Fig.2** Li 1s spectra of EG after electrochemical cycles with various take-off angle

[1] Elad Pollak *et al*, Nano.lett. **10**, 3386 (2010) [2] Jingshu Hui *et al*, ACS.Nano. **10**, 4248 (2016)

Corresponding Author: Kazuyuki Takai

Tel: +81-42-387-6138, Fax: +81-42-387-7002, E-mail: takai@hosei.ac.jp

## Detection of photo current arising from atom-thin MoS<sub>2</sub> Schottky junction fabricated by electron beam irradiation

Y. Katagiri, C. Ohata, Y. Inoue<sup>1</sup>, S. Maruyama<sup>1</sup>, T. Nakamura<sup>2</sup>, S. Katumoto<sup>2</sup>, A. Ishi<sup>3</sup>,  
M. Hasegawa<sup>3</sup>, G. Fioli<sup>4</sup>, S. Roche<sup>5</sup>, J. Haruyama

Depts. Electrical Eng. and Electro. <sup>3</sup>Chemi. and Bio., Aoyama Gakuin University, 5-10-1  
Fuchinobe, Sagamihara, Kanagawa252-5258, Japan

<sup>1</sup>Department of Mechanical Eng., The University of Tokyo, Tokyo 113-8656, Japan

<sup>2</sup>Institute for Solid State Physics, The University of Tokyo, 5-1-5 Kashiwanoha, Kashiwa,  
Chiba 277-8581, Japan

<sup>4</sup>University of Pisa, <sup>5</sup>Barcelona Institute of Sci. and Tech

Research of post-graphene atom-thin two-dimensional layers are highly active and its advancement as van der Waals engineering is significant. Among them, molybdenum disulfide (MoS<sub>2</sub>) is attracting considerable attention as atom-thin semiconductor with direct energy band gap [1]. Our group reported creation of atom-thin MoS<sub>2</sub> lateral Schottky junction with barrier height of 0.18 eV, fabricated only by irradiating electron beam (EB) and causing semiconductor(2H)/metal(1T) transition. We revealed weak Fermi-level pinning as unique property of this atom-thin Schottky junction [2]. Here, we report on photo current properties arising from this junction.

Few-layer MoS<sub>2</sub> has been fabricated on SiO<sub>2</sub>/Si substrate following mechanical exfoliation method of bulk material using scotch tape. EB has been irradiated to this MoS<sub>2</sub> with dose in 160Me for 1.5μm<sup>2</sup> at room temperature. Two electrode-pairs, in which one locates on 1T-metal region (i.e., EB irradiated region) while the other on 2H, have been fabricated both sides of this junction with different distance from the junction. Figure 1 shows PL property of the MoS<sub>2</sub> including 1T metal region as a basic feature. Laser beam has been irradiated with wave length of 488 nm under applied no bias voltage in inset. The number (#1-5) noted on each spectrum corresponds to position of PL mapping shown in inset. Two PL peaks unique to direct exciton transition in 2H semiconductor phase are observed at position #1-3, while no peak is detected at position #4, which corresponds to 1T metal region. These suggest presence of expected 2H/1T regions. In contrast, clear 2H/1T interface cannot be observed in the inset with 0.25 μm space resolution. This may be due to carbon contamination existing around the junction, because of the large EB dose. Figure 2 shows photo current ( $I_{sd}$ ) as a function of photo intensity observed in forward and reverse voltage bias ( $V_{sd}$ ) regions in the Schottky junction. Large increase in  $I_{sd}$  in reverse voltage region suggests concentration of high electric field on the Schottky junction. These promise high-efficient photo sensor using this structure.

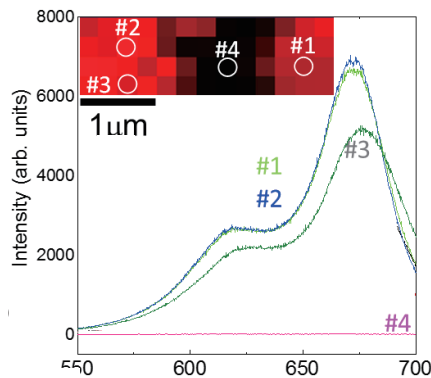


**Fig.1** Wavelength (nm)

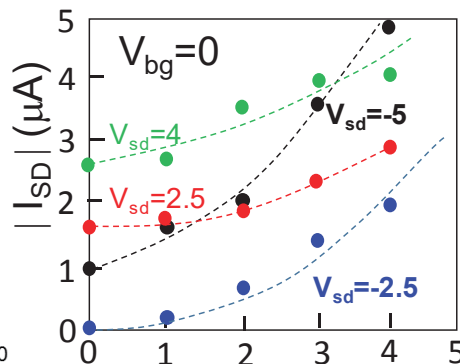


**Fig.2** Photo intensity (mW)

[1] M. Acerce, M. Chhowalla et al., *Nature Nanotechnology* **10**, 313 (2015).

[2] Y. Katagiri, T. Nakamura, S. Katsumoto, S. Roche, J. Haruyama et al., *Nano Lett.* **16**, 3788 (2016).

Corresponding Author: J. Haruyama

Tel: +81-42-759-6256, E-mail: J-haru@ee.aoyama.ac.jp

## Mechanism of contact-resistance improvement in suspended device of bi-layer WSe<sub>2</sub> by mild oxygen plasma treatment

○Reito Nagai, Toshiro Kaneko, Toshiaki Kato

*Department of Electronic Engineering, Tohoku University, Sendai 980-8579, Japan*

Mono or few-layer transition metal dichalcogenide (TMD) is known as an atomically-thin two-dimensional (2D) material with excellent optical and electrical properties. For the fabrication of high performance optoelectrical devices, it is required to reduce the contact resistance between TMD and metals used for electrodes. Suppressing the impurity scattering from the substrate is also another critical issue for their high performance applications. The suspended-device structure of 2D materials is one of the ideal structures, which can reduce impurity scattering from the substrate obtaining better optoelectrical-device performance such as ballistic carrier transport and bright photoluminescence (PL) of graphene and carbon nanotubes. However, the contact between TMD and electrodes in the suspended device is usually very poor due to the van der Waals gap caused by atomically-flat TMD surface. Therefore, developing the post process, which can reduce the contact resistance of suspended-TMD device with maintaining the original high optical properties becomes as an important issue for realizing high performance optoelectrical device with TMD.

Here, we developed a simple method to obtain the low contact resistance of suspended TMD device. The short time (a few tens of seconds) mild oxygen plasma treatment [1,2] can improve the contact resistance of bi-layer WSe<sub>2</sub> field effect transistor (FET), resulting in high on current density of 2.8  $\mu\text{A}$  and relatively low  $\sim 10^6 \Omega\mu\text{m}$  contact resistance with suspended configuration, which is about  $10^5$  times higher and  $10^7$  times lower than that of before plasma treatment, respectively. The bright PL can be obtained even after the mild-plasma treatment.

Through the systematic investigations, we found that mild O<sub>2</sub> plasma treatment can introduce local defects such as vacancies of W atom or partial oxidation (WO<sub>x</sub>) in bi-layer WSe<sub>2</sub>. These local defects may introduce the formation of covalent bonds between WSe<sub>2</sub> and metal electrode, suppressing the original van der Waals gap.

We also measured photoresponse of suspended bi-layer WSe<sub>2</sub>. Our plasma-treated device showed the relatively fast response time of  $\sim 20$  ms and high photoresponsivity of  $\sim 12000$  A/W at a wavelength of 400 nm, indicating the mild plasma treatment is very useful for the fabrication of TMD-based high performance optoelectrical devices.

[1] T. Kato, L. Jiao, X. Wang, H. Wang, X. Li, L. Zhang, R. Hatakeyama, and H. Dai, *Small* **7**, 574 (2011).

[2] T. Kato and R. Hatakeyama, *Nat. Nanotechnol.* **7**, 651 (2012).

Corresponding Author: R. Nagai

Tel: +81-22-795-7046

E-mail: nagai14@ecei.tohoku.ac.jp

## Optical spectroscopy on monolayer transition metal dichalcogenides immersed in an aqueous solution

Wenjin Zhang, Yusuke Hasegawa, Kazunari Matsuda, and Yuhei Miyauchi

*Institute of Advanced Energy, Kyoto University, Uji, Kyoto 611-0011, Japan*

Monolayer (1L) transition-metal dichalcogenides (TMDCs)  $\text{MX}_2$ , where M and X are a transition metal (typically Mo, W) and a chalcogen (typically S, Se, or Te), respectively, have recently emerged as two-dimensional (2D) direct gap semiconductors [1,2] promising for future electronics and optoelectronics applications. To date, various intriguing optical properties of atomically thin TMDCs in vacuum or ambient air conditions have been intensively studied using optical spectroscopy techniques [1-4]. However, knowledge on the optical spectra of these materials in liquids has still been quite limited, although variety of phenomena occurring at the interfaces of liquid and atomically thin TMDCs may considerably modify their physical properties and affect their usefulness in applications.

Here we demonstrate a simple procedure for optical spectroscopic studies on mechanically exfoliated TMDCs immersed in a liquid, which will provide an excellent platform for examining impacts of various physical chemistry phenomena at the liquid/TMDC interface on their physical properties. 1L-TMDCs were prepared using standard mechanical exfoliation method, and transferred on transparent glass substrates. The substrate with the transferred 1L-TMDC was then tightly bonded with a glass tube to compose a liquid reservoir in which an enough amount of liquid can be kept over the sample during the measurements. The optical measurements were performed through the glass substrate using oil immersion objective lens and a home-made confocal optical measurement system.

Figure 1 shows PL spectra of 1L- $\text{MoS}_2$  in water and air conditions, respectively. Considerable modifications in the PL intensity and spectral line shape (inset) were observed for the 1L- $\text{MoS}_2$  just by immersion in water. Dependence of the PL spectra on the solution pH and the mechanism of the spectral modulation will be discussed.

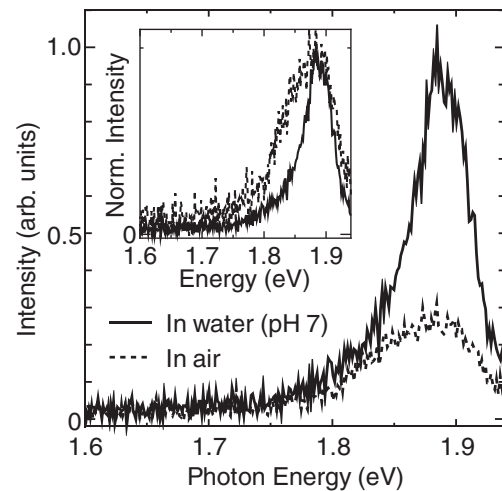


Fig. 1. PL spectra of 1L- $\text{MoS}_2$  in water of pH 7 (solid curve) and air conditions (dashed curve). Inset compares the PL spectra normalized by their intensities at the peak maxima.

[1] K. F. Mak, *et al.*, *Phys. Rev. Lett.* **105**, 136805 (2010).

[2] A. Splendiani, *et al.*, *Nano Lett.* **10**, 1271 (2010).

[3] K. Matsuda, *J. Phys. Soc. Jpn.* **84**, 121009 (2015).

[4] S. Mouri, Y. Miyauchi, and K. Matsuda, *Nano Lett.* **3**, 5944 (2013).

Corresponding Author: Y. Miyauchi

Tel/Fax: +81-774-38-3463/+81-774-38-4567

E-mail: miyauchi@iae.kyoto-u.ac.jp

## Helicity-resolved first order resonant Raman spectra of graphene and transition metal dichalcogenides

○Yuki Tatsumi and Riichiro Saito

*Department of Physics, Tohoku University, Sendai 980-8578, Japan*

Raman spectroscopy is one of the conventional method to verify the crystal and electronic structure of materials. Recently, helicity-resolved and angle-resolved Raman spectroscopies of atomic layer materials attract many interests due to their unique properties depending on the crystal structure, phonon modes, and the polarization direction of incident light. Recent experimental study by S.-Y. Chen *et al.* [1] shows that the  $E'$  Raman mode switches the helicity of photon [right-handed circular polarized ( $\sigma_-$ ) light is scattered], but the  $A'_1$  mode does not switch the helicity [left-handed circular polarized ( $\sigma_+$ ) light is scattered] in Raman scattering of monolayer  $\text{MoS}_2$  when we apply the  $\sigma_+$  incident light. This fact implies that the phonon transfers the angular momentum to the photo-excited electron in the process of Raman scattering. L. Zhang, *et al.* [2] discusses the chirality of the phonon which switches the helicity of photon at high-symmetry points in monolayer hexagonal lattices. However, there is no actual calculation result to show the Raman intensity of the helicity-resolved Raman spectra up to now.

In order to know the property of helicity-resolved Raman spectra, we develop the program to calculate the first order resonant Raman spectra based on the first-principles calculation. Raman intensity is proportional to the product of two electron-photon matrix elements and an electron-phonon matrix element. We obtain the electron-photon matrix element with dipole approximation given from the wave function calculated by Quantum Espresso package [3] and electron-phonon matrix element by EPW package [4].

In Fig. 1, we show the resonant Raman spectrum of G band in graphene calculated by our program. As Fig. 1 shows, scattered light of G band changes the helicity of photon. This result is in good agreement with previous theoretical study [2] and implies that the phonon transfers the angular momentum to the photo-excited electron in the process of Raman scattering. In this presentation, we discuss the helicity-resolved selection rule of first order Raman scattering in graphene and monolayer  $\text{MoS}_2$  by considering the symmetry of electron-phonon matrix elements.

- [1] S.-Y. Chen, *et al.*, Nano Lett. 15, 2526 (2015)  
 [2] L. Zhang, *et al.*, Phys. Rev. Lett. 115, 115502 (2015)  
 [3] P. Giannozzi, *et al.*, J. Phys.: Condens. Matter 21, 395502 (2009)  
 [4] J. Noffsinger, *et al.*, Compt. Phys. Commun. 181, 2140 (2010)

Corresponding Author: Yuki Tatsumi  
 Tel: +81-22-795-6442, Fax: +81-22-795-6447,  
 E-mail: tatsumi@flex.phys.tohoku.ac.jp

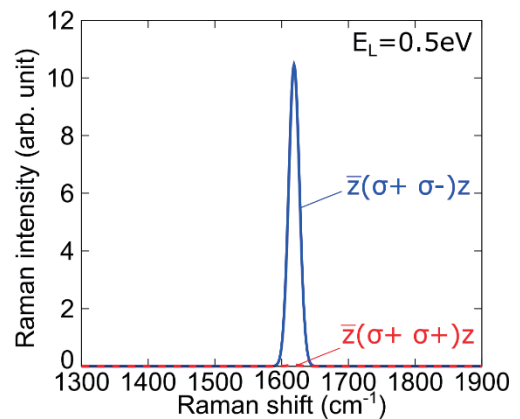


Fig1. Calculated resonant Raman spectrum of G band in graphene. Solid (Dashed) line is the helicity-resolved Raman intensity with (without) switching of helicity of photo-excited electron. Incident laser energy is 0.5 eV.

## Energetics and electronic properties of $C_{60}$ adsorbed on graphene

○Yamato A. Saucier, Mina Maruyama, and Susumu Okada

*Graduate school of Pure and Applied Sciences, University of Tsukuba, Tsukuba  
305-8571, Japan*

Graphite intercalation compounds (GICs) are the representative van der Waals heterostructures consisting of graphene and intercalant layers which are characterized by the staging structure corresponding to the number of graphene layers sandwiching intercalant layers. An early theoretical work has predicted a GIC consisting of graphene and  $C_{60}$  sheets, which are alternately stacked each other [1]. Following the theoretical prediction, an experimental work demonstrated that the possibility of the  $C_{60}$ -GIC and  $C_{60}$  molecular layer on graphene [2]. Motivated by these early works, we are now aiming to investigate the physical properties of the all carbon thin film consisting of monolayer graphene and  $C_{60}$  molecular sheet as the thinnest version of the all carbon van der Waals heterostructure with mixed dimensionality, using the density functional theory combined with the effective screening medium method. Owing to the work function difference between  $C_{60}$  and graphene, the sheet exhibits dipole moment normal to the sheet with the potential difference of 0.15 V [Fig. 1(a)]. We also demonstrated that the biaxial compressive strain causes the electron transfer from graphene to  $C_{60}$ , because of the different compressibility between graphene and  $C_{60}$  layers [Fig. 1(b)].

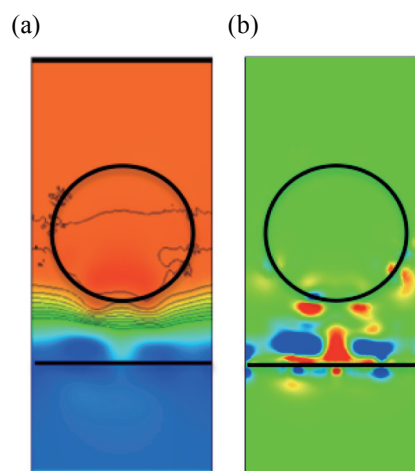


Fig. 1, Contour plots of (a) electrostatic potential and (b) charge redistribution of  $C_{60}$  adsorbed on graphene.

### References:

- [1] S. Saito and A. Oshiyama, Phys. Rev. B **49**, 17413 (1994).
- [2] E. V. Rut'kov, A. Ya. Tontegode, and M. M. Usufov, Phys. Rev. Lett. **74** 758 (1995).

Corresponding Authors: Y. A. Saucier and S. Okada

E-mail: sokada@comas.frsc.tsukuba.ac.jp

## Upconversion photoluminescence spectra of carbon nanotubes in mice tissues

○Saki Okudaira<sup>1</sup>, Yoko Iizumi<sup>2</sup>, Masako Yudasaka<sup>2</sup>, Toshiya Okazaki<sup>2</sup>, Kazunari Matsuda<sup>1</sup>, and Yuhei Miyauchi<sup>1</sup>

<sup>1</sup> Institute of Advanced Energy, Kyoto University, Uji, Kyoto 611-0011, Japan

<sup>2</sup> National Institute of Advanced Industrial Science and Technology (AIST), Tsukuba, Ibaraki 305-8562, Japan

Single-walled carbon nanotubes (SWNTs) have been considered as promising luminescent probes for deep-tissue bioimaging because of their intrinsic photoluminescence (PL) in the near infrared wavelength range of ~1000-1300 nm called NIR-II [1,2]. The near infrared light readily penetrates into highly scattering media such as biological tissues; this enables PL imaging of deep inside of them. However, it is necessary to use Stokes PL at longer wavelengths than ~1100 nm to avoid autofluorescence from the biological tissues, and standard Si-based detectors cannot be used in this wavelength range. Recently, efficient upconversion PL (UCPL) of SWNTs has been discovered [3]. The UCPL phenomena enable SWNTs excited at wavelengths longer than ~1050-1200 nm to emit PL shorter than 1000 nm in which standard Si-based detectors have finite sensitivity. The availability of the UCPL thus drastically enhances the usefulness of SWNTs as luminescent probes in their bioimaging applications.

In this study, we examine UCPL spectra of SWNTs in biological tissues of mice using a Si-based CCD and an InGaAs photodiode array detector. We measured both PL and UCPL spectra of sectioned liver tissues of mice into which SWNTs were intravenously injected. Figure 1(a) and 1(b) show a UCPL image and a UCPL spectrum of SWNTs in the sectioned liver tissue excited at 1064 nm, respectively. A circle in Fig. 1(a) indicates the position at which the UCPL spectrum shown in Fig. 1(b) was measured. The UCPL showed a major peak at about 1010 nm; similar UCPL peak was also observed for the SWNTs before the injection. Relatively broad UCPL feature implies bundling of SWNTs [4]. Results for the UCPL imaging and spectroscopy in other conditions will also be discussed.

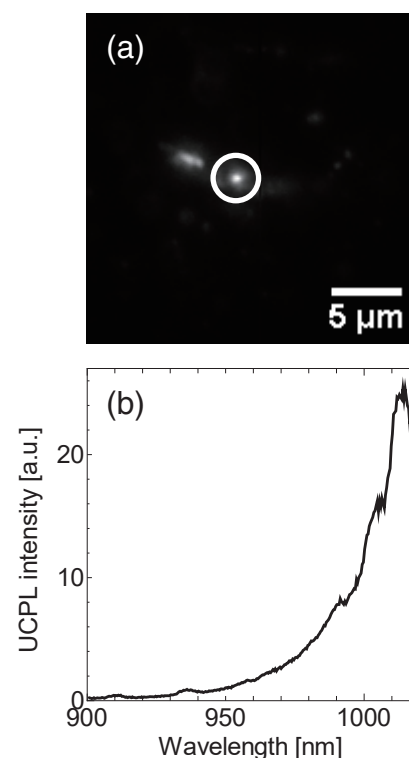


Fig. 1. (a) UCPL image of SWNTs in a sectioned tissue of a mouse liver excited at 1064 nm. (b) UCPL spectrum taken at the position indicated by a circle in (a).

[1] K. Welsher *et al.*, Nat. Nanotechnol. **4**, 773 (2009).

[2] Y. Iizumi, *et al.*, ACS Appl. Mater. Interfaces **5**, 7665 (2013).

[3] N. Akizuki *et al.*, Nat. Commun. **6**, 8920 (2015).

[4] S. Aota, *et al.*, Appl. Phys. Express **9**, 045103 (2016).

Corresponding Author: Y. Miyauchi

Tel: 81-774-38-3463, Fax: +81-774-38-4567

E-mail: miyauchi@iae.kyoto-u.ac.jp

## Electrical properties of defective hexagonal boron nitride nanosheet

○ Ho-Kyun Jang, Jun Hee Choi, Kook Jin Lee, Do-Hyun Kim, Gyu Tae Kim

*School of Electrical Engineering, Korea University, Seoul 02841, Korea*

Boron nitride (BN) has a good thermal conductivity [1] but, it has no electrical conductivity due to its large bandgap. Theoretical calculations predicted that hexagonal BN nanosheet (BNNS) with some defects can have an electrical conductivity because of new energy states of these defects between conduction and valence band [2]. In this study, we created vacancy defects on BNNS by the method of forming multi-vacancies on BN nanotubes [3]. As a result, we observed a change in the electrical properties of the BNNS.

BNNS was transferred on SiO<sub>2</sub>/Si substrate using mechanical exfoliation method. The source and drain electrodes for BNNS were patterned by E-beam lithography and gold was deposited by chemical vapor deposition to form the electrodes. Then, the BNNS was impregnated with Co precursor and heated at about 200 °C under air atmosphere to form defective structures in BNNS by catalytic oxidation. In the electrical measurements, the pristine BNNS did not show any electrical properties. However, BNNS with defects exhibited an electrically metallic behavior. To investigate this phenomenon, the electronic structures of BNNS with mono- and di-vacancy defects were calculated based on density functional theory. Calculation results and actual experimental results were compared and analyzed.

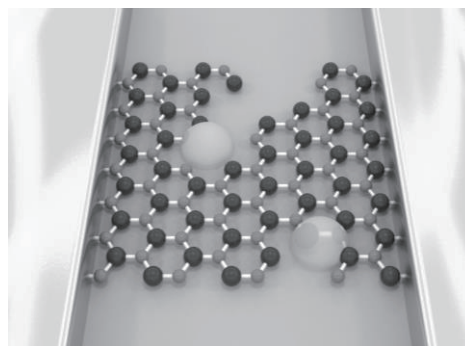


Fig.1 Schematic image of defective BNNS device

[1] J. H. Lan *et al.* Phys. Rev. B. **79**(11), 115401 (2009)

[2] P. Tang *et al.* RSC Adv. **2**, 6192-6199 (2012)

[3] D.-H. Kim *et al.* Phys. Chem. Chem. Phys. **19**, 976-985 (2017)

Corresponding Author: Ho-Kyun Jang

Tel: +82-2-3290-3801, Fax: +82-2-953-3780,

E-mail: pleastandup@korea.ac.kr

## Modification of Electrical Properties in MoS<sub>2</sub> by Using Catalytic Oxidation

○ Jun Hee Choi, Ho-Kyun Jang, Jun Eon Jin, Jong Mok Shin, Do-Hyun Kim  
Gyu-Tae Kim

*School of Electrical Engineering, Korea University, Seoul 136-701, South Korea*

Modulation of electrical properties in MoS<sub>2</sub> attracts much attention in terms of complementary circuit design based on monolayer two-dimensional material [1-3]. In this work, we demonstrate an effective method to change electronic transport characteristics of MoS<sub>2</sub> by using catalytic oxidation ( $\text{MoS}_2 + \text{O}_2 \rightarrow \text{MoO}_x + \text{SO}_x$ ). Ambipolar behavior in MoS<sub>2</sub> field effect transistors (FETs) can be easily obtained by heating MoS<sub>2</sub> flakes under air atmosphere in the presence of cobalt oxide catalyst. From the microscopic observation by SEM and AFM, the catalytic oxidation of MoS<sub>2</sub> flakes between source-drain electrodes resulted in lots of nanoparticles (NPs) on MoS<sub>2</sub> flakes with thickness reduction. The oxidation state of the NPs was confirmed by XPS analysis to be MoO<sub>x</sub>, meaning that catalytic oxidation happened on the top layer of MoS<sub>2</sub> flakes. N-type behavior of MoS<sub>2</sub> FETs was converted to ambipolar transport characteristics by MoO<sub>x</sub> NPs which inject hole carriers to MoS<sub>2</sub> flakes [4]. Theoretical calculations were performed to investigate the change in the electronic structure of MoS<sub>2</sub> by MoO<sub>x</sub> NPs.

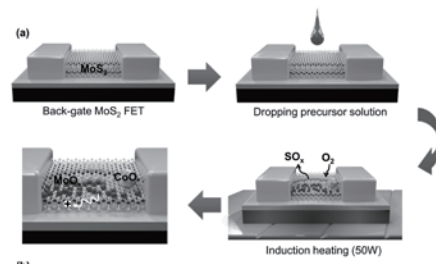


Fig.1 Schematic diagram of achieving ambipolar behavior in FETs by partially modifying MoS<sub>2</sub> flakes via catalytic oxidation using CoO NPs.

- [1] K. Dolui *et al.* S. Phys. Rev. B, **88**, 075420 (2013).  
 [2] M. R. Laskar *et al.* S. Appl. Phys. Lett. **104**, 092104 (2014).  
 [3] J. Suh *et al.* Nano Lett. **14**, 6976 (2014).  
 [4] S. Chuang *et al.* A. Nano Lett. **14**, 1337 (2014).

Corresponding Author: Jun Hee Choi  
 Tel: +82-2-3290-3801, Fax: +82-2-953-3780,  
 E-mail: cjuny426@gmail.com

## Hidden symmetries in one-dimensional photonic crystals

M. Shoufie Ukhtary, Haihao Liu, and Riichiro Saito

*Department of Physics, Tohoku University, Sendai 980-8578, Japan*

Nowadays, transferring information across a long distance efficiently has been the main subject in communication field of science. Light is used mainly for this purpose due to its velocity and its versatile properties which is sensitive to the medium it passes. Photonics is a branch of science that studies how the light propagates through the material and how to modify its propagation, such as how to prevent the propagation or to localize the light [1]. One-dimensional photonic crystal (PC), which is a system containing  $N$  layers of varying dielectric media, is usually used to achieve this purpose. By manipulating the sequence of dielectric media within the PC, we can control the light propagation through it [2].

Previous studies have shown that by controlling the sequence of PC, the light propagation can be controlled. This allows the development of optical devices such as optical filter and optical switches. However, the studies focus only on some specific sequences of PC, such as Fibonacci and Cantor sequences [3,4]. A study for optical properties of arbitrary sequences is not yet done as far as we know. In this work, we study theoretically the light propagation within arbitrary sequences. We use one-dimensional PC containing  $N$  layers made of two kinds of dielectric media. In contrast to previous studies, we study all the possible sequences of the PC, which is in total of  $2^N$  sequences [5]. We will show that the number of light transmission probability ( $T$ ) values for the  $N$  layers is not arbitrary, instead there are either  $(N/2 + 1)$  or  $(N + 1)$  discrete values of  $T$  for even or odd number  $N$ , respectively. This high degeneracy implies the existence of hidden symmetries within the PC, which we will explain in this work. One of symmetries found in this work is shown in figure 1. Studying the symmetries within the PC can be useful for designing a sequence of PC with desirable properties, such as a PC with specific  $T$ .



**Figure 1:** The mirror symmetry: Mirrored sequence of dielectric media will give the same transmission probability ( $T$ ).

[1] J.D. Joannopoulos et al. Photonics crystal : molding the flow of light. (2011)

[2] B.E Saleh et al. Fundamentals of photonics. (1991).

[3] R. Endo and R. Saito. JOSA B 28, 2537. (2011)

[4] P. Xu et al. JOSA B27, 640. (2010)

[5] H. Liu et al. in preparation. (2017)

Corresponding Author: M. Shoufie Ukhtary

TEL: +81-22-795-6442, FAX: +81-22-795-6447, E-mail: shoufie@flex.phys.tohoku.ac.jp

## Theoretical estimation for the electronic property and reactivity of activated fullerenes

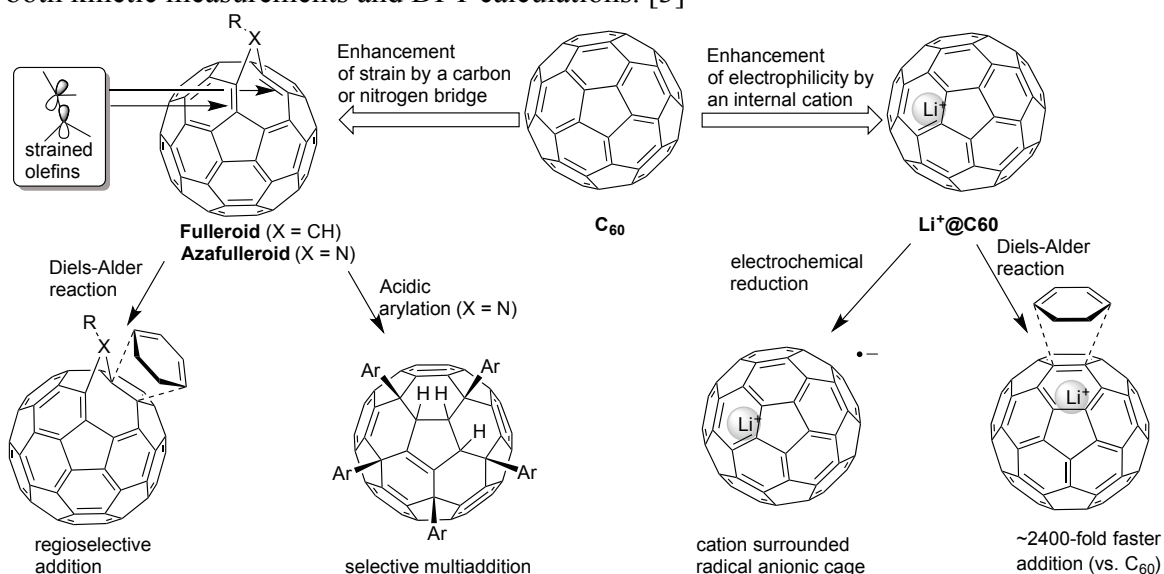
○Naohiko Ikuma, Ken Kokubo and Takumi Oshima<sup>1</sup>

<sup>1</sup>*Division of Applied Chemistry, Graduate School of Engineering, Osaka University, Suita 565-0871, Japan*

One of the advantages of nanocarbon materials is the modification of properties and solubility by various organic reactions; therefore, control of the reactivity and regioselectivity is an important issue for obtaining new materials effectively. To enhance the reactivity and regioselectivity of fullerene, we have investigated on the activated fullerenes with increasing cage strain or introducing an electrophilic cation. In this presentation, we will show theoretical evaluation for the reactivity and regioselectivity on these reactions.

**Activation by cage modification:** Carbon- or nitrogen-bridged fullerenes, named as fulleroids or azafulleroids respectively, showed high reactivity and regioselectivity on Diels–Alder reaction, *m*CPBA oxidation, acidic arylation [1] and Grignard reaction, because of increased strain on the adjacent bridgehead olefins. These reactivities and regioselectivities were well explained by DFT transition state (TS) calculations.

**Activation by an internal cation:** Li-encapsulated fullerene  $\text{Li}^+\text{@C}_{60}$  has higher electrophilicity due to the internal "naked" lithium cation. Electrochemical reduction gave the stable ion pair of a radical anionic cage and the internal Li-cation. [2] Moreover, the internal cation promoted Diels–Alder reaction (2400-fold vs.  $\text{C}_{60}$ ) due to its Lewis acidity estimated by both kinetic measurements and DFT calculations. [3]



[1] N. Ikuma, Y. Doi, K. Fujioka, T. Mikie, K. Kokubo, T. Oshima., *Chem. Asian J.* **9**, 3084 (2014).

[2] (a) H. Ueno, K. Kokubo, Y. Nakamura, K. Ohkubo, N. Ikuma, H. Moriyama, S. Fukuzumi, T. Oshima, *Chem. Commun.* **49**, 7376 (2013); (b) H. Ueno, S. Aoyagi, Y. Yamazaki, K. Ohkubo, N. Ikuma, H. Okada, T. Kato, Y. Matsuo, S. Fukuzumi, K. Kokubo, *Chem. Sci.* **7**, 5770 (2016).

[3] H. Ueno, H. Kawakami, K. Nakagawa, H. Okada, N. Ikuma, S. Aoyagi, K. Kokubo, Y. Matsuo, T. Oshima, *J. Am. Chem. Soc.* **136**, 11162 (2014).

Corresponding Author: N. Ikuma

Tel: +81-6-6879-4592, Fax: +81-6-6879-4593 ; E-mail: ikuma@chem.eng.osaka-u.ac.jp

## Palladium-Catalyzed Functionalization of C<sub>60</sub> Derivatives: Regioselectivity and Structures

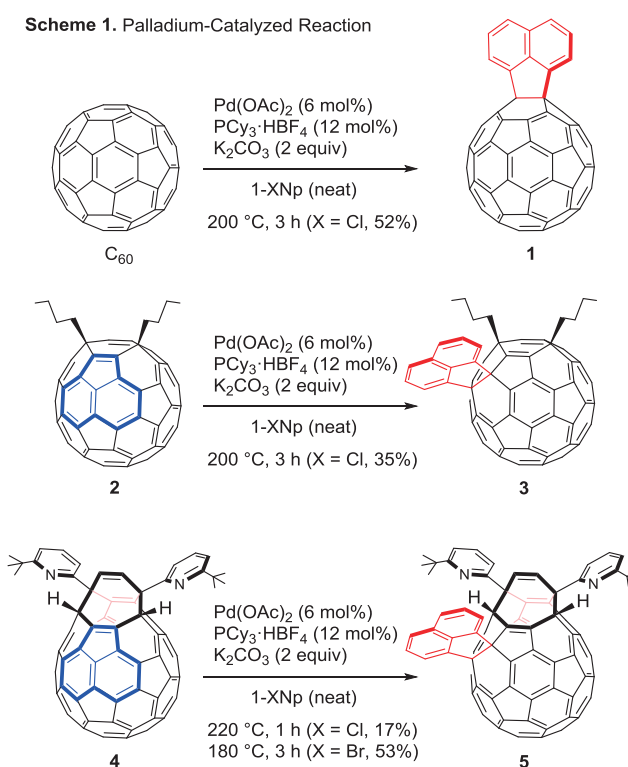
○Yoshifumi Hashikawa, Michihisa Murata, Atsushi Wakamiya, Yasujiro Murata

*Institute for Chemical Research, Kyoto University, Uji, Kyoto 611-0011, Japan*

The multi-functionalized fullerene C<sub>60</sub> derivatives have been studied for the elucidation of their nature and for application in electronic devices.<sup>1</sup> Though a number of methods for multi-functionalization of C<sub>60</sub> have been reported, in some cases, reactions are unctrollable and/or isolation of a desired compound from a reaction mixture is not facile.

We developed a method for the synthesis of arene-fused C<sub>60</sub> derivatives by utilizing a catalytic amount of palladium. Firstly, we optimized conditions using different palladium sources for the reaction of C<sub>60</sub> and 1-halogenated naphthalene (1-XNp). Under the optimized conditions, compound **1** was found to be obtained in 52% yield (Scheme 1). To investigate the reaction scope, we applied the same conditions to 1,4-di-*n*-butyl C<sub>60</sub> (**2**), which resulted in the regioselective formation of **3** in 35% yield. This reaction can be applied to open-cage C<sub>60</sub> derivative **4** to give **5**, albeit in 17% yield. The relatively low yield of **5** arises from the side reaction, thermal dehydrogenation from the opening of **4**. However, when 1-BrNp was used as an arene-source instead of 1-ClNp, compound **5** was obtained in 53% yield since the temperature required for this reaction decreased to 180 °C from 220 °C, which prevented the thermal dehydrogenation of **4**. It is noteworthy that the compounds **2** and **4** have the same structural motif of acenaphthylene where the palladium-catalyzed reaction takes place. The DFT calculations suggested that the HOMO is predominantly localized on this moiety.

To get further insights into the reaction mechanism, we performed the DFT calculations on the reaction of C<sub>60</sub> and 1-BrNp along with two plausible reaction pathways, Heck-type and concerted metalation-deprotonation mechanisms.<sup>2</sup> The optimized conditions, DFT calculations, and the single crystal X-analysis will be presented in detail.



[1] Hirsch, A. *Fullerenes: Chemistry and Reactions*; Wiley-VCH: Weinheim, 2005.

[2] (a) Lapointe, D.; Fagnou, K. *Chem. Lett.* **2010**, *39*, 1118–1126. (b) Tang, S.-Y.; Guo, Q.-X.; Fu, Y. *Chem.–Eur. J.* **2011**, *17*, 13866–13876. (c) Tan, Y.; Hartwig, J. F. *J. Am. Chem. Soc.* **2011**, *133*, 3308–3311.

Corresponding Author: Y. Murata

Tel: +81 774-38-3172, Fax: +81 774-38-3178,

E-mail: yasujiro@scl.kyoto-u.ac.jp

## Synthesis of Lithium-ion-encapsulated Fluoreno[60]fullerenes

○Yutaka Matsuo<sup>1,2,3</sup>, Hiroshi Okada<sup>2</sup>, Hiroshi Ueno<sup>3</sup>

<sup>1</sup>Hefei National Laboratory for Physical Sciences at the Microscale, University of Science and Technology of China, Hefei, Anhui 230026, China

<sup>2</sup>Department of Mechanical Engineering, School of Engineering, The University of Tokyo, Bunkyo-ku, Tokyo 113-8656, Japan

<sup>3</sup>Department of Chemistry, Northeast Normal University, Changchun, Jilin 130024, China

Lithium-ion-containing [60]fullerene,  $\text{Li}^+\text{@C}_{60}$ , is a highly electron accepting material, which have been utilized in electron transfer chemistry, supramolecular chemistry, photovoltaics, singlet oxygen generation, and so on. Considering what chemical modification of fullerene has played in, that for  $\text{Li}^+\text{@C}_{60}$  would be a significant step for further functionalization of this compound.<sup>[1-7]</sup>

In this presentation, we will report the modification of  $\text{Li}^+\text{@C}_{60}$  by using the fluoreno group. The reaction of  $\text{Li}^+\text{@C}_{60}$  and diazofluorene gave the desired product smoothly. Difference in the reactivity in the synthesis of diphenylmethano-modified  $\text{Li}^+\text{@C}_{60}$  and fluoreno-modified one will be discussed.

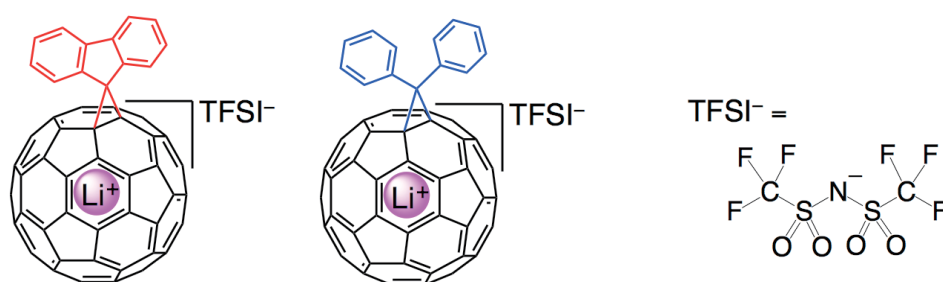


**Figure.** Structures of Lithium-ion-encapsulated fluoreno- and diphenylmethano[60]fullerenes.

### References

- [1] Y. Matsuo *et al.*, *Org. Lett.* **2012**, *14*, 3784–3787.
- [2] H. Okada *et al.*, *RSC Adv.* **2012**, *2*, 10624–10631.
- [3] Y. Noguchi *et al.*, *J. Phys. Chem. C* **2013**, *117*, 15362–15368.
- [4] H. Kawakami *et al.*, *Org. Lett.* **2013**, *15*, 4466–4469.
- [5] Y. Kawashima *et al.*, *ChemPhysChem* **2014**, *15*, 3782–3790.
- [6] H. Ueno *et al.*, *J. Am. Chem. Soc.* **2014**, *136*, 11162–11167.
- [7] H. Ueno *et al.*, *Chem. Sci.* **2016**, *7*, 5770–5774.

Corresponding Author: Y. Matsuo

Tel: +81-3-5841-0978, E-mail: matsuo@ustc.edu.cn; matsuo@photon.t.u-tokyo.ac.jp

## Nanoscale Control of Polymer Assembly on Fullerene Bilayer Membranes

○Koji Harano, Ricardo M. Gorgoll, Eiichi Nakamura

*Department of Chemistry, The University of Tokyo, Tokyo 113-0033, Japan*

Preparation of nanostructured polymer materials templated by self-assembled scaffolds has long been inspired by biosynthetic machinery on cell membranes, but has still remained to be a challenging subject of research in laboratories. Noticing that one of the fundamental problems in this challenge is the excessive fluidity of a lipid or lipid-mimetic membrane, we conjectured on the use of a self-assembled bilayer made of an anionic fullerene amphiphile **1–3** (Figure), from which an aqueous solution of a vesicle of a uniform size (typically 30 nm in diameter) is formed spontaneously upon dissolution in water (**V1–V3**, respectively). The fullerene bilayer keeps the hydrophilic fullerene anion inside and exposes the hydrophobic groups on an aqueous environment to create three regions: surface, interior and fullerene-rich core. Herein we report a catalyst–membrane system where catalyst **6** doped on the vesicle for ring-opening metathesis polymerization (ROMP) controls the assembly of polymer products from a norbornene diethyl ester (**4a**) in three different ways by the choice of the fluorinated vesicle **V1**, the octyl vesicle **V2** and the eicosanyl vesicle **V3**, depending on the miscibility of the growing polymer to the interior of the bilayer. Thus, the polymerization of **4a** on the fluorinated vesicle **V1** occurred heterogeneously on the vesicle surface to afford 6-nm sized spherical particles composed mostly of a single polymer chain. In contrast, polymerization of **4a** on the octyl vesicle **V2** occurred homogeneously near the fullerene core of the bilayer to afford a hollow polymer capsule of 35-nm size composed of tightly entangled 20–30 polymer chains. Polymerization on **V3** occurred in the eicosanyl alkyl environment to afford a soft and sticky capsule.

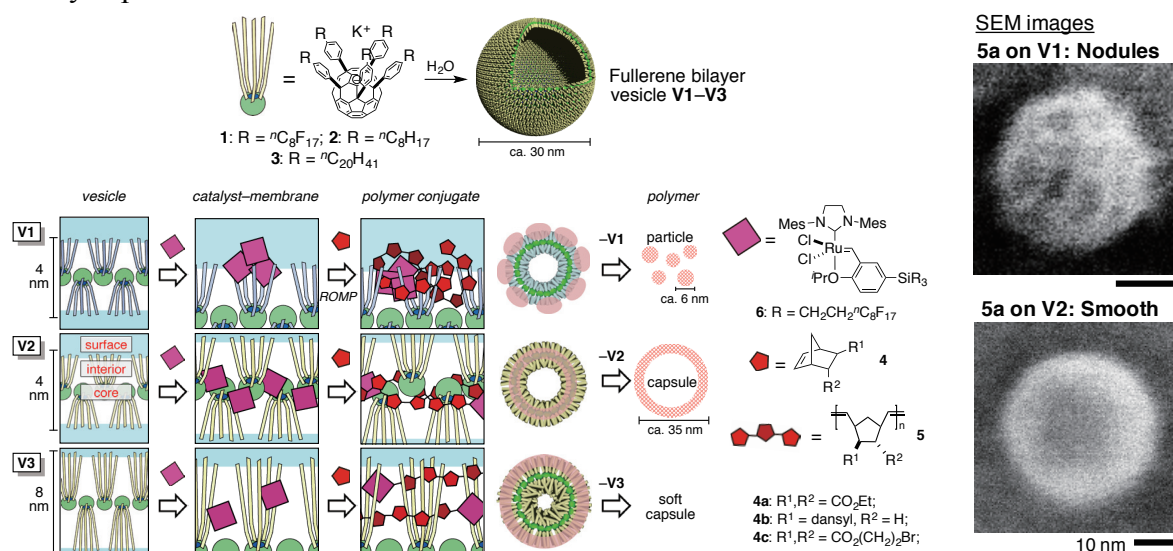


Fig. Controlled polymer growth and assembly in a synthetic catalyst–bilayer system made of fullerene amphiphiles **1–3**.

[1] R. M. Gorgoll, K. Harano, E. Nakamura, *J. Am. Chem. Soc.*, **138**, 9675 (2016).

Corresponding Author: E. Nakamura

Tel: +81-3-5841-4369, Fax: +81-3-5841-4369,

E-mail: harano@chem.s.u-tokyo.ac.jp

## Metallic Polymerization of C<sub>60</sub> Thin Film by Electron-Beam Irradiation

Hiroto Uenoyama<sup>1</sup>, Yu Tanaka<sup>1</sup>, Shingo Yamanouchi<sup>1</sup>, Yuichi Ochiai<sup>1</sup>, and Nobuyuki Aoki<sup>1,2</sup>

1 Chiba University, Chiba, Japan, 2 JST-PRESTO

Although C<sub>60</sub> molecules form fcc (3d) structure in the van der Waals crystal, various kinds of crystalline structures have been found in the polymers by using different triggers for the polymerization. For example, orthorhombic (1d) structure by visible or ultraviolet light irradiation, tetragonal and rhombohedral (2d) structure by high pressure application at high temperature, and peanut shape (1d) polymer by electron beam (EB) irradiation [1] have been reported. Different structure leads to different physical properties such as electrical properties. Here, we are interested in EB irradiation using electron beam lithography system, because we can expose EB toward the selected area to form metallic patterns in electrical circuits within a semiconducting C<sub>60</sub> thin film.

We prepared the sample of C<sub>60</sub> thin film FET on SiO<sub>2</sub>/p<sup>++</sup>-Si substrate by vacuum evaporation. The sample was extracted to the atmosphere and settled into a vacuum chamber of a scanning electron microscope (SEM). Before EB irradiation, the sample was heated to 453 K for 19 hours in the SEM chamber to remove oxygen absorbed on the sample surface. And then, the sample was irradiated by EB with an acceleration voltage of 2 kV. We measured the FET property of the sample before and after irradiation for 2 hours. As shown in Fig. 1, n-type semiconductor property changed to a metallic one which exhibits conductive but no dependence of current in the gate voltage sweep. The resistivity is an order of 10 Ω·m or less. The change must be due to the polymerization of C<sub>60</sub> molecules during the EB exposure. Moreover, we confirmed the metallic properties are still kept after exposure to air. We will discuss the characteristics including the surface morphology using atomic-force microscope observation and the results of micro Raman scattering spectroscopy.

[1] J. Onoe et al, Fullerenes, Nanotubes, and Carbon Nanostructures. 20, 1 (2012)

Corresponding Author: N.Aoki

Tel: +81-43-290-3430, Fax: +81-43-290-3427,

E-mail: n-aoki@faculty.chiba-u.jp

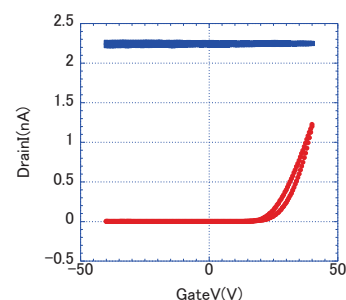


Fig. 1. Gate voltage dependence of drain current of C<sub>60</sub> thin film before (lower) and after (upper) EB irradiation.

## Synthesis of CdS-Mn-[C<sub>60</sub>]Fullerene Nanocomposites and Their Photocatalytic Activities for Degradation of Organic Dyes

○ Jeon Won Ko<sup>1</sup>, Jiulong Li<sup>1</sup> and Weon Bae Ko<sup>1,2</sup>

<sup>1</sup> Department of Convergence Science, Graduate School,

<sup>2</sup> Department of Chemistry, Sahmyook University, Seoul 139-742, Korea

Manganese doped CdS nanocomposites were prepared by using manganese (II) sulfate monohydrate (MnSO<sub>4</sub>·H<sub>2</sub>O), cadmium sulfate 8/3 hydrate (3CdSO<sub>4</sub>·8H<sub>2</sub>O) and sodium sulfide (Na<sub>2</sub>S) as source reagent in basic aqueous solution. Manganese (II) sulfate monohydrate (MnSO<sub>4</sub>·H<sub>2</sub>O) and cadmium sulfate 8/3 hydrate (3CdSO<sub>4</sub>·8H<sub>2</sub>O) were added with a mole ratio of 1:10. CdS-Mn-[C<sub>60</sub>]Fullerene nanocomposites were synthesized through heating CdS-Mn nanocomposites and [C<sub>60</sub>]Fullerene at a mass ratio of 2:1 in the electric furnace at 700 °C for 2 h. The synthesized nanocomposites were characterized by X-ray diffraction (XRD), Raman spectroscopy, scanning electron microscopy (SEM) and transmission electron microscopy (TEM).

As a photocatalyst, CdS-Mn-[C<sub>60</sub>]Fullerene nanocomposites were used in the degradation of organic dyes like BG, MB, MO and RhB under 254 nm ultraviolet light. The photocatalytic activities and kinetics study of CdS-Mn nanocomposites and CdS-Mn-[C<sub>60</sub>]Fullerene nanocomposites were evaluated by UV-vis spectrophotometer.

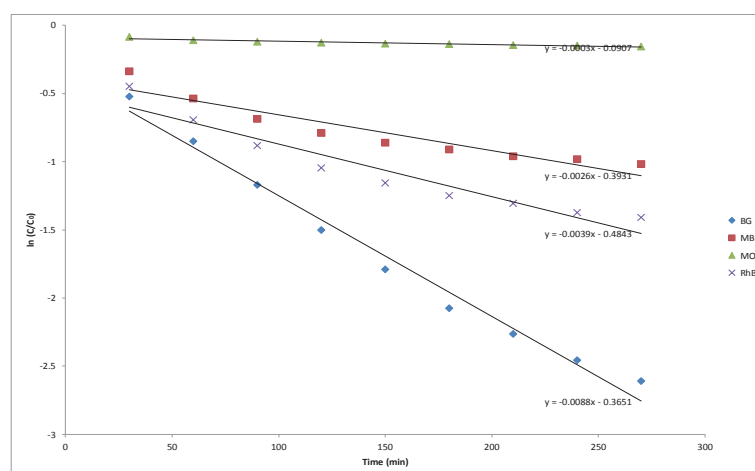


Fig.1 Kinetics study of various organic dyes with CdS-Mn-[C<sub>60</sub>]Fullerene nanocomposites at 254 nm.

[1] M. Grandcolas, J. Ye and K. Miyazawa, *Ceram. Int.* **40**, 1297 (2014).

[2] Z. Lian, P. Xu, W. Wang, D. Zhang, S. Xiao and G. Li, *Appl. Mater. Interfaces* **7**, 4533 (2015).

[3] H.S. Park and W.B. Ko, *J. Nanosci. Nanotechnol.* **15**, 8125 (2015).

Corresponding Author: W. B. Ko

Tel: +82-2-3399-1700, Fax: +82-2-979-5318,

E-mail: kowb@syu.ac.kr

## Studies on the Aggregated Structures and Crystallinities of Bulk Heterojunction Films Constituting Organic Solar Cells

○Saki Kawano<sup>1</sup> and Hironori Ogata<sup>1,2</sup>

<sup>1</sup>Grad. School of Sci. and Engin., Hosei Univ., <sup>2</sup>Res.Center for Micro-Nano Technol., Hosei Univ.

E-mail: hogata@hosei.ac.jp

Bulk heterojunction (BHJ) organic solar cells are an emerging technology that has the potential to provide a low cost photovoltaic devices. It is well known that the nanomorphology of the polymer:fullerene BHJ is a critical factor which affects the solar cell performance. The addition of processing additives such as 1,8-diiodooctane (DIO) is widely used approach to increase power conversion efficiencies for many organic solar cells<sup>[1-2]</sup>. Solid-state solar NMR spectroscopy offers several techniques for the investigation of the morphological, structural, and dynamics properties of BHJ organic solar cells.

We have explored the effects of DIO, 1,8-Octanedithiol(ODT) and 1-Chloronaphthalene(CN) addition of P3HT/1-(3-methoxy- carbonyl)propyl-1-phenyl-(6, 6)(C61-PCBM) BHJ films on the local crystallinity and morphology by using solid-state NMR spectroscopy. In this study, we have investigated the change in the crystallinity, morphology, and the properties of molecular motions of P3HT/C71-PCBM BHJ film by changing material by using <sup>13</sup>C and <sup>1</sup>H solid-state NMR spectroscopy.

Mixed solution of P3HT/C71-PCBM of 1:1(w/w) was prepared by mixing P3HT and PCBM into chlorobenzene at a concentration of 1 wt% for 50 hrs in a glove box under argon atmosphere. Additives were then dropped into the solution and then stirred for 1 hr. The solution was filtered using 0.45μm filter before making films to remove undissolved materials. P3HT/C-71PCBM BHJ films were prepared by dropping the solution in a glass plate and dried in a glove box under argon atmosphere using different drying rates. Dried film were removed from the glass plate and sealed into 4 mm zirconia NMR rotor. Solid-state NMR spectra were collected on Bruker AVANCE300 spectrometer.

Detailed results of their crystallinities, morphologies, and the properties of P3HT/C71-PCBM BHJ film the will be presented.

### References:

- 1) J. K. Lee et al., *J.Am.Chem.Soc.*, **130**(2008)3619.
- 2) B.R.Aïch et al, *Organic Electronics*, **13** (2012)1736.
- 3) Ryan C. Nieuwendaal et al., *ACS Macro Lett.* **3**(2014)130–135.

## Production and Characterization of Hetero-dimetallofullerene: GdY@C<sub>80</sub>(I<sub>h</sub>)

○Takuji Mitani<sup>1</sup>, Natsumi Nakatori<sup>1</sup>, Takahisa Yamaguchi<sup>2</sup>, Ko Furukawa<sup>3</sup>, Tatsuhisa Kato<sup>2,4</sup>,  
Koichi Kikuchi<sup>1</sup>, Yohji Achiba<sup>1</sup>, Takeshi Kodama<sup>1</sup>

<sup>1</sup>Department of Chemistry, Tokyo Metropolitan University, Hachioji 192-0397, Japan

<sup>2</sup>Graduate School of Human and Environmental Studies, Kyoto University, Kyoto 606-8501,  
Japan

<sup>3</sup>Department of Chemistry, Niigata University, Niigata 950-2181, Japan

<sup>4</sup>Institute for Liberal Arts and Sciences, Kyoto University, Kyoto 606-8501, Japan

In the previous symposium, we reported the isolation and characterization of Gd<sub>2</sub>@C<sub>80</sub>(I<sub>h</sub>)<sup>-</sup> anion, which are not stable as a neutral form but stable as an anion form[1]. In (Gd<sub>2</sub>@C<sub>80</sub>(I<sub>h</sub>))<sup>-</sup>, an excess electron is located on the internal Gd dimer and Gd takes the trivalent state. Then, the spin system of (Gd<sub>2</sub>@C<sub>80</sub>(I<sub>h</sub>))<sup>-</sup> consists of one doublet spin and two octet spins. From the ESR study, the spin state of (Gd<sub>2</sub>@C<sub>80</sub>(I<sub>h</sub>))<sup>-</sup> was found to be S=15/2, that is, the ferromagnetic interaction between three spins was suggested. On the other hand, the antiferromagnetic interaction was reported in mono-metallofullerene encapsulating a Gd atom: Gd@C<sub>82</sub>, whose spin system consists of one octet spin of the encapsulated Gd<sup>3+</sup> and one doublet spin of an unpaired electron on the π orbital of the carbon cage[2]. Here, we report the production and characterization of (GdY@C<sub>80</sub>(I<sub>h</sub>))<sup>-</sup>. To clarify more simply the magnetic interaction between the spins of Gd<sup>3+</sup> and an excess electron on the internal metal dimer, we exchange one Gd<sup>3+</sup> of Gd<sub>2</sub>@C<sub>80</sub>(I<sub>h</sub>) for Y<sup>3+</sup> that is a nonmagnetic ion.

Soot containing Gd,Y-metallofullerenes was produced by a direct-current arc discharge, and the raw soot was extracted with a mixed solvent of triethylamine and acetone. MM'C<sub>80</sub> mixture (M, M'=Gd, Y) was separated by two-stage HPLC using acetone with an ion-pair reagent, tetrabutylammonium bromide, as an eluent. The presence of GdYC<sub>80</sub> was confirmed by LD-TOF-MS (Fig.1). Furthermore, since the UV-vis-NIR absorption spectrum of MM'C<sub>80</sub> mixture was found to be very similar to those of (Gd<sub>2</sub>@C<sub>80</sub>(I<sub>h</sub>))<sup>-</sup> and (Y<sub>2</sub>@C<sub>80</sub>(I<sub>h</sub>))<sup>-</sup> as shown in Fig.2, it is suggested that the GdYC<sub>80</sub> would be GdY@C<sub>80</sub>(I<sub>h</sub>)<sup>-</sup>. The results of ESR measurements on (GdY@C<sub>80</sub>(I<sub>h</sub>))<sup>-</sup> will also be discussed in the presentation.

[1] T. Mitani, et al. *The 50<sup>th</sup> Fullerenes-Nanotubes-Graphene General Symposium 95* (2016).

[2] K. Furukawa, et al. *J. phys. Chem.* **107**, 10933-10937 (2003).

Corresponding Author: Takeshi Kodama

Tel:+81-42-677-2530, Fax:+81-42-677-2525

E-mail: kodama-takeshi@tmu.ac.jp

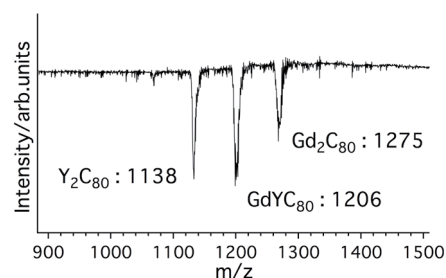


**Fig.1** LD-TOF-MS spectrum (negative ion mode) for MM'C<sub>80</sub> mixture (M, M'=Gd, Y).

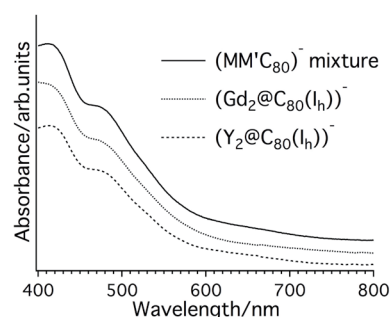


**Fig.2** UV-vis-NIR absorption spectra of (MM'C<sub>80</sub>)<sup>-</sup> mixture (M, M'=Gd, Y), (Gd<sub>2</sub>@C<sub>80</sub>(I<sub>h</sub>))<sup>-</sup> and (Y<sub>2</sub>@C<sub>80</sub>(I<sub>h</sub>))<sup>-</sup>.

## Isolation and structural analysis of La@C<sub>60</sub>(CF<sub>3</sub>)<sub>5</sub>

○Makiko Nishino<sup>1</sup>, Shinobu Aoyagi<sup>2</sup>, Haruka Omachi<sup>1</sup>, Zhiyong Wang<sup>1</sup>,  
Ayano Nakagawa<sup>1</sup>, Ryo Kitaura<sup>1</sup>, and Hisanori Shinohara<sup>1</sup>

<sup>1</sup> Graduate School of Science, Nagoya University, Nagoya 464-8602, Japan.

<sup>2</sup> Department of Information & Biological Science, Nagoya City University, Nagoya  
467-8501, Japan.

La@C<sub>60</sub> is historical fullerene, which is first metallofullerene found on earth<sup>[1]</sup> and is theoretically predicted to have properties like superconductivity. Despite such a big prospect, M@C<sub>60</sub> have not been easily isolated since 1985 because of severe instability. Accordingly, there were some opinions even claiming that La atom is not encapsulated inside fullerene. To solve this issue, the stabilization technique of metallofullerenes by introducing CF<sub>3</sub> substituents has been developed in our group<sup>[2]</sup>.

We finally isolated La@C<sub>60</sub>(CF<sub>3</sub>)<sub>3</sub>, La@C<sub>60</sub>(CF<sub>3</sub>)<sub>5</sub>(isomer I) and La@C<sub>60</sub>(CF<sub>3</sub>)<sub>5</sub>(isomer II) by multi-step HPLC purification with two types of buckyprep columns alternately (Fig.1 (a)). Furthermore, first X-ray crystallographic structure of La@C<sub>60</sub>(CF<sub>3</sub>)<sub>5</sub>(I) was revealed. The ORTEP drawing was shown in Fig1 (b). La atom was definitely incorporated within the fullerene cage. One of C–CF<sub>3</sub> bonds was formed at a point distant from other four CF<sub>3</sub> groups. Although single crystal of M@C<sub>60</sub> has not been found so far because of high degree of freedom, this crystal was neither co-crystal nor including solvent. This miracle is supposed to have happened by existence of solely distant CF<sub>3</sub> substituent.

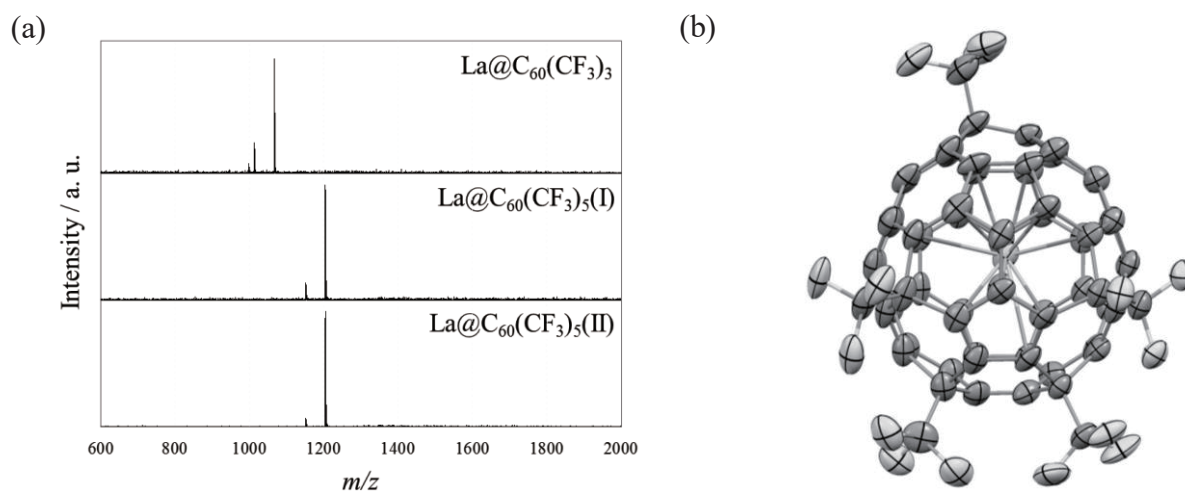


Fig.1 (a) Negative MALDI-MS of isolated CF<sub>3</sub>-functionalized La@C<sub>60</sub> derivatives. (b) X-ray structure of La@C<sub>60</sub>(CF<sub>3</sub>)<sub>5</sub>(I). Thermal ellipsoids are shown at 50% probability.

[1] J. R. Heath *et al.*, *J. Am. Chem. Soc.*, **107**, 7779 (1985).

[2] (a) Z. Wang *et al.*, *Angew. Chem. Int. Ed.*, **52**, 11770 (2013). (b) Z. Wang *et al.*, *Angew. Chem. Int. Ed.*, **55**, 199 (2016)

Corresponding Author: Hisanori Shinohara

Tel: +81-52-789-2482, Fax: +81-52-747-6442, E-mail: noris@nagoya-u.jp

## Photoreactions of Cyclic Organosilanes with Trimetallic Nitride Template Endohedral Metallofullerenes

○Shinpei Fukazawa<sup>1</sup>, Takeshi Sugiura<sup>1</sup>, Kyosuke Miyabe<sup>1</sup>,  
Masahiro Kako<sup>\*1</sup>, Takeshi Akasaka<sup>2,3,4</sup>

<sup>1</sup>Department of Engineering Science, The University of Electro-Communications, Chofu,  
Tokyo 182-8585, Japan

<sup>2</sup>Life Science Center of Tsukuba Advanced Research Alliance, University of Tsukuba,  
Tsukuba, Ibaraki 305-8577, Japan

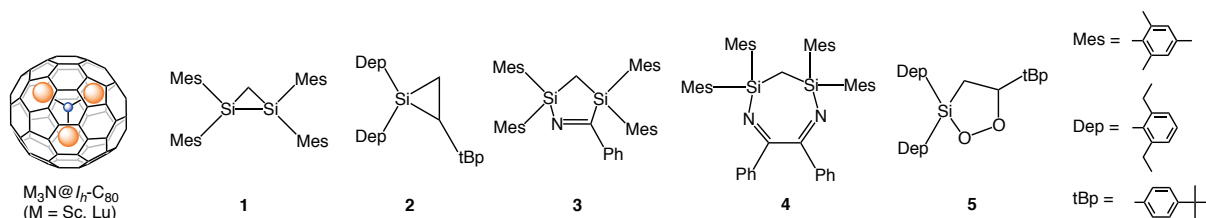
<sup>3</sup>Department of Chemistry, Tokyo Gakugei University, Tokyo 184-8501, Japan

<sup>4</sup>Foundation for Advancement of International Science, Ibaraki 305-0821, Japan

Endohedral metallofullerenes (EMFs) have acquired a lot of interest from researchers because of their fascinating structural and electronic properties. Exohedral functionalization is a crucial method that enables the utilization of EMFs for various applications in molecular electronics and biomedicine. As a part of our continuing study of functional EMF derivatives, we have been developing reactions of disiliranes and siliranes with EMFs to afford the corresponding silylated derivatives, which exhibit remarkable electronic properties compared with their parent EMFs [1]. Previously, it was reported that the photoreaction of disilirane **1** with C<sub>60</sub> in benzonitrile produced **3** and **4** as the adducts of **1** and benzonitrile instead of the adduct of **1** and C<sub>60</sub> [2]. These results prompted us to examine the solvent effect on the photoreactions of disilirane **1** and silirane **2** with M<sub>3</sub>N@I<sub>h</sub>-C<sub>80</sub> (M = Sc, Lu).

When Sc<sub>3</sub>N@I<sub>h</sub>-C<sub>80</sub> and **1** was irradiated in a mixed solvent of toluene and benzonitrile by two 500 W halogen lamps under an argon atmosphere, two benzonitrile adducts **3** and **4** were obtained in 42% and 14% yields, respectively. In the case of Lu<sub>3</sub>N@I<sub>h</sub>-C<sub>80</sub>, a similar reaction took place to produce **3** and **4** in 44% and 23% yields, respectively. In contrast, the photoreaction of Sc<sub>3</sub>N@I<sub>h</sub>-C<sub>80</sub> (or Lu<sub>3</sub>N@I<sub>h</sub>-C<sub>80</sub>) and **2** under the same conditions afforded the corresponding oxygenated product **5**, and no benzonitrile adduct of **2** was obtained. The formation of **5** may result from oxygenation by the residual oxygen in the solvent during the photolysis. The mechanistic pathway of photochemical conversions of **1** and **2** in the presence of M<sub>3</sub>N@I<sub>h</sub>-C<sub>80</sub> (M = Sc, Lu) will be discussed.

### Scheme 1.



[1] M. Yamada and T. Akasaka, *Bull. Chem. Soc. Jpn.* **87**, 1289–1314 (2014).

[2] T. Akasaka, *et al. Org. Lett.* **1**, 1509–1512 (1999).

Corresponding Author: Masahiro Kako Tel: +81-42-442-5570 E-mail: [kako@e-one.uec.ac.jp](mailto:kako@e-one.uec.ac.jp)

## Energetics and electronic structure of SIMEF chains

Sho Furutani and Susumu Okada

*Graduate School of Pure and Applied Sciences, University of Tsukuba, 1-1-1 Tennodai,  
Tsukuba, Ibaraki 305-8571, Japan*

Fullerene and fullerene derivatives are widely used for electron acceptor in organic photovoltaic devices because of their deep lowest unoccupied state resulting in the high open voltage to the electron donor materials. Silylmethyl[60]fullerene (SIMEF) is one of representative fullerene derivatives which has high electron mobility due to their crystal packing structure in device structures. Although experiments are advancing the efficiency of the devices, a little is known the detailed electronic properties of SIMEF in packed structure. In particular, because of the complicated crystalline structure, the effective mass of SIMEF is not sufficiently address to date. Therefore, in this work, we aim to investigate the energetics and electronic structures of SIMEF chains with various intermolecular arrangements to give theoretical insight into the preferable geometries and physical origin of the high

electron mobility in terms of their electronic energy band. All calculations are conducted using the density functional theory with local density approximation and ultrasoft pseudopotentials. To unravel the physical origin of the high carrier mobility, we evaluate the electron effective mass along SIMEF chains with various intermolecular arrangements under the optimum spacing (Fig. 1).

Our calculations show that the chain chains possess the effective masses of  $3.0m_e$ ,  $15.2m_e$ ,  $10.1m_e$ , and  $871.0m_e$  for the intermolecular angles of  $0^\circ$ ,  $30^\circ$ ,  $60^\circ$ , and  $90^\circ$ , respectively. Thus, the chain with molecular angle of  $0^\circ$  give the smallest electron effective mass among these chains. On the other hand, the biding energy of the chain with  $60^\circ$  is the most favorable intermolecular arrangement.

Corresponding author: S. Furutani

Tel: +81-29-853-5600 (ext.8233), Fax: +81-29-853-5924,

E-mail: sfurutani@comas.frsc.tsukuba.ac.jp

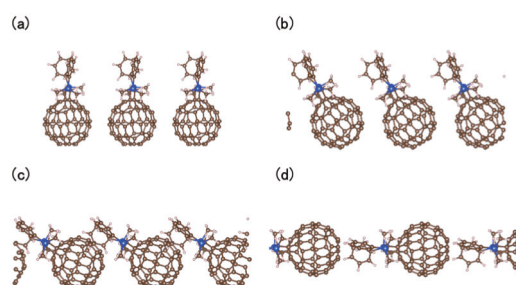


Fig. 1 The structural model of SIMEF chains with molecular angles of (a)  $0^\circ$ , (b)  $30^\circ$ , (c)  $60^\circ$ , and (d)  $90^\circ$ .

## Absolute yield of fullerene formed by graphite laser ablation at medium-high ambient temperatures

○Haruka Suzuki, Yuki Taguchi, Takeshi Kodama, Yohji Achiba, and Haruo Shiromaru

*Department of Chemistry, Tokyo Metropolitan University, Tokyo 192-0397, Japan*

In our previous paper, we have shown that a macroscopic amount of C<sub>60</sub> is produced by laser ablation of graphite in a room temperature gas flow and the yield is considerably higher than that expected from the extrapolation of the yields by high-temperature laser ablation, above 500 °C [1-3]. In the present study, we produced C<sub>60</sub> in a similar way while the irradiation cell was gently heated up to 200 °C. The experimental setup is the same with that employed in Ref. [1] except for an external heating device, a kanthal electric heating wire around a glass, as schematically shown in Fig. 1. Flowing Ar gas (100 mL/min), Nd: YAG laser (10 Hz, 532 nm) with the power of 300 mJ/pulse was irradiated for 30 minutes. The gas temperature was measured with a thermocouple placed 5 mm downstream of the ablation area, in an independent measurement with the same flow rate of Ar. It should be noted that the gas temperatures rise about 85 degrees under laser ablation at room temperature.

The ablation products carried by Ar gas flow were captured in 5 mL toluene. Soluble products attached to the glass cell were extracted by sonication for about 20 minutes in excessive amounts of toluene. The solution was then concentrated to a volume of 5 mL. The amount of vaporized graphite was measured as the difference in the weight before and after irradiation.

The products, which were carried by Ar gas flow and attached to the cell, were analyzed by HPLC (column: Buckyprep, eluent: toluene). The yields are shown in Fig. 2 together with the reference data. At 23 °C, the total amount of C<sub>60</sub>, the average of six independent runs, was 1.0 × 10<sup>-3</sup> mg and the yield of C<sub>60</sub> was 0.034 wt%. At 100 °C and 200 °C, the yields of C<sub>60</sub> show a nearly flat behavior with respect to the gas temperature, suggesting a need of reconsideration of the formation mechanism of C<sub>60</sub>.

[1] H. Endo *et al.*, *Chem. Phys. Lett.* **642**, 35 (2015).

[2] T. Wakabayashi *et al.*, *Structure and Dynamics of Clusters*, p. 535 (1996).

[3] D. Kasuya *et al.*, *Eur. Phys. J. D*, **9** 355 (1999).

Corresponding Author: H. Suzuki,

Tel: +81-42-677-1111, Fax: +81-42-677-2525,

E-mail: suzuki-haruka4@ed.tmu.ac.jp

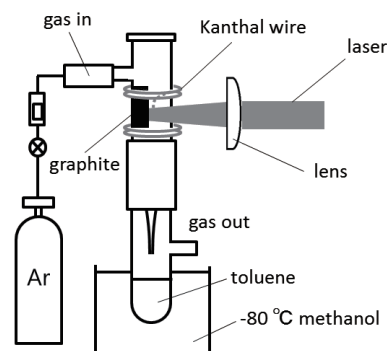


Fig. 1 Schematic drawing of the experimental setup.

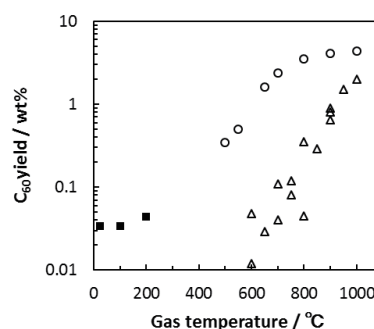


Fig. 2 C<sub>60</sub> yield vs. temperature graph.  
 △: “Laser-furnace” at 500 Torr [2],  
 ○: “Laser-furnace” at 200 Torr [3],  
 ■: present study.

## **Energetics and electronic properties of fullerenes consisting of fused pentagonal rings**

Susumu Okada

*Graduate school of Pure and Applied Sciences, University of Tsukuba, Tsukuba  
305-8571, Japan*

A fused pentagon trimer, an acepentalene structure, can be a constituent unit of a two-dimensional covalent network of  $sp^2$  C atoms, by assembling them in hexagonal manner, which exhibits ferromagnetic spin ordering throughout the sheet owing to the flat dispersion band at the Fermi level [1,2]. In the case, the network contains dodecagonal ring as the pore in the network. By substituting the other polygons smaller than dodecagon, we can get hollow cage structures of fused pentagonal rings as the zero dimensional version of graphitic network of fused pentagons. In this work, we theoretically studied the energetics and electronic structures of the hollow-cage pentagonal network,  $C_{28}$ ,  $C_{56}$ , and  $C_{140}$  fullerenes, using the density functional theory with generalized gradient approximation. Our calculation showed that the total energies of these fullerenes are almost the same as that of the planar sheet of fused pentagons, while those are higher by about 0.2 eV than that of  $C_{60}$ . According to the small gap between the highest occupied and the lowest unoccupied states,  $C_{140}$  exhibits spin polarization in which the polarized electron spins are extended throughout their cage.

### Reference

- [1] M. Maruyama and S. Okada, *Appl. Phys. Express* **6**, 095101 (2013).
- [2] M. Maruyama and S. Okada, *Jpn. J. Appl. Phys.* **53**, 06JD02 (2014).

Corresponding Author: S. Okada

E-mail: sokada@comas.frsc.tsukuba.ac.jp

## Macroscopic aligned single-walled carbon nanotubes achieved with vacuum filtration

○ Hao Zhang<sup>1</sup>, Rong Xiang<sup>1</sup>, Taiki Inoue<sup>1</sup>, Shohei Chiashi<sup>1</sup>, Shigeo Maruyama<sup>1,2</sup>

<sup>1</sup> Department of Mechanical Engineering, the University of Tokyo, Tokyo 113-8656, Japan

<sup>2</sup> National Institute of Advanced Industrial Science and Technology (AIST), Ibaraki 305-8564, Japan

Excellent electronic, thermal and optical properties found in individual single-walled carbon nanotubes has made this one-dimensional material one of the best candidates for many new-generation applications such as nanoprobe, molecular reinforcements in composites, displays, sensors, energy-storage media and molecular electronic devices [1]. Recently, a novel vacuum filtration method (Fig. 1) was proposed by Xiaowei He et al. [2] for fabricating well aligned SWNT films at macro scale. However, the aligned films made from different SWNTs vary markedly in quality and the detailed mechanism is still unclear. Here, we are trying to build a connection between starting materials and the degree of the alignment.

By far, with the recipe from this pioneering paper, horizontally aligned SWNT arrays at centimeter scale have been successfully reproduced as confirmed by SEM. (Fig. 2) Further, the characterization of the films with Resonance Raman spectroscopy, UV-vis-NIR spectrometer, TEM and etc. will be presented.

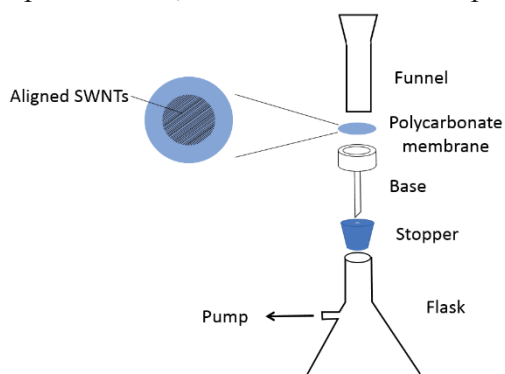


Fig. 1. A schematic of the vacuum filtration setup.

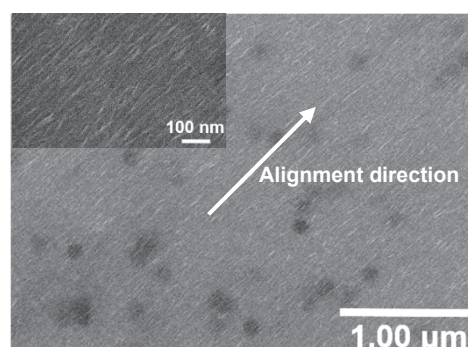


Fig. 2. SEM image of aligned SWNT film produced with vacuum filtration method and SEM image of higher magnification (Inset).

[1]. R. H. Baughman et al., Science 297, 787-792 (2002)

[2]. X. He et al., Nature Nanotech, 10.1038 (2016)

Corresponding Author: Shigeo Maruyama

Tel: +81-3-5841-7434, Fax: +81-3-5841-7437

E-mail: maruyama@photon.t.u-tokyo.ac.jp

## Selective phonon mode generations in single wall carbon nanotubes and graphene nanoribbons

○ Ahmad R.T. Nugraha, Eddwi H. Hasdeo, Riichiro Saito  
*Department of Physics, Tohoku University, Sendai 980-8578, Japan*

Ultrashort laser pulses given to a single wall carbon nanotube (SWNT) sample with duration less than a phonon period in the SWNT may generate lattice oscillations coherently, known as coherent phonons. By using sub-10-fs laser pulses, many coherent phonon modes with frequency around  $100\text{-}3000\text{ cm}^{-1}$  could be observed in an enriched SWNT sample [1]. This opened up a possibility to utilize particular coherent phonon modes of the SWNT as a nanoresonator with a wide frequency range. Besides SWNTs, graphene nanoribbons (GNRs) also have several modes available in the THz regime [2]. However, in order to take advantage of each coherent phonon mode as a basis of phononic devices [3], we have to select a single coherent phonon mode among many phonon modes that have been excited.

In this work, we theoretically investigate the ultrafast pulse-train technique in pump-probe spectroscopy to keep a single coherent phonon mode while suppressing the other phonon modes in SWNTs and GNRs. In particular, we focus on the selectivity of the radial breathing mode (RBM) and the G band for a given SWNT [4]. By adjusting the laser pulse width and pulse train repetition period, we find that if the repetition period matches with integer multiple of the RBM phonon period, the RBM phonon could be kept while the other modes are suppressed. As for the G band, which has a higher frequency (shorter period) than the RBM, the number of pulses in the pulse train also affects the selectivity through the ratio of the G band and RBM's periods so that some special values of the pulse number could give a good selectivity (Figure 1). By understanding the selectivity of each phonon mode, we expect that it could be possible to develop SWNT and GNR's phononic devices in the near future.

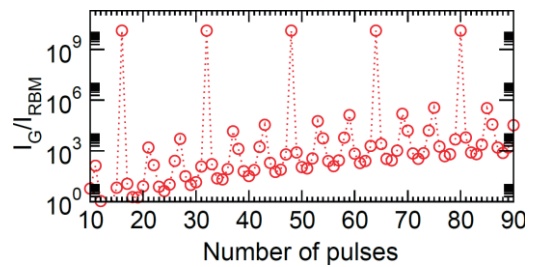


**Figure 1** Ratio of coherent G band and RBM intensities for a (11,0) SWNT.

- [1] Y.-S. Lim et al., *Nano Lett.* 14, 1426-1432 (2014).
- [2] G. D. Sanders et al., *Phys. Rev. B* 85, 205401 (2012).
- [3] R. Ruskov and C. Tahan, *J. Phys.: Conf. Ser.* 398, 012011 (2012).
- [4] A. R. T. Nugraha et al., *J. Phys. Condens. Matter* 29, 055302 (2017).

Corresponding Author: A.R.T. Nugraha

Tel: +81-22-795-6442, Fax: +81-22-795-6447, E-mail: nugraha@flex.phys.tohoku.ac.jp

## Electrically conductive multi-walled boron nitride nanotubes by catalytic etching

○Do-Hyun Kim<sup>1</sup>, Ho-Kyun Jang<sup>1</sup>, Min-Seok Kim<sup>2</sup>, Sung-Dae Kim<sup>2</sup>, Dong-Jin Lee<sup>3</sup>, Gyu Tae Kim<sup>1</sup>

<sup>1</sup> School of Electrical Engineering, Korea University, 5-Ga, Anam-dong, Seongbuk-Gu, Republic of Korea

<sup>2</sup> Metallic Materials Division, and Advanced Characterization and Analysis Group, Korea Institute of Materials Science, 797 Changwondaero, Changwon, Republic of Korea

<sup>3</sup> New Functional Components Research Team, Korea Institute of Footware & Leather Technology, 152 Danggamseo-ro, Busanjin-gu, Busan 614-100, Republic of Korea

Boron nitride nanotubes (BNNTs) are hardly oxidized below 1000 °C due to their superior thermal stability and electrically almost insulators with a band gap of 5 eV in the electronic structure. Hence, oxidizing BNNTs at low temperature and converting their electrical properties to a conductive behavior are challenging tasks.

In this work, we report that BNNTs can be etched at low temperature in the air by catalytic oxidation. To realize this, multi-walled BNNTs (MWBNTs) were impregnated with Co precursor ( $\text{Co}(\text{NO}_3)_2 \cdot 6\text{H}_2\text{O}$ ) and simply heated at 350 °C under air atmosphere. Consequently, various shapes of etched structures like pits and thinned walls were formed on the surface of MWBNTs. Furthermore, the original crystallinity and the tubular structure of MWBNTs were kept in the etched MWBNTs in spite of oxidation. Interestingly, insulating MWBNTs showed a conductive behavior in the electrical measurement after etching by catalytic oxidation. It was revealed by theoretical calculations that a new energy state in the gap and a Fermi level shift contributed to MWBNTs being conductive.

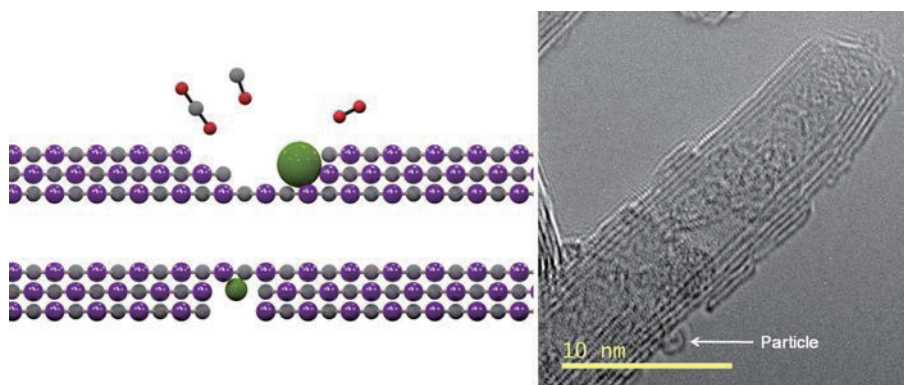


Fig.1 Etched multi-walled boron nitride nanotubes by catalytic oxidation

Corresponding Author: Do-Hyun Kim, Gyu Tae Kim

Tel: +82-2-3290-4791

E-mail: nanotube@korea.ac.kr, gtkim@korea.ac.kr

## Artificial muscle using single wall carbon nanotube bundles

○ Nguyen T. Hung, Ahmad R. T. Nugraha, Riichiro Saito  
*Department of Physics, Tohoku University, Sendai 980-8578, Japan*

An artificial muscle is a novel actuator based on a variety of polymers or composites that change their shape when excited electrically. A composite of single wall carbon nanotubes (SWNTs) is known to be one of the strongest and stiffest materials [1, 2], and it can reversibly contract and expand in volume under an applied voltage, similar to the natural muscle. Almost two decades ago, Baughman et al. [3] built an ultra-strong artificial muscle from bundles of SWNTs with electrochemical charging, in which the artificial muscle could be about 100 times stronger than the natural muscle in terms of force generated per unit area. Their work indicated importance of understanding the effects of doping on the structural deformation of the *bundles* of SWNTs. However, while both structural deformation and electronic structure of the *individual* SWNTs under electromechanical charging have been extensively investigated by theory [4, 5], a detailed first-principles study for the SWNT *bundles* is necessary to discuss since most of the actuators are made of the *bundles*. Now since SWNTs are commercially available, the application for artificial is now getting promising.

In this work, we perform a first-principles simulation to discuss the effects of electron and hole doping on the structural deformation and on the electronic structure of SWNT bundles. We use a (6, 6) SWNT bundle as a model [Fig. 1] and we predict a mechanical deformation in the (6, 6) SWNT bundle as a function of gate voltage, which provides the basis for electromechanical actuators. The (6, 6) SWNT bundle exhibits a broken symmetry and pseudogaps around the charge neutral condition with a band gap of about 0.41 eV. We find that the magnitude of the actuation response of hole-doped (6, 6) SWNT bundle is larger than that of electron-doped (6, 6) SWNT bundle, suggesting the hole-doped SWNT bundle for a building block of artificial muscles.

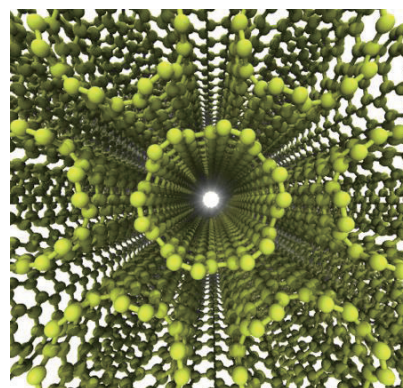


**Figure 1** (6, 6) SWNT bundle model.

- [1] M. F. Yu et al., *Science* **28**, 637 (2000).
- [2] N. T. Hung et al. *Comput. Mater. Sci.* **114**, 167 (2016).
- [3] R. H. Baughman et al., *Science* **284**, 1340 (1999).
- [4] L. C. Yin et al., *Carbon* **49**, 4774 (2011).
- [5] Y. N. Gartstein et al., *Phys. Rev. Lett.* **89**, 045503 (2002).

Corresponding Author: Nguyen Tuan Hung

Tel: +81-22-795-6442, Fax: +81-22-795-6447, E-mail: [nguyen@flex.phys.tohoku.ac.jp](mailto:nguyen@flex.phys.tohoku.ac.jp)

## Electrochemical Properties of Nitrogen-Doped Vertically Aligned Multi-Walled Carbon Nanotubes Prepared by Defluorination

○Rei Nonomura<sup>1</sup>, Takashi Itoh<sup>2</sup>, Yoshinori Sato<sup>3</sup>, Masashi Yamamoto<sup>3</sup>, Tetsuo Nishida<sup>3</sup>, Kenichi Motomiya<sup>1</sup>, Kazuyuki Tohji<sup>1</sup>, Yoshinori Sato<sup>1,4,\*</sup>

<sup>1</sup>Graduate School of Environmental Studies, Tohoku University, Sendai 980-8579, Japan

<sup>2</sup>Frontier Research Institute for Interdisciplinary Sciences, Tohoku University, Sendai 980-8579, Japan

<sup>3</sup>Stella Chemifa Co., Osaka 595-0075, Japan

<sup>4</sup>Institute for Biomedical Sciences, Interdisciplinary Cluster for Cutting Edge Research, Shinshu University, Matsumoto 390-8621, Japan

Vertically aligned carbon nanotubes (VACNTs) have been utilized as electrodes of electric double-layer supercapacitors (EDLSCs) because of their excellent electrical properties by which the EDLSCs exhibit high power densities with keeping specific capacitances, in compared with activated carbon electrodes. In chemically functionalized CNTs, the specific capacitances are larger than those of unfunctionalized CNTs. Therefore, functionalized VACNTs are great candidates as electrodes for high-performance EDLSCs. Here, we report the synthesis of nitrogen-doped vertically aligned multi-walled carbon nanotubes (VAMWCNTs) via defluorination<sup>[1,2]</sup> and their electrochemical properties.

As-grown VAMWCNTs synthesized by a chemical vapor deposition method were fluorinated using a mixture of F<sub>2</sub> (20%) and N<sub>2</sub> (80%) at 250 °C for 30 min. The fluorinated-VAMWCNTs (F-VAMWCNTs) placed at the center into a quartz tube were reacted with flowing a mixture of NH<sub>3</sub> (1%) and N<sub>2</sub> (99%) at the temperature of 573-873 K for 30 min (N-VAMWCNTs). The samples were characterized using scanning electron microscopy (SEM), high-resolution transmission electron microscopy (HRTEM), X-ray photoelectron spectroscopy (XPS), and Raman scattering spectroscopy. Electrochemical properties were evaluated by cyclic voltammetry and AC impedance spectroscopy using a two or three electrode coin-type cell in propylene carbonate (PC) electrolyte containing triethylmethylammonium tetrafluoroborate (TEMABF<sub>4</sub>)<sup>[3]</sup>. We will report the detailed data in this presentation.

[1] K. Yokoyama *et al.* Carbon **94**, 1052 (2015).

[2] K. Yokoyama *et al.* J. Mater. Chem. A **4**, 9184 (2016).

[3] Y. Honda *et al.* J. Power Sources **185**, 1580 (2008).

\*Corresponding Author: Yoshinori Sato

Tel: +81-22-795-3215, Fax: +81-22-795-3215,

E-mail: yoshinori.sato.b5@tohoku.ac.jp

## Synthesis and morphology control of carbon nanotubes on substrates for electron emitter application

○Sae Kitagawa<sup>1</sup>, Hisashi Sugime<sup>2</sup>, Suguru Noda<sup>1,\*</sup>

<sup>1</sup>Department of Applied Chemistry, Waseda University, Tokyo 169-8555, Japan

<sup>2</sup>Waseda Institute for Advanced Study, Waseda University, Tokyo 169-8050, Japan

Electron emitters are used for display, X-ray tube and so on. In conventional electron emitters, thermionic emission is widely used, in which electrons are emitted from heated filament. But this method has some problems, such as large power consumption and short lifespan. Field emission (FE), in which electrons are emitted by high electric field, is an alternative method, which can solve these problems [1]. Carbon nanotubes (CNTs) are a suitable material for electron emitters due to their high aspect ratio, electric conductivity, thermostability and mechanical strength. In order to enhance electric field and increase current and lifespan, adequate density of CNT tips is necessary. Lithography is often used to form microstructure of CNTs and previously our laboratory reported that morphology controlled CNTs by e-beam lithography showed good FE performance [2,3].

In this work, we fabricate CNT-FEs with controlled morphology via quick self-organization processes without using lithography. Textured Si wafers and stainless steel mesh (SUS 304) are used as growth substrates for CNTs. Si wafers are treated with HF to remove surface SiO<sub>2</sub> and then etched in 2 wt% NaOH solution to form surface texture (Fig. 1). Fe/TiN and Fe/Al/Ti are sputtered on the textured Si substrate and SUS mesh, respectively. These substrates are set in a CVD reactor (inner diameter of 34 mm, heating zone length of 300 mm) and annealed for 3 min at 700 °C under H<sub>2</sub> flow. Subsequently, C<sub>2</sub>H<sub>2</sub> as carbon source is introduced to grow CNTs under 1.0 vol% C<sub>2</sub>H<sub>2</sub>/10 vol% H<sub>2</sub>/Ar for 1–5 min. Obtained CNTs are evaluated in a diode configuration at  $<4 \times 10^{-5}$  Pa. CNTs/substrate is used as cathode, which opposes to anode of ITO glass with a 500 μm gap using glass spacer. Emitter array size is approximately 0.8×0.8 cm<sup>2</sup>. Sweep voltage (0–600V) is applied for 100 times and FE properties and lifespan are evaluated.

Fig. 2 shows a SEM image of CNTs synthesized for 5 min on a SUS mesh. The Ti/Al under layer enables CNTs growth on the SUS mesh, which results in morphologically controlled CNTs. Fig. 3 shows FE currents extracted from the CNTs on SUS mesh. Electrons are efficiently emitted by external field with 2 mA at 600 V.

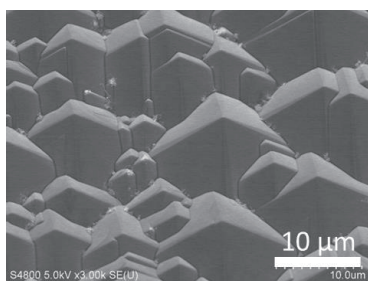


Fig. 1. Textured Si substrate

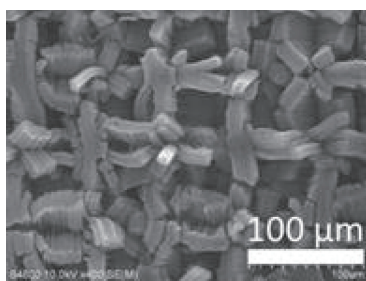


Fig. 2. CNTs on mesh (5 min)

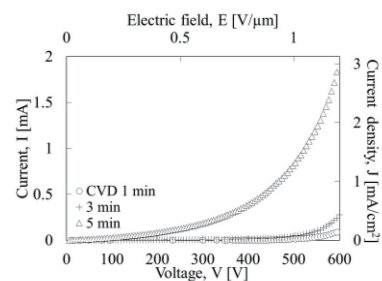


Fig. 3. I-V curves

[1] Yuan Cheng *et al*, C. R. Physique 4 (2003).

[2] Y. Shiratori *et al*, Nanotechnology 20 (2009).

[3] K. Sekiguchi *et al*, Carbon 50 (2012).

Corresponding Author: S. Noda, Tel&Fax: +81-3-5286-2769, E-mail: noda@waseda.jp

## Analysis of Pt catalyst for SWNT growth by In-situ XANES

○Makoto Kumakura<sup>1</sup>, Hoshimitsu Kiribayashi<sup>1</sup>, Takahiro Saida<sup>2</sup>, Shigeya Naritsuka<sup>1</sup>,  
Takahiro Maruyama<sup>2</sup>

<sup>1</sup> Department of Material Science and Engineering, Meijo Univ, 1-501 Shiogamaguchi,  
Tempaku, Nagoya 468-8502, Japan

<sup>2</sup> Department of Applied Chemistry, Meijo Univ, 1-501 Shiogamaguchi, Tempaku, Nagoya  
468-8502, Japan

Single-walled carbon nanotubes (SWNTs) have been anticipated for applications to electronic devices because SWNTs have superior electrical characteristics. The smaller an SWNT diameter, the wider its bandgap, so it is important to grow small-diameter SWNTs. So far, using Pt catalyst, we have succeeded in obtaining SWNTs with small diameters below 1.0 nm [1]. However, growth mechanism of SWNTs from Pt catalysts has been unclear. In this study, we investigated chemical states of Pt catalysts during SWNT growth by in-situ X-ray absorption near edge structure (XANES).

Using Pt catalysts, SWNTs were grown on SiO<sub>2</sub>/Si substrates by CVD method in in-situ CVD chamber. The growth temperature and the ethanol pressure were 700 °C and 20 Pa, respectively. The growth time was 60 min. In addition, Pt catalysts just before and after heating at 700 °C were analyzed. XANES were carried out at BL5S1 of Aichi SR.

Fig. 1 shows Pt L<sub>3</sub>-edge XANES spectra of Pt catalysts at each process. After deposition, the white line intensity was larger than that of Pt foil, but became smaller after heating. During SWNT growth, XANES spectra did not change. This indicates that Pt catalysts were reduced after heating and that Pt catalysts were metallic during SWNT growth [2]. This means that carbon atoms did not solved into Pt catalysts and diffused on the catalyst surface during SWNT growth. Our results indicate that SWNTs grew from Pt catalysts based on the vapor-solid-solid (VSS) model.

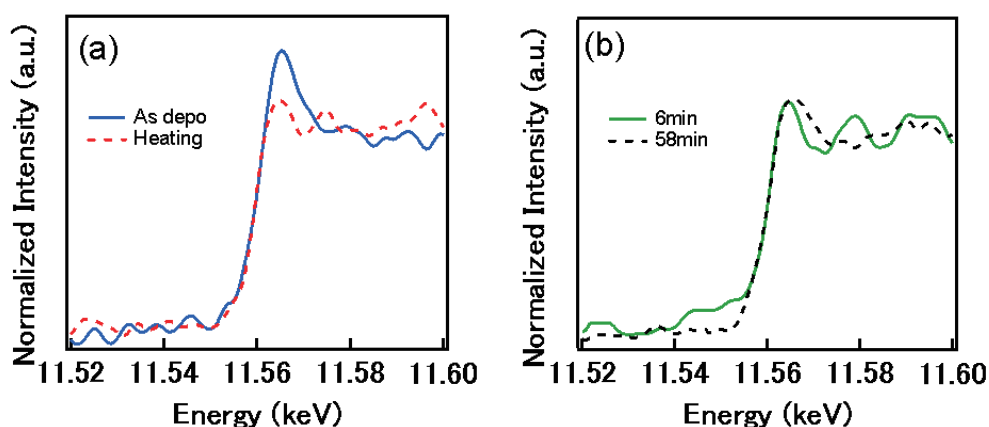


Fig.1 In-situ Pt L<sub>3</sub>-edge XANES spectra of Pt catalysts for the samples (a) as deposition and during heating at 700 °C and (b) after SWNTs growth for 6 and 58 min.

[1] T. Maruyama et al. Mater. Express 1 (2011) 267.

[2] T. Shishido et al., Catal. Lett. 131 (2009) 413.

Corresponding Author: Takahiro Maruyama

Tel: 052-838-2386

E-mail: takamaru@meijo-u.ac.jp

## Time-dependent selective synthesis and growth mechanism of single-walled carbon nanotubes from sputtered W-Co catalyst

○ Hua An<sup>1</sup>, Rong Xiang<sup>1</sup>, Akihito Kumamoto<sup>2</sup>, Taiki Inoue<sup>1</sup>, Shohei Chiashi<sup>1</sup>, Yuichi Ikuhara<sup>2</sup>, Shigeo Maruyama<sup>1,3</sup>

*1 Department of Mechanical Engineering, The University of Tokyo, Tokyo 113-8656, Japan*

*2 Institute of Engineering Innovation, The University of Tokyo, Yayoi 2-11-16, Bunkyo-ku, Tokyo 113-8656, Japan*

*3 Energy NanoEngineering Laboratory, National Institute of Advanced Industrial Science and Technology (AIST), 1-2-1 Namiki, Tsukuba, 305-8564, Japan*

The potential industrial applications are impeded by the mixed chiralities of as-grown SWNT assemblies. Direct synthesis of SWNTs with single chirality is challenging but always attracts considerable attention among researchers. Catalyst plays an important role in the chirality definition of SWNTs during growth process. Bimetallic catalysts have been explored for the selective growth of SWNTs because of their inhibition for the aggregation of catalyst particles at growth temperature. The  $\text{Co}_7\text{W}_6$  clusters were reported to successfully grow a single chirality SWNT (12, 6), with over 90% abundance and a zigzag SWNT (16, 0), with near 80%, by controlling the catalyst structure and growth conditions with a high-temperature reduction and growth [1, 2]. We have proposed a simple sputtering method to prepare W-Co catalyst to selectively grow (12, 6) SWNTs with the enrichment of 50%-70% where the selectivity is strongly associated with the intermediate structure of  $\text{Co}_6\text{W}_6\text{C}$  [3]. A 5 min-growth with alcohol catalytic chemical vapor deposition (ACCVD) [4] will give only Co particles indicating a complicated evolution of catalyst structure. Here we will present a detailed time-dependent study on the selectivity and the structural evolution within 5 min-growth with ethanol. The complicated structure evolution will be illustrated by electron diffraction and energy-dispersive X-ray spectroscopy (EDS) mapping. The as-reduced catalyst particles are confirmed to be W and  $\text{W}_6\text{Co}_6\text{C}$ . Upon the introduction of ethanol, additional W will be removed gradually through a gas phase reaction and the ratio of W decreases. The further loss of W will result in the precipitation of Co from the carbide particles. A possible mechanism will be discussed in detail.

[1] F. Yang et al., *Nature*, **510**, 522(2014).

[2] F. Yang et al., *J. Am. Chem. Soc.* **137**, 8688 (2015).

[3] H. An, et al., *Nanoscale*, **8** (2016) 14523.

[4] S. Maruyama et al., *Chem. Phys. Lett.* **360**, 229 (2002).

Corresponding Author: Shigeo Maruyama

Tel: +81-3-5841-6421, Fax: +81-3-5800-6983

E-mail: maruyama@photon.t.u-tokyo.ac.jp

## Extraction of High-Purity Single-Chirality Single-Wall Carbon Nanotubes by Precise Tuning of pH using CO<sub>2</sub> Bubbling

○Yota Ichinose, Junko Eda, Yutaka Maniwa, Yohei Yomogida, Kazuhiro Yanagi

*Tokyo Metropolitan University, Tokyo 192-0397, Japan*

Gel-column chromatography is known as a powerful tool to extract a specific chirality of single-chirality single-wall carbon nanotubes (SWCNTs) in high-purity from a solution with a mixture of different chiralities of SWCNTs [1]. In this purification processes, we sometimes find that extraction results vary how long eluent solutions are left in ambient air. It is reported that pH of eluent solutions influences on the extraction results [2]. Thus we thought that the CO<sub>2</sub> in the air would induce the pH changes and then influence the result. To clarify this hypothesis, we adjusted the the pH of the eluent solutions using CO<sub>2</sub> bubbling, and then investigated how slight difference of pH influences on extraction results.

In this study, we investigated the influence of pH on the basis of a reported technique to extract the single-chirality SWCNTs without pH adjustment [1]. We found that metallic SWCNTs were residual (original, Fig.1) after (6,5) chirality extraction. However, to systematically and precisely adjust the pH value of the eluent solutions, from 8.2 to 7.7 in 0.1 steps by CO<sub>2</sub> bubbling, we found that the residual metallic SWCNTs could be completely removed at a proper condition (at the pH of ~8.0). As a result, we could obtain high-purity single-chirality (6,5) SWCNTs (Fig. 2). The purity of the sample was evaluated to be more than 99% from optical absorption spectra, and preparation of such purity sample was crucial for correct evaluation of thermo-electric performance of SWCNTs.

Reference:

[1] Yomogida et al., Nature Commun 7, 12056 (2016)

[2] Hirano et al., ACS Nano 7, 10285 (2013)

Corresponding Author: K. Yanagi

Tel: +81-42-677-2493,

E-mail: yanagi-kazuhiro@tmu.ac.jp

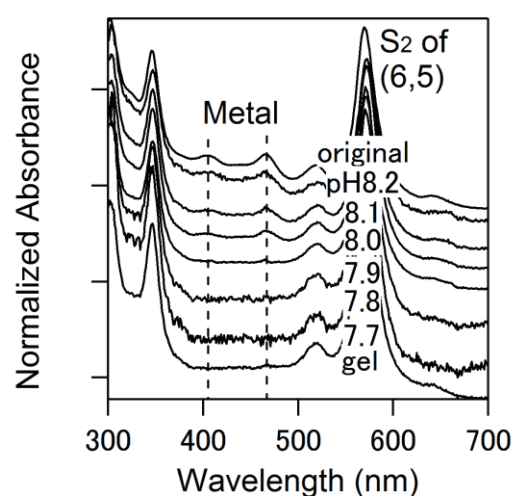


Fig. 1. Removal of metallic SWCNTs using systematically different pH solutions

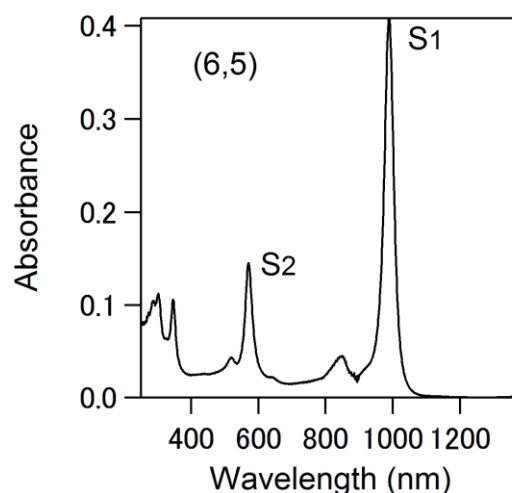


Fig. 2. Optical absorption spectrum of (6,5) SWCNTs

## Magnetic field effects on the growth process of SWCNTs and examination of its mechanism

○Yasumasa Takashima, Atom Hamasaki, Jin Uchimura, Sumio Ozeki

*Graduate School of Science and Technology, Shinshu University,  
Matsumoto, Nagano 390-8621, Japan*

Magnetic fields have possibility controlling carbon structure, which leads to various functions. We reported magnetic field effects (MFEs) on a few carbon materials [1-2]. Number of crystallite of graphite precursor was increased by magnetic fields during heat-treatment of coal tar pitch and multi-walled carbon nanotubes aligned to the direction of a magnetic field. These structural changes were explained by magnetic orientation of carbon hexagonal layer. In this study, MFEs on single-walled carbon nanotubes (SWCNTs) was found, although the magnetic orientation was not observed in its growth process.

Carbon materials including SWCNTs grew on carbon paper substrate by thermal decomposition of alcohols dissolving cobalt (II) acetate tetrahydrate. The liquid decomposition method was carried out at 1053 K by resistance-heating of a solution under magnetic field of up to 10 T using a superconducting magnet.

Metallic SWCNTs of just 1.0 nm diameter grew preferentially under magnetic fields (Fig. 1). Sub-peak of C 1s in X-ray photoelectron spectra at 288.5 eV decreased with increasing magnetic field, which corresponds to a change in carbon-oxygen bond (Fig. 2). Structural changes in SWCNTs were possibly brought about by an anomalous growth environment due to magnetic fields.

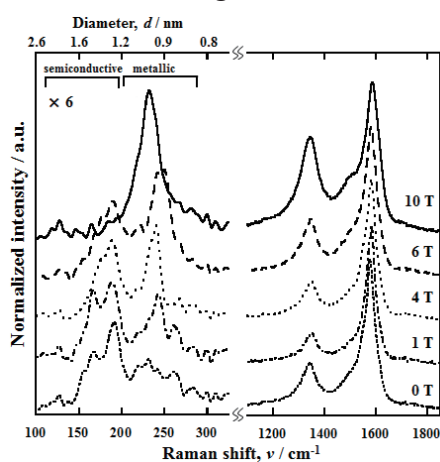


**Fig. 1.** Raman spectra excited with 532 nm of carbon materials prepared under various magnetic fields.

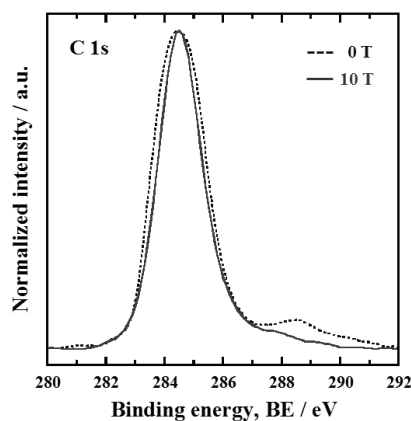


**Fig. 2.** C 1s spectra of carbon materials prepared under 0 and 10 T.

[1] A. Sakaguchi, A. Hamasaki, T. Sadatou, Y. Nishihara, S. Yamamoto, Y. Sekinuma, S. Ozeki, *Chem. Lett.*, **2012**, *41*, 1576.

[2] A. Sakaguchi, A. Hamasaki, S. Ozeki, *Chem. Lett.*, **2013**, *42*, 304.

Corresponding Author: Atom Hamasaki

Tel: +81-263-37-2466, Fax: +81-263-37-2559, E-mail: atom@shinshu-u.ac.jp

## Chemical reaction analysis of Fe-Co and Co-Cu clusters with ethanol by FT-ICR mass spectrometer

○Ken Mizutani<sup>1</sup>, Yoshinori Sato<sup>1</sup>, Hiroya Minowa<sup>1</sup>, Ryohei Yamada<sup>1</sup>,  
Taiki Inoue<sup>1</sup>, Shohei Chiashi<sup>1</sup>, Shigeo Maruyama<sup>1,2</sup>

<sup>1</sup> Department of Mechanical Engineering, The University of Tokyo, Tokyo 113-8656, Japan

<sup>2</sup> Energy NanoEngineering Lab. National Institute of Advanced Industrial Science and Technology (AIST), Ibaraki. 305-8564, Japan

The alcohol catalytic chemical vapor deposition (ACCVD) is an efficient method to synthesize single walled-carbon nanotubes (SWCNTs). In ACCVD method, alcohol is used as the carbon source and metal nanoparticles, such as Fe, Co, Cu, or binary alloy of these metals are used as the catalyst. The alcohol molecules are decomposed on the catalyst and supply carbon atoms. The choice of catalysts affects the quality and quantity of SWCNTs. For instance, Fe-Co gives highly crystalline SWCNTs with high yield [1], while Co-Cu gives small-diameter SWCNTs compared to other catalysts [2]. However, the chemical reactions between these metal catalysts and alcohol molecules are unclear and understanding the reactions contributes to the development of the synthesis method.

In this study, the chemical reactivity of Fe-Co and Co-Cu clusters was investigated by Fourier transform ion cyclotron resonance (FT-ICR) mass spectrometer. These clusters generated by laser vaporization are trapped in a strong magnetic field and reacted with ethanol. The reaction processes can be observed as the change of the mass spectra depending on the reaction time. Figure 1 (a) shows that an ethanol molecule is simply chemisorbed to Fe-Co clusters. On the other hand, Fig. 1 (b) shows that an ethanol molecule is not simply chemisorbed to Co-Cu clusters, and  $\text{Co}_{n-1}\text{Cu}$  cluster is more stable than other compositions.

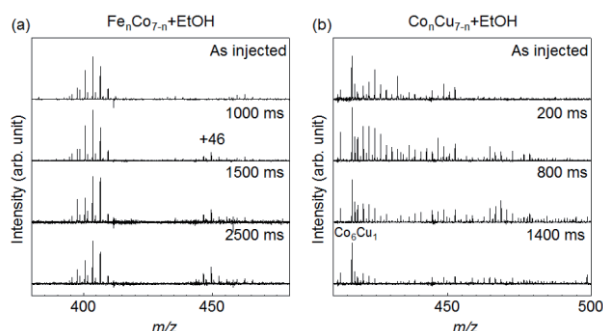


Fig. 1 Mass spectra of (a)  $\text{Fe}_n\text{Co}_{7-n}$  and (b)  $\text{Co}_n\text{Cu}_{7-n}$  clusters reacted with ethanol.

[1] E. Flahaut et al., *Chem. Phys. Letters* **300**, 236 (1999).

[2] K. Cui et al., *Nanoscale* **8**, 1608 (2016).

Corresponding Author: S. Maruyama

Tel: +81-3-5841-6421, Fax: +81-3-5841-6421, E-mail: maruyama@photon.t.u-tokyo.ac.jp

## Carrier injection in nearly free electron states of graphene nanoribbons by edge hydroxylation

Remi Taira, Ayaka Yamanaka, and Susumu Okada

*University of Tsukuba, 1-1-1 Tennodai, Tsukuba, Ibaraki, 305-8571 Japan*

Work function of the graphene edges is sensitive to the edge shapes and edge functional groups. It has been demonstrated that the work function of edges of graphene ribbons is tunable by attaching appropriate chemical functional group; a work function of zigzag edges functionalized by hydroxyl group is smaller than those by carboxyl, ketone, and carbonyl groups [1]. The fact implies that the free electron carriers are induced by the asymmetrical edge functionalization of graphene nanoribbon, one of which edges is functionalized by hydroxyl group. Thus, in this work, we aim to investigate the electronic properties of asymmetrically edge functionalized graphene nanoribbons containing hydroxyl group, using the density functional theory with the local density approximation. To investigate their electronic structures, we consider the graphene nanoribbon with width of 1.5 nm and zigzag edges of which edges are terminated by functionalized groups, -H, -O, -OH, -COH, and -COOH. Figure 1 shows the electronic structure of the asymmetrically terminated graphene ribbons containing hydroxyl group. For the edges with hydroxyl group, we found that the nearly free electron (NFE) state substantially shifts downward and crosses the Fermi level, indicating the free electron carriers are generated alongside the hydroxylated edge of graphene ribbons.

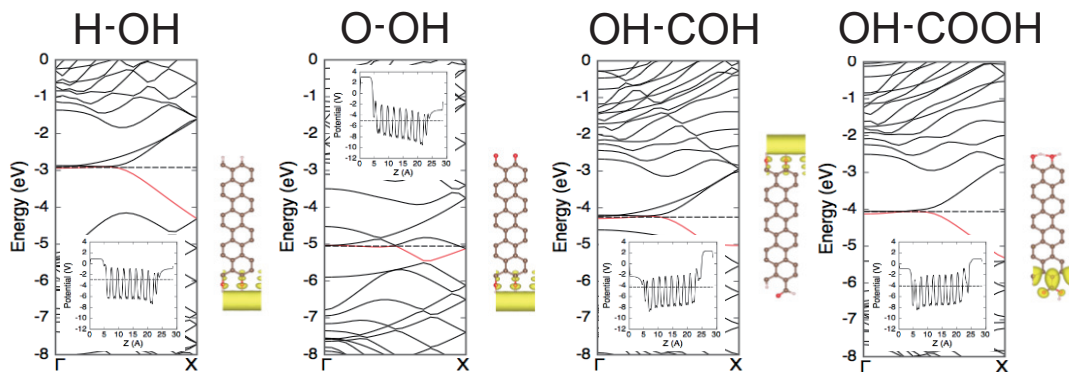


Fig. 1: Electronic structure and the wave function of the branch of conduction band of asymmetrically edge functionalized graphene ribbons containing hydroxyl group.

[1] R. Taira, A. Yamanaka, and S. Okada, *Appl. Phys. Express* **9**, 115102, (2016).

Corresponding author: R. Taira (resoccermi222@gmail.com)

**Fermi level tuning of N-doped graphene by an external electric field**

Manaho Matsubara and Susumu Okada

*Graduate School of Pure & Applied Sciences, University of Tsukuba, Tsukuba 305-8571  
Japan*

Graphene has been keeping a premier position not only in the field of nanoscale sciences but also in the field of nanotechnology due to its unique structural and electronic properties. For application in nanotechnology, owing to the tunable electronic structure by the external condition and the high carrier mobility, graphene could be a constituent material for electronic, optical, optoelectronic, and catalytic devices, being expected to exhibit remarkable efficiency. For the applications, the Fermi level tuning is the one of important issues for controlling their functionality and operation. In addition to pristine graphene, graphene can form hybrid structure with foreign materials, resulting in further variation in their electronic properties that allow them emerging materials for future devices. N-doped graphene is one of representative hybrids exhibiting unusual electronic properties being applicable for electronic and catalytic devices. In such devices, to tailor the device properties, it is mandatory to precisely tune the Fermi level by the external electric field. Thus, in this work, we are interested in the effect of external electric field on band structures and carrier accumulation, and aim to give theoretical insight into the electronic properties of N-doped graphene under the external electric field, using the density functional theory combined with effective screening medium method. Here, we consider four possible N-doped graphene; graphitic, pyridinic, and pyrrolic structures (Fig. 1).

Our calculations show that N-doped graphene does not possess the Dirac cone but a finite energy gap in their  $\pi$  electron state irrespective to the defect species. On the other hand, the electronic structures near the Fermi level are sensitive to the defect species. Under the external electric field, the electronic states near the Fermi level exhibit unusual modulation that depends on the distribution of wave function of these states: The electronic state associated with the dangling bonds substantially shifts under the external electric field while the  $\pi$  states are insensitive to the electric field. According to the asymmetric shift of the electronic states, the electronic structure of N-doped graphene under the electric field does not exhibit ridged band nature.

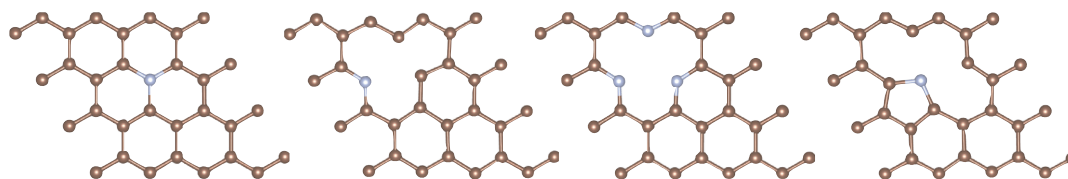


Fig.1 : Geometric structures of N-doped graphene.

Corresponding author: M. Matsubara  
Email: mmatsubara@comas.frsc.tsukuba.ac.jp

## Electronic structures of graphene exposed to electrolyte solution

○Mari Ohfuchi<sup>1,2</sup>

<sup>1</sup> *Fujitsu Laboratories Ltd., Atsugi 243-0197, Japan*

<sup>2</sup> *Institute of Materials and Systems for Sustainability, Nagoya University, Nagoya 464-8603, Japan*

Power generation from the flow of electrolyte solution is an emerging technology for environmental energy harvesting. A voltage of a few millivolts has been generated by using graphene [1] or carbon nanotube thin films [2]. However, the underlying physics is poorly understood. In this work, we study the graphene exposed to electrolyte solution using density functional theory, considering the oxygen molecules ( $O_2$ ) that can be dissolved in the solution.

When the solution has only electrolyte ions, as shown in Fig. 1(a), the graphene has no net charge (see the band diagram). The sodium ion ( $Na^+$ ) near the graphene produces a negative charge distribution in the graphene; however, the same amount of the opposite charge is induced around it. The chlorine ion ( $Cl^-$ ) near the graphene gives the same results. On the other hand, when  $O_2$  lies on the graphene (Fig. 1(b)), the band diagram and the charge distribution show that electronic charge is transferred from the graphene to  $O_2$ . When electrolyte ions and  $O_2$  coexist, as shown in Fig. 1(c),  $Cl^-$  near the graphene makes more electronic charge transfer from the graphene to  $O_2$ . The  $O_2$  molecules seem to be able to act as a charge source or sink. This may be related to the voltage generation from the electrolyte solution flow using nanocarbon materials. This work was supported by CREST, JST.

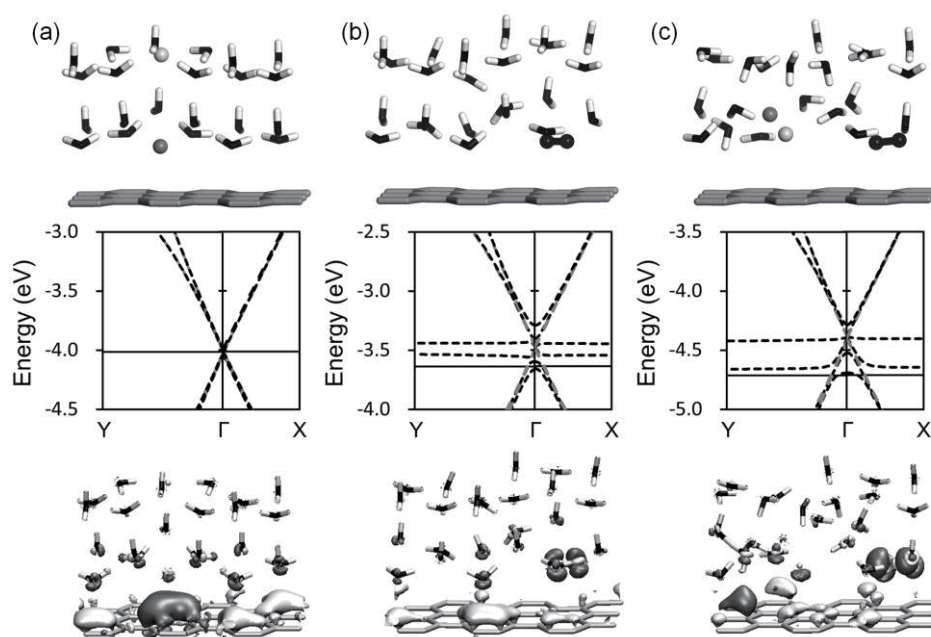


Fig.1: Optimized atomic structures, band diagrams, and induced charge distribution for electrolyte solution on graphene. The solution has (a) only  $Na^+$  and  $Cl^-$ , (b) only  $O_2$ , and (c) both of electrolyte ions and  $O_2$ . The gray (black and white) sticks represent graphene (water). The black, dark gray, and light gray spheres indicate O, Na, and Cl atoms. The solid line and the two dotted curves in the band diagrams show the chemical potential and the majority and minority spins. The dark and light gray colors indicate negative and positive charges, respectively.

[1] J. Yin *et al.*, *Nat. Nanotechnol.* **9**, 378 (2014). [2] T. Yasunishi *et al.*, *The 51th FNTG Symp.*, 3P-10 (2016).  
Corresponding Author: M. Ohfuchi, E-mail: mari.ohfuchi@jp.fujitsu.com

## Magnetic interactions between Edge-state spins and Ferrocenium ion spins

○Akira Suzuki<sup>1</sup>, Kazuyuki Takai<sup>1,2</sup>

<sup>1</sup>Graduate School of Science and Engineering, Hosei University, Tokyo 184-8584, Japan

<sup>2</sup>Department of Chemical Science and Technology, Hosei University, Tokyo 184-8584, Japan

Activated Carbon Fibers (ACFs) is promising as nanographene-based host material having localized spins originating in zigzag edges of graphene. We have successfully developed a magnetic host-guest system between ACFs and Ferrocene ( $\text{FeCp}_2$ ) based on  $\pi$ - $\pi$  stack design [1]. The spin magnetism of guest  $\text{FeCp}_2^+$  was induced by charge-transfer host-guest interaction between nanographene host and  $\text{FeCp}_2$ , resulting in the 5 times larger spin concentration of  $\text{FeCp}_2$ -ACFs synthesized with  $\text{FeCp}_2$  vapor of  $5.6 \times 10^3$  Pa than that of ACFs. In this study, we investigated the magnetic interactions between induced ferrocenium ion spin and nanographene spin by using ESR and FT-IR.

No X-band ESR signal was observable even for the sample prepared at 100 Pa due to extremely broad linewidth. ESR linewidth  $\Delta H_{\text{pp}}$  for the sample prepared at 15 Pa (1/300 lower pressure than that in the previous study) shows the 7 times larger than that for ACFs (**Fig. 1**), where  $\text{FeCp}_2$  doping of at the lower pressure was confirmed by FT-IR (**Fig. 2**). Taking only dipole interaction into consideration,  $\Delta H_{\text{pp}}$  should be only 5 times larger than that for ACFs even for  $\text{FeCp}_2$ -ACFs synthesized at  $5.6 \times 10^3$  Pa. The observed “excess” broadening suggests the presence of the exchange interaction between non-identical spins (nanographene spin and  $\text{FeCp}_2^+$  spin).

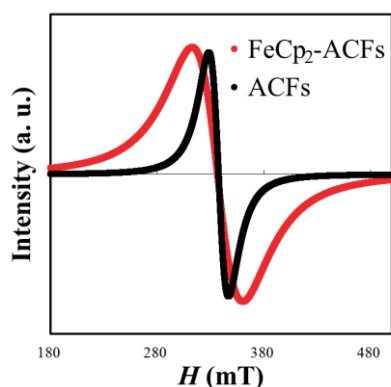


**Fig. 1** RT ESR spectra for ACFs and  $\text{FeCp}_2$ -ACFs synthesized at 55 °C

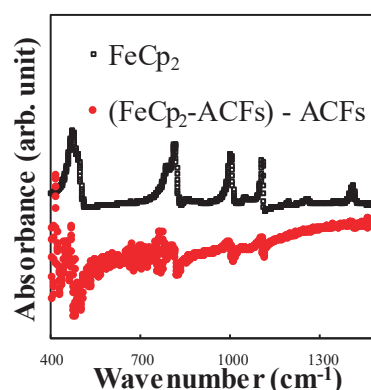


**Fig. 2** The infrared spectrum of  $\text{FeCp}_2$  and differential absorbance spectrum between  $\text{FeCp}_2$ -ACFs synthesized at 55 °C and ACFs

Corresponding Author: Kazuyuki Takai

Tel: +81-42-387-6138, Fax: +81-42-387-7002

E-mail: takai@hosei.ac.jp

## Electrical properties of reduced graphene oxide by thermal annealing

○Takuya Ishida<sup>1</sup>, Yuta Nishina<sup>2</sup>, and Nobuyuki Aoki<sup>1</sup>

<sup>1</sup> Graduate School of Advanced Integration Science, Chiba University,  
Chiba 263-8522, Japan

<sup>2</sup> Research Core for Interdisciplinary Sciences, Okayama University, Okayama 700-8530,  
Japan

Graphene oxide (GO) is one of the well-known materials studied since 1850's. It can be synthesized easily from carbon black. The electrical properties are almost insulating however it becomes conductive after the reduction process by thermal annealing, UV irradiation in vacuum, chemical treatment using hydrazine, and so on. Since large scale sheets of graphene oxide can be provided easily due to recent development of the method, reduced graphene oxide (r-GO) is expected for the use in electrical devices. Since the hydroxyl groups and oxygen atoms removed from the GO sheet during the annealing process, holey structures are introduced in the carbon skeleton structure. Such a GO sheet having voids is called as "holey graphene oxide (hGO)". And then, such a holey structure can be expected as a network of graphene-nano-ribbon. However the transport properties of r-hGO sheets have been studied mainly in the macroscopic scale so far. In this study, we confirmed a transition of transport properties of r-GO (r-hGO) sheet from macroscopic to mesoscopic transport regime.

The GO material was synthesized from Kish Graphite oxidized by  $\text{KMnO}_4$  in  $\text{H}_2\text{SO}_4$  solution [1]. The GO flakes are dispersed on a  $\text{SiO}_2/\text{Si}$  substrate by a spin-coating and reduced by thermal annealing at 473 K in vacuum condition for 20 hours to obtain r-GO films. Electric contacts were fabricated by electron beam lithography to form square-shape channels. The sizes of each channel are 100 nm, 300 nm, 1  $\mu\text{m}$ , 3  $\mu\text{m}$  and 10  $\mu\text{m}$ , respectively. These contacts were prepared on the same monolayer r-GO sheet to confirm the size dependence of the resistance. Figure 1 shows channel size dependence of the resistance. The resistance drastically increases when it is reduced to submicron scale. In a two-dimensional square sample, the sheet resistance should be independent on the size (scale). The experimental results suggest that the transport regime of the r-GO sample changes when it is reduced in the submicron scale.

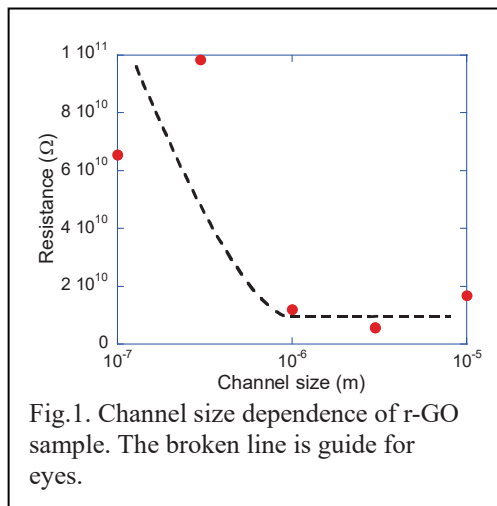


Fig.1. Channel size dependence of r-GO sample. The broken line is guide for eyes.

[1] N. Morimoto *et al.*, Sci. Rep., **6**, 21715, (2016).

Corresponding Author: N. Aoki

Tel:+81-43-290-3430, Fax:+81-43-290-3427

E-mail:n-aoki@faculty.chiba-u.jp

## Influence of Water Molecules on Molecular Adsorption induced Charge Transfer in Graphene

○Takai Umehara<sup>1</sup>, Kazuyuki Takai<sup>1,2</sup>

<sup>1</sup> Graduate School of Science and Engineering, Hosei University, Tokyo 184-8584, Japan

<sup>2</sup> Department of Chemical Science and Technology, Hosei University, Tokyo 184-8584, Japan

Electronic and Structural properties of Graphene as an actual carbon material rather than an ideal model for two dimensional systems with novel Dirac Fermion is significantly influenced by the presence of edges, defects and impurities [1], and so on. Especially, surrounding guest chemical species play an important role for two dimensional host materials like graphene, where the host-guest interactions through the surface and the interface between supporting substrate is classified into three types according to the energy scale of interactions; chemical modification by covalent bonding, charge transfer by electrostatic interaction, and mechanical strain by physisorption [3]. In this talk, I would like to focus mainly on the charge transfer interactions caused by guest chemical species facing with graphene. Indeed, surface modification of supporting substrate by self-assemble monolayer of molecules having various electric dipole and eigen frequency of molecular vibration enables tuning of the Fermi energy  $E_F$  of graphene [5]. Interestingly, such molecular proximity effects for adsorbed molecules on the surface of graphene show significant dependence on  $E_F$  experimentally tuned by gate voltage, where hole and electron doping by oxygen [4] and hydrazine molecules, respectively, exhibit opposite dependence on  $E_F$ . In addition, the kinetic for the charge transfer induced by molecular adsorption is quite slower in comparison with usual time scale for the electron system. Moreover, the absolute value of the characteristic times of the charge transfer by hydrazine (1.25 min) is much faster than that for oxygen (18 min), in the former of which large amount of water molecules coexist as hydration water in contrast to oxygen as dry gas. This is explained by a mechanism by electrochemical process involving co-existing water molecule for charge transfer phenomena by molecular adsorption on graphene. Indeed, the is a graphene FET characteristic measurement under precise controlling of atmosphere in UHV chamber reveals that the oxygen induced charge transfer process is much accelerated accompanied with increasing in partial pressure of water in oxygen gas.

[1] T. Enoki, S. Fujii, and K. Takai, Carbon, 50, 3141-3145 (2012).

[2] Y. Kudo, K. Takai, and T. Enoki, J. Mater. Res., 8, 1097-1104 (2013).

[3] K. Takai, H. Kumagai, H. Sato, T. Enoki, Phys. Rev. B, 73, 035435 (2006).

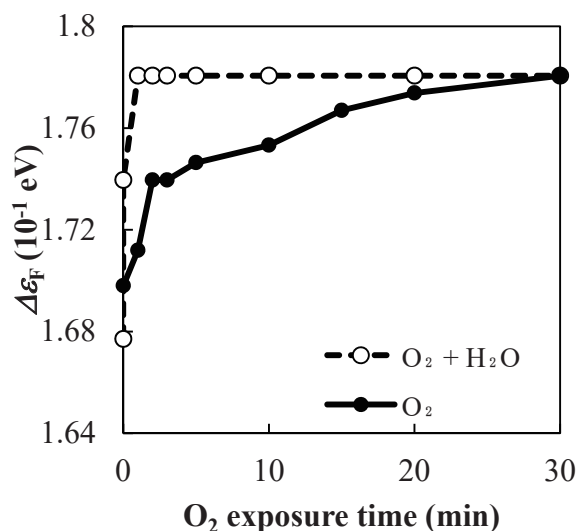
[4] Y. Yokota, K. Takai, and T. Enoki, Nano Lett., 11, 3669-3675 (2011).

[5] Y. Sato, K. Takai, and T. Enoki, Nano Lett., 11, 3468-3475 (2011).

Corresponding Author: Kazuyuki Takai

Tel: +81-42-387-6138, Fax: +81-42-387-7002

E-mail: takai@hosei.ac.jp



## Growth of large-area and uniform multilayer hexagonal boron nitride as an ideal 2D insulator

○Sho Nakandakari<sup>1</sup>, Kenji Kawahara<sup>2</sup>, Yuki Uchida<sup>1</sup>, Shigeto Yamasaki,<sup>1</sup>  
Masatoshi Mitsuhashi,<sup>1</sup> Hiroki Ago<sup>1,2,3,\*</sup>

<sup>1</sup> Interdisciplinary Graduate School of Engineering Sciences, Kyushu University, Fukuoka 816-8580, Japan

<sup>2</sup> Global Innovation Center (GIC), Kyushu University, Fukuoka 816-8580, Japan

<sup>3</sup> PRESTO, Japan Science and Technology Agency, Saitama 332-0012, Japan

Recently, hexagonal boron nitride (h-BN, Fig. 1a) has become an important 2D insulator which significantly improves electrical and optical properties of various 2D materials, including graphene and TMDCs [1-3]. When these 2D materials are stacked on multilayer h-BN, influences from the SiO<sub>2</sub> substrate surface, such as charge impurity, surface roughness, and optical phonons, are screened by the h-BN, realizing the intrinsic properties of the 2D materials. However, most of the h-BN films employed in previous works are obtained by mechanical exfoliation from bulk h-BN crystal [1-3], which limits further development of 2D device applications. Although CVD has been applied to the growth of h-BN, monolayer h-BN is widely obtained by CVD [4,5] which is not thick enough to screen the influence from a SiO<sub>2</sub>, while there exists a problem in uniformity of CVD-grown multilayer h-BN [6,7].

In this study, we demonstrate the synthesis of highly uniform multilayer h-BN by catalytic CVD. Growth of multilayer h-BN requires the controlled segregation of B and N atoms from a metal catalyst. We found that there are three essential factors that determine the crystallinity and uniformity of multilayer h-BN; (i) precursor feedstock, (ii) [B]/[N] balance, and (iii) catalyst composition. Throughout a systematic study, we succeeded in growing the large-area, highly uniform multilayer h-BN by using borazine (B<sub>3</sub>N<sub>3</sub>H<sub>6</sub>) feedstock and epitaxial metal alloy thin film catalysts. Figure 1b shows the optical image of a transferred multilayer h-BN film, indicating the uniformity of the film. The Raman spectra confirmed the growth of h-BN (Fig. 1b inset). To assess the quality of the CVD-grown multilayer h-BN, monolayer WS<sub>2</sub> grains were grown on the h-BN and SiO<sub>2</sub> substrates (Fig. 1c). Much more intense and narrower PL spectrum was observed for the WS<sub>2</sub> grains grown on the h-BN than those grown on SiO<sub>2</sub>. This suggests that our multilayer h-BN film is almost comparable to exfoliated h-BN flakes [3]. Our achievement of the synthesis of uniform multi-layer h-BN is expected to stimulate industrial applications of 2D materials.

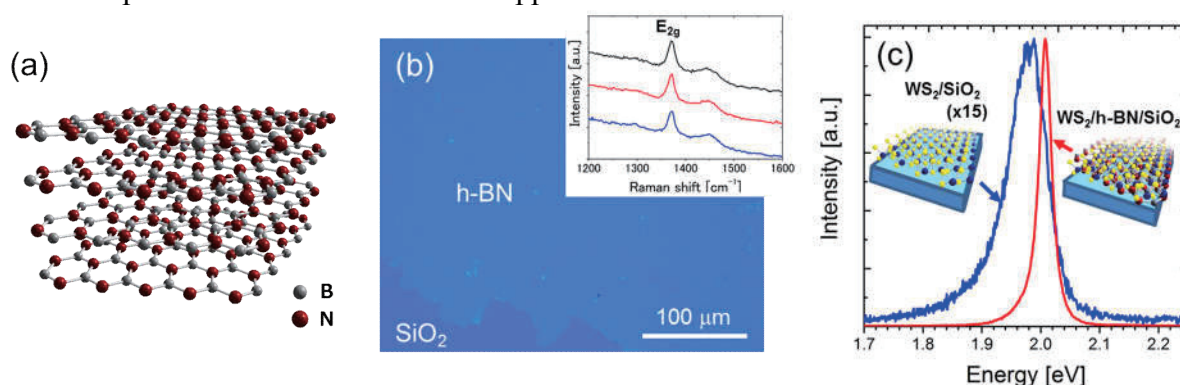


**Fig. 1** (a) Atomic model of multilayer h-BN. (b) Optical micrograph and Raman spectra of uniform multilayer h-BN transferred on SiO<sub>2</sub>. (c) PL spectra of WS<sub>2</sub> grown on h-BN/SiO<sub>2</sub> and SiO<sub>2</sub> substrates.

**References:** [1] C. R. Dean, *Nat. Nanotechnol.*, **5**, 722 (2010). [2] X. Cui, *Nat. Nanotechnol.*, **10**, 534 (2015). [3] M. Okada, *ACS Nano*, **8**, 8273 (2014). [4] K. K. Kim, *Nano Lett.*, **12**, 161 (2012). [5] Y. Stehle, *Chem. Mater.*, **27**, 8041 (2015). [6] S. K. Jang, *Sci. Rep.*, **6**, 30449 (2016). [7] S. M Kim, *Nat. Commun.*, **6**, 8662 (2015).

**Correspondence:** H. Ago (Tel&Fax: +81-92-583-8815, E-mail: h-ago@gic.kyushu-u.ac.jp)

## Enhancement of laser-induced water decomposition by 2D sheets studied by first-principles simulations II

○Yoshiyuki Miyamoto<sup>1</sup>, Hong Zhang<sup>2</sup>, Xinlu Cheng<sup>3</sup> Angel Rubio<sup>4</sup>

<sup>1</sup> *Research Center for Computational Design of Advanced Functional Materials, AIST, Umezono, 1-1-1 Central 2, Tsukuba 305-0685, Japan*

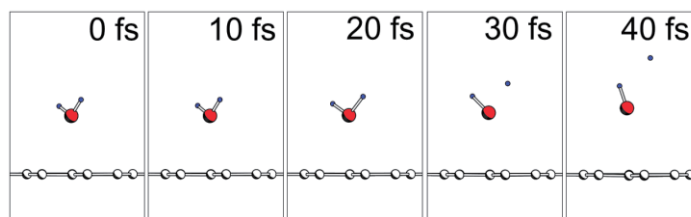
<sup>2</sup> *College of Physical Science and Technology, Sichuan University, Chengdu 610065, China*

<sup>3</sup> *Key Laboratory of High Energy Density Physics and Technology of Ministry of Education; Sichuan University, Chengdu, 610064, China*

<sup>4</sup> *Max Planck Institute for the Structure and Dynamics of Matter and Center for Free-Electron Laser Science, Luruper Chaussee 149, 22761 Hamburg, Germany*

This work was motivated by recent report of metal-free photocatalysis consisting of graphitic carbon nitride (gC<sub>3</sub>N<sub>4</sub>) [1,2] and we have proposed usage of high-intensity pulse laser as an alternative to ordinary light-source for achieving higher yield of H<sub>2</sub>O decomposition. Continuing to our presentation in the last meeting, we are still investigating property of 2D material in enhancement of laser-induced H<sub>2</sub>O decomposition by means of the first-principles simulation. Here we present updated results; 1) We have compared threshold laser intensity of H<sub>2</sub>O decomposition for an isolated molecule and for molecules above 2D-sheets, and we will present dependence of pulse-width of the laser. 2) We have proposed an idea to combine electrical hole-doping in graphene and pulse-laser H<sub>2</sub>O decomposition for higher yield of H and OH generation.

We have obtained significantly lower threshold laser-intensity of H<sub>2</sub>O decomposition when H<sub>2</sub>O is above 2D sheets. [3] The cause of the threshold lowering is attributed as a field enhancement effect by the 2D sheets studied by this work. The threshold is further decreased when we extended the full-width-of-half-maximum (FWHM) from 10 fs to 20fs, yet the estimated laser fluence for the H<sub>2</sub>O becomes larger with wider FWHM. The details of the computational method, results, and potential application for generating hydrogen fuel will be discussed. The figure shows snapshot of the H<sub>2</sub>O dynamics which was strongly bind to graphene under electrical hole-doping condition. (At the beginning, the O-side of water is closer to graphene due to polar nature of the H<sub>2</sub>O molecule.)



Snapshots of H<sub>2</sub>O dynamics upon pulse-laser illumination (FWHM=10fs, 800nm) with laser field intensity 7V/Å.

This work is supported by the fund from JSPS KAKENHI, Project No.JP16H00925.

[1] X. Wang *et al*, Nature Mat. **8**, 76 (2009).

[2] J. Liu *et al*, Science **347**,970 (2015).

[3] Paper in preparation.

Corresponding Author: Y. Miyamoto

Tel: +81-29-849-1498, Fax: +81-29-851-5428,

E-mail: yoshi-miyamoto@aist.go.jp

## Photoluminescence and photocurrent properties of monolayer WSe<sub>2</sub> FETs fabricated by dry-transfer process

○Xiaofan Wang, Wenjin Zhang, Nur Baizura Mohamed, Dezhi Tan, Hong En Lim,  
Yuhei Miyauchi, Kazunari Matsuda

*Institute of Advanced Energy, Kyoto University, Uji, Kyoto 611-0011, Japan*

Recently, transition metal dichalcogenides (TMDs) have attracted much attention as novel two-dimensional semiconductors, which opens the new research fields [1,2]. These materials are also promising candidates for the future optical and electronic devices such as light emitting diodes and field effect transistors (FETs) [3]. The standard TMD FETs reported to date have been fabricated using conventional electron-beam or photo-lithography technique followed by multiple wet processes, in which the process using the polymer may affect the device performance and optical properties [4]. As an alternative method, the multilayer MoS<sub>2</sub> FET fabricated by dry-transfer process has been reported [5].

In this work, we investigated the device performance and optical properties of monolayer (1L) WSe<sub>2</sub> FET fabricated by the dry-transfer process with Pt electrode. Figure 1(a) shows the transfer characteristics of 1L WSe<sub>2</sub> device. The sharp and large on/off current ratio of  $\sim 10^4$  are observed. We extract the high field-effect hole mobility of 86.3 cm<sup>2</sup>/V·s, which is a high value to compare with the devices fabricated by standard method. This suggests that the quality of 1L WSe<sub>2</sub> FET device fabricated by the dry-transfer method shows high quality. Figure 1(b) shows the photoluminescence (PL) spectra of 1L WSe<sub>2</sub> with varying the bias-voltages ( $V_G$ ) at room temperature. The spectral change of PL spectra depending on the  $V_G$  is observed. We will discuss the detail of PL and photocurrent properties in high quality 1L WSe<sub>2</sub> fabricated by the dry-transfer process.

- [1] Q. H. Wang *et al.*, Nat. Nanotechnol. **7**, 699 (2012).  
 [2] S. Mouri *et al.*, Nano Lett. **14**, 5944 (2013).  
 [3] B. Radisavljevic *et al.*, Nat. Nanotechnol. **6**, 147(2011).  
 [4] A. G. F. Garcia *et al.*, Nano Lett. **12**, 4449 (2012).  
 [5] Yang *et al.*, J. Vac. Sci. Tech. B **32**, 061203 (2014).

Corresponding Author: Kazunari Matsuda  
 Tel/Fax: +81-774-38-3460  
 E-mail: matsuda@iae.kyoto-u.ac.jp

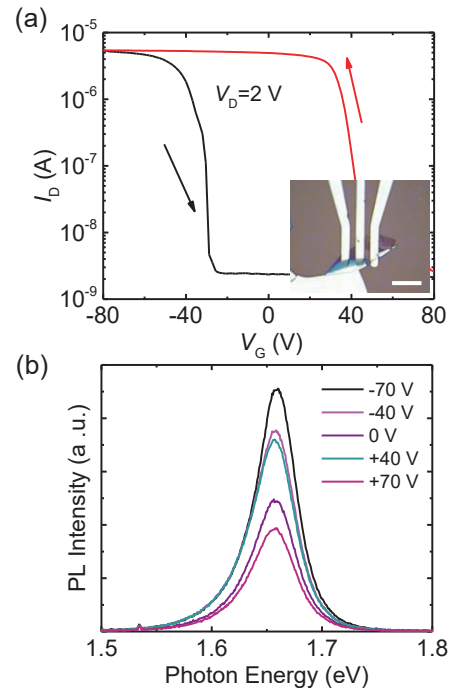


**Figure 1** (a) Transfer characteristics (optical image) of 1L WSe<sub>2</sub> device (inset: bar is 10 μm). (b) PL spectra under different  $V_G$ .

**Piezoelectric properties of 3R bulk transition metal dichalcogenides**○Satoru Konabe<sup>1,2</sup> and Takahiro Yamamoto<sup>1,2,3</sup><sup>1</sup>*RIST, Tokyo University of Science, Tokyo, Japan*<sup>2</sup>*Department of Electrical Engineering, Faculty of Engineering,  
Tokyo University of Science, Tokyo, Japan*<sup>3</sup>*Department of Liberal Arts (Physics), Faculty of Engineering,  
Tokyo University of Science, Tokyo, Japan.*

The bulk transition metal dichalcogenides (TMDCs) mainly exhibit two different types of crystal structures, *i.e.*, 2H and 3R. While TMDCs with 2H structure have the centrosymmetry, TMDCs with 3R structure lose their centrosymmetry, resulting in the valley related physics such as valley selectivity by a circular polarized light [1]. The non-centrosymmetry structure of 3R bulk TMDCs could lead to the other important property like piezoelectricity, where strain gives rise to electrical polarization. Besides the bulk TMDCs, it has been shown that the monolayer TMDCs, which also have the non-centrosymmetry structure, exhibit a large piezoelectric response. The first principles calculation predicted the large piezoelectric coefficients in monolayer TMDCs such as MoS<sub>2</sub>, MoSe<sub>2</sub>, WS<sub>2</sub>, and WSe<sub>2</sub> [2]. After the theoretical calculation, the piezoelectricity of monolayer TMDCs is confirmed experimentally and the measured values are consistent with the theoretical calculations [3-6]. Similarly to the TMDC monolayers, we expect piezoelectricity in the bulk 3R-TMDCs. If both monolayer and bulk structures exhibit the piezoelectricity, it opens a variety of applications from the usual piezoelectric devices to flexible energy harvesting devices.

In the present work, we perform a systematic investigation of piezoelectric properties of the bulk 3R-TMDCs (MoS<sub>2</sub>, MoSe<sub>2</sub>, WS<sub>2</sub>, and WSe<sub>2</sub>) using the first principles calculations based on the density functional theory. We calculate the elastic constant  $C_{ij}$ , the piezoelectric constant  $e_{ij}$ , and the piezoelectric constant  $d_{ij}$  from  $C_{ij}$  and  $e_{ij}$ . We find that the piezoelectric constants are sufficiently large or comparable compared with the conventional bulk piezoelectric materials such as  $\alpha$ -quartz, wurtzite GaN, and wurtzite AlN. Our simulation demonstrates that the bulk 3R-TMDCs are potential materials for piezoelectric applications as well as the monolayer counterparts.

## References:

- [1] R. Suzuki, *et al*, Nature Nanotechnology **9**, 611 (2014).
- [2] K.-A. N. Duerloo, *et al*, The Journal of Physical Chemistry Letters **3**, 2871 (2012).
- [3] W. Wu, *et al*, Nature **514**, 470 (2014).
- [4] H. Zhu, *et al*, Nature Nanotechnology **10**, 151 (2014).
- [5] T. Wu, *et al*, Angewandte **54**, 4432 (2015).
- [6] J. Qi, *et al*, Nature Communications **6**, 1 (2015).

Corresponding Author: Satoru Konabe

E-mail: konabe@rs.tus.ac.jp

Tel: +81-3-5876-1494 (ext. 2713)

## Molecular beam epitaxy growth of molybdenum diselenide atomic layers on hexagonal boron nitride substrates

○Takuto Tokuda<sup>1</sup>, Takato Hotta<sup>1</sup>, Kenji Watanabe<sup>2</sup>, Takashi Taniguchi<sup>2</sup>, Hisanori Shinohara<sup>1</sup> and Ryo Kitaura<sup>1</sup>

<sup>1</sup>Department of Chemistry, & Institute for Advanced Research Nagoya University, Nagoya 464-8602, Japan, <sup>2</sup> National Institute for Materials Science, Tsukuba 305-0044, Japan

The progress on graphene research has yielded the discovery of its fascinating properties including the extremely high carrier mobility ( $\sim 500,000 \text{ cm}^2/\text{Vs}$ ), the room temperature quantum hall effect and the fractional quantum hall effect, etc [1]. The fascination with graphene research has led to searching for other two-dimensional systems, and hexagonal boron nitrides (hBN) and transition metal dichalcogenides (TMDs) have been isolated in its monolayer form. In particular, TMD provides a family of two-dimensional systems, including semiconductors, metals and superconductors, and they provide an excellent and widespread platform to explore novel chemistry and physics in two-dimensions. To further explore the fundamental properties and possibility in future device applications of TMDs, development of controlled growth of high-quality sample is indispensable. As a controlled growth method of TMDs, chemical vapor deposition has been intensively studied, whereas another representative thinfilm growth technique, molecular beam epitaxy (MBE), has not been explored very well [2]. In this study, we have focused on application of MBE method to grow a TMD, MoSe<sub>2</sub>. Figure 1 shows AFM image of grown MoSe<sub>2</sub> at 885 K on hBN substrate; Mo and Se are supplied with e-beam heating and low temperature K-cell, respectively. As clearly seen, MoSe<sub>2</sub> are grown as a hexagonal flake, which is consistent with the hexagonal crystal system of MoSe<sub>2</sub>. The PL spectrum shown in Figure 2 exhibits the single peak at 1.57 eV, which is assigned to the emission from free excitons. Temperature dependence of the PL spectrum have shown that PL from trions is very weak, which indicates minimal amount of unintentionally doping. In the presentation, further details of MBE growth and discussion of optical properties will be given.

[1] A. S. Mayorov, *et al.*, *Nano Lett.*, **11**, 2396 (2011). [2] K. Kang et al., *Nature*, **520**, 656 (2015).

Corresponding Author: Hisanori Shinohara and Ryo Kitaura

Tel: +81-52-789-2477, Fax: +81-52-747-6442, E-mail: noris@nagoya-u.jp and r.kitaura@nagoya-u.jp

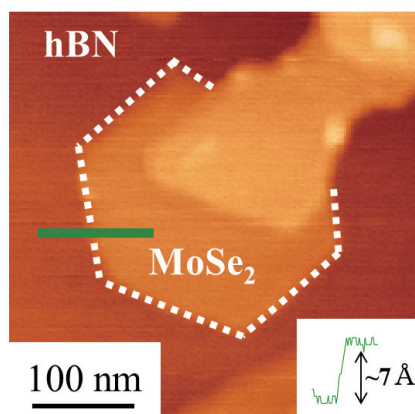


Fig.1 AFM image of grown MoSe<sub>2</sub>

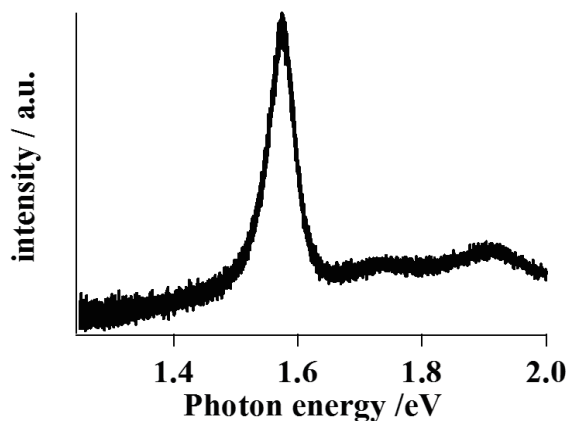


Fig.2 PL spectra of grown MoSe<sub>2</sub>

## Meteorite- and detonation-nanodiamonds are the same substances

Eiji Ōsawa<sup>1</sup>, Amanda S. Barnard<sup>2</sup>, Toshihiko Tanaka<sup>3</sup> and Masayoshi Fukaya<sup>3</sup>

<sup>1</sup>*NanoCarbon Research Institute, Asama Research Extension Center, Faculty of Textile Science and Technology, Shinshu University, Ueda, Nagano 386-8567, Japan*

<sup>2</sup>*CSIRO Material Science and Engineering, Parkville, Victoria 3052, Australia*

<sup>3</sup>*Department of Chemistry and Biochemistry, National Institute of Technology, Fukushima College, Iwaki, Fukushima 970-8034, Japan*

Nanodiamond was first isolated from the well-known presolar ‘Allende/Murchison meteorite’ as fine-grained tan-colored carbon by R. S. Lewis and his coworkers, who initially expected that the meteorite carbon could be C<sub>60</sub> buckminsterfullerene[1]. This lucky incidence took place in 1987, two years after the discovery of C<sub>60</sub>[2]. Later, Danilenko disclosed that they had synthesized nanodiamond by using detonation method earlier in 1963[3]. Although this discovery was a brilliant achievement, he isolated only micron-sized agglutinates. Single-crystalline, elementary particles of detonation nanodiamond (EPDND) have long defied isolation. However, once isolated in dispersed state and characterized[4], EPDND proved identical with Lewis’ meteorite nanodiamond despite vastly different origins!

The first indication of identity came from comparison of particle sizes. Disintegration of crude agglutinates of detonation nanodiamond by attrition milling initially produced complex mixture of oligomers like dimers and trimers in addition to the monodisperse elementary particles, and used to give average diameters exceeding 3nm. Careful optimization of milling conditions finally led to a minimum and constant diameter of  $2.63 \pm 0.4$  nm, which we believe to represent the true EPDND[4]. As shown in **Table 1**, the diameter of EPDND perfectly agrees with those from meteorites [5-7].

**Table 1.** Reported average sizes of meteorite nanodiamond in nm

Meteorite \ Method	TEM point countin [5,6]	MALDI-TOF-MS [7]	
		mode average	mean average
Murchison	2.6, 2.579	2.4	2.4
Allende	2.841	2.6	2.7

The second evidence was obtained by comparing LDI-TOF-MS of EPDND[8-9] with those of meteorite nanodiamond [7]. Convergence of the single-nano diamonds grown in different environments into the same size and internal structure [8-9] suggests that similar circumstances for diamond growth were created by shock waves generated from the detonation of military explosives in closed vessel or from the grandiose explosion of a supernova considered responsible for the eventual formation of our solar system billions of years ago.

[1] R. S. Lewis *et al.*, *Nature* **326**, 160-162 (1987). [2] H. Kroto *et al.*, *Nature* **318**, 162-163 (1985). [3] V. V. Danilenko, *Phys. Solid State*, **46**, 595-599 (2004). [4] E. Ōsawa *et al.*, manuscript in preparation. [5] R. S. Lewis *et al.*, *Nature* **339**, 117-121 (1989). [6] T. L. Daulton *et al.*, *Geochim. Cosmochim. Acta*, **60**, 4853-4872 (1996). [7] I. C. Lyon, *Meteorit. Planet. Sci.* **40**, 981-200 (2005). [8] M. Fukaya *et al.*, FNTG 52<sup>th</sup> General Symposium, 2017, Tokyo. [9] T. Tanaka *et al.*, FNTG 52<sup>th</sup> General Symposium, 2017, Tokyo.

Corresponding Author: E. Ōsawa, Tel: +81-(0)268-75-8381, E-mail: osawa@nano-carbon.jp

## Synthesis of N-doped carbon nanoballoons with nitrogen plasma

○Ryota Takahashi<sup>1</sup>, Toru Harigai<sup>1</sup>, Hirofumi Takikawa<sup>1</sup>, Yoshiyuki Suda<sup>1</sup>

<sup>1</sup> Department of Electrical and Electronic Information Engineering, Toyohashi University of Technology, Toyohashi, Aichi 441-8580, Japan

Doping a carbon nanomaterial with other atomic species (like nitrogen) provides a means of altering its electronic and transport properties. Carbon nanoballoons (CNBs) have a pentagonal ring in a part of a graphite layer with hexagonal rings. CNBs are a hollow and spherical structure, and has high conductivity. To control the electronic properties of CNBs, we performed a substitutional doping of nitrogen atoms by using N<sub>2</sub> plasma.

CNBs were synthesized by heat treatment of arc black at 2600°C in Ar gas [1]. CNBs mixed with polyvinylidene difluoride (PVDF) in a mass ratio of 9:1 was applied to a silicon substrate and dried. N<sub>2</sub> radio frequency (RF) magnetron plasma was applied to CNBs fixed on a substrate. X-ray photoelectron spectroscopy (XPS) was used to determine the chemical bonding of CNBs.

Fig. 1 shows the C 1s and N 1s XPS spectra of CNBs treated with N<sub>2</sub> plasma. In Fig. 1(a), there is a possibility that the asymmetric C 1s spectra is influenced by C-N bonding [2]. The main C 1s peak (284.4 eV) shows a shift to higher binding energy. This shift is in agreement with increasing structural disorder due to the disruptions in the *sp*<sup>2</sup> carbon framework by the incorporation of nitrogen [3]. In Fig. 1(b), the two peaks at 398.5 eV and 400.1 eV can be assigned to pyridinelike N and pyrrolelike N, respectively. The small peak at 401.7 eV can be considered to graphitelike N, i.e., threefold coordinated *sp*<sup>2</sup> N in the hexagonal rings of CNBs [4].

This work has been partly supported by the JSPS KAKENHI Grant Number 15K13946.

[1] Y. Okabe *et al.* *Electrochim. Acta.* **131**, 207 (2014).

[2] C. Morant *et al.* *Phys. Status. Solidi A.* **203**, 1069 (2006).

[3] S. Maldonado *et al.* *J. Phys. Chem. B.* **109**, 4707 (2005).

[4] Y. C. Lin *et al.* *Appl. Phys. Lett.* **96**, 133110 (2010).

Corresponding Author: Y. Suda

Tel: +81 532 44 6726, Fax: +81 532 44 6757

E-mail: suda@ee.tut.ac.jp

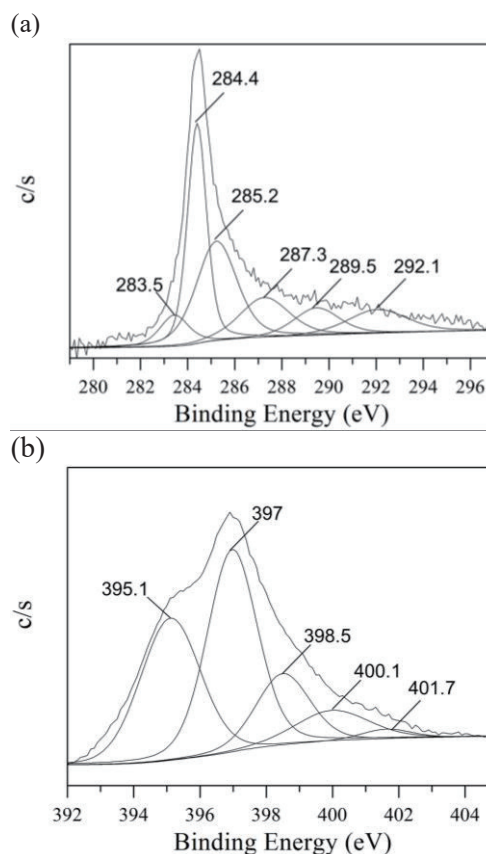


Fig. 1 XPS spectra of (a)C 1s(b)N 1s of CNBs treated with N<sub>2</sub> plasma.

## Separation of iron oxide nanotubes from the products prepared by surfactant assisted sol-gel method and characterization

Yuka Tanaka, ○ Shunji Bandow

*Department of Applied Chemistry, Meijo University, Nagoya 468-8502, Japan*

Co-polymerization of iron-nitrate hydrate on the surface of non-ionic surfactant of a Pluronic F-127 in 1-propanol gives a scrolled type of iron oxide nanotubes (Fe-ox NTs) with outer diameter around 10 nm and the thickness of tube wall about 2 – 3 nm (inter-wall spacing of ~0.6-0.8 nm). Lengths of these nanotubes are not clear but mostly over 100 nm long. Although such tube structured material can be prepared, there are numerous number of nano-particulate materials are formed simultaneously. Iron oxide has optical bandgap of ca. 2 eV which corresponds to the red light with the wavelength of ~600 nm, and so that there are some studies focused on the sun light energy utilization [1,2]. Tube structure is one of fascinated structure for the use of both side surfaces, and nano-scale size has great advantage because of less dead space for attaching the molecules to the inner surface.

Detail of the sample preparation is in Ref. 3 [3]. Transmission electron microscopy (TEM) images of as-prepared sample are indicated in Fig. 1, where one can see faint contrasted rod-like or tube-like materials embedded in particulate materials. Therefore, the nanotube content is not so high for as-prepared sample. Separation of iron oxide nanotubes was based on the centrifugal method using surfactant. Surfactants that we examined are classified into cationic and anionic surfactants of benzalkonium chloride (BKC) and sodium deoxycholate (SDC), respectively. Briefly, 20 mg of as-prepared material was dispersed into 50 ml of 2 wt% aqueous solution of surfactant by sonication, and first centrifuged at 100 G for 30 min. Then the sediments were removed, and supernatant was again centrifuged at 150 G for 30 min. After this two-step separation, sediments and supernatant were observed by TEM. Results are in Fig. 2. From Fig. 2, we found that the nanotubes are in the sediments and BKC gives better separation than SDC.

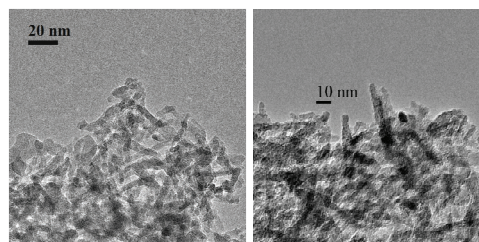


Fig. 1. TEM of as-prepared Fe-ox NTs

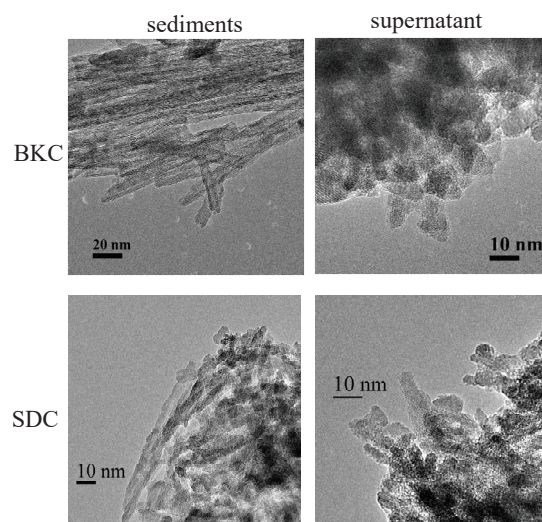


Fig. 2. Separated Fe-ox NTs by centrifugation

- [1] X.P. Shen *et al.*, Z. Xu, Chem. Lett. 33, 1128 (2004). [2] C.J. Jia *et al.*, Angew. Chem. Int. Ed. 44, 4328 (2005). [3] Y. Kosugi, S. Bandow, J. Inorg. Organomet. Polym. 24, 933 (2014).

Corresponding Author: S. Bandow, E-mail: bandow@meijo-u.ac.jp, Tel: +81-52-838-2404

## 多段トラップ気相移動度測定装置の開発とナノ物質の分離

(東邦大理) ○菅井 俊樹・陣内 涼太・星野 裕大・寺田 夏樹・椎野 恭平・浜野 裕太・森田 博暉

Development of Multi-stage Ion Trap Ion Mobility Measurement System and Separation of Nano Materials (*Department of Chemistry, Toho University*) ○Toshiki Sugai, Ryota Jinnouchi, Yuudai Hoshino, Natsuki Terada, Kyohei Shiino, Yuuta Hamano, Hiroki Morita

Ion mobility together with mass spectrometry has been utilized to reveal novel structures of nano materials<sup>1)</sup>. However, almost no long-term successive structural measurements have been performed. We have been developing ion trap ion mobility measurement system with optical observation on particles with the sizes from several tens of  $\mu\text{m}$  to 50 nm by enhancing the sensitivity. Here we present newly developed system that realize separation based on mobility. Figure 1 shows a schematic view of the system with multiply stacked ring ion guide (SRIG) electrodes, which operate as many connected ion traps. The potential of the electrodes are controlled by newly developed power supplies which control both of ion trap radio frequency high-voltage (RF) and low frequency low-voltage (LF) simultaneously. With this system we have succeeded to observe and separate charged NaCl water solution particles and fluorescent nano materials. We are now improving the separation resolution.

*Keywords* : Ion Mobility; Ion Trap; Multi-stage

気相移動度測定は質量分析と組み合わせることでナノ物質の新規構造解明などに有用である<sup>1)</sup>。しかし、長時間の構造変化の追跡観測はこれまでなされていなかった。我々はこれまで、複数個のイオントラップとトラップ電位の制御により、移動度測定を行いながら、数時間にわたる継続観察を蛍光や散乱光を用いて行ってきた。さらに光検出感度を向上させることにより、測定対象を直径数  $10\ \mu\text{m}$  の微粒子から直径  $50\ \text{nm}$  のナノ物質まで縮小させてきた。今回我々は、これらの技術を発展させ、新たに移動度に基づいた空間分離を試みた。図 1 にシステムを示す。このシステムは多数の多段積層リング型電極(SRIG)で構成された、複数連結イオントラップとこれらのトラップ用高周波電場と移動度用低周波電場を制御する、多チャンネル電源で構成される。このシステムを用いて NaCl 水溶液荷電微粒子と蛍光ナノ物質の観測と移動度分離保持を実現した。現在分離分解能向上を図っている。

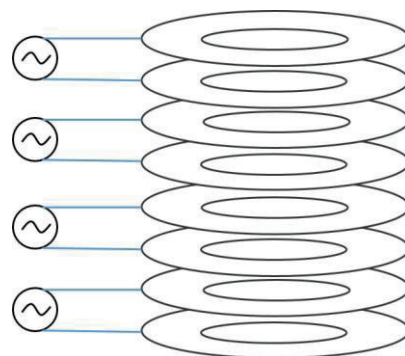


Fig. 1 Schematic View of Multiple SRIG type Ion Mobility Ion Trap Measurement System with control power supplies.

1) T. Sugai et al., J. Am. Chem. Soc. 123, 6427 (2001).

## Mechanical properties of nano-rotors: Energetics of triptycene derivatives

Miki Akiba and Susumu Okada

*Graduate school of Pure and Applied Sciences, University of Tsukuba, Tsukuba 305-8571, Japan*

Following the experimental demonstration of nanoscale machines, much effort has been devoted to design further variations of nanoscale machines and to elucidate their mechanical properties. Hydrocarbon molecules are one of representative constituent units for such nanoscale machines due to their ridged covalent network within the molecules and flexible intermolecular covalent bonds. Although, the experiments reported various nanoscale mechanical machines, fundamental mechanics of the nano-machines is still unclear. In the present work, we aim to elucidate the nanomechanics for the rotational motion of nano-rotors consisting of triptycene and other hydrocarbon molecules, using the density functional theory with the generalized gradient approximation. In this work, we focus on triptycene derivatives in which hydrocarbon molecules, naphthalene, anthracene, and triptycene, are attached to the triptycene via linear  $C_2$  unit (Fig. 1). Our calculations show that the energy barrier for the rotational motion strongly depends on the attached hydrocarbon species: Triptycene gives the largest barrier while the symmetrically attached anthracene gives the smallest barriers (Fig. 2). We further studied the angular velocity and torque for the rotational motion of these hydrocarbon molecules.

Corresponding Authors: M. Akiba and S. Okada  
E-mail: sokada@comas.frsc.tsukuba.ac.jp

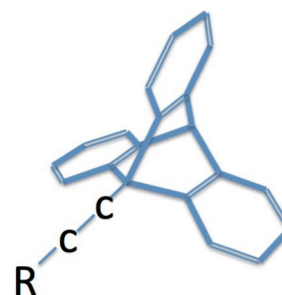


Fig. 1. Geometric structure of triptycene derivatives where R is naphthalene, anthracene, and triptycene

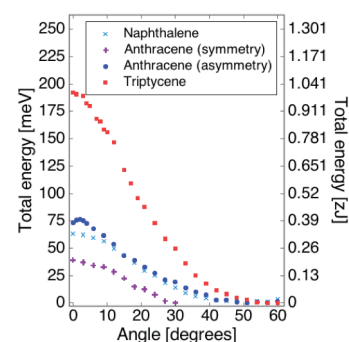


Fig 2. Total energy of triptycene derivatives as a function of the rotational angle.

## Study of deactivation mechanism of carbon catalyst by thermo-catalytic decomposition of methane

○Haruki Nishii<sup>1</sup>, Yoshito Umeda<sup>2</sup>, Hiroaki Hamaguchi<sup>3</sup>, Masashi Suzuki<sup>3</sup>, Toru Harigai<sup>1</sup>, Hirofumi Takikawa<sup>1</sup>, Yoshiyuki Suda<sup>1</sup>

<sup>1</sup> Toyohashi Univ. of Technol., Japan

<sup>2</sup> Chubu Region Institute for Sorcial and Economic Reserach, Japan

<sup>3</sup> Aichi Science & Technology Foundation, Japan

Thermo-catalytic decomposition (TCD) of methane is the attractive hydrogen production process to mitigate CO<sub>2</sub> emissions commonly associated with the conventional processes (such as steam methane reforming). However, the problem of process is catalyst deactivation. [1] The purpose of this study is to investigate deactivation mechanism of carbon catalyst by analyzing carbon deposited over carbon catalysts.

Activated carbon sample was used as the catalyst for the TCD of methane. Experiments were carried out in a fixed-bed reactor. After heating to 920°C under nitrogen, methane was flowed for different time periods. [2] After experiments, methane conversion ratio was calculated by the following equation. The obtained carbon was analyzed by X-ray diffraction (XRD) and scanning electron microscopy (SEM).

$$\text{Methane conversion ratio} \equiv \frac{\text{Molecules of produced carbon [mol]}}{\text{Molecules of inlet methane [mol]}} \quad (1)$$

Temporal change of methane conversion at 920°C is shown in Fig. 1. Although the methane conversion of initial reaction (at 20 min) reached 60%, after 40 min, the methane conversion dropped to 33% rapidly. Subsequently, it decreased gradually, and after 330 min, reached 23%. Fig. 2 shows SEM micrographs of as-prepared catalyst and used ones for methane conversion after 20 to 330 min. From Fig. 2 (a), it is confirmed that AC had a lot of pores on the surface. However, in Fig. 2 (b), pores diameter of 5 nm disappeared. From Figs. 2 (c) and (d), it is confirmed that carbon grown spherically, and completely covered the catalyst, respectively.

From these results and study of N. Muradov et al. [3], initial drop of reaction and subsequent gradual decrease are considered to be attributed to block micro-pores, meso-pores and macro-pores by carbon deposition.

### Acknowledgements

A part of this work was supported by “Development project of near-term hydrogen economy forming technology” for priority of research project of Knowledge Hub Aichi. The authors would like to thank K. Azato for emeritus prof. of Gifu Univ. and H. Yamashita for emeritus prof. of Nagoya Univ. with discussion about correlation between produced carbon and methane conversion.

[1] Lee, Eun Kyoung, et al. *Carbon* **42**, no. 12–13 (2004): 2641–48.

[2] Abánades, et al. *International Journal of Hydrogen Energy*, **36**, no. 20 (2011): 12877–86.

[3] N. Muradov, et al. *Catalysis Communications* **2**, no. 3–4 (2001): 89–94.

Corresponding Author: Y. Suda

Tel: +81-3-0532-44-6726

E-mail: suda@ee.tut.ac.jp

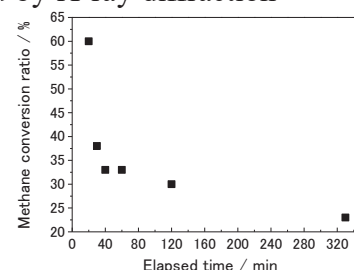


Fig. 1 Temporal change of Methane conversion ratio

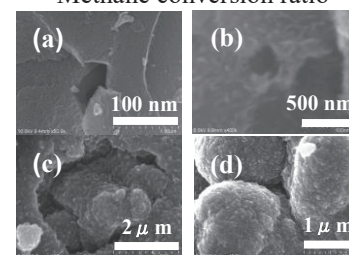


Fig. 2 SEM micrograph of (a) AC (as prepared), (b) after 20 min, (c) after 40 min, and (d) after 330 min.

## Effect of PtRu alloying degree on catalytic activity of catalysts for direct methanol fuel cells

OK. Kawasaki<sup>1</sup>, T. Ohiro<sup>1</sup>, T. Harigai<sup>1</sup>, H. Takikawa<sup>1</sup>, H. Ue<sup>2</sup>, Y. Suda<sup>1</sup>

<sup>1</sup> Department of Electrical and Electronic Information Engineering, Toyohashi University of Technology, Toyohashi, Aichi 441-8580, Japan

<sup>2</sup> Fuji Research Laboratory, Tokai Carbon Co., Ltd., Oyama, Shizuoka 410-1431, Japan

Carbon black, nanometer-size carbon particles, is commercially used as a catalyst support in fuel cells owing to its high surface area, porosity, electric conductivity, low density, and low cost. In the previous work, we have used various carbon nanomaterials as a catalyst support for direct methanol fuel cells (DMFC) [1]. In this study, we used carbon nanocoils (CNCs) as a catalyst support and measured the catalytic activity and PtRu alloying degree of CNC-supported PtRu catalyst.

An automatic chemical vapor deposition (CVD) system was used for CNC synthesis. CNC was prepared by using Fe/Sn catalytic solution [1]. CNCs are helical-shaped carbon nanofibers (CNFs). CNCs are graphitic. We supported PtRu catalysts for the DMFC anode. Sodium boron hydrate (NaBH<sub>4</sub>) was used as a reducing agent in the reduction method [2]. Deionized water was used as solvent in the reduction method. We mixed CNCs-dispersed solution, PtRu precursor solution, and reducing agent solution. We changed the concentration of mixed solution by adjusting the amount of solvent and prepared PtRu catalysts.

Table 1 shows the electrochemically active surface area (ECSA), onset potential of methanol oxidation reaction (MOR) of the PtRu catalysts, and PtRu alloying degrees. The PtRu alloying degree was evaluated from the X-ray diffraction spectra of the PtRu catalysts. The alloying degrees decreased with reducing of concentration. Low alloying degree caused to low MOR onset potential. This is mainly due to increase of unalloyed Ru in PtRu catalyst [3].

**Table 1.** Electrochemical properties and alloying degrees of CNC-supported PtRu catalyst

Concentration /L g <sub>CNC</sub> <sup>-1</sup>	ECSA /m <sup>2</sup> g <sub>Pt</sub> <sup>-1</sup>	MOR onset potential /V	Alloyed Ru /%
2.5	100.6	0.214	4
5.0	96.7	0.263	12
10.0	109.9	0.264	13

This work has been partly supported by JSPS KAKENHI Grant Number 15K13946.

[1] Y. Suda *et al.* Materials Today Communications. Vol. 3, pp. 96-103 (2015).

[2] T.C. Deivaraj *et al.* Journal of Power sources. Vol. 142, pp. 43-49 (2005)

[3] J. Guo *et al.* Journal of Power sources. Vol. 168, pp. 299-306 (2007).

Corresponding Author: Y. Suda

Tel: +81 532 44 6726, Fax: +81 532 44 6757

E-mail: suda@ee.tut.ac.jp

## Microfabrication of carbon nanocoil using Focused Ion Beam

○Munehiro Takahashi<sup>1</sup>, Toru Harigai<sup>1</sup>, Hirohumi Takikawa<sup>1</sup>, Hitoshi Ue<sup>2</sup>, Yoshiyuki Suda<sup>1</sup>

<sup>1</sup>Toyohashi Univ. of Technol., <sup>2</sup>Tokai Carbon Co., Ttd.

Carbon nanocoils (CNCs), which are synthesized by chemical vapor deposition (CVD) method, have a coil diameter of 500-1500 nm [1]. CNCs are expected such as electromagnetic wave shielding and counter electrode of solar cells [2,3]. CNCs are expected to be used as a nanoinductor. However the effect of nanoinductor on CNCs are low due to high resistivity [4]. In addition, we do not know magnetic property of single CNCs, and CNCs are obtained as an aggregate when synthesized. In this study, we have made the CNC substrate for measuring magnetic property

CNCs are obtained by chemical vapor deposition method. Fig. 1 shows processing of the measurement substrate. Au film having a thickness of 150 nm was formed on SiO<sub>2</sub> substrate using an ion coater. A single CNC is extracted by using focused ion beam (FIB). Au on SiO<sub>2</sub> substrate was etched to draw a line by using FIB. The single CNC was bridged there. Then Pt gas deposited at both ends of the bridged single CNCs to fix it, and the measurement substrate was prepared. A plural of measurement substrates were prepared.

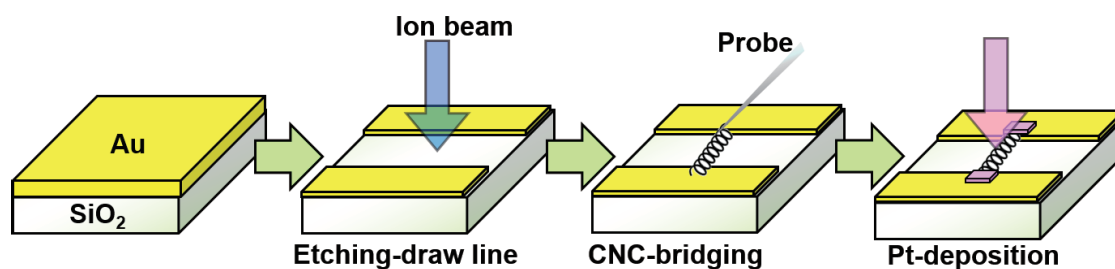


Fig. 1 Processing of the measurement substrate

Table 1 shows the geometry of the bridged single CNCs. The number of turns and fiber length tend to increase when the pitch angle is decreased. From these results, we can expect to measure the magnetic properties by using the measurement substrate.

**Table 1.** Configuration of CNCs.

Sample number	Coil diameter [nm]	Fiber diameter [nm]	Pitch angle [deg]	Number of turns	Fiber length [ $\mu$ m]
1	765	385	35.1	7.91	23.3
2	582	130	14.8	21.5	40.8
3	551	124	14.4	17.2	30.8

[1] G. Xu, *et. al*, Jpn. J. Appl. Phys, **44**, 1569 (2005)

[2] G. Kang, *et. al*, Applied Surface Science, **380**, 114 (2016)

[3] G. Wang, *et. al*, Materials Letters, **174**, 14 (2016)

[4] Y. Nakamura, *et. al*, Appl. phys. Lett, **108**, 153108 (2016)

## Attempt to produce dimetallofullerenes containing Yb

○Kazuhiro Kobayashi, Takuji Mitani, Natsumi Nakatori, Koichi Kikuchi, Yohji Achiba,  
Takeshi Kodama

*Department of Chemistry, Tokyo Metropolitan University, Hachioji 192-0397, Japan*

So far,  $M_2@C_{80}(I_h)$  ( $M=La, Ce, Pr$ ) have been isolated and characterized, but  $M_2@C_{80}(I_h)$  containing other metals like Y, Gd, etc. have never been obtained, then called as a “hidden” or “missing” metallofullerenes. Quite recently, however, we succeeded in the isolation of  $Y_2@C_{80}(I_h)$  [1] and  $Gd_2@C_{80}(I_h)$  [2] as an anion form using the method combining the ion-pair chromatography with the mixed solvent extraction. In other words,  $Y_2@C_{80}(I_h)$  and  $Gd_2@C_{80}(I_h)$  are unstable and unable to be extracted as a neutral form but are produced in the raw soot.

For Yb-metallofullerenes, the isolations of monometallofullerenes,  $Yb@C_n$  ( $n=74, 76, 78, 80, 82, 84$ ), have been reported [3], but there is no report on the Yb-dimetallofullerenes,  $Yb_2@C_n$ . Because there is a possibility of the production of  $Yb_2@C_n$  in the raw soot like that for  $Y_2@C_{80}(I_h)$  and  $Gd_2@C_{80}(I_h)$ , we tried to extract and separate  $Yb_2@C_n$  as an anion form.

First, we carried out direct-current (DC) arc discharge (60 ~ 65 A) of Yb/C composite rods (Yb:C=2:98) or Yb/Ni/C composite rods (Yb:Ni:C=2:1:97) under a 500 Torr He atmosphere. In the latter, Ni was used as a catalyst. Unfortunately, in the both experiments, the obtained soot was little and no evidence of Yb-metallofullerenes in the extract was presented. Then, we next executed DC arc discharge (60 A) of Yb/Y/C composite rods (Yb:Y:C=1:1:98) under a 500 Torr He atmosphere, and the sufficient soot was obtained. The raw soot was extracted for 8 h with a mixed solvent of triethylamine and acetone. The extract was separated by HPLC using a Buckyprep column and acetone with an ion-pair reagent, tetrabutylammonium bromide, as an eluent. Figures 1 and 2 show HPLC chromatogram and LD-TOF mass spectra of the fraction A and B, respectively. In the fraction A, the peak of  $Y_2C_{78}$ , which should be  $Y_2@C_{78}(D_{3h})$ , was observed but no peak of  $YYbC_{78}$  and  $Yb_2C_{78}$ . Similarly, in the fraction B, the peak of  $Y_2C_{80}$ , which should be  $Y_2@C_{80}(I_h)$ , was observed but no peak of  $YYbC_{80}$  and  $Yb_2C_{80}$ . Therefore, it was suggested that dimetallofullerenes containing Yb, not only  $Yb_2@C_n$  but also  $YYb@C_n$ , were not produced or not extracted as an anion form if existed in the raw soot.

[1] N. Nakatori, et al. *The 49<sup>th</sup> Fullerenes-Nanotubes-Graphene General Symposium* 46 (2015).

[2] T. Mitani, et al. *The 50<sup>th</sup> Fullerenes-Nanotubes-Graphene General Symposium* 95 (2016).

[3] J. Xu, et al. *Chem. Mater.* **16**, 2959-2964 (2004).

Corresponding Author: Takeshi Kodama

Tel: +81-42-677-2530, Fax: +81-42-677-2525

E-mail: kodama-takeshi@tmu.ac.jp

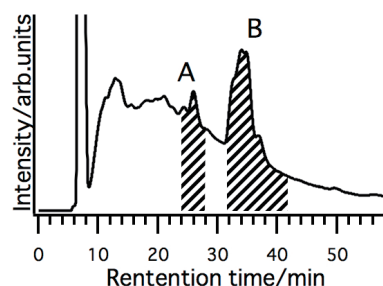


Fig. 1 HPLC chromatogram of the extract.

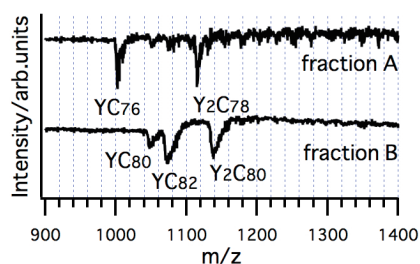


Fig. 2 LD-TOF-MS spectra of the fraction A and B.

## Spectroscopic studies of $\text{La}_2@C_{78}$ anion

○Shinya Nishimoto<sup>1</sup>, Kazuhiro Kobayashi<sup>1</sup>, Takaaki Hirayama<sup>1</sup>, Takuji Mitani<sup>1</sup>,  
 Natsumi Nakatori<sup>1</sup>, Takahisa Yamaguchi<sup>2</sup>, Ko Furukawa<sup>3</sup>, Tatsuhisa Kato<sup>2,4</sup>,  
 Koichi Kikuchi<sup>1</sup>, Yohji Achiba<sup>1</sup>, Takeshi Kodama<sup>1</sup>

<sup>1</sup>Department of Chemistry, Tokyo Metropolitan University, Hachioji 192-0397, Japan  
<sup>2</sup>Graduate School of Human and Environmental Studies, Kyoto University, Kyoto 606-8501,  
 Japan

<sup>3</sup>Department of Chemistry, Niigata University, Niigata 950-2181, Japan

<sup>4</sup>Institute for Liberal Arts and Sciences, Kyoto University, Kyoto 606-8501, Japan

In 2004, Cao et al. reported that  $\text{La}_2@C_{78}$  has  $C_{78}(D_{3h})$  cage and exhibits the absorption spectrum with several characteristic features in the visible region [1]. Recently, we succeeded in the isolation of  $M_2@C_{78}(M=Y, Gd)$  anion and measured their UV-vis-NIR absorption spectra [2,3]. The obtained spectra are very similar to that of  $\text{La}_2@C_{78}(D_{3h})$  neutral. In order to interpret such a similarity between anion and neutral forms of metallofullerenes, it was speculated that  $M_2@C_{78}(M=Y, Gd)$  anion has  $C_{78}(D_{3h})$  cage and an excess electron is located on  $M_2$ . To confirm this speculation, it has been desired to measure the absorption spectrum of  $\text{La}_2@C_{78}(D_{3h})$  in anion form and compare it with that of its neutral form. In this study, we isolated  $\text{La}_2@C_{78}$  anion and measured its absorption spectrum. Moreover, its ESR spectrum was also measured to check whether an excess electron of  $\text{La}_2@C_{78}$  anion is located on  $\text{La}_2$ .

Soot containing La-metallofullerenes was produced by direct-current (60 A) arc discharge of La/C composite rods (La:C=2:98) under a 500 Torr He atmosphere. The raw soot was extracted for 8 h with a mixed solvent of triethylamine and acetone. The isolation of  $\text{La}_2@C_{78}$  anion was accomplished by two-stage HPLC. Acetone with an ion-pair reagent, tetrabutylammonium bromide (TBABr), was used as an eluent in all the stages. For the isolated  $\text{La}_2@C_{78}$  anion, the UV-vis-NIR absorption and ESR spectra were measured. After the solvent was replaced to neutralize  $\text{La}_2@C_{78}$  anion from acetone to  $\text{CS}_2$ , or toluene, the UV-vis-NIR absorption spectra were measured for each solution.

Figure 1 shows the UV-vis-NIR absorption spectra of each solution of  $\text{La}_2@C_{78}$ . All the spectra are almost the same, though their positions of a characteristic peak near 650 nm are slightly different from each other (TBABr/acetone: 648 nm,  $\text{CS}_2$ : 662 nm, toluene: 652 nm). Figure 2 shows the ESR spectrum of  $\text{La}_2@C_{78}$  anion, showing the presence of the very large hyperfine constant. These results indicate the assumed speculation for  $M_2@C_{78}(M=Y, Gd)$  anion is valid.

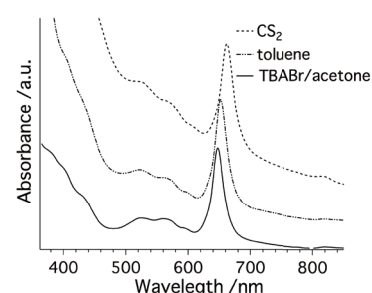


**Fig.1** UV-vis-NIR absorption spectra of each solution of  $\text{La}_2@C_{78}$ .

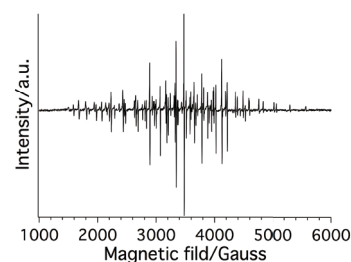


**Fig.2** X-band ESR spectrum of  $\text{La}_2@C_{78}$  anion at 4 K in TBABr/acetone.

[1] B. Cao, et al. *J. Am. Chem. Soc.* **126**, 9164-9165 (2004).

[2] N. Nakatori, et al. *The 50<sup>th</sup> Fullerenes-Nanotubes-Graphene General Symposium* 44 (2016).

[3] T. Mitani, et al. *The 10<sup>th</sup> Annual Meeting of Japan Society for Molecular Science* 3P077(2016).

Corresponding Author: Takeshi Kodama

Tel: +81-42-677-2530, Fax: +81-42-677-2525

E-mail: kodama-takeshi@tmu.ac.jp

## Evaluation of dispersion states of nanomaterials by disc centrifuge sedimentation technique

○Naoko Tajima<sup>1</sup>, Takahiro Morimoto<sup>1,2</sup>, Yuichi Kato<sup>1,2</sup>, Kazufumi Kobashi<sup>1,2</sup>, Takeo Yamada<sup>1,2</sup>, Toshiya Okazaki<sup>1,2</sup>

<sup>1</sup> Technology Research Association for Single Wall Carbon Nanotubes (TASC), Tsukuba, 305-8565, Japan

<sup>2</sup> CNT Application Research Center, National Institute of Advanced Industrial Science and Technology (AIST), Tsukuba, 305-8565, Japan

To evaluate the dispersion state of nanomaterials such as carbon nanotubes (CNTs) is very important for the application of the material. As one of the evaluation methods, we have measured the particle size (Stokes diameter) distribution of the dispersion using disk centrifuge (DC24000, CPS Instruments Inc.), which is based on differential sedimentation according to Stokes' law.

Figure 1 shows the particle size distribution of multi-walled CNT (MWCNT) in the water dispersion (CNT-Aqua, Microphase Co., Ltd.). The distribution is bimodal, the smaller size fraction is associated with individual CNTs and the larger size fraction with aggregated CNTs. For rod-like substance, Henn [1] suggested its Stokes diameter ( $D$ ) is calculated from relational equation with the substance diameter ( $d$ ) and length ( $L$ ) concerning the sedimentation process of the substance.

$$D = d\sqrt{\ln(2L/d)}$$

By using the dimensions of the MWCNT ( $d$  :  $\sim 0.01\mu\text{m}$ ,  $L$  :  $30\text{-}600\mu\text{m}$ ) specified by the manufacturers used for CNT-Aqua in this equation,  $D$  is calculated  $0.029$  to  $0.034\mu\text{m}$ , which is close to the obtained peak value ( $0.025\mu\text{m}$ ) of the smaller size fraction in Fig. 1.

Similarly, for the other MWCNTs, the diameters measured by DC24000 were compared with the calculated values with this equation. Here,  $d$  and  $L$  of each CNT were obtained from SEM and/or AFM observation. As a result, they agreed with each other within a certain range, and it was found that the equation is effective also for individual CNT. The dispersion states of graphene oxide and cellulose nanofiber will also be discussed in detail.

This study is based on results obtained from a project commissioned by the New Energy and Industrial Technology Development Organization (NEDO).

[1] A. R. Henn. Part. Part. Syst. Charact. 13, 249 (1996).

Corresponding Author: Toshiya Okazaki

E-mail: toshi.okazaki@aist.go.jp

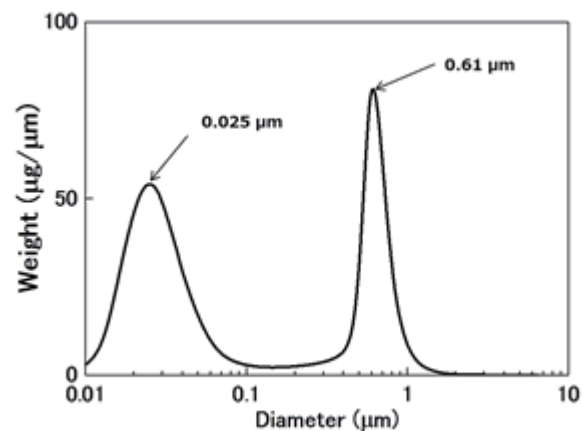


Fig.1 Particle size distribution of MWCNT in the water dispersion

## Unified analysis of quantum and classical transport properties on metallic carbon nanotubes

○Keisuke Ishizeki<sup>1</sup>, Kenji Sasaoka<sup>2,3</sup>, Satoru Konabe<sup>1,4</sup>, Satofumi Souma<sup>3</sup>,  
Takahiro Yamamoto<sup>1,4,5</sup>

<sup>1</sup> *Department of Engineering, Tokyo University of Science, Tokyo 125-8585, Japan*

<sup>2</sup> *Organization of Advanced Science and Technology, Kobe University, Kobe 657-8501, Japan*

<sup>3</sup> *Department of Engineering, Kobe University, Kobe 657-8501, Japan*

<sup>4</sup> *RIST, Tokyo University of Science, Tokyo 125-8585, Japan*

<sup>5</sup> *Department of Liberal Arts (Physics), Tokyo University of Science, Tokyo 125-8585, Japan*

Metallic carbon nanotubes (CNTs) are expected to be wiring materials of next-generation LSIs because of their high carrier mobility. It is known that a CNT shows different electronic transport properties depending on the system size. While the transport property shows diffusive transport when the system size is much longer than a mean free path, it shows ballistic transport when the system size is much shorter than a mean free path [1]. On the other hand, a phase coherence length is a characteristic length to divide coherent and incoherent transport. Conventionally, each transport property has been studied by different transport theories. However, a transport theory that can treat the two transport regimes including the crossover has not been established in spite of the importance for designing LSIs.

In this study, we developed a new quantum transport simulation method that can treat an open system of millions of atoms with atomic vibration at finite temperature. Using the new simulation method, we investigated the electronic transport properties of metallic CNTs at room temperature. As a result, we succeeded to calculate electrical resistance from ballistic to diffusive transport regime in a unified manner, and estimate a mean free path at room temperature (Fig. 1. (a)). Moreover, we also succeeded to extract the coherent component of electronic current which goes through a system with preserving an initial energy, and estimate a phase coherence length (Fig. 1. (b)).

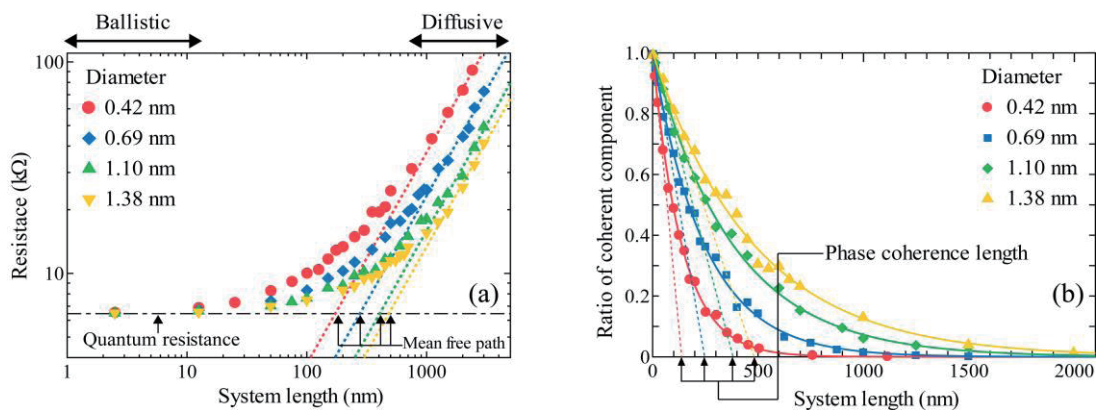


Fig. 1. System length dependence of (a) electrical resistance and (b) the coherent component

### References:

[1] S. Datta, *Electronic transport in Mesoscopic Systems* (Cambridge University Press, Cambridge, 1995)

**Corresponding Author: T. Yamamoto**

E-mail: takahiro@rs.tus.ac.jp

## High Temperature Surface Enhanced Raman Scattering of Single-Walled Carbon Nanotubes

Ming Liu<sup>1</sup>, Keigo Otsuka<sup>1</sup>, Rong Xiang<sup>1</sup>, Taiki Inoue<sup>1</sup>, Shohei Chiashi<sup>1</sup>, Shigeo Maruyama<sup>1,2</sup>

<sup>1</sup> Department of Mechanical Engineering, The University of Tokyo, Tokyo 113-8656, Japan

<sup>2</sup> National Institute of Advanced Industrial Science and Technology (AIST), Ibaraki 305-8564, Japan

In situ Raman scattering is a significant technique to characterize the growth process of single-walled carbon nanotubes (SWNTs), which can provide both formation dynamics and population evolution of the obtained SWNTs. [1] However, Raman intensity obtained at high temperature is too weak to explicitly identify the structure-related fingerprints, e.g. position and shape of G- peak. [2] In our previous work, the poor stability of metal nanoparticles at high temperature was the main restriction to achieve surface-enhanced Raman scattering (SERS) of SWNTs during growth process. [3] In this study, Ag@SiO<sub>2</sub> core shell particle was investigated to be the stable SERS particle to enhance Raman scattering of SWNTs at high temperature. By detection of Rhodamine B at room temperature, this Ag@SiO<sub>2</sub> structure (Fig. 1(a)) was confirmed to be an effective SERS substrate, which could be a promising application for detecting other organic pollutants. The stability of Ag@SiO<sub>2</sub> particle at high temperature was verified by a series of heating experiments and characterization. Additionally SERS enhancement of horizontally aligned SWNTs (HA-SWNTs) at different temperatures was confirmed to be stable and temperature insensitive in our experiment (Fig. 1(b)). Besides, the annealing process of nanodiamond at high temperature was also monitored in real time on this SERS substrate (Fig. 1(c)). This study paves a way to achieve in situ characterizing of growth process of SWNTs at high temperature by Raman scattering.

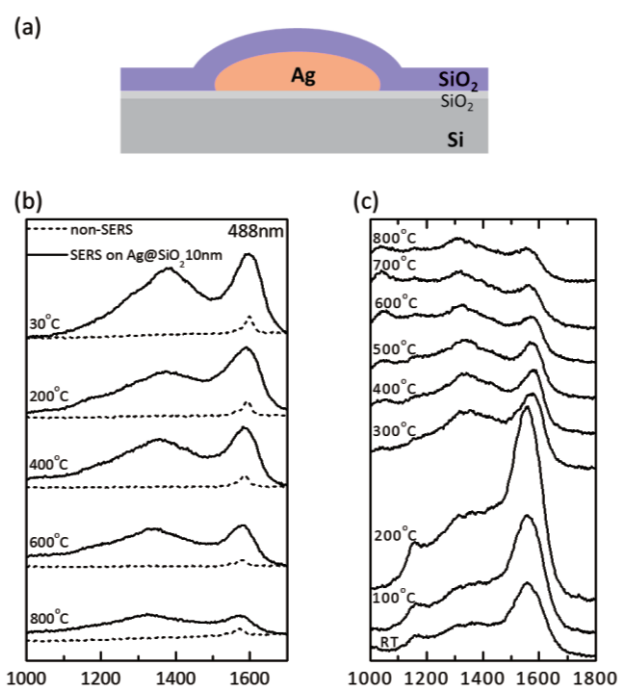


Fig. 1 (a) Schematic illustration of Ag@SiO<sub>2</sub> SERS substrate. (b) Non-SERS spectra of HA-SWNTs on silicon substrate and SERS spectra of the same HA-SWNTs on Ag@SiO<sub>2</sub> 10nm substrate at different temperatures; (c) Temperature dependent Raman spectra of nanodiamond on Ag@SiO<sub>2</sub> 10nm substrate during annealing process; Excitation laser 488 nm for (b) and (c).

[1]. Li-Pook-Than A. *et al.* J. Phys. Chem. C **114**, 11018 (2010).

[2]. Huong, P. V. *et al.* Phys. Rev. B **51**, 10048 (1995).

[3]. Liu, M. *et al.* Carbon **80**, 311 (2014).

Corresponding Author: Shigeo Maruyama

Tel: +81-3-5841-7437, Fax: +81-3-5841-7437,

E-mail: maruyama@photon.t.u-tokyo.ac.jp

## Fabrication and photoluminescence characterization of carbon nanotube dual-gate devices

○Akihiro Sasabe<sup>1,2</sup>, Takushi Uda<sup>1,2</sup>, Masahiro Yoshida<sup>1,3</sup>, Akihiro Ishii<sup>1,4</sup>, Yuichiro K. Kato<sup>1,3</sup>

<sup>1</sup> *Nanoscale Quantum Photonics Laboratory, RIKEN, Saitama 351-0198, Japan*

<sup>2</sup> *Department of Applied Physics, The University of Tokyo, Tokyo 113-8656, Japan*

<sup>3</sup> *Quantum Optoelectronics Research Team, RIKEN center for Advanced Photonics, Saitama 351-0198, Japan*

<sup>4</sup> *Department of Electrical Engineering, The University of Tokyo, Tokyo 113-8656, Japan*

Photoluminescence from carbon nanotubes subjected to a DC gate voltage is quenched due to induced carrier accumulation [1], whereas applying a square-wave gate voltage to nanotubes causes luminescence recovery as a result of carriers being swept into contact electrodes [2]. Here we characterize photoluminescence of carbon nanotubes in dual-gate devices which allow for simultaneous and independent application of a DC gate voltage and a square-wave gate voltage. The devices are fabricated from silicon-on-insulator substrates, where trenches isolate two regions of the top silicon layer for use as the dual gates. We then perform thermal oxidation to form a gate dielectric, and air-suspended carbon nanotubes are grown over the trench between the dual gates. Photoluminescence measurements are used to identify the chirality of the as-grown individual nanotubes, and we examine the response of the nanotube emission to various combinations of the dual-gate voltages.

Work supported by KAKENHI (JP16H05962), Asahi Glass Foundation, and MEXT (Photon Frontier Network Program, Nanotechnology Platform). T.U. is supported by ALPS and A.I. is supported by MERIT and JSPS Research Fellowship.

[1] S. Yasukochi, T. Murai, S. Moritsubo, T. Shimada, S. Chiashi, S. Maruyama, Y. K. Kato, Phys. Rev. B 84, 121409(R) (2011).

[2] M. Jiang, Y. Kumamoto, A. Ishii, M. Yoshida, T. Shimada, Y. K. Kato, Nature Commun. 6, 6335 (2015).

Corresponding Author: Yuichiro K. Kato

Tel: +81-48-462-1111 (ext. 3432)

E-mail: [yuichiro.kato@riken.jp](mailto:yuichiro.kato@riken.jp)

## Optical Measurement of Single-walled Carbon Nanotubes Using Rayleigh Scattering Spectroscopy

○Takeshi Okochi<sup>1</sup>, Toru Osawa<sup>1</sup>, Yoritaka Furukawa<sup>1</sup>, Tatsuro Ogamoto<sup>1</sup>, Shun Kamakura<sup>1</sup>, Taiki Inoue<sup>1</sup>, Shohei Chiashi<sup>1</sup>, Shigeo Maruyama<sup>1,2</sup>

<sup>1</sup> *Department of Mechanical Engineering, The University of Tokyo, Hongo 7-3-1, Bunkyo-ku, Tokyo, Japan*

<sup>2</sup> *Energy NanoEngineering Laboratory, National Institute of Advanced Industrial Science and Technology (AIST), Tsukuba*

Because SWNTs are nano-materials and have large specific surface, the interaction between SWNTs and the environments sometimes changes the electronic property. This change needs to be studied because it may influence the performance and reliability of SWNT devices. In this study, we measured Rayleigh scattering spectra [1] to investigate the electronic structure of various SWNT samples. We constructed the optical system for measuring Rayleigh scattering spectra and Rayleigh scattering images. The continuum laser (the range of wavelength was 400 – 2500 nm) was used as the excitation light. To improve the S/N ratio of measurement, we utilized cross polarization technique [2]. We measured Rayleigh scattering spectra of suspended SWNTs, SWNTs on Si substrates, dispersed SWNTs in the surfactant solutions [3] and dry-deposited SWNT films [4]. For example, we obtained Rayleigh spectra of a suspended SWNT as shown in fig. 1, and we estimated its chirality. We will discuss the influence of the environmental conditions on the electronic structures of SWNTs led to by environmental conditions on the basis of on experimental results.

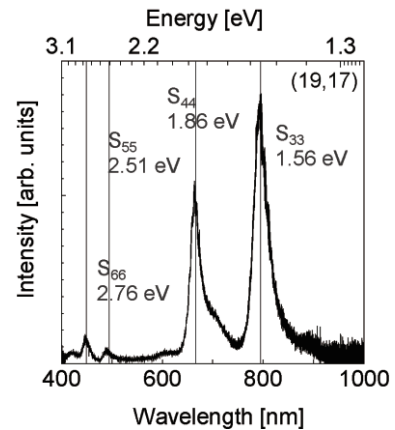


Fig. 1: Rayleigh scattering spectrum of a suspended SWNT.

[1] M. Y. Sfeir *et al.*, *Science* **306**, 1540 (2004).

[2] K. Liu *et al.*, *Nat. Nanotechnol.* **8**, 917 (2013)

[3] H. Liu *et al.*, *Nat. Commun.* **2**, 309 (2011).

[4] A. Kaskela *et al.*, *Nano Lett.* **10**, 4349 (2010).

Corresponding author: S. Maruyama

Tel: +81-3-5841-6421

Email: okochi@photon.t.u-tokyo.ac.jp

## Synthesis and structure control of vertically aligned carbon nanotubes on Cu foils for thermal interface materials

○Shunji Kobayashi<sup>1</sup>, Kei Hasegawa<sup>1</sup>, Hisashi Sugime<sup>2</sup>, Masanao Obori<sup>3</sup>,  
Junichiro Shiomi<sup>3</sup>, Xiaosong Zhou<sup>4</sup>, Mizuhisa Nihei<sup>4</sup>, Suguru Noda<sup>1</sup>

<sup>1</sup> Department of Applied Chemistry, Waseda University, Tokyo 169-8555, Japan

<sup>2</sup> Waseda Institute for Advanced Study, Waseda University, Tokyo 169-8050, Japan

<sup>3</sup> Department of Mechanical Engineering, The University of Tokyo, Tokyo 113-8656, Japan

<sup>4</sup> Huawei Technologies Japan K. K., Kanagawa 221-0056, Japan

In order to release heat from electronic device chip to heat sink, thermal interface materials (TIMs) are used. To fill the air gap between the chips and heat sinks, composites of polymer and metal particles are widely used as TIMs. Many researchers have studied TIMs with carbon nanotubes (CNTs), which have high thermal conductivity and high flexibility. We have previously reported ~50  $\mu\text{m}$ -tall, 0.2-0.3  $\text{g}/\text{cm}^3$ -dense vertically-aligned (VA) CNTs grown both faces of Cu foils, which showed TIM performance comparable to the typical indium sheet [1]. This time we propose Cu-CNT composite, in which Cu particles are held by thermally conductive VA-CNTs instead of thermally less conductive polymer matrix.

VA-CNTs were synthesized following the previous method [1]. Fe (2 nm)/TiN (15 nm)/Ta (10 nm) was sputter-deposited on both sides of Cu foil, and VA-CNTs were synthesized by CVD using  $\text{C}_2\text{H}_2$  (0.2 Torr)/ $\text{H}_2$  (2 Torr)/Ar (12.8 Torr) at 700 °C for 30 min. Then the VA-CNTs were coated with carbon using  $\text{C}_2\text{H}_2$  (21.3 Torr)/Ar (78.7 Torr) at 800 °C for 30 min to prevent them from shrinking during the electrodeposition process. Then Cu was electrodeposited on VA-CNTs using  $\text{Cu}(\text{NO}_3)_2$  aq under condition shown in Table 1.

As grown VA-CNTs shrank after dipping-drying with water, but the carbon-coated VA-CNTs stayed stable. Cu particles were electrodeposited on the carbon-coated VA-CNTs by applying electric pulses; high overpotential promotes nucleation of Cu particles while interval enables sufficient diffusion of  $\text{Cu}^{2+}$  from outside to inside of the VA-CNTs. Fabricated Cu/VA-CNT is shown in Fig.1. Cu was deposited fairly uniformly with volume fractions of 7.73 vol%, 7.61 vol% and 10.55 vol% at the top, middle and bottom of the VA-CNTs.

The thermal resistance of VA-CNT will be measured and reduced by optimizing electrodepositing condition.

**Table 1.** Condition for Cu electrodeposition on VA-CNTs.

Target Cu fraction	Total charge	Pulse current	Pulse width	Number of pulses	Pulse interval	Total time
30 vol%	81.6 C	0.4 A	1.5 s	136	100 s	$1.37 \times 10^4$ s

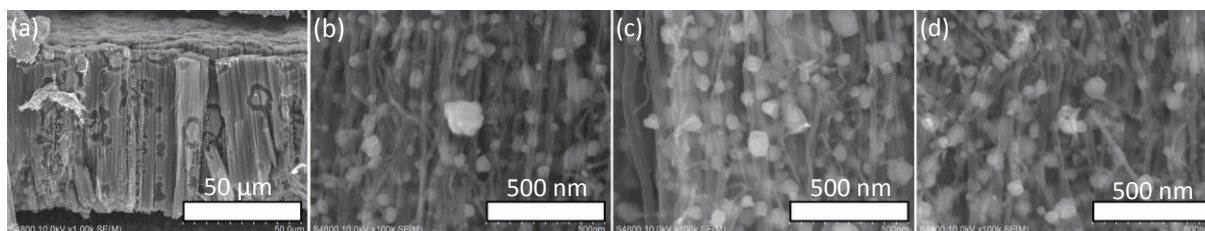


**Fig. 1.** Cross-sectional SEM images of Cu/VA-CNTs. (a) Overall view (b) top (c) middle (d) bottom.

Acknowledgement: This work is supported by Huawei Innovation Research Program.

[1] N. Na et al., Jpn. J. Appl. Phys. 54, 095102 (2015).

Corresponding Author: S. Noda, Tel&Fax: +81-03-5286-2769, E-mail: noda@waseda.jp

## Selective detection of neurotransmitters by adsorption voltammetry with carbon nanotube film

○Takuya Ushiyama<sup>1</sup>, Shigeru Kishimoto<sup>1</sup>, and Yutaka Ohno<sup>1,2</sup>

<sup>1</sup>Graduate School of Engineering, Nagoya University, Nagoya 464-8603, Japan

<sup>2</sup>Institute of Materials and Systems for Sustainability, Nagoya University, Nagoya 464-8603, Japan

Neurotransmitters are emitted by nerve cells to convey information in brain. They are also known as one of stress markers in saliva. The concentrations of neurotransmitters are 10-1000 nM in cerebrospinal fluid and ~100 pM in saliva [1, 2]. Carbon nanotube (CNT) is promising electrode material for electrochemical sensors to detect neurotransmitters [3]. We had proposed adsorption voltammetry using a CNT film, and demonstrated ultra-high sensitivity detection of neurotransmitters of 100 pM [4]. This method consists of pre-concentration and detection processes; neurotransmitters are concentrated by adsorption onto electrode surface and subsequently detected by cyclic voltammetry. In practical biological samples, many impurity substances are contained as well as small amount of objective molecule. Therefore, electrochemical sensors are required to have selectivity in addition to sensitivity. In this work, we investigated the selectivity in detection of neurotransmitters by the adsorption voltammetry.

We fabricated electrochemical sensors with clean single-walled CNTs on a plastic substrate, using the dry transfer and micro-fabrication process as our previous work [4]. Adsorption voltammetry was performed for PBS solutions containing dopamine (DA), serotonin (5-HT) or their mixture. First, we applied fixed potential to CNT electrode for 600 s in sample solution in the pre-concentration process. Then, we scanned potential in the detection process to measure oxidation current similar to cyclic voltammetry.

Figure 1 shows the voltammogram for 10- $\mu$ M 5-HT (dashed curve) and a mixture of 10- $\mu$ M 5-HT and 1- $\mu$ M DA (solid curve). We observed a sharp oxidation peak at ~0.1 V for the mixture sample (5-HT+DA) although broad peak at ~0.35 V appeared for both 5-HT and 5-HT+DA. According to our previous work, the peak originating from adsorbed DA is presumed to appear at the potential of ~0.1 V [4]. The potential of oxidation peak for adsorbed species is lower than that of peak observed in conventional cyclic voltammetry [5]. The result shows DA can be detected selectively in presence of 5-HT by the adsorption voltammetry.

[1] K. O. Schwab *et al.*, *Eur. J. Clin. Chem. Clin. Biochem.*, **30**, 541 (1992)

[2] T. Okumura *et al.*, *J. Chromatogr. B*, **694**, 305 (1997)

[3] C. B. Jacobs *et al.*, *Analyst*, **136**, 3557 (2011)

[4] T. Ushiyama *et al.*, *The 51st FNTG General Symp.*, 2P-14 (2016)

[5] A. S. Kumar *et al.*, *J. Electroanal. Chem.*, **641**, 131 (2010)

Corresponding Author: Y. Ohno

Phone & Fax: +81-52-789-5387, E-mail: yohno@nagoya-u.jp

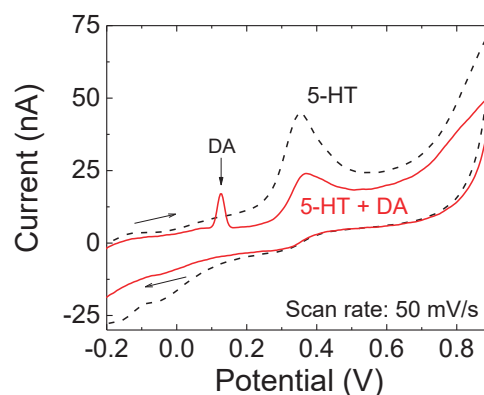


Fig. 1 Voltammograms for 5-HT (dashed curve) and a mixture of 5-HT and DA (solid curve) obtained by adsorption voltammetry

## Time-dependent change of the semiconducting-CNT ink evaluated from the performance of CNT-TFTs

○Yuki Kuwahara<sup>1,3</sup>, Fusako Sasaki<sup>3</sup>, Fumiyuki Nihey<sup>2</sup>, Takeshi Saito<sup>1,3</sup>

<sup>1</sup> National Institute of Advanced Industrial Science and Technology, Tsukuba 305-8565, Japan

<sup>2</sup> IoT Devices Research Laboratories, NEC Corporation, Tsukuba 305-8501, Japan

<sup>3</sup> Technology Research Association for Single Wall Carbon Nanotubes, Tsukuba 305-8565, Japan

The network of carbon nanotubes (CNTs) has been used as a channel of thin film transistors (TFTs) which enables us fabricating flexible, large-area, and low-cost electronic devices by a printed-electronics technique. Usually, CNT dispersion is used as ink that can be deposited on various substrates. The uniformity of CNT network, as well as the purity of semiconducting CNTs, is one of the important factors to produce high performance CNT-TFTs for their practical use. Recently, we have investigated the electric-field-induced layer formation (ELF) method [1] in order to separate metallic and semiconducting CNTs. By using the CNT ink extracted by ELF, high device performance with low variability have been demonstrated [2]. Although the condition of CNT-ink deposition was investigated for improving the device performance, the temporal stability of CNT ink was still remained as an open question. In this study, we have investigated the time-dependent change of the semiconducting-CNT ink by the evaluation on the basis of the CNT-TFTs' performances.

CNTs synthesized by eDIPS method [3] were dispersed in the aqueous solution of polyoxyethylene (100) stearyl ether (Brij S 100). Then the semiconducting-CNT ink was extracted from the CNT dispersion by ELF, in which the semiconductor purity of >95% was obtained by the optical-absorption-spectroscopy characterization. We have stored the CNT ink in the refrigerator for up to ca. 2 months to check the temporal stability. The CNT network films were prepared moment to moment by depositing the ink on silicon substrates, and then rinsing with isopropyl alcohol (IPA) after several minutes. On the CNT network film, Au electrodes were deposited through a metal mask to fabricate CNT-TFTs. Figure 1 plotting the performance of CNT-TFTs fabricated at different ink ages shows that the deterioration of the CNT ink is negligible from the viewpoint of the TFT performance. In presentation, we will also discuss the morphological changes of CNT networks by AFM observation.

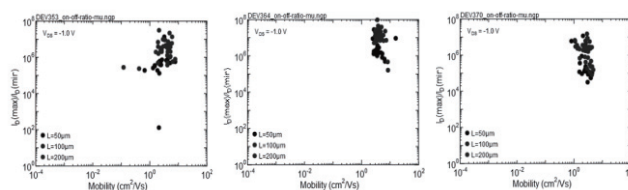


Fig. 1 Performance of CNT-TFTs prepared in 1day (left), 18days later (center) and 51days later (right).

### Acknowledgment

This presentation is based on results obtained from a project subsidized by the New Energy and Industrial Technology Development Organization (NEDO).

### References

- [1] K. Ihara *et al.*, *J. Phys. Chem. C* **115**, 22827 (2011).
- [2] S. Ohmori *et al.*, *RSC Adv.*, **2**, 12408 (2012).
- [3] T. Saito *et al.*, *J. Nanosci. Nanotechnol.* **8**, 6153 (2008).

Corresponding Author: T. saito, Tel: +81-29-861-4863, Fax: +81-29-861-4413, E-mail: takeshi-saito@aist.go.jp

## Lamination of Vertically Aligned Single-Walled Carbon Nanotube Forests on Perovskite Solar Cells via Membrane Filter Transfer Method

○Seungju Seo<sup>1</sup>, Il Jeon<sup>1</sup>, Takahiro Sakaguchi<sup>1</sup>, Taiki Inoue<sup>1</sup>, Rong Xiang<sup>1</sup>, Shohei Chiashi<sup>1</sup>, Yutaka Matsuo<sup>1,2</sup>, Shigeo Maruyama<sup>1,3</sup>

<sup>1</sup> Department of Mechanical Engineering, The University of Tokyo, Tokyo 113-8656, Japan

<sup>2</sup> Hefei National Laboratory for Physical Sciences at the Microscale, University of Science and Technology of China, Hefei, Anhui 230026, China

<sup>3</sup> Energy NanoEngineering Lab, National Institute of Advanced Industrial Science and Technology(AIST), Ibaraki 305-8564, Japan

Single-walled carbon nanotubes (SWNTs) are well-known as an outstanding electrical conductor with their excellent mobility, about  $100,000 \text{ cm}^2/\text{Vs}$  at room temperature. Also, the fact that they have an alignment orientation makes SWNTs stand out among other carbon conductors such as graphite, graphene. Arrays of vertically-aligned single-walled carbon nanotubes (VA-SWNTs) [1] so called SWNTs forests, offer remarkable vertical conductivity, which is not observed with disordered SWNTs. VA-SWNTs can be viewed as a new type of functional bulk material that is useful for numerous applications. Their potential can be maximized if their unique features are met with the device's properties, and a successful transfer is accomplished.

Over the past five years, the rapid emergence of perovskite solar cells (PSCs) are attracting increased attention on account of their high power conversion efficiency (PCE) and simple processes in addition to low material costs. Along with the optimization of perovskite crystal formation, the approach from the diversity of device concepts and new material, the PCE has risen from 3% to over 20%, which is close to that of conventional solar cell families such as Si, CIGS, and CdTe [2].

Thus far, VA-SWNTs application in perovskite solar cells has not been reported. This is because VA-SWNTs are non-transparent and their conventional transfer method involves water, which prompts perovskite degradation. Other alternative dry transfer methods, such as PDMS infiltration also take too much time and difficult to accomplish [3].

In our work, we demonstrate an application of VA-SWNTs in perovskite solar cells using a new transfer method using membrane filter, which offers a facile and reproducible way to laminate VA-SWNTs film (Fig.1) without moisture contact to the perovskite layer. PSCs with a structural configuration of glass/fluorine-doped tin oxide (FTO)/ $\text{C}_{60}$ / $\text{CH}_3\text{NH}_3\text{PbI}_3$ /VA-SWNTs/Au were fabricated. The inclusion of VA-SWNTs enhanced both power conversion efficiency (PCE) and stability of the devices. Improved PCE was due to the increase in open-circuit voltage originated from energy level matching between perovskite layer and gold. Improved stability is attributed to hydrophobic and densely packed nature of the VA-SWNTs.

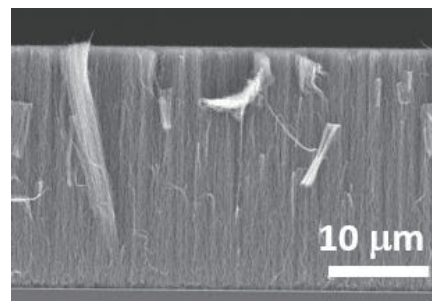


Fig.1 SEM image of VA-SWNTs film on Si/SiO<sub>2</sub> Substrate

[1] Y. Murakami et al., *Chem. Phys. Lett.*, **385** (2004) 298.

[2] [http://www.nrel.gov/ncpv/images/efficiency\\_chart.jp](http://www.nrel.gov/ncpv/images/efficiency_chart.jp)

[3] D. H. Lee et al., *Adv. Mat* **22.11** (2010): 1247.

Corresponding Author: S. Maruyama

Tel: +81-3-5841-6421, Fax: +81-3-5841-6421, E-mail: maruyama@photon.t.u-tokyo.ac.jp

## Yields of carbon nanotube integrated circuits on flexible plastic film

○Jun Hirotsani<sup>1</sup>, Shigeru Kishimoto<sup>1</sup>, and Yutaka Ohno<sup>1,2</sup>

<sup>1</sup>Graduate School of Engineering, Nagoya University, Nagoya 464-8603, Japan

<sup>2</sup>Institute of Material and Systems for Sustainability, Nagoya University, Nagoya 464-8603, Japan

Carbon nanotube thin-film transistors (CNT TFTs) are attracted much attention in flexible electronics because of their high carrier mobility [1] and excellent mechanical flexibility. To realize integrated circuits in large scale, an improvement of yield of devices is essential. We have reported wafer-scale and high-yield fabrication of CNT TFTs with small characteristic variation by using purified semiconducting CNTs [2]. In this work, we have investigated the yields of integrated circuits such as inverters and ring oscillators which consist of TFTs with purified semiconductor CNTs.

The integrated circuits were fabricated on a poly(ethylene naphthalate) (PEN) substrate. Purified semiconducting CNTs were used as the channel. The gate oxide of a 40-nm-thick Al<sub>2</sub>O<sub>3</sub> layer was deposited by atomic layer deposition. The channel width and length were 100 μm. The inverters were constructed in E/D configuration. The load TFT was slightly doped with F<sub>4</sub>TCNQ (tetrafluoro-tetracyano quinodimethane) to shift the threshold voltage to be depletion mode. Ring oscillators of 3, 11, and 24 stages with an output buffer were fabricated.

Figure 1 shows input-output characteristics of 24 inverters. All of the inverters worked successfully. The voltage gain was as high as ~30 in average. Although their large logic threshold voltages dispersed from -3.5 to -2.2 V, logic signal transfer to the subsequent stage would be possible even under an existence of hysteresis. The yields of ring oscillators degraded with an increase in integration scale, i.e., 3-stage (100%), 11-stage (75 %), and 21-stage (50%). The yield of TFTs were 96.2 %, which should be improved further for high yield fabrication of integrated circuits.

Acknowledgments: The semiconducting CNTs were provided by TASC. This work was partially supported by Grant-in-Aid by MEXT, JST/SICORP, and JST/CREST.

[1] D.-M. Sun, *et al.*, *Nature Nanotechnol.* **6**, 156 (2011).

[2] J. Hirotsani et al., *The 48th FNTG symposium*, 3P-12

Corresponding Author: Yutaka Ohno, Phone & Fax: +81-52-789-5387, E-mail: yohno@nagoya-u.jp

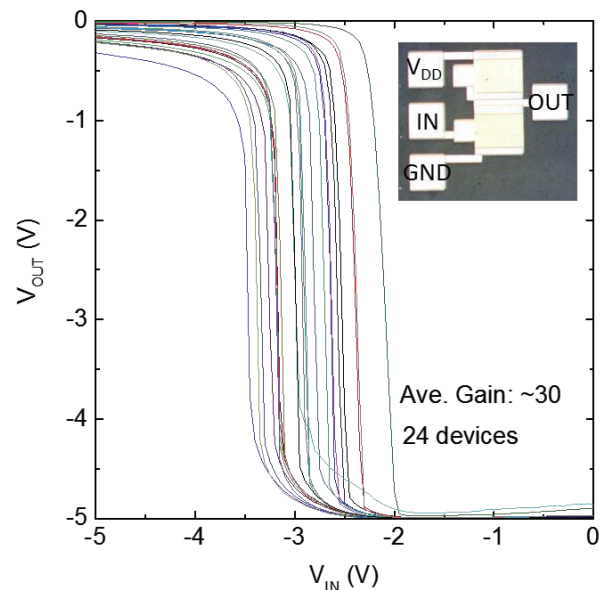


Fig. 1 Input-output characteristics of 24 inverters.

## Modeling of carbon nanotube thin-film transistor on flexible plastic film

○Taiga Kashima<sup>1</sup>, Tomoki Matsuura<sup>2</sup>, Jun Hirotsu<sup>2</sup>, Shigeru Kishimoto<sup>2</sup>, and Yutaka Ohno<sup>2,3</sup>

<sup>1</sup>*School of Engineering, Nagoya University, Nagoya 464-8603, Japan*

<sup>2</sup>*Graduate School of Engineering, Nagoya University, Nagoya 464-8603, Japan*

<sup>3</sup>*Institute of Material and Systems for Sustainability, Nagoya University, Nagoya 464-8603, Japan*

Carbon nanotube thin-film transistors (CNT TFTs) are promising active devices for flexible electronics because of their high carrier mobility [1] and excellent mechanical flexibility. In recent years, high-yield fabrications of CNT TFTs with small characteristic variation have become possible with purified semiconductor CNT materials. This leads to progressive researches on large-scale integration and analog circuit applications of CNT TFTs. To design functional integrated circuits, the modeling of transistors for circuit simulations are indispensable. In this work, we have built a model of CNT TFTs on the basis of the electrical characterizations.

The device structure of the CNT TFTs is shown in the inset of Fig. 1(b). The device was fabricated on poly(ethylene naphthalate) (PEN) substrate. Purified semiconducting CNTs were used as the channel. The gate oxide of a 40-nm-thick  $\text{Al}_2\text{O}_3$  layer was deposited by atomic layer deposition. The channel width was 100  $\mu\text{m}$ , and the channel length was from 5 to 100  $\mu\text{m}$ .

We constructed a device model based on Shichman and Hodges's MOSFET model [2]. Some modifications were applied to express subthreshold current and off current. Figure 1 shows measured characteristics and the fitted model. The developed model can well express the both output and transfer characteristics. The model was also applicable to n-type CNT TFTs.

Acknowledgments: The semiconducting CNTs were provided by TASC. This work was partially supported by Grant-in-Aid by MEXT, JST/SICORP, and JST/CREST.

[1] D.-M. Sun, *et al.*, *Nature Nanotechnol.* **6**, 156 (2011).

[2] H. Shichman and D. A. Hodges, *J. Solid-State Cir.* **3**, 285 (1968).

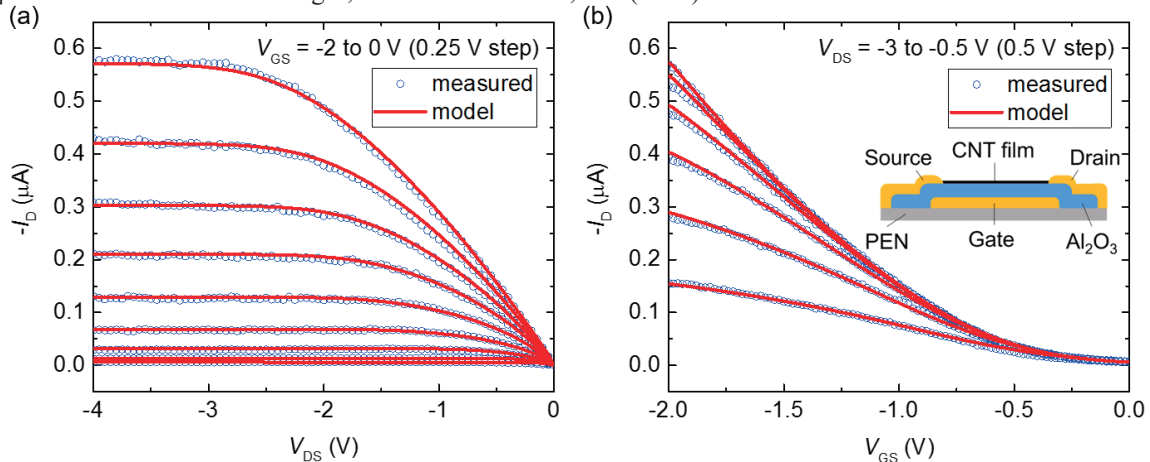


Fig. 1 Measured characteristics and fitted model. (a) Output and (b) transfer characteristic.

Corresponding Author: Yutaka Ohno, Phone & Fax: +81-52-789-5387, E-mail: yohn@nagoya-u.jp

## Improved Efficiency and Stability of Perovskite Solar Cells with Single-Walled Carbon Nanotube Electrodes

○Takahiro Sakaguchi<sup>1</sup>, Jeon Il<sup>1</sup>, Hiroki Suko<sup>1</sup>, Taiki Inoue<sup>1</sup>, Rong Xiang<sup>1</sup>, Shohei Chiashi<sup>1</sup>, Esko I. Kauppinen<sup>2</sup>, Nam-Gyu Park<sup>3</sup>, Yutaka Matsuo<sup>1,4</sup>, Shigeo Maruyama<sup>1,5</sup>

<sup>1</sup> Department of Mechanical Engineering, The University of Tokyo, Tokyo 113-8656, Japan

<sup>2</sup> Department of Applied Physics, Aalto University School of Science, Espoo 15100, Finland

<sup>3</sup> School of Chemical Engineering and Department of Energy Science, Sungkyunkwan University, Suwon 440-746, Korea

<sup>4</sup> Hefei National Laboratory for Physical Sciences at Microscale, University of Science and Technology of China, Hefei, Anhui 230026, China

<sup>5</sup> Energy NanoEngineering Lab, National Institute of Advanced Industrial Science and Technology (AIST), Ibaraki 305-8564, Japan

Perovskite solar cells [1] are attracting a lot of attention due to their high power conversion efficiency (PCE) with low-cost materials. The PCE was 3.8 % in 2009 [1] and has drastically increased to 22.1 % [2]. As anodes, gold electrodes and Spiro-MeOTAD are used in conventional perovskite solar cells. Both gold and Spiro-MeOTAD are expensive, and the latter is unstable in ambient. Single-walled carbon nanotubes (SWNTs) have been reported to act as anodes in perovskite solar cells by substituting gold and Spiro-MeOTAD [3]. However, PCEs of perovskite solar cells with SWNT anodes have not yet attained those with conventional anodes.

In this study, we improved stability and efficiency of perovskite solar cells using SWNTs as anodes by adding polymethyl methacrylate (PMMA) onto SWNTs. Dry-deposited SWNT films [4] were employed, and solar cell structures were fabricated by deposition of TiO<sub>2</sub> layers, perovskite crystals, and SWNT films on FTO/glass substrates. Figure 1 shows the *J-V* characteristics of cells with PMMA and without PMMA. While the PCE of 10 % was obtained in the case of cell without PMMA, we achieved the PCE of 11.8 % by adding PMMA on SWNT films. Figure 2 shows the time change of the PCEs of both cells. The cell with PMMA was found to have higher stability than the cell without PMMA. These indicate that the PMMA densifies and mildly dopes SWNT films, and protects cells from moisture.

[1] A. Kojima *et al.*, *J. Am. Chem. Soc.*, **131**, 6050 (2009).

[2] [http://www.nrel.gov/ncpv/images/efficiency\\_chart.jpg](http://www.nrel.gov/ncpv/images/efficiency_chart.jpg)

[3] Z. Li *et al.*, *ACS Nano*, **8**, 6797 (2014).

[4] A. Kaskela *et al.*, *Nano Lett.*, **10**, 4349 (2010).

Corresponding Author: S. Maruyama

Tel: +81-3-5841-6421,

Fax: +81-3-5841-6421,

E-mail: maruyama@photon.t.u-tokyo.ac.jp

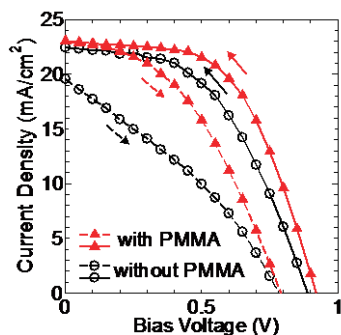


Fig. 1 *J-V* characteristics of cells with PMMA and without PMMA.

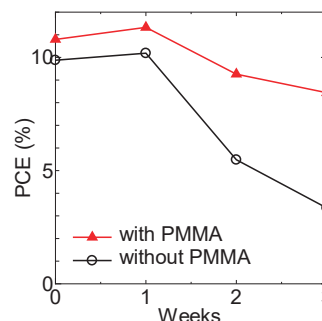


Fig. 2 Stability plots of perovskite solar cells with and without PMMA.

## Evaluation of the ratio of metal/semiconductive SWNTs by utilizing ATP technique and Raman spectroscopy

Kento Uratani<sup>1</sup>, Naoki Kanazawa<sup>1</sup>, ○Shinzo Suzuki<sup>1</sup>

<sup>1</sup>Department of Physics, Kyoto Sangyo University, Kyoto 603-8555, Japan

In this presentation, ATP technique and Raman spectroscopy were applied in order to evaluate the ratio of metal/semiconductive SWNTs by changing excitation wavelength (532 nm and 633 nm). Briefly, mono-dispersed sodium cholate (SC) solution (2 wt%) of SWNTs produced by arc-burning of Ni/Y-carbon composite rod in helium atmosphere was utilized for two immiscible aqueous solution phases (ATP), i.e., PEG and DX solution phases, following the recipe by C.Y. Khripin et al. [1]. After recognizing that each solution phase shows different color because of the difference in the ratio of metal/semi-conductive SWNTs, Raman spectra were obtained by different excitation photon energy (532 nm and 633 nm) for each solution phase, and the ratio of metal / semiconductive SWNTs was evaluated by analyzing those spectra [2].

Figure 1 shows the reproducibility of the ratio of metal/semiconductive SWNTs obtained by this technique, in case that the concentration of SC in ATP was slightly varied. It was confirmed that the reproducibility of the ratio was reasonable, indicating that this technique can be useful for in-situ evaluation of the ratio of metal /semiconductive SWNTs in ATP separation procedure.

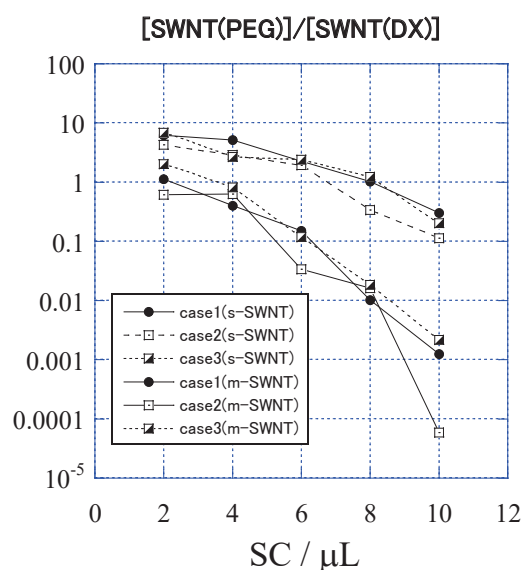


Fig. 1.

[1] C.Y. Khripin et al., *J. Am. Chem. Soc.*, **135**, 6822-6825(2013).

[2] N. Kanazawa et al., The 46<sup>th</sup> fullerenes-nanotubes-graphene general symposium, 1P-27.

Corresponding Author: S. Suzuki

Tel: +81-75-705-1631, Fax: +81-75-705-1640,

E-mail: suzukish@cc.kyoto-su.ac.jp

## Removing catalyst metals from various carbon nanotubes by halogen gas

○Koki Hamada<sup>1</sup>, Hisashi Sugime<sup>2</sup>, Suguru Noda<sup>1</sup>

<sup>1</sup> *Department of Applied Chemistry, Waseda University, Tokyo 169-8555, Japan*

<sup>2</sup> *Waseda Institute for Advanced Study, Waseda University, Tokyo 169-8050, Japan*

Extensive efforts have been made to remove catalyst metals from as-produced carbon nanotubes (CNTs). Two-step purification is popular; first the carbon shells (C-shells) covering catalyst particles are removed by gas-phase or liquid-phase oxidation and then the catalyst metals are dissolved by acids [1]. But the oxidation step causes damage to CNTs and the solution process causes aggregation of CNTs upon drying and yields liquid wastes. Some groups recently reported dry purification process in which catalyst metals such as Ni [2] or Fe [3] are etched away by the reaction with Cl<sub>2</sub> gas at elevated temperatures of ~1000 °C. However, this method is not widely used and reaction mechanism remains unclear.

In this research, we applied this method for various CNTs including single-wall CNTs (SWCNTs) by arc discharge (from Meijo Nano Carbon), multi-wall CNTs (MWCNTs) by chemical vapor deposition (CVD) (from Meijo Nano Carbon), and Tuball SWCNTs (from OCSiAl). We examined the process parameters (temperature, Cl<sub>2</sub> and Br<sub>2</sub> pressures, and reaction time) and discuss the rate determining step and reaction mechanism.

Fig. 1 shows transmission electron microscope (TEM) images of the CNTs before and after purification with 10 vol% Cl<sub>2</sub>/Ar. Both Ni (a) and Fe (b,c) catalysts are efficiently removed (d-f), leaving hollow carbon spheres. Mercier, et al. reported such structure and proposed a mechanism that Cl<sub>2</sub> diffuses through the C-shells, metal expands upon chlorination, causing cracks in the shells, promoting Cl<sub>2</sub> diffusion and metal chloride vaporization [4]. Following this mechanism, metal in crack-free shells cannot be removed. We propose another model that metal diffuses through the shells at a small probability and metal on the shells immediately be etched away by Cl<sub>2</sub>. To identify diffusion species (halogen or metal), we examined Br<sub>2</sub> as etchant and found that it can also remove metal efficiently (Fig. 2). We are now studying the rate process at milder condition to identify the diffusion species and rate determining step.

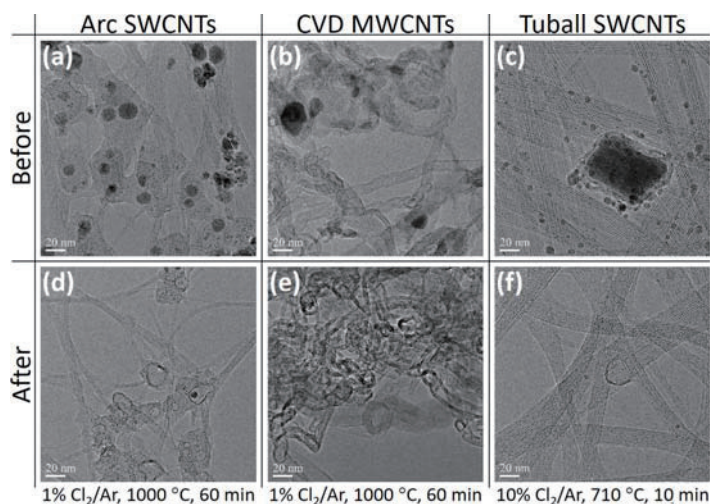


Fig. 1. CNTs before and after purification.

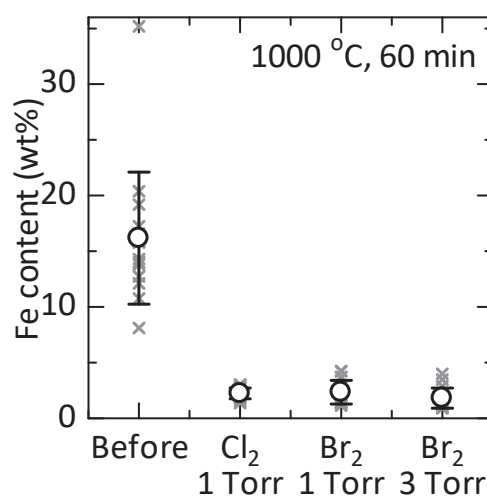


Fig. 2. Fe contents in Tuball.

[1] J. Vejpravova, et al., *Analyst* 141, 2639 (2016). [2] A. Desforges, et al., *Carbon* 76, 275 (2014).

[3] E. Remy, et al., *Carbon* 93, 933 (2015). [4] G. Mercier, et al., *New J. Chem.* 37, 790 (2013).

Corresponding Author: S. Noda, Tel&Fax: +81-3-5286-2769, E-mail: noda@waseda.jp

## Controllable growth of single-walled carbon nanotubes in quality and uniformity by extended alcohol catalytic chemical vapor deposition

○Bo Hou<sup>1</sup>, Cheng Wu<sup>2</sup>, Yoko Iizumi<sup>3</sup>, Takahiro Morimoto<sup>3</sup>, Toshiya Okazaki<sup>3</sup>, Taiki Inoue<sup>2</sup>, Shohei Chiashi<sup>2</sup>, Rong Xiang<sup>2</sup>, and Shigeo Maruyama<sup>1,2</sup>

<sup>1</sup> Energy NanoEngineering Lab., Department of Energy and Environment, AIST, Tsukuba 305-8564, Japan

<sup>2</sup> Department of Mechanical Engineering, The University of Tokyo, Tokyo 113-8656, Japan

<sup>3</sup> Nanotube Research Center, AIST, Tsukuba 305-8564, Japan

In the extended conventional alcohol catalytic chemical vapor deposition (ACCVD), CVD temperature was varied from 350 °C to 1050 °C combined with the pressures range over 6 magnitudes. In this work, we will report the high-quality SWNTs which are nearly none defect were obtained within a specific work window of extended ACCVD using zeolite-supported Fe-Co system. Furthermore, several other catalysts (zeolite-supported Rh-Co, Cu-Co and Rh) were also studied in the extended ACCVD. By using Rh-Co as the catalyst, the efficient growth of uniform diameter SWNTs was achieved in extended ACCVD. Scanning Raman with many laser lines, absorption, and photoluminescence (PL) were used to characterize the chirality and abundance of SWNTs. TEM was employed to examine the quality of SWNTs and explore the condition of catalysts near the growth boundary. The success of the direct growth of high-quality SWNTs and the realization of diameter uniformity SWNTs in extended ACCVD suggest the promising future for application and fundamental understanding of growth of SWNTs.

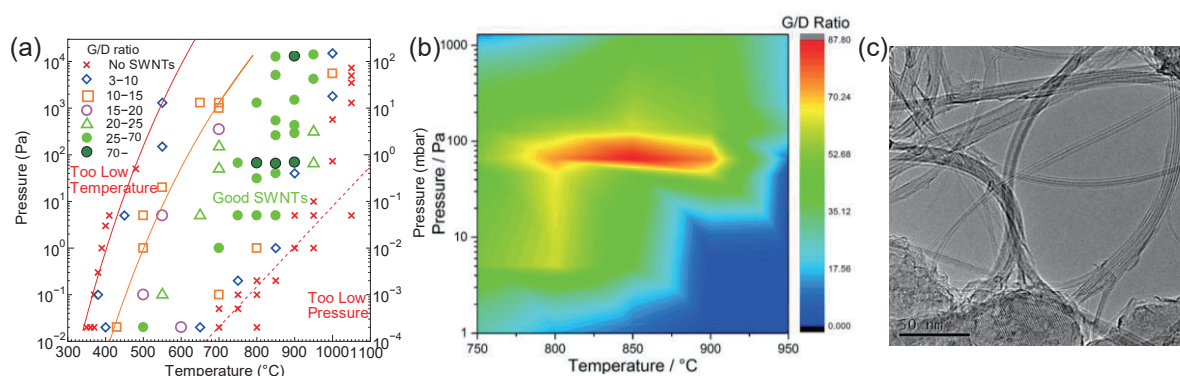


Fig (a). Extended ACCVD map. (b). 3D mapping of G/D ratio. (c) TEM image of high-quality SWNTs.

Corresponding Author: Shigeo Maruyama

Tel: +81-29-861-2073, Fax: +81-29-851-7523,

E-mail: maruyama.nano@aist.go.jp

## Synthesis and Characterization of SWNTs Using W-Co Catalyst

○Shinnosuke Ohyama<sup>1</sup>, Shun Yamamoto<sup>1</sup>, Hua An<sup>1</sup>, Feng Yang<sup>2</sup>, Taiki Inoue<sup>1</sup>, Rong Xiang<sup>1</sup>, Shohei Chiashi<sup>1</sup>, Yan Li<sup>2</sup>, Shigeo Maruyama<sup>1,3</sup>

<sup>1</sup> Department of Mechanical Engineering, The University of Tokyo, Tokyo 113-8656, Japan

<sup>2</sup> Beijing National Laboratory for Molecular Science, Key Laboratory for the Physics and Chemistry of Nanodevices, State Key Laboratory of Rare Earth Materials Chemistry and Applications, College of Chemistry and Molecular Engineering, Peking University, Beijing 100871, China.

<sup>3</sup> Energy NanoEngineering Lab, National Institute of Advanced Industrial Science and Technology (AIST), Ibaraki 305-8564, Japan

Chirality controlled growth of SWNTs is highly expected toward the applications of SWNTs. Recently, it was reported that  $W_6Co_7$  alloy catalyst realized the growth of single-chirality SWNTs with purity over 90% through pretreatment and growth at high temperature using molecular cluster as a catalyst precursor [1, 2]. Furthermore, in our group, (12, 6) SWNTs were selectively grown at lower temperature by using a sputtered bimetallic W-Co in the alcohol catalytic chemical vapor deposition [3, 4]. The structure of the sputtered catalyst identified by TEM analysis was  $W_6Co_6C$ , which is different from that from the molecular cluster.

In this report, we deposited W-Co catalyst by dip-coating of solution of  $WCl_6$  and  $Co(CH_3COO)_2$ , and compared the grown SWNTs with those from sputtering and the molecular cluster. We succeeded in producing SWNTs with high yield and chirality selectivity to some extent by relatively lower temperature growth. We changed ratio of W/Co and investigated the effects of W by using Raman spectra (Fig. 1). From the spectra, we found that sample (c) exhibited the highest selectivity of (12, 6). We will also discuss the effects of water vapor treatment during the reduction process.

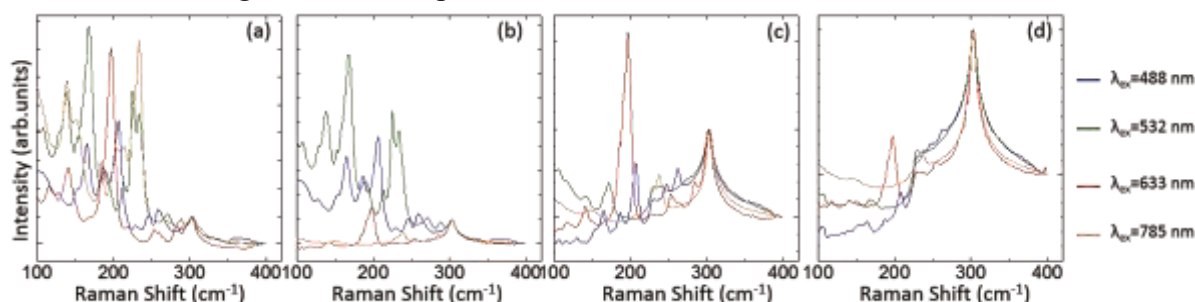


Fig. 1 Raman spectra of SWNTs from W-Co catalyst deposited by dip-coat method (a) Co: 1.68 mM, (b) W: 5.0 mM, Co: 1.0 mM, (c) W: 5.0 mM, Co: 3.0 mM and (d) W: 5.0 mM, Co: 5.0 mM.

[1] F. Yang *et al.*, Nature **510**, 522 (2014). [2] F. Yang *et al.*, J. Am. Chem. Soc. **137**, 8688 (2015).

[3] S. Maruyama *et al.*, Chem. Phys. Lett. **360**, 229 (2002). [4] H. An *et al.*, Nanoscale **8**, 14523 (2016).

Corresponding Author: S.Maruyama Tel: +81-3-5841-6408, Fax: +81-3-5841-6408,  
E-mail: maruyama@photon.t.u-tokyo.ac.jp

## Growth of Semiconducting (14,4) Carbon Nanotubes Using W-Co Salts as Catalyst Precursor

○Xiulan Zhao, Feng Yang, Yan Li

*Beijing National Laboratory for Molecular Science, College of Chemistry and Molecular Engineering, Peking University, Beijing 100871, China*

Tungsten-based intermetallic catalyst with high melting points can maintain their specific crystal structure during the chemical vapor deposition (CVD) process and regulate the chirality of the grown SWNTs [1-2]. Instead of the previously used molecular clusters, here, we simply used salts containing W and Co, respectively, as precursors to prepare intermetallic  $W_6Co_7$  catalysts.  $(NH_4)_6W_7O_{24}\cdot 6H_2O$  and  $Co(CH_3COO)_2\cdot 4H_2O$  with rational molecular ratio were mixed, annealed and reduced at suitable conditions to prepare  $W_6Co_7$  intermetallic compounds. Using the resultant  $W_6Co_7$  nanoparticles as catalysts, we realized the synthesis of semiconducting SWNTs with the purity of  $\sim 97\%$ , in which (14,4) tubes are at the abundance of  $\sim 62\%$  under the optimized growth condition. It seems that this is a flexible pathway to grow semiconducting SWNTs with one enriched chirality.

[1] F. Yang, Y. Li *et al.* Nature. **510**, 522 (2014).

[2] F. Yang, Y. Li *et al.* ACS Nano. 10.1021/acsnano.6b06890 (2014)

Corresponding Author: Yan Li

Tel: +86-10-6275-6773, Fax: +86-10-6275-6773,

E-mail: yanli@pku.edu.cn

## Single-Walled Carbon Nanotube Growth from Bimetallic Catalyst by Molecular Dynamics Simulations

○Ryo Yoshikawa<sup>1,2</sup>, Hiroyuki Ukai<sup>1</sup>, Yukai Takagi<sup>1</sup>, Shohei Chiashi<sup>1</sup>, Shigeo Maruyama<sup>1,2</sup>

<sup>1</sup> Department of Mechanical Engineering, The University of Tokyo, Tokyo 113-8656, Japan

<sup>2</sup> National Institute of Advanced Industrial Science and Technology, Ibaraki 305-8564, Japan

It is reported that some of bimetallic catalyst can control the chirality of single-walled carbon nanotubes (SWCNTs) during growth and it is suggested that a specific chirality of SWCNTs fit the structure of the catalyst alloy [1].

In this study, we conducted molecular dynamics (MD) simulations to investigate SWCNT growth from two types of bimetallic catalyst, Cu-Co and W-Co. We constructed Tersoff-type potential for the triatomic system including two metal elements of the catalyst and carbon. Brenner-Tersoff potential was applied among carbon atoms forming covalent bonds and Lennard-Jones potential was applied between non-bonded carbon atoms. The catalyst metal nanoparticle was put at the center of  $10 \times 10 \times 10 \text{ nm}^3$  cell with periodic boundary condition along the three axes. The temperature of the catalyst metal nanoparticle was controlled with Nosé-Hoover thermostat. Carbon atoms were supplied into the cell so that the number of gas-phase carbon atoms ( $n$ ) was constant.

Figure 1 shows SWCNT caps formed on W-Co catalyst and Co monometallic catalyst. On W-Co catalyst, SWCNT caps were formed at high temperature (1500-2000 K), compared to Co monometallic catalyst (1350-1550 K). Since few W atoms were bonded to  $sp^2$  carbon atoms, W atoms were considered to support Co atoms rather than to catalyze the cap formation. The size of the caps was almost the same as that on Co monometallic catalysts.

Figure 2 shows a Cu-Co particle after reaction with carbon atoms. The Cu-Co catalyst was divided into Cu-rich and Co-rich parts, and amorphous carbon formed between two parts. Over 700 K, the catalysts were completely separated into the two parts.

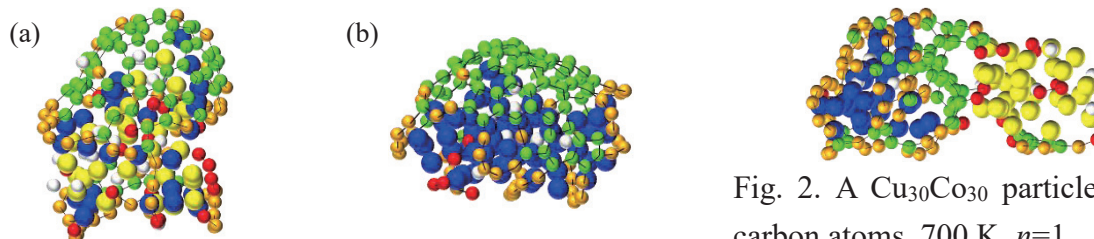


Fig. 1. (a) Cap formed on a  $W_{30}Co_{30}$  particle. 2000 K,  $n=1$ . The blue atoms are Co, the yellow atoms are W, and the others are C. (b) Cap on a  $Co_{60}$  particle. 1400 K,  $n=3$ .

Fig. 2. A  $Cu_{30}Co_{30}$  particle with carbon atoms, 700 K,  $n=1$ .

The blue atoms are Co, the yellow atoms are Cu, and the others are C.

[1] F. Yang, et al., *Nature*, **510** (2014) 522.

Corresponding Author: S. Maruyama

Tel: +81-3-5841-6421 Fax: +81-3-5800-6983 E-mail: maruyama@photon.t.u-tokyo.ac.jp

## Template Synthesis of $\pi$ -Conjugated Nanomaterials using Inner Space of Carbon Nanotubes

○Yasuhiro Kinno<sup>1</sup>, Haruka Omachi<sup>1,2</sup>, Ryo Kitaura<sup>1</sup>, and Hisanori Shinohara<sup>1,3</sup>

<sup>1</sup> Graduate School of Science, Nagoya University, Nagoya 464-8602, Japan.

<sup>2</sup> Research Center for Materials Science, Nagoya University

<sup>3</sup> Institute for Advanced Research, Nagoya University

It is possible to stably contain substances such as fullerene in the internal space of the CNTs, and it is expected to develop new physical properties [1,2]. Recently, we have demonstrated the synthesis of 1D diamondoid polymer by using the internal space of CNTs as a reaction platform [3]. Utilizing the selective cleavage of carbon–halogen bonds, biradical diamantine species reacted each other inside of the nanotubes. However, this synthetic methodology has been applicable to only  $sp^3$  carbon nanomaterials.

In this study, we developed the template synthesis of 1D  $\pi$ -conjugated nanomaterials into the CNTs under milder reaction conditions. Vapor-phase reaction of oligothiophenes substituted with bromine atoms at  $\alpha$  positions furnished the linear polythiophenes into CNTs (Figure 1a). Using experimental techniques, we revealed that the oligothiophenes moieties were linked each other inside CNTs. Our new synthetic method might provide various 1D aromatic polymer utilizing a huge number of dihalogenated aromatic compounds.

In the TEM observation, a 1D substance could be confirmed inside the CNTs (Figure 1b), and the peaks of polythiophene could be detected by the Raman spectra measurement (Figure 1c). These results suggest that 1D polythiophene was synthesized successfully.

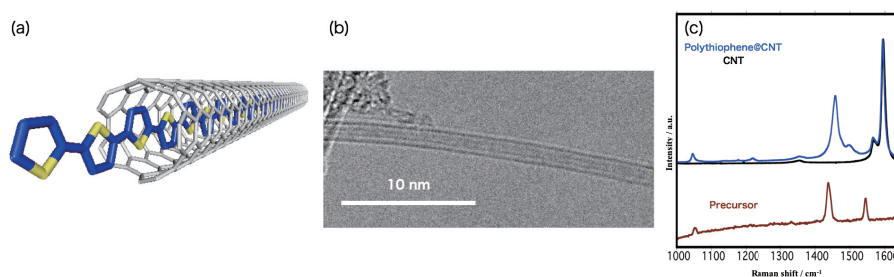


Fig.1 (a) Structural model of a polythiophene@CNTs ;(b) TEM image of 1D polythiophene@CNT ;(c) Raman spectra of 1D polythiophene@CNT

[1] J. Lee, *et al.*, *Nature*, **415**, 683 (2002).

[2] T. Takenobu, *et al.*, *Nat. Mater.*, **2**, 683 (2003).

[3] Y. Nakanishi, *et al.*, *Angew. Chem., Int. Ed.*, **54**, 10802 (2015).

Corresponding Author: Hisanori Shinohara

Tel: +81-52-789-2482, Fax: +81-52-747-6442,

E-mail: noris@nagoya-u.jp

## Electronic states of chalcogen encapsulated in single-walled carbon nanotubes studied by First-Principles DFT calculations(II)

○<sup>1</sup>Yutaka Sato, <sup>2</sup>Yousuke Kataoka, <sup>1</sup>Eita Yokokura and <sup>1,2,3</sup> and Hironori Ogata

<sup>1</sup> Graduate School of Science and Engineering, Hosei University, Koganei 184-8584, Japan

<sup>2</sup>Department of Faculty of Bioscience and Applied Chemistry, Hosei University, Koganei, 184-8584, Japan

<sup>3</sup>Research Center for Micro-Nano Technology, Hosei University, Koganei 184-0003, Japan

Single-walled carbon nanotubes(SWNTs) have a hollow space in the nanometer size that can be encapsulated various functional molecules. The confined molecular assemblies is expected to exhibit unique low-dimensional structures and solid state properties that can not be realized in the bulk states. Recently, syntheses of sulfur encapsulated SWNTs or selenium encapsulated DWNTs and unique one-dimensional conductive sulfur chain structure or double-helices selenium structure were reported. In this study, we report the effects of chirality and diameter of CNTs on the electronic states of the chalcogens encapsulated by SWNTs by using First-Principles DFT calculations.

In the First-Principles DFT calculations, we used a code package PWscf and GIPAW in Quantum ESPRESSO. We have calculated the electronic states of encapsulated chalcogen assemblies and their solid-state NMR parameters(chemical shift and electric field gradient (EFG) tensor) with several kinds of SWNTs. Fig.1. show the predicted static <sup>33</sup>S-NMR spectrum in S@(5,5)SWNT or S@(7,0)SWNT at 21.1 tesla. The detailed results will be presented.

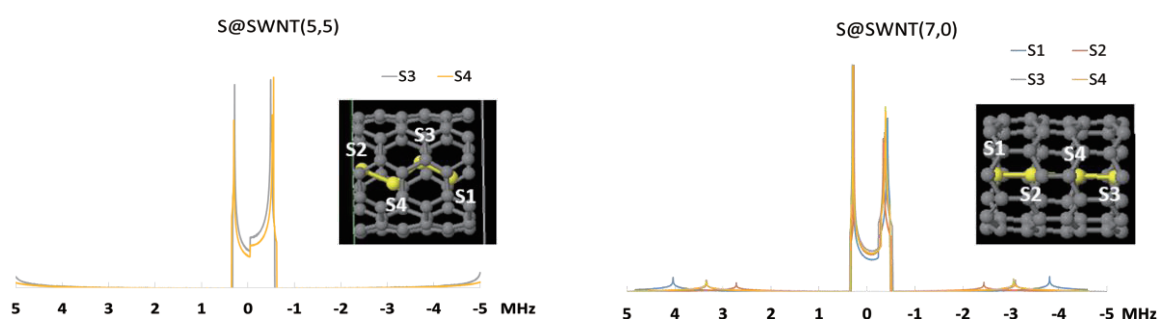


Fig.1. Predicted <sup>33</sup>S-NMR spectrum in S@(5,5)SWNT and S@(7,0)SWNT

### References

- [1] Toshihiko Fujimori et al. Nature Communications4(2013)2162.
- [2] Toshihiko Fujimori et al. ACS Nano vol.7 No.6(2013)5067-5613.
- [3]T.A wagler et al. Journal of Magnetic resonance 161 (2003) 191-197.
- [4]L.A. O'Dell, I.L. Moudrakovski. Journal of Magnetic Resonance 207 (2010) 345-347.
- [5] P. Giannozzi et al., J.Phys.:Condens.Matter, 21(2009)395502.

Corresponding Author: H. Ogata Tel: +81-42-387-6229, Fax: +81-42-387-6229, E-mail: hogata@hosei.ac.jp

## Effect of carbon nanohorns on lipopolysaccharide-induced RAW264.7 macrophage cells

○Maki Nakamura<sup>1</sup>, Kiyoko Kuroiwa<sup>1</sup>, Sumio Iijima<sup>2</sup>, Masako Yudasaka<sup>1,2</sup>

<sup>1</sup> National Institute of Advanced Industrial Science and Technology (AIST), 1-1-1 Higashi, Tsukuba 305-8565, Japan

<sup>2</sup> Meijo University, 1-501 Shiogamaguchi, Nagoya 468-8502, Japan

Carbon nanohorns (CNHs, Fig. 1) have great potential for delivery carriers of drug delivery systems. For the treatment of inflammatory diseases, drug delivery of anti-inflammatory steroid drugs to the diseased site is expected to minimize the systemic side effects. Determination of interleukin-6 (IL-6) produced from lipopolysaccharide (LPS)-induced RAW264.7 macrophage cells can be one of the effective way to evaluate an anti-inflammatory effect of steroid drug-loaded CNHs *in vitro*. In this report, we investigated the effect of CNHs on the production of IL-6 from LPS-induced RAW264.7 macrophage cells, and discussed the suitability of this evaluation method.

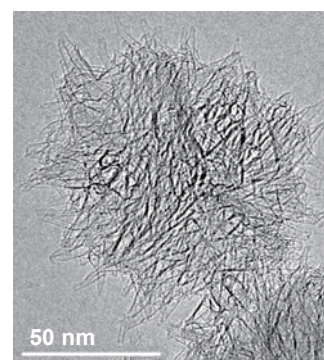


Fig. 1 A transmission electron microscopy image of CNHs

The oxidized CNHs (oxCNHs) were prepared by simultaneous light irradiation and heating of as-grown CNHs in an aqueous hydrogen peroxide solution [1]. The resultant oxCNHs were dispersed in ultrapure water and sterilized. This oxCNH solution was added to the RAW264.7 macrophage cells that were cultured at 37 °C in a 5% CO<sub>2</sub> atmosphere (final concentration of oxCNH: 0, 1.46, 7.3, 36.5 µg/mL). After incubation for 3 h, LPS was added to each well in order to induce inflammation (final concentration of LPS: 0, 0.1 µg/mL). After incubation for 44 h, culture medium was collected and centrifuged at 18,000 g for 50 min to remove oxCNHs. The amounts of IL-6 in the supernatants were quantified by enzyme-linked immunosorbent assay.

The amounts of IL-6 produced from the LPS (0.1 µg/mL)-induced RAW264.7 macrophage cells incubated with oxCNHs (1.46, 7.3, 36.5 µg/mL) were larger than those without oxCNHs (0 µg/mL). With increasing concentration on oxCNHs, the amounts of IL-6 increased. In contrast, without LPS treatment (0 µg/mL), IL-6 was seldom produced even in the presence of oxCNHs. These results indicated that LPS induced inflammation more strongly in the presence of oxCNHs. It was considered that LPS adsorbed on oxCNHs in culture medium and was incorporated into the cells with oxCNHs, resulting in the large quantity of LPS inside the cells. Therefore, the LPS, a commonly-used reagent to induce inflammatory response, is not suitable to be employed for the evaluation of an anti-inflammatory effect of steroid drug-loaded CNHs *in vitro*.

[1] M. Zhang, M. Yudasaka, K. Ajima, J. Miyawaki, S. Iijima, ACS Nano, 1, 265 (2007).

Corresponding Authors: M. Nakamura

Tel: +81-29-861-4604, Fax: +81-29-861-3005,

E-mail: ma-ki-nakamura@aist.go.jp (M.N.)

## A study of Preparation Conditions of Carbon Nanobrush

○Ryota Yuge<sup>1</sup>, Fumiya Nihey<sup>1</sup>, Kiyohiko Toyama<sup>1</sup>, and Masako Yudasaka<sup>2,3</sup>

<sup>1</sup>*IoT Devices Research Laboratories, NEC Corporation, Tsukuba 305-8501, Japan*

<sup>2</sup>*National Institute of Advanced Science and Technology (AIST), Tsukuba, 305-8565, Japan*

<sup>3</sup>*Graduate School of Science and Technology, Meijo University, Nagoya 468-8502, Japan*

Single-walled carbon nanohorns (SWCNHs) are generally in spherical aggregates [1], and they are attractive due to high dispersibility in solutions and large specific surface area. However, when used for energy devices such as electrical capacitors and fuel cells, high electrical conductivity has been also required. Recently, we have succeeded in preparing the radially-assembled and fibrously connecting SWCNHs, named as carbon nanobrushes [2]. They have high dispersibility in solutions, large specific surface areas, and high electrical conductivity [2]. Therefore, the carbon nanobrush is an excellent candidate for the electrode materials of various energy devices. Although the carbon nanobrushes are prepared by CO<sub>2</sub> laser ablation of iron-containing carbon target at room temperature, the yield is quite small and the major products are the spherical SWCNHs. In this study, we have changed the laser power and the rotation speed of target to increase the yield.

In the laser ablation, the CO<sub>2</sub> laser was operated at 2.5-4.5 kW in the continuous-wave mode. The iron-containing carbon target with cylindrical form (diameter 3 cm, length 10 cm) was used. The iron content in the target was 1 at. %. The target was rotated at 0.5-4 rpm for 30 sec during the laser ablation. The gas pressure in the growth chamber was sustained at 700-800 Torr by controlling the evacuation rate while the buffer gas of N<sub>2</sub> was kept at the flow rate of 10 Lmin<sup>-1</sup>.

SEM and STEM observations showed that the samples obtained at 2.5-4.5 kW of the laser power and 2 rpm of target rotation speed were mainly spherical SWCNHs. The preparation of carbon nanobrushes did not strongly depend on the laser power. When the rotation speed of target was changed, a variety of carbon materials was obtained. At low rotation speed, the graphitic particles and/or carbon nanotubes were dominantly formed. On the other hand, at high rotation speed, spherical SWCNHs were formed. Thus, we found that carbon nanobrushes were obtained at the intermediate rotation speed of the target. The details will be discussed in the presentation.

[1] S. Iijima *et al.* Chem. Phys. Lett. **309**, 165 (1999).

[2] R. Yuge *et al.* Ad. Mater. **28**, 7174 (2016).

Corresponding Author: R. Yuge

Tel: +81-29-850-1566, Fax: +81-29-856-6137

E-mail: [r-yuge@bk.jp.nec.com](mailto:r-yuge@bk.jp.nec.com)

## Analysis of Initial Formation Process of Graphene on SiC(0001) Surfaces Based on the First-Principles Molecular Dynamics

○Fumihiko Imoto <sup>1</sup>, Jun-Ichi Iwata <sup>1</sup>, Mauro Boero <sup>2</sup>, Atsushi Oshiyama<sup>1</sup>

<sup>1</sup> *Department of Applied Physics, The University of Tokyo, Tokyo 113-8656, Japan*

<sup>2</sup> *Institut de Physique et Chimie des Matériaux de Strasbourg UMR 7504, and University of Strasbourg and CNRS, F-67034 Strasbourg, France*

Thermal decomposition of SiC (0001) surfaces is a promising way to form graphene because it provides large-area graphene supported on regular SiC substrates. It is experimentally known that Si atoms are desorbed selectively from the SiC, leading to the growth of graphene layers on a carbon-rich  $6\sqrt{3}\times 6\sqrt{3}$  buffer layer[1]. Before the thermal decomposition, hydrogen etching of the SiC is performed and ordered nanofacets appear on the surface[2]. Several experiments[1,3] have revealed that graphene layers grow from such nanofacets toward terraces. This nanofacet is theoretically identified as a bunched structure of single bilayer atomic steps[4].

The aim of our work is to unravel the microscopic mechanisms of graphene formation from the step edge, which constitutes the nanofacet. In our previous calculations based on the density functional theory, we found that the energy barrier for the desorption of an Si atom at the step edge is lower than that of a C atom by 0.75 eV, which indicates the selective desorption of Si atoms[5]. However, this result does not provide sufficient information on free energy barriers, which should be overcome at finite temperature ( $\sim 1500$  K) during the heating.

In this talk, we report Car-Parrinello molecular dynamics calculations that clarify atom-scale mechanisms of the initial formation process of graphene from 4H-SiC (0001)  $[11\bar{2}0]$  step edge. Free energy profiles have been calculated by metadynamics, in which Si desorption is forced to occur by filling up the free energy surface. The stacking of Si-C bilayers along the  $[0001]$  direction in 4H-SiC is  $\dots ABCB\dots$ , which results in two possible step edge configurations, the cubic upper terrace (A as the upper terrace and B as the lower terrace) and the hexagonal upper terrace (B as the upper terrace and C as the lower terrace). Our calculation has been performed for these two possible step edges. We find that an Si is desorbed toward the lower terrace with the rate-determining barrier of 1.50 eV for the cubic upper terrace and 1.10 eV for the hexagonal upper terrace. The obtained reaction pathways are in good agreement with our previous results and we further study subsequent Si desorption to clarify carbon bond formation process near the step edge.

[1] J. B. Hannon *et al.* Phys. Rev. B **77**, 241404(R) (2008).

[2] T. Kimoto *et al.* Appl. Phys. Lett. **66**, 3645 (1995).

[3] W. Norimatsu *et al.* Physica E **42**, 691 (2010).

[4] K. Sawada *et al.* Appl. Phys. Lett. **104**, 051605 (2014).

[5] F. Imoto *et al.* [arXiv:1611.04404] (2016).

Corresponding Author: F. Imoto

Tel: +81-80-3157-8122

E-mail: fimoto@comas.t.u-tokyo.ac.jp

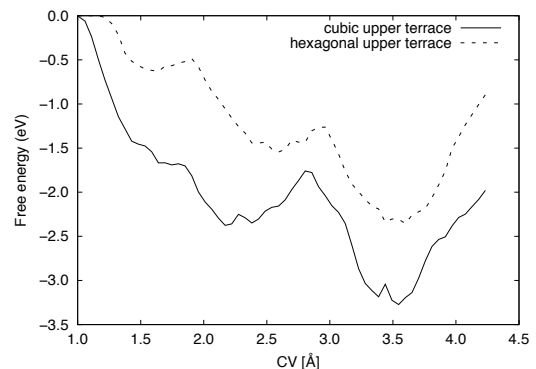


Fig.1: Free energy profiles of Si desorption

## Growth of Single-Crystal Single-Layer and Bi-Layer Graphene Using Alcohol Catalytic CVD

○Masaki Sota<sup>1</sup>, Kotaro Kashiwa<sup>1</sup>, Naomasa Ueda<sup>1</sup>, Keigo Otsuka<sup>1</sup>,  
Taiki Inoue<sup>1</sup>, Rong Xiang<sup>1</sup>, Shohei Chiashi<sup>1</sup>, Shigeo Maruyama<sup>1,2</sup>

<sup>1</sup> *Department of Mechanical Engineering, The University of Tokyo, Tokyo 113-8656, Japan*

<sup>2</sup> *Energy NanoEngineering Lab., National Institute of Advanced Industrial Science and Technology (AIST), Ibaraki 305-8564, Japan*

Graphene, an  $sp^2$ -bonded single-layer honeycomb lattices, is a promising material due to its extraordinary mechanical, thermal, and electrical properties. However, single-layer graphene (SLG) is conductor and inapplicable to semiconductor applications. Several groups reported that a bandgap up to 250 meV can be induced by an external electric field in AB-stacked bi-layer graphene (BLG) [1]. Therefore, the synthesis of BLG is essential for electronic applications of graphene. Chemical vapor deposition (CVD) is an effective method for the synthesis of large-scale graphene. Since grain boundaries in poly-crystal graphene degrade its superior properties, many efforts have been focused on enlarging the size of single-crystal graphene. As a result, single-crystal SLG of large size has been synthesized using CVD, but there is a problem that the size of the single-crystal BLG is still not large.

In this research, we synthesized single-crystal SLG and BLG using the alcohol catalytic CVD (ACCVD) [2]. We used a copper foil as the catalyst and oxidized and folded it into a pocket before synthesis. CVD was performed at 1065 °C with various pressures of Ar/H<sub>2</sub> and ethanol. We found that single-crystal BLG can be grown by low pressure of the CVD condition. Figure 1 is a dark field (DF) optical image of graphene on copper foil, which shows the crystal orientation of single-crystal BLG matches that of SLG. Figure 2 shows large-size flakes of single-crystal BLG and many of them have the same orientation. This indicates BLG are epitaxially grown on SLG in the ACCVD.

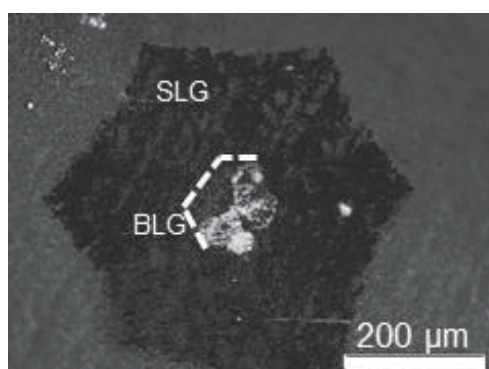


Fig. 1 DF optical image of SLG and BLG.

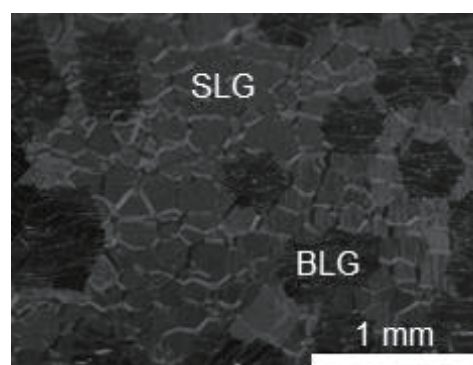


Fig. 2 DF optical image of large flakes of single-crystal BLG.

[1] Y. Zhang *et al.* Nature, **459**, 820 (2009).

[2] X. Chen *et al.* Carbon, **107**, 852 (2016).

Corresponding Author: S. Maruyama

Tel: +81-03-5841-6421, Fax: +81-03-5841-6421,

E-mail: maruyama@photon.t.u-tokyo.ac.jp

## Highly Oriented CuInS<sub>2</sub> Thin-Films on Graphene Electrodes for Solar Cells Applications

○Ryousuke Ishikawa, Tomoya Oya, Tonan Yamada, Takahiro Nomoto, and Nozomu Tsuboi  
*Faculty of Engineering, Niigata University, Niigata 950-2181, Japan*

Thin-film solar cells based on multinary compound semiconductors represented by Cu(In,Ga)Se<sub>2</sub> (CIGS) have demonstrated a high conversion efficiency over 20%. Other multinary compound semiconductors such as CuInS<sub>2</sub> (CIS), Cu<sub>2</sub>SnS<sub>3</sub> (CTS), and Cu<sub>2</sub>ZnSn(S,Se) have been also considered to be potential photovoltaic materials for next-generation solar cells with high efficiency. Graphene, a single atomic layer of sp<sup>2</sup> graphitic carbon, is a promising material for transparent electrodes due to its high electrical conductivity and optical transparency over a wide range of wavelength [1]. We attempted using the high-crystalline graphene layers on several types of substrates to grow highly oriented CuInS<sub>2</sub> films.

High quality graphene was fabricated by chemical vapor deposition (CVD) growth technique using Cu foil for monolayer (1L-graphene) or Ni thin film for multilayer graphene (ML-graphene) as catalyst substrates. After CVD growth, deposited graphene was then transferred by polymethyl methacrylate (PMMA) assisted process onto glass substrates. The CuInS<sub>2</sub> films were deposited by reactive-sputtering with facing targets system on obtained graphene or Mo.

The peak intensity and intensity ratio of (112) in CuInS<sub>2</sub> films on graphene were greater than that on Mo as shown in Fig. 1. Especially, the SLG/1-L graphene sample indicated a highly orientation. Because the CuInS<sub>2</sub> (112) plane has hexagonal symmetry, CuInS<sub>2</sub> thin-film might cause quasi-superlattice matching with highly-oriented graphene which consists of perfect honeycomb structure. The cross-sectional images revealed that larger and columnar grains were grown in the CuInS<sub>2</sub> films on graphene as shown in Fig. 2 (a) compared to the films on Mo as shown in Fig. 2 (b). The top-surface view of the CuInS<sub>2</sub> films on graphene exhibited the dense microstructure as shown in Fig. 2 (c). On the other hand, the CuInS<sub>2</sub> films on Mo had many boundaries and voids as shown in Fig. 2 (d). Moreover, the electrical junction of graphene/CIS interface exhibited perfect ohmic characteristics comparable to Mo/CIS interface.

Here we demonstrated the potential of graphene as transparent electrode in the compound semiconductors based thin-film solar cells toward to multi-junctions solar cells with ultra-high efficiency.

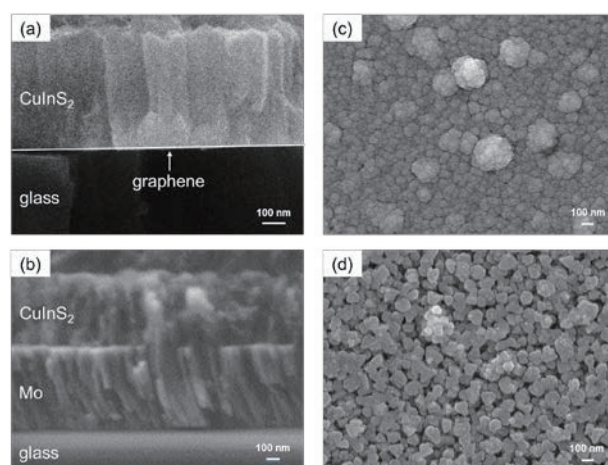
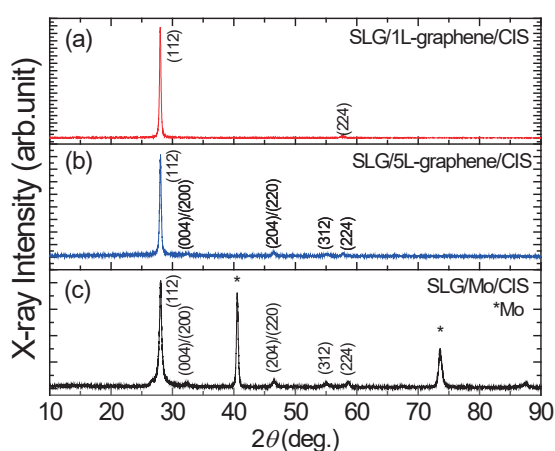


Fig. 1 The XRD patterns of CuInS<sub>2</sub> films      Fig. 2 The cross-sectional and top-surface SEM images of CuInS<sub>2</sub> films

[1] R. Ishikawa et al. *Jpn. J. Appl. Phys.*, **51** 11PF01 (2012).

Corresponding Author: R. Ishikawa, Tel & Fax: +81-25-262-6736, E-mail: ishikawa@eng.niigata-u.ac.jp

## Controlled fabrication of graphene liquid cells

○Yoshimasa Michiya,<sup>1</sup> Tomohiro Yasunishi,<sup>2</sup> Yutaka Ohno,<sup>2</sup> Hisanori Shinohara,<sup>1</sup>  
and Ryo Kitaura<sup>1</sup>

<sup>1</sup> *Department of Chemistry, Nagoya University, Nagoya 464-8602, Japan.*

<sup>2</sup> *Graduate School of Engineering, Nagoya University, Nagoya, 464-8603, Japan*

Transmission electron microscopy (TEM) is a very powerful tool to visualize structure of materials at the nanoscale. If TEM can be applied to observations of liquid, there is a possibility that a wide range of phenomena including dissolution, precipitation and various liquid phase reactions can be directly visualized at the nanoscale. In conventional TEM observations of liquid, liquid is encapsulated in a liquid cell with thick membranes (typically, 50 nm SiN) to prevent the liquid from vaporization under the high vacuum. In this case, scattering of electrons arising from the membranes greatly limits resolution and contrast of TEM images. In order to solve this problem, we have been focusing on graphene liquid cells (Figure.1), where graphene completely prevents liquid from vaporization with minimal degradation of resolution and contrast. In this work, in order to develop controllable fabrication method of the graphene cells, we have applied a semiconductor microfabrication technique including electron beam lithography (EBL).

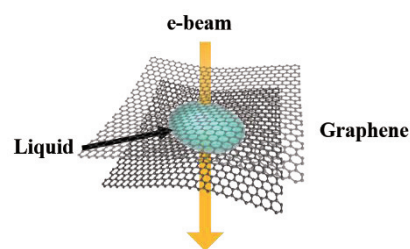


Figure.1 Schematic view of a graphene liquid cell.

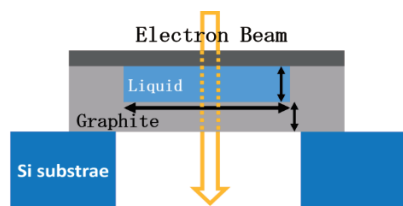


Figure.2 Cross-sectional view of a designed graphene liquid cell. It is possible to control the part indicated by the black arrow.

Figure.2 shows a schematic cross-sectional view of the graphene liquid cell; in this liquid cell, graphite is used as bottom and side walls of the cell. To make the graphite vessel structure, graphite with thickness of about 100 nm was etched with reactive ion etching on a hole penetrating through a Si substrate. The width, depth and shape can be microly controlled with accuracy of about 10 to 100 nm. After putting Liquid (water) in the vessel, graphene is transferred on the structure. In the presentation, in addition to details of sample fabrication, TEM observations of the graphene liquid cells will be shown.

Corresponding Author: R.Kitaura and H.Shinohara Tel: +81-52-789-2477, Fax: +81-52-747-6442

E-mail: r.kitaura@nagoya-u.jp and noris@nagoya-u.jp

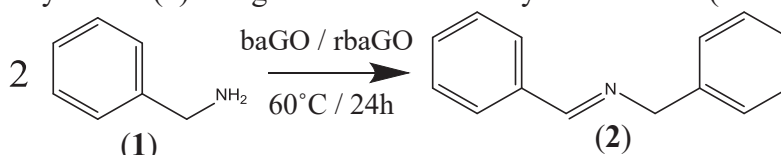
## Factors for reactivity of GO regarding oxidative amine coupling reaction

○Takuya Isaka<sup>1</sup>, Kentaro Tajima<sup>1</sup>, Tomoki Yamashina<sup>1</sup>, Kazuyuki Takai<sup>1,2</sup>

<sup>1</sup>Graduate School of Science and Engineering, Hosei University, Tokyo 184-8584, Japan

<sup>2</sup>Department of Chemical Science and Technology, Hosei University, Tokyo 184-8584, Japan

Investigating Graphene Oxide (GO) properties before / after the catalytic reaction is a promising strategy for clarification of the mechanism for GO catalytic activity. Additionally, it is known that removing oxidative debris on GO by base-treatment is important factor to get the higher yield for the following catalytic reaction [1]. We have reported that base-treated GO (baGO) used as catalyst once gives the higher yield than that in the 1st cycle reaction in oxidative amine coupling reaction [2]. In this study, the principle for reactivity is investigated by conducting the oxidative amine coupling reaction of benzylamine (1) to *N*-benzylidenebenzylamine (2) using baGO and thermally reduced one (rbaGO) (Scheme 1).



Scheme 1 Oxidative amine coupling reaction of benzylamine to *N*-benzylidenebenzylamine

baGO-Pristine was obtained by washing GO, synthesized by Hummers method, with NaOH. rbaGO was prepared by reducing baGO at 450°C. After Scheme 1, the reaction media filtered for removing the catalyst was characterized by GC-MS. After the 1st cycle reaction, the recovered catalyst was used as that for the 2nd cycle (baGO-1st cycle, rbaGO-1st cycle). The chemical structure of each catalyst after the reaction was evaluated by XPS (Al K $\alpha$ ), where it was washed with ethanol after the reaction.

The GC-MS yields of (2) for each catalyst is summarized in Table 1. The atomic ratio O/C of catalyst much decreases after the reduction or 1st cycle reaction and rbaGO shows poor yield, suggesting roles of baGO / rbaGO not as catalyst but as oxidant (Fig.1). However, baGO-1st cycle exhibits the highest yield in spite of C1s spectrum and O/C similar to that of rbaGO and rbaGO-1st cycle, which also indicates no more reduction for rbaGO in the 1st cycle reaction. Taking these results and appearance of nitrogen content after the 1st cycle reaction into consideration, a different mechanism in the 2nd cycle reaction is suggested, where nitrogen incorporated into rbaGO / baGO in the 1st cycle reaction plays an important role for the reactivity.

Table 1 Yield for (2) using each baGO

Catalyst sample	Yield (%)
baGO-Pristine	13
baGO-1st cycle	39
rbaGO	6
rbaGO-1st cycle	6

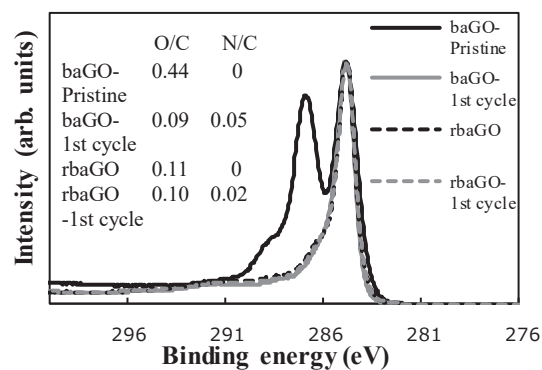


Fig.1 XPS C1s peak for each baGO after the reaction

[1]C. Su, M. Acik, K. Takai *et al.* Nat. Commun., 3, 1298 (2012) [2]T. Isaka *et al.* FNTG51 conference (2016)

Corresponding Author: Kazuyuki Takai

Tel: +81-42-387-6138, Fax: +81-42-387-7002, E-mail: takai@hosei.ac.jp

## Highly conductive and transparent large-area bilayer graphene realized by MoCl<sub>5</sub> intercalation

○Hiroki Kinoshita,<sup>1</sup> Kenji Kawahara,<sup>2</sup> Yuri Terao,<sup>1</sup> Il Jeon,<sup>3</sup> Mina Maruyama,<sup>4</sup>  
Rika Matsumoto,<sup>5</sup> Susumu Okada,<sup>4</sup> Yutaka Matsuo,<sup>3</sup> Hiroki Ago<sup>1,2,6,\*</sup>

<sup>1</sup> Interdisciplinary Graduate School of Engineering Sciences, Kyushu University, Fukuoka 816-8580, Japan

<sup>2</sup> Global Innovation Center (GIC), Kyushu University, Fukuoka 816-8580, Japan

<sup>3</sup> School of Engineering, The University of Tokyo, Tokyo 113-8656, Japan

<sup>4</sup> Graduate School of Pure and Applied Sciences, University of Tsukuba, Tsukuba 305-8577, Japan

<sup>5</sup> Faculty of Engineering, Tokyo Polytechnic University, Kanagawa 243-0297, Japan

<sup>6</sup> PRESTO, Japan Science and Technology Agency, Saitama 332-0012, Japan

Being different from monolayer graphene, bilayer graphene (BLG) possesses a unique two-dimensional (2D) nanospace sandwiched by the two graphene sheets. Intercalation of molecules/ions into this 2D nanospace provides a new avenue for realizing novel functionalities without deteriorating the graphene  $\pi$ -network. P-type doping of few-layer graphene was demonstrated by intercalating FeCl<sub>3</sub>, reducing the sheet resistance [1,2]. However, the intercalation has been mostly applied to small, exfoliated graphene flakes, thus limiting its practical applications. Also, most of the previous literature employed FeCl<sub>3</sub> as an intercalant [1-3]. Here, we demonstrate the intercalation of a new metal chloride, MoCl<sub>5</sub>, into large-area, uniform BLG sheets which are grown by CVD.

A uniform BLG sheet grown by CVD on a Cu-Ni alloy catalyst [4] was sealed with MoCl<sub>5</sub> powder in a glass tube, followed by heating in vacuum. The Raman G-band of the BLG upshifted from 1585 cm<sup>-1</sup> to 1616 cm<sup>-1</sup> after the intercalation, indicating significant p-type doping of the BLG. We found that the MoCl<sub>5</sub> intercalation proceeds at lower temperature and more uniformly, as compared with FeCl<sub>3</sub>. Interestingly, the intercalation of MoCl<sub>5</sub> was found to strongly depend on the stacking order of the BLG, as shown in Fig. 1a,b. Figure 1a shows a Raman mapping image ( $I_{2D}/I_G$  ratio) of the as-grown BLG, indicating the coexistence of AB- and twist-stacked areas. After the exposure to MoCl<sub>5</sub>, the twisted area showed a fully intercalated state, while the AB area showed only surface doping without intercalation (Fig. 1b). Figure 1c compares the sheet resistance of BLG sheets. Here, AB- and twist-rich BLG sheets were selectively synthesized by controlling the CVD condition. The twist-rich BLG showed much lower sheet resistance, 80  $\Omega/\square$  (~95% transmittance), which is the lowest value reported so far for BLG. Moreover, the intercalated state was stable in air for more than 30 days. Our work offers a new route to functionalize graphene which can be applied to transparent electrodes in various flexible devices.

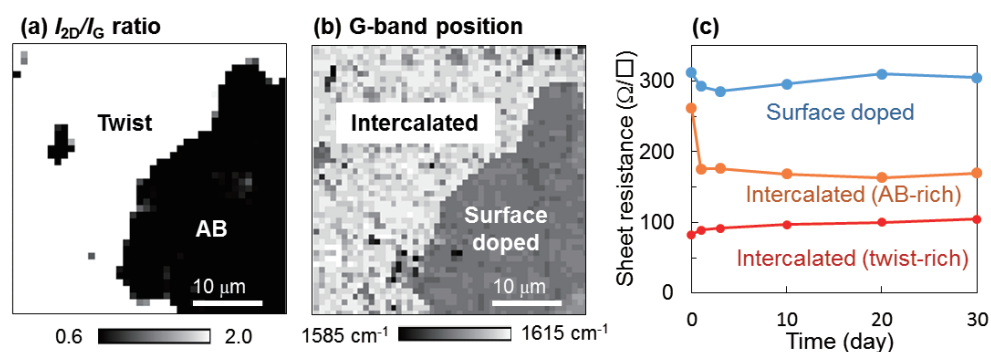


**Fig. 1** Raman mapping of  $I_{2D}/I_G$  ratio of pristine BLG (a) and G-band position after intercalation (b). (c) Sheet resistance of different BLG samples (in air).

[1] I. Khrapach *et al.*, *Adv. Mater.*, **24**, 2844 (2012). [2] D. Zhan *et al.*, *Small*, **11**, 1177 (2015). [3] N. Kim *et al.*, *Nano Lett.*, **11**, 860 (2012). [4] Y. Takesaki *et al.*, *Chem. Mater.*, **28**, 4583 (2016).

Corresponding Author: H. Ago (Tel&Fax: +81-92-583-8852, E-mail: h-ago@gic.kyushu-u.ac.jp)

## Energetics of edge oxidization of graphene nanoribbons with clean edges

○ Airi Yasuma, Ayaka Yamanaka, and Susumu Okada

*Graduate School of Pure and Applied Sciences, University of Tsukuba, 1-1-1 Tennodai,  
Tsukuba, Ibaraki 305-8571, Japan*

Graphene has been keeping premier position in nanoscale science and technology in this decade, because of their unique geometric and electronic structure, allowing them an emerging material for future functional devices in the near future. To utilize graphene for devices, it is mandatory to control their geometries and elucidate their stability against the formation of hybrid structures with foreign materials. Edge stability against chemical attachment is one of important factors to determine the graphene geometries. In this work, we aim to elucidate the energetics of GNRs by the edge oxidization in terms of their detailed edge geometries, using the density functional theory with generalized gradient approximation. As for the structural model, we consider the GNR with clean edges and five edge angles from armchair ( $0^\circ$ ) to zigzag ( $30^\circ$ ) (Fig.1).

Figure 2 shows the adsorption energy of O atoms to the edges of GNRs with edge angles from  $0^\circ$  to  $30^\circ$ . The adsorption energy strongly depends not only on the edge angle but also on the edge atomic site in each edge shape. Our calculations demonstrate that the edges with zigzag shape are preferentially oxidized compared with the edge with armchair portion. Furthermore, O atoms attached to the step edge lead to the substantial structural deformation around the edges.

Corresponding Author: A. Yasuma

Tel: +81-29-853-5921, Fax: +81-29-853-5924

E-mail: [ayasuma@comas.frsc.tsukuba.ac.jp](mailto:ayasuma@comas.frsc.tsukuba.ac.jp)

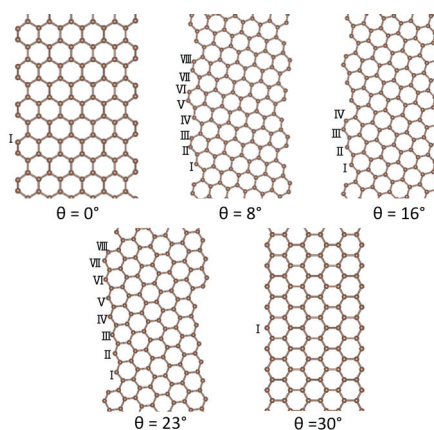


Fig.1 Optimized structures of GNRs with clean edges.

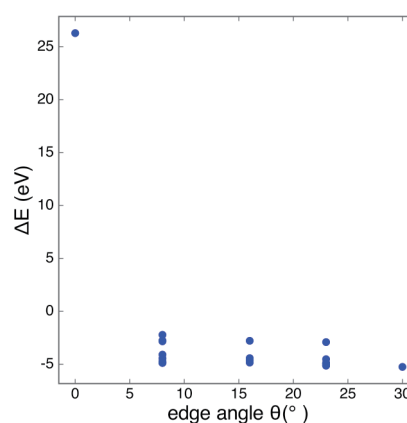


Fig.2 Adsorption energy of oxygen to GNRs

## Band unfolding study on Fermi-level-velocity reduction induced by Dirac cone interaction in twisted bilayer graphene

○Hirofumi Nishi, Yu-ichiro Matsushita, Atsushi Oshiyama

*Department of Applied Physics, The University of Tokyo, Tokyo 113-8656, Japan*

Graphene shows the linear dispersion (Dirac cone) which causes great notable properties such as high mobility, Klein tunneling, and the anomalous quantum Hall effect. It is reported that when two sheets of graphene are stacked, Dirac cones are modified depending on the way of the stacking. In particular, in twisted bilayer graphene (tBLG), the Fermi velocity drastically reduces in tiny twisted angles. The origin of this mysterious modification of the Fermi velocity in tBLG has been discussed: The continuum theory shows that the interactions between Dirac cones located at different K points causes this reduction [1]. However, why this long-range modulation of atomistic structure in real space causes the cone-cone interactions in reciprocal space is unclear yet.

In this study, we have adopted the band-unfolding method with the tight-binding model, by which we can unfold the electronic band structure calculated in the supercell Brillouin zone (BZ) of tBLG to that in primitive cell BZ of monolayer. Using this technique, we can easily visualize how the Dirac cones of the monolayer graphene are modulated in tBLG, and clarify the relation between atomistic structure modulation in real space and Dirac-cone modulation in reciprocal space. As a result, we find the band-gap opening at particular points in the reciprocal space, that elucidates the drastic reduction of the Fermi-level velocity with the tiny twisted angles in tBLGs. Moreover, it is found that the band-gap openings correspond to low energy van Hove singularity in the density of states as shown in FIG. We find that moiré pattern caused by the twist of the two graphene layers generates interactions among Dirac cones, otherwise absent, and the resultant cone-cone interactions peculiar to each point in the reciprocal space causes the energy gap and thus reduced the Fermi-level velocity [2].

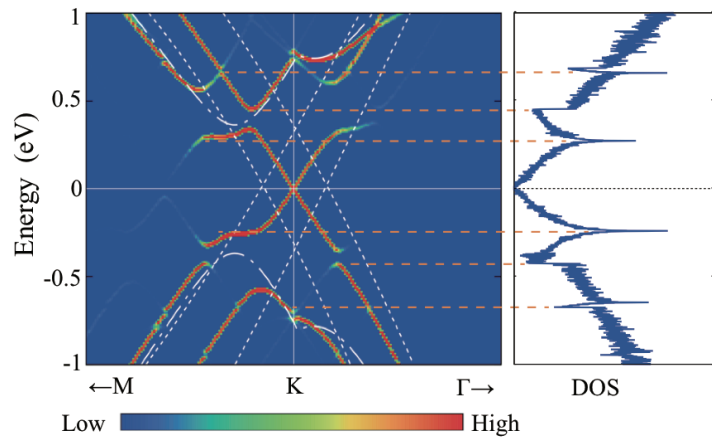


FIG. Contour plots of the unfolded bands and total density of states of tBLGs near the Fermi energy with twisted angle  $\theta=5.09^\circ$ .

[1] R. Bistritzer and A. H. MacDonald, Proc. Natl. Acad. Sci. USA 108, 12233 (2011).

[2] H. Nishi, Y. Matsushita, and A. Oshiyama arXiv:1609.05297 (2016).

Corresponding Author: H. Nishi

Tel: +81-3-5841-6812,

E-mail: nishi@comas.t.u-tokyo.ac.jp

## Energetics of Edge Formation Processes of Graphene

○Ayaka Yamanaka, Susumu Okada

*Graduate School of Pure and Applied Sciences, University of Tsukuba, Tennodai, Tsukuba  
305-8577, Japan*

Ever since the synthesis of graphene by mechanical exfoliation technique, graphene has attracted a great deal of attention in both pure and applied sciences due to its unique structural and electronic properties. For the application of graphene, it is very important to precisely control their geometric and electronic structure. Theoretical works demonstrated that near-zigzag edges are less stable than near-armchair edges because of the large number of states at the Fermi level in nanoribbons with near-zigzag edges. However, on the other hand, graphene with zigzag edges have been occasionally observed in TEM and STM experiments. The fact implies that the edge shape of graphene flakes strongly depends on their formation process. In this study, we aim to investigate the energetics of graphene edges with atomic desorption to clarify the formation process of graphene edges by using the density functional theory.

We consider the several edge structure of graphene generated by atomic desorption from the pristine armchair and zigzag edges as shown in Fig. 1. Figure 2 shows the stability of graphene edges with atomic desorption of C atoms from pristine graphene edges. We consider the methane and ethane as the references of the desorbed C atoms. As shown in Fig. 2, the A-2 structure is remarkably stable than the perfect armchair edges. This defective edge possesses zigzag portions in accordance to the diatomic desorption. This result indicates that the zigzag edges are preferentially generated under the certain condition.

Corresponding Author: A. Yamanaka  
Tel: +81-29-853-5600 (ext. 8233),  
Fax: +81-29-853-5924,  
E-mail:  
ayamanaka@comas.frsc.tsukuba.ac.jp

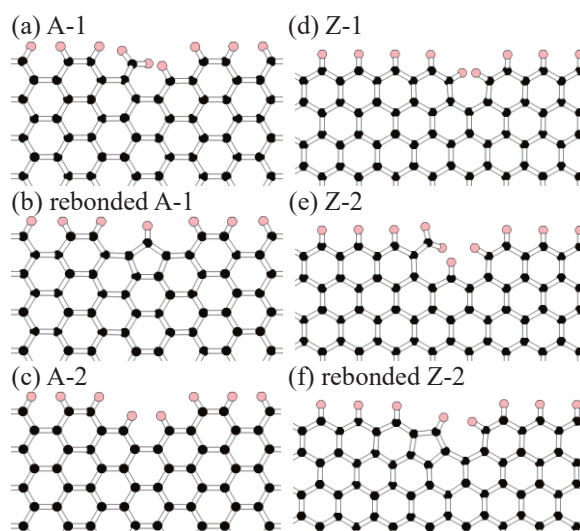


Fig.1 Optimized structures of nanoribbons with atomic desorption. Black and pink disks denote the carbon and hydrogen atoms, respectively.

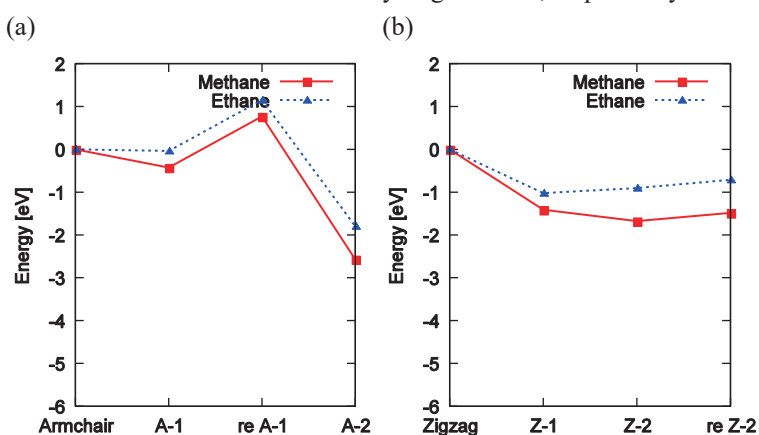


Fig.2 Desorption energies for (a) armchair and (b) zigzag edges. Energies are measured from the total energy of the pristine armchair and zigzag edges. Red and blue lines denote the energies calculated by using the chemical potentials of methane and ethane, respectively.

## Electronic structure of edge functionalized graphene under an external electric field

○Yanlin Gao, Susumu Okada

*Graduate School of Pure and Applied Sciences, University of Tsukuba,  
Tsukuba, 305-8571, Japan*

Graphene has attracted a great deal of attention in the fields of nanoscience and nanotechnology due to its peculiar physical property and extensive application prospects. Graphene has atom thickness, high electrical conductivity, and remarkable chemical stability, which allow it to be a possible candidate for a field emission source in field emission devices. In the ambient condition, edges of graphene are usually terminated by functional groups, depending on the environment. In this work, we aim to elucidate the correlation between the work function and critical electric field of the field emission from the zigzag edges of graphene, which is terminated by functional groups (ketone, aldehyde, hydrogen or carboxyl group), using the density functional theory combined with the effective screening medium method.

Figure 1(a) shows the structure model for simulating the field emission from the edges of graphene terminated by functional groups. The edge is simulated by the graphene nanoribbon with zigzag edges which are terminated by H and functional groups. The ribbons are located in front of the planar electrode with 6 Å vacuum spacing. Our calculations show that functional groups affect the critical electric field resulting in the field emission at which the electrostatic potential at the electrode crosses the Fermi level [Fig. 1(b)]. For the edges functionalized by H, ketone, aldehyde, and carboxyl groups, the critical electric field leading to the electron emission is proportional to their work function. In contrast, the edge terminated by the hydroxyl group has a larger critical electric field in spite of its small work function. The large critical electric field for the hydroxylated edge is ascribed to the spilled electron outside the edges arising from the nearly free electron states: The electron distribution outside the edge causes the potential barriers at this region preventing the electron emission from the edge.

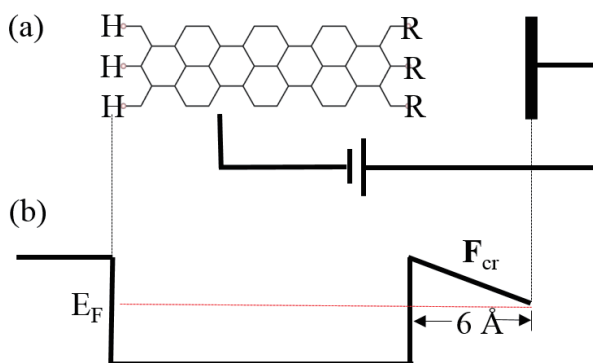


Fig.1(a) A structural model and (b) schematic diagram of the electrostatic potential for functionalized graphene nanoribbon under the electric field.

Corresponding Author: Y. Gao

TEL: +81-29-853-5921, FAX: +81-29-853-5924

E-mail: ylgao@comas.frsc.tsukuba.ac.jp

## Brillouin zone topology and band structure of four-dimensional diamond

Yuichi Kato, Masanori Yamanaka

*Department of Physics, College of Science and Technology, Nihon University, Tokyo  
101-8308, Japan*

We study the diamond lattice in 4d [1] which is a descendant of the 3d diamond lattice, or 2d hexagonal lattice. We determine the first Brillouin zone explicitly as a 4d polytope and draw the band structure of the tight-binding model on a normal piece of 2d paper. By the polyhedral decomposition, we find the zone boundary of the first Brillouin zone in 4d to be the omnitruncated 5-cell, otherwise known as the great prismatic decachoron, which comprises 10 truncated octahedra glued to 20 hexagonal prisms. The irreducible zone is determined to be a 4d polytope with the heptahedron as the base polyhedron and the origin in the momentum space as the apex. We found the 2d isotropic Dirac cone at the W-point and the 2d anisotropic Dirac cone on the line node to the D-point where the coefficients of two components differ. Gapless line nodes are characterized by a linear dispersion relation and we have a total of 60 line nodes inside the hexagonal prisms in the first Brillouin zone.

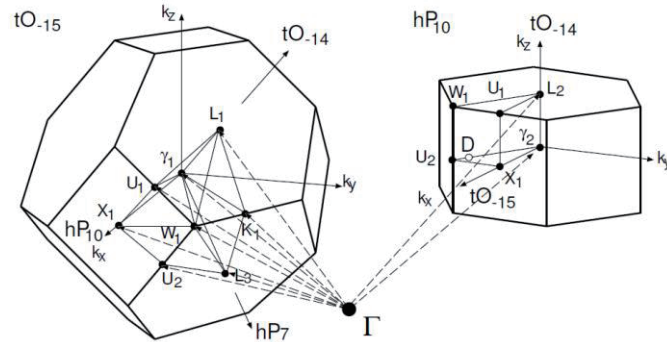


Fig.1 Irreducible zone and the  $k$ -points defined on the zone boundary. We obtained these polyhedra by projecting the 4d zone boundary polyhedra onto the perpendicular bisecting 3d space. The axes ( $k_x$ ,  $k_y$ ,  $k_z$ ) are the local coordinate systems on the projected 3d spaces. The  $\Gamma$ -point is the origin of the 4d momentum space and is outside of the projected 3d spaces. The dotted lines between the  $\Gamma$ -point and the  $k$ -points on these polyhedra stretch to the 4th axes and are also outside of these projected 3d spaces. Then, the irreducible zone is a 4d polytope with the heptahedron as the base polyhedron and the  $\Gamma$ -point as the apex. There is a Dirac line node on the plane  $\gamma_2 U_2 W_1 L_2$  from point  $W_1$  to  $W_1'$  and  $D$  where  $D$  is a point that internally divides points  $U_2$  and  $\gamma_2$  in a ratio of 1:5.

[1] Y. Kato and M. Yamanaka, accepted for publication in J. Phys. Soc. Japan.

Corresponding Author: M. Yamanaka, Tel: +81-3-3259-0921, Fax: +81-3-3259-0921,

E-mail: yamanaka@phys.cst.nihon-u.ac.jp

## Transport property of bilayer graphene with monovacancy

○Ken Kishimoto and Susumu Okada

*Graduate school of Pure and Applied Sciences, University of Tsukuba, Tsukuba 305-8571, Japan*

Graphene has unique geometric and electronic structures, allowing it an emerging material for various functional devices in the near future. On the other hand, its electronic structure is fragile against the formation of hybrid structures with foreign materials, such as molecules, insulating substrate, metal electrode, and other atomic layer materials. Furthermore, atomic and topological defects also modulate the electronic structure of graphene near the Fermi level. In the hybrid structure, interaction between constituents cooperatively and competitively affects the electronic structures of resultant hybrids. Indeed, the bilayer graphene, in which one of two layers possesses defects, possesses finite energy gap in  $\pi$  states instead of a pair of linear dispersion bands [1] owing to the defect and interlayer interaction. The result indicates that the transport properties of graphene hybrids may also exhibit unusual features, which are not the simple sum of that of each constituent. In this work, we aim to investigate the transport property of the bilayer graphene, one of which layers possesses monovacancies using the non equilibrium Green's function method within the framework of the density functional theory.

Our calculations show that the I-V characteristics of bilayer graphene with monovacancy (MV) exhibit unusual feature. Although the bilayer graphene contains pristine graphene layer, the current density is smaller than that for the pristine monolayer graphene (Fig. 1). Thus, the transport properties of graphene hybrids are sensitive to their geometries which cooperatively affect their electronic structures.

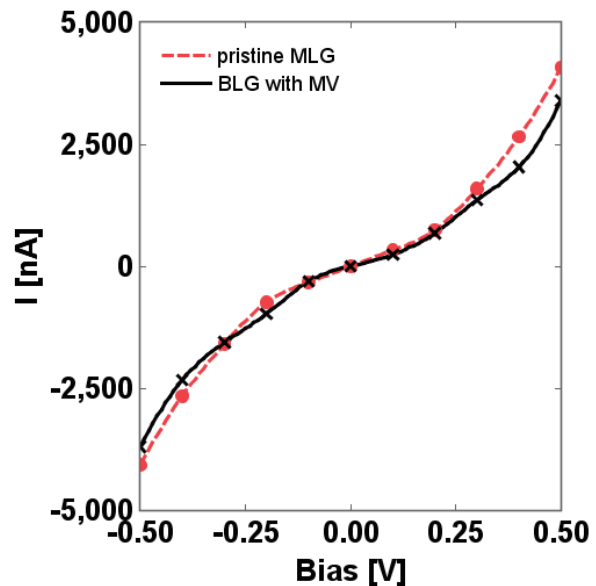


Fig. 1. I-V characteristics of pristine monolayer graphene (MLG) and bilayer graphene (BLG) with monovacancy (MV).

### Reference

[1] K. Kishimoto and S. Okada, *Sur. Sci.* **644**, 18, (2016).

Corresponding Author: K. Kishimoto

Tel: +81-29-853-5600(ext.; 8233)

E-mail: [kkishimoto@comas.frsc.tsukuba.ac.jp](mailto:kkishimoto@comas.frsc.tsukuba.ac.jp)

## Tuning of local optical properties of MoS<sub>2</sub> monolayer and its structural control using electric-field-effect scanning near-field optical microscopy techniques

○Junji Nozaki, Musashi Fukumura, Takaaki Aoki, Yutaka Maniwa, Yohei Yomogida, and Kazuhiro Yanagi

*Department of Physics, Tokyo Metropolitan University, Hachioji, Tokyo 192-0397, Japan*

Transition metal dichalcogenides (TMDCs) attract a lot of interests because of their remarkable physical characteristics. Especially, unique optical properties, such as single photon emission and non-linear optical processes, have been reported at peculiar sites on a monolayer TMDC, such as defects, grain boundaries, and hetero interfaces.<sup>1,2</sup> How to tune such optical characteristics is of great importance for their optoelectronic applications. It is known that optical properties of TMDCs can be modulated by application of electric field.<sup>3</sup> Thus here, as shown in Fig. 1(a), we developed scanning near-field optical microscopy (SNOM)<sup>4</sup> measurement techniques under electric fields in order to reveal relationships between local optical properties and applied biased voltages on monolayer TMDCs.

A schematic illustration of our experimental setup is shown in Fig. 1(a). We applied a bias voltage to a monolayer sample from a cantilever of our SNOM system and then optical properties of a site under electric field were measured. As shown in Fig. 1(b), photoluminescence (PL) on a site of MoS<sub>2</sub> monolayer was reversibly modulated in the spatial resolution of about 100 nm by this method, indicating that electron injection control and evaluation of its optical properties on the site were achieved at the same time by this method. In addition, in hole injection regime, we found the structure of monolayer MoS<sub>2</sub> was unstable and sometimes decomposed. On the basis of this observation, we developed a method to etch MoS<sub>2</sub> crystal using near-field light in combination with negatively biased voltages. Furthermore, using this technique, we fabricated a MoS<sub>2</sub> nanoribbon with a width of approximately 500 nm from a triangle MoS<sub>2</sub> monolayer crystal. This technique enables us to tune local optical properties of atomic monolayer samples and to freely design their structural forms.

References: [1] Y. He *et al.* Nat Nanotechnol. **10**, 497 (2015). [2] X. Yin *et al.* Science. **344**, 488 (2014). [3] K. F. Mak *et al.* Nat Mater. **12**, 207 (2012). [4] J. Nozaki *et al.* JJAP **55**, 038003, 06GB01 (2016).

Corresponding Author: K. Yanagi, Tel: +81-42-677-2494, E-mail: yanagi-kazuhiro@tmu.ac.jp

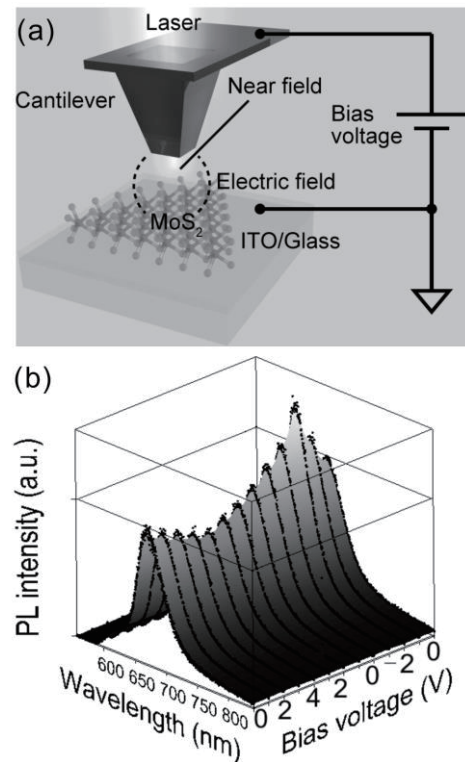


Fig.1 PL modulation in a site of a monolayer MoS<sub>2</sub> by local carrier injection control using our electric-field-effect scanning near-field optical microscopy system. (a) Schematic illustration of our experimental setup. (b) Modulation of local PL spectra on MoS<sub>2</sub> monolayer at a site in the spatial resolution of about 100 nm.

## Optical properties of superacid-treated MoS<sub>2</sub>

○Hong En Lim, Nur Baizura Mohamed, Yuhei Miyauchi, Kazunari Matsuda

*Institute of Advanced Energy, Kyoto University, Uji, Kyoto 611-0011, Japan*

Research on 2D materials, such as transition metal dichalcogenides (TMDCs), has generated profound interests for their application in optoelectronics, valleytronics, and spintronics [1]. Nevertheless, because of the defects and surface contamination, monolayers of TMDCs have been suffering from low photoluminescence (PL) quantum yields (QY). Molybdenum disulfide, MoS<sub>2</sub> for instance, has a maximum reported QY of <1 % with an extremely short PL life time of less than hundreds picoseconds. This prevents the thorough understanding on details of their excitation dynamics, as well as valley polarization/coherence physics, and therefore limiting their immediate use in nano-optical devices. Recently, a breakthrough was achieved by Amani *et al.* [2,3], where the QY of MoS<sub>2</sub> had been significantly improved to >95 % by using an organic superacid, bis(trifluoro-methane) sulfonamide (TFSI). However, detailed understanding on the optical properties of superacid-treated MoS<sub>2</sub> has not been fully understood.

Here we examined the optical properties of such chemically treated MoS<sub>2</sub> monolayer. Under the excitation of 2.33 eV, a substantial increase (~100 times) in the PL intensity of the treated sample is observed (Fig. 1(a)) at 298 K. The value is comparable to those reported ones, implying the effectiveness of this method towards PL enhancement. Besides, the treatment has resulted in a decrease in the full width half maximum (FWHM) of the peak registered from 87 to 59 meV. We decomposed the PL spectra of the as-exfoliated and TFSI-treated MoS<sub>2</sub> into exciton and charged peaks [4] as shown in Fig. 1(b) and (c), respectively. These results reveal a distinct change in each component, with a noticeable increase in the exciton population after the reaction. Further details on the results obtained at low temperature (5 K) will be discussed.

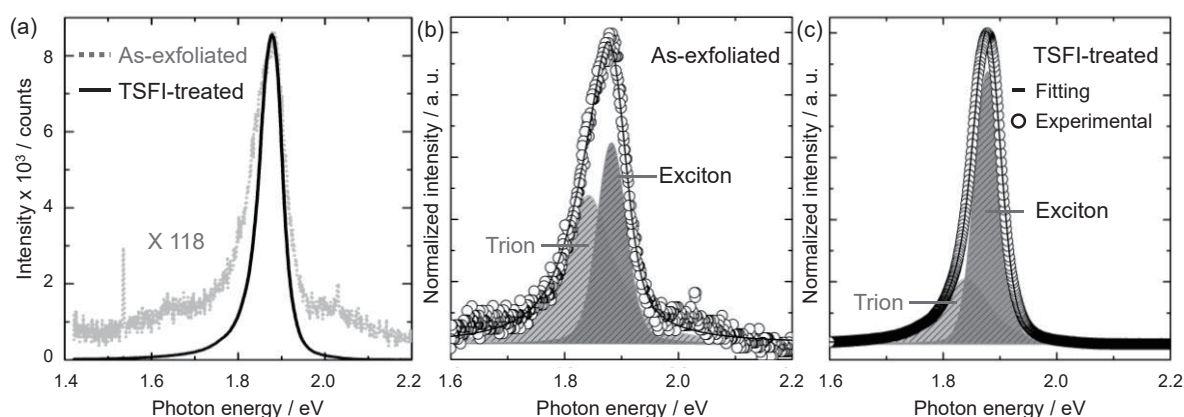


Fig.1 (a) PL spectra for the as-exfoliated and TFSI-treated MoS<sub>2</sub> monolayer with exciton and trion features fitted using Voigt function in (b) and (c).

- [1] F. Xia *et al.* Nat. Photonics **8**, 12 (2014). [2] M. Amani *et al.* Science **350**, 6264 (2015).  
 [3] M. Amani *et al.* Nano Lett. **16**, 4 (2016). [4] S. Mouri, Y. Miyauchi, and K. Matsuda, Nano Lett. **13**, 5944 (2016).

Corresponding Author: H. E. Lim

Tel: +81-774-38-3460, Fax: +81-774-38-3460,  
 E-mail: limhongen@gmail.com

## Relaxation Mechanism of Interlayer Excitons in 2D van der Waals Heterostructures

○Mitsuhiro Okada<sup>1</sup>, Yusuke Kureishi<sup>1</sup>, Yusuke Hasegawa<sup>2</sup>, Alex Kutana<sup>3</sup>, Kenji Watanabe<sup>4</sup>, Takashi Taniguchi<sup>4</sup>, Yuhei Miyauchi<sup>2</sup>, Kazunari Matsuda<sup>2</sup>, Hisanori Shinohara<sup>1</sup>, Ryo Kitaura<sup>1</sup>

<sup>1</sup> *Department of Chemistry and Institute for Advanced Research, Nagoya University, Nagoya 464-8602, Japan*

<sup>2</sup> *Institute of Advanced Energy, Kyoto University, Uji 611-0011, Japan*

<sup>3</sup> *Department of Materials Science and Nanoengineering, Rice University, Houston, TX 77005, USA*

<sup>4</sup> *National Institute for Materials Science, Tsukuba 305-0044, Japan*

Two-dimensional (2D) semiconductors, including MoS<sub>2</sub>, WS<sub>2</sub>, MoSe<sub>2</sub>, etc., have provided a fascinating opportunity to explore optical properties in 2 dimensions. In particular, van der Waals (vdW) heterostructures composed of these 2D semiconductors, such as WS<sub>2</sub>/MoS<sub>2</sub>, offer a novel platform for optical physics, where strong inter-layer interaction drastically alters optical transitions. To explore the intrinsic PL properties of TMDC vdW heterostructures, we have focused on fabricating high-quality samples achieved by fully-hBN encapsulated WS<sub>2</sub>/MoS<sub>2</sub> heterostructures (Fig.1). In this work, we report drastic excitation energy dependence in PL spectra, where relaxation pathway of photoexcited carriers plays an important role.

We synthesized monolayer MoS<sub>2</sub> and WS<sub>2</sub> by chemical vapor deposition method and prepared thin hBN flakes by mechanical exfoliation method. hBN-encapsulated heterostructures (hBN/WS<sub>2</sub>/MoS<sub>2</sub>/hBN) were prepared with the polymer-assisted dry-transfer method. Fabricated heterostructure shows PL emission from interlayer excitons around 1.4 to 1.7 eV in addition to A-excitons from WS<sub>2</sub> and MoS<sub>2</sub> at RT (Fig. 2). The interlayer excitons in WS<sub>2</sub>/MoS<sub>2</sub> vdW heterostructures were observed in previous papers, giving a single broad peak at around 1.4 eV. [1] In contrast, the observed interlayer PL peak gives more detailed spectral features, which might originate from high-quality (clean interface and surface flatness) of our sample. At 15 K, the PL spectra show strong excitation energy dependence at interlayer exciton region. At low excitation energy (under 2.38 eV), PL spectra show single and sharp interlayer exciton peak at 1.77 eV, whereas broad interlayer exciton emission at 1.4-1.77 eV is observed with 2.54 eV excitation. We think this is caused by a characteristic relaxation pathway at “band nesting” region, which is consistent to DFT calculation.

[1] Y.Gong *et al.* Nature Mater. **13**, 1135 (2014).

Corresponding Author: H. Shinohara and R. Kitaura  
Tel: +81-52-789-2477, Fax: +81-52-747-6442,  
E-mail: noris@nagoya-u.jp, r.kitaura@nagoya-u.jp

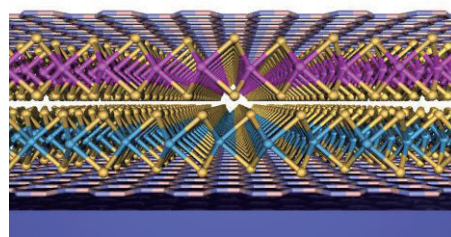


Fig. 1 A structure model of the fabricated heterostructure.

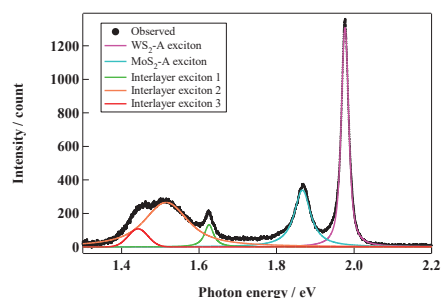


Fig.2 PL spectrum of hBN-encapsulated WS<sub>2</sub>/MoS<sub>2</sub> vdW heterostructure measured at RT.

## Transition of crystal structure and electrical property of MoTe<sub>2</sub> crystal by laser irradiation

○Kota Kamiya<sup>1</sup>, Tomoki Yamanaka<sup>1</sup>, Masahiro Matsunaga<sup>1</sup>, Ayaka Higuchi<sup>1</sup>, Yuichi Ochiai<sup>1</sup>, Michio Kida<sup>1</sup>, Jonathan P. Bird<sup>2</sup> and Nobuyuki Aoki<sup>1</sup>

<sup>1</sup> Graduate School of Advanced Integration Science, Chiba University, Chiba 263-8522, Japan

<sup>2</sup> Department of Electrical Engineering, University at Buffalo, SUNY, Buffalo, New York 14260-1920, USA

Transition metal dichalcogenides (TMDCs) have attracted a lot of interests due to its various properties[1]. One of its unique properties is that the transport property can be changed from semiconducting (2H) to metallic (1T') depending on the structure. It is known that such a structural change occurs relatively easily in MoTe<sub>2</sub> [2]. Recently, S. Cho *et al.*, achieved the phase transition from 2H to 1T' in MoTe<sub>2</sub> by laser patterning [3]. In this study, we fabricated 1T' structure in a MoTe<sub>2</sub> crystal by optical laser irradiation and confirmed the electronic properties.

In our study, we used multilayer MoTe<sub>2</sub> crystals exfoliated onto Si/SiO<sub>2</sub> substrates. The green laser ( $\lambda = 532$  nm) was irradiated by a single line scan at various laser powers through an objective lens under atmospheric condition. After the exposure, the phase transition was confirmed from the Raman scattering spectra. Fabricating several FET structures with or without 1T' phase region, we confirmed the difference of the electrical properties. Figure 1 shows a Raman spectra of MoTe<sub>2</sub> crystal after a laser scanning. The Raman peak shifts from  $\sim 230$  cm<sup>-1</sup> to 125 cm<sup>-1</sup> after the irradiation, which is consistent with the peak positions of 2H and 1T' structures. It indicated that the phase transition occurred within the irradiated region with decreasing the thickness of the crystal by a local heating. Figure 2 shows transfer curves obtained in 1T' and 2H phase devices. No gate voltage dependence was observed at 1T' channel device while the usual 2H device showed ambipolar characteristic.

In conclusion, we observed the phase transition from 2H to 1T' structure in MoTe<sub>2</sub> crystals by optical laser thinning. In addition, we confirmed that the 1T' phase shows metallic behavior.

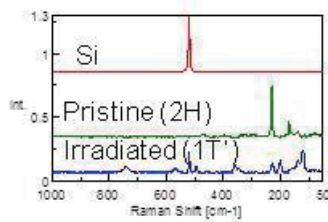


Figure 1. Raman map and spectra of the laser patterned MoTe<sub>2</sub> crystal.

[1] Q. H. Wang *et al.* Nature Nanotech, **7**, 699 (2012).

[2] K.-A. Alexander *et al.*, Nature Comm. **5**, 4214 (2014).

[3] S. Cho *et al.* Science, **349**, 625 (2015).

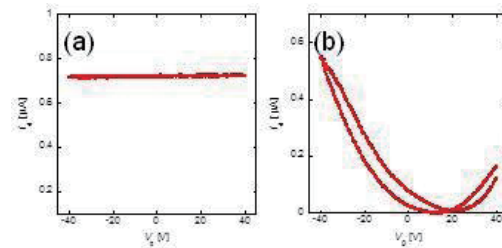


Figure 2. Transfer curves obtained (a) 1T' channel and (b) 2H channel device.

Corresponding Author: N. Aoki

Tel: +81-43-290-3430, Fax: +81-43-290-3427

E-mail: n-aoki@faculty.chiba-u.jp

## The LDI spectra of Detonation Nanodiamonds

○Masayoshi Fukaya<sup>1</sup>, Toshihiko Tanaka<sup>1</sup>, Amanda S. Barnard<sup>2</sup>, Eiji Osawa<sup>3</sup>

<sup>1</sup> Department of Chemistry and Biochemistry, National Institute of Technology, Fukushima College, 30 Aza-nagao, Tairakamiarakawa, Iwaki, Fukushima, 970-8034, Japan

<sup>2</sup> CSIRO Materials Science and Engineering, 343 Royal Parade, Parkville, Victoria 3052, Australia

<sup>3</sup> Nano Carbon Research Institute Ltd., Asama Research Extension Center, Faculty of Textile Science and Technology, Shinshu University 3-15-1 Tokida, Ueda, Nagano, 386-8567 Japan

We reported previously the laser desorption ionization mass spectra (LDI MS) of the detonation nanodiamonds deposited on a stainless plate from the aqueous solution of well dispersed primary particles of detonation nanodiamonds (PPDNDs).<sup>1-3</sup> Among five positive-peaks (<0.5kDa, 1~5kDa, ~12kDa, ~40kDa broad, ~120kDa broad) observed, the third peak was assigned to the remnant of PPDNDs after losing all the shell and about one-third of the core. Abundant peaks under 5kDa represent the fragments from the shell and outer core. Although the solution was dried before LDI measurements, they were observed from it and not from raw detonation materials, thus the third peak having not been explained well. The purpose of this poster is to substantiate the unusual assignment.

Recent LDI MS results herein show that a 12kDa ion should be attributable to the inner sp<sup>3</sup> core of PPDND. We think that the inner core ions can be generated from the colloidal crystals of PPDNDs [Fig.1]. Whiskers<sup>5</sup> prepared from the aqueous solution also shows similar inner core peaks whereas a freeze-dried solution does not surprisingly. Slow drying from dispersed PPDNDs probably forms the crystals that cannot desorb themselves because of their huge mass. The shell and outer core decomposes harder, thus emerging the stable inner core ions. The 12kDa peak is observed by both a linear and reflector modes, whereas two larger peaks (~40kDa, ~120kDa) are lost in the reflector mode, thereby demonstrating the stability of the 12kDa peak during the flight in the analyzer to a detector. The inner core size was also estimated to be ~12kDa by a confined mode of Raman spectra.<sup>4</sup> Such a stable ion is therefore the inner core.

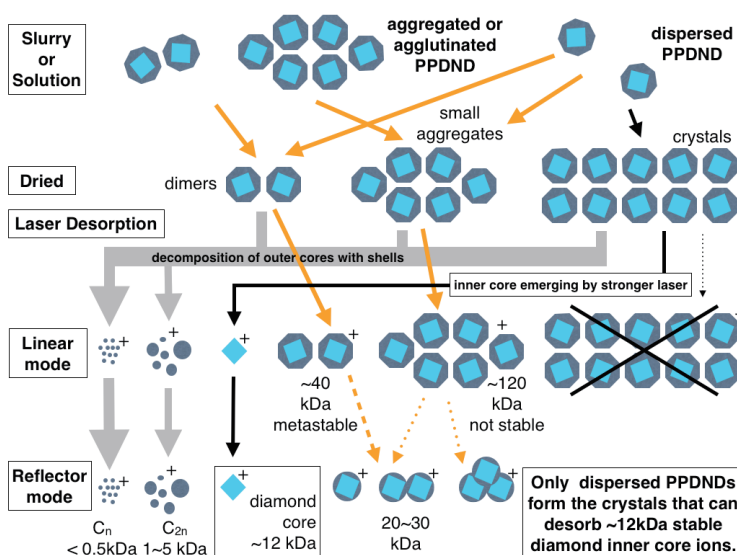


**Fig.1** generation of the core peak in the LDI from the precipitation from the solution of highly dispersible PPDNDs.

[1] E. Osawa, D. Ho, H. Huang, M. V. Korobov, N. N. Rozhkova; *Dia. Rel. Mat.* 18, 904(2009). [2] M.Fukaya, Y.Otsubo, T. Tanaka, R.Yamanoi, E.Osawa; *FNTG 50 Proceedings* 85(2016). [3] T. Tanaka, R.Yamanoi, E.Osawa; *FNTG 48 Proceedings* 19(2015). [4] V. I. Korepanov, H. Witek, H. Okajima, E. Osawa, and H. Hamaguchi; *J. Chem. Phys.* 140, 41107 (2014). [5] E. Osawa, *Diamond & Related Materials* 16, 2018–2022 (2007). Corresponding Author: Toshihiko Tanaka / Tel: +81-246-46-0810 / E-mail: ttanaka@fukushima-nct.ac.jp

## Impact synthesis of amino acids on carbon nano-particles in nitrogen gas

○Tetsu Mieno<sup>1,2</sup>, Kazuki Okochi<sup>2</sup>, Syunsuke Sekiguchi<sup>2</sup>, Sunao Hasegawa<sup>3</sup>

<sup>1</sup> Graduate School of Science & Technology, Shizuoka University, Shizuoka 422-8529, Japan

<sup>2</sup> Department of Physics, Shizuoka University, Shizuoka 422-8529, Japan

<sup>3</sup> Institute of Space & Astronautical Science, JAXA, Sagami-hara, 252-5210, Japan

We are interested in synthesis of carbon clusters and carbon molecules in space. Carbon materials have been produced by impacts of asteroids onto surfaces of planets/satellites like Titan. We have done impact experiment using a light-gas gun simulating the space-impacts, and found synthesis of many kinds of carbon clusters (fullerenes, nanotubes, metal-encapsulated carbon capsules, balloon-like carbons). [1] Here, we analyzed smaller carbonaceous molecules, which can not be observed by TEM. A poly-carbonate bullet is accelerated by a gas-gun (6.5 km/s) and injected onto an iron target (an ice + iron target, a hexane + ice + iron target) under 1 atm of nitrogen gas. Figure 1 shows scheme of the pressurized chamber in which the impact takes place. After the impact, a hog-gas plume generates for about 50  $\mu$ s, and strong emission from CN and C<sub>2</sub> molecules ( $T_{rot} \sim 5000$  K) is observed. Then, the gas-plume cools down and many carbon nanoparticles deposit on the inner surface. The carbon sample is carefully collected to avoid contamination, refluxed using pure water, filtered and condensed. The sample is dabsyllized and analyzed using a HPLC. As a result, strong peaks of amino acids (glycine and alanine) are obtained. [2] Figure 2 shows the HPLC chart. In 1 mg of soot, 2 nmol of glycine and 0.9 nmol of alanine are included. We conjecture that during the cooling process of carbon particles, carbon radicals and CN radicals react on the particle's surface, and amino acids are synthesized.

[1] T. Mieno *et al.*, Jpn. J. Appl. Phys. **50** (2011) 125102. [2] K. Okochi, T. Mieno *et al.*, Org. Life Evol. Biosp. **45** (2015) 195.

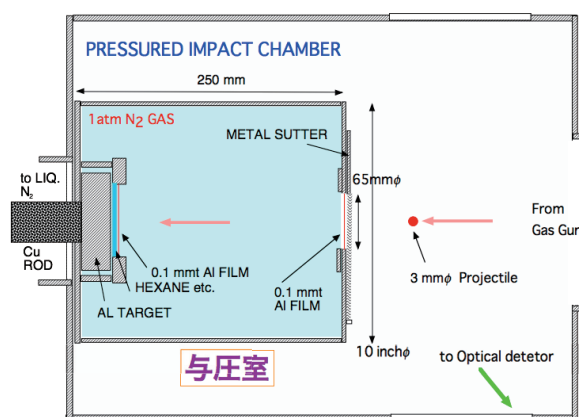


Fig.1 Scheme of the pressurized chamber.

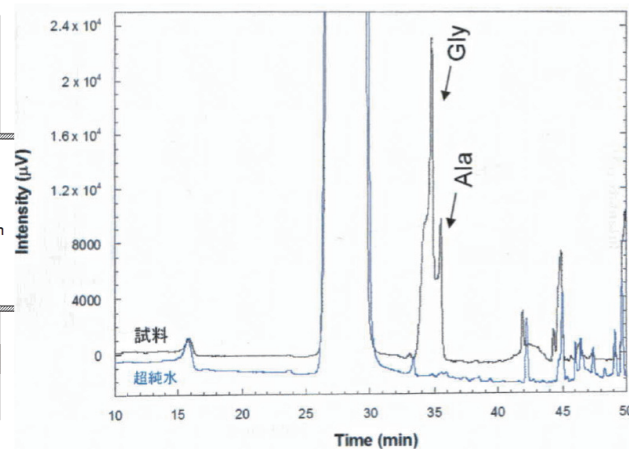


Fig.2 HPLC chart detecting glycine & alanine.

発表索引  
**Author Index**

## Author Index

### < A >

Achiba, Yohji 2-10, 2-13, 2P-8,  
2P-12, 3P-1, 3P-2  
Ago, Hiroki 2P-31, 3P-30  
Ahn, Namyoung 1P-25, 3-7  
Akasaka, Takeshi 1P-1, 2P-10  
Akiba, Miki **2P-40**  
Amagai, Yuri 3-4  
An, Hua **2P-21**, 3P-18  
Aoki, Nobuyuki 2P-5, 2P-29, 3P-40  
Aoki, Takaaki 3P-37  
Aoyagi, Shinobu 1P-2, 2P-9  
Arai, Miho 2-7  
Asaka, Koji 3-5  
Ata, Seisuke 2-4

### < B >

Bandow, Shunji **2P-38**  
Barnard, Amanda 2-14, 2P-36, 3P-41  
Bichara, Christophe **1S-3**  
Bird, Jonathan P. 3P-40  
Boero, Mauro 3P-25

### < C >

Chen, Zhongming 1P-15  
Cheng, Xinlu 2P-32  
Chiashi, Shohei 1-1, 1-3, 2P-14,  
2P-21, 2P-24, 3P-5,  
3P-7, 3P-11, 3P-14,  
3P-17, 3P-18, 3P-20,  
3P-26  
Choi, Jun Hee 1P-9, 1P-40, **1P-41**  
Choi, Mansoo 1P-25, 3-7  
Cong, Kankan 3S-8

### < D >

D'Arsié, Lorenzo 3-10  
De Silva, Kanishka 3-8  
Dinda, Diptiman 2S-6

### < E >

Eda, Junko 2P-22  
Einarsson, Erik **3S-10**

Endo, Hitomi 2-13  
Endo, Norifumi 1P-29  
Endoh, Hiroyuki 1P-16  
Esconjauregui, Santiago 3-10

### < F >

Fioli, G. 1P-34  
Fujii, Shunjiro 1P-6  
Fujimoto, Yoshitaka **1-6**  
Fujiwara, Kyosuke 1P-21  
Fukaya, Masayoshi 2-14, 2P-36, **3P-41**  
Fukazawa, Shinpei **2P-10**  
Fukidome, Hirokazu 1P-29  
Fukumura, Musashi 3P-37  
Fukuzumi, Shunichi 1P-2  
Furukawa, Ko 2-10, 2P-8, 3P-2  
Furukawa, Yoritaka 3P-7  
Furutani, Sho **2P-11**  
Futaba, Don 2-1, 2-3

### < G >

Gao, Weilu 1P-8, 3S-8  
Gao, Yanlin **3P-34**  
Gorgoll, Ricardo M. 2P-4  
Guo, Jingdong 1P-1

### < H >

Hachiya, Soichiro **1P-15**  
Hada, Masahiko 2-9  
Hamada, Koki **3P-16**  
Hamaguchi, Hiroaki 2P-41  
Hamano, Yuuta 2P-39  
Hamasaki, Atom 2P-23  
Hao, Zhang **2P-14**  
Hara, Masanori **3-8**  
Harano, Koji **2P-4**  
Harigai, Toru 2P-37, 2P-41, 2P-42,  
2P-43  
Haruyama, J. 1P-32, 1P-34  
Hasdeo, Eddwi H. 2P-15  
Hasegawa, Kei 1P-15, 1P-22, 3P-8  
Hasegawa, M. 1P-34  
Hasegawa, Sunao 3P-42

Hasegawa, Yusuke	1P-36, 3P-39	Ishizeki, Keisuke	<b>3P-4</b>
Hashikawa, Yoshifumi	<b>2P-2</b>	Itoh, Takashi	2P-18
Hata, Kenji	2-1, 2-3	Iwata, Jun-Ichi	3P-25
Hatakeyama, Kazuto	1P-7	Iwata, Nobuyuki	1P-23
Hayamizu, Yuhei	2-6		
Hayashi, Hironobu	3-9	< J >	
He, Xiaowei	1P-8	Jang, Ho-Kyun	<b>1P-40</b> , 1P-41, 2P-16
Higashide, Noriyuki	3-6	Jeon, Il	<b>3-7</b> , 3P-11, 3P-14,
Higuchi, Ayaka	3P-40		3P-30
Hiraide, Rineka	1-5	Jin, Jun Eon	1P-41
Hirano, Atsushi	1P-6, <b>1P-8</b> , 1P-17	Jinnouchi, Ryota	2P-39
Hirayama, Takaaki	3P-2	Jippo, Hideyuki	<b>3-9</b>
Hirofumi, Jun	1P-13, <b>3P-12</b> , 3P-13	Jnag, Ho-Kyun	1P-9
Homma, Yoshikazu	1P-3		
Honda, Shirou	1P-18	< K >	
Hoshino, Ryo	1P-23	Kako, Masahiro	1P-1, 2P-10
Hoshino, Yuudai	2P-39	Kamakura, Shun	3P-7
Hotta, Takato	2P-35	Kamiya, Kota	<b>3P-40</b>
Hou, Bo	<b>3P-17</b>	Kanazawa, Naoki	3P-15
Huang, Hsin-Hui	3-8	Kanda, Akinobu	1-5, 1P-30
Hung, Nguyen T.	<b>2P-17</b>	Kaneko, Toshiro	1P-35
		Karmakar, Arka	3S-10
< I >		Kasama, Yasuhiko	2-11
Ichinose, Yota	1P-5, <b>2P-22</b>	Kashima, Taiga	<b>3P-13</b>
Iijima, Sumio	3P-23	Kashiwa, Kotaro	3P-26
Iizumi, Yoko	1P-39, 3P-17	Katagiri, Y.	1P-32, <b>1P-34</b>
Ikeda, Kozo	1P-7	Kataoka, Yosuke	1P-20
Ikuhara, Yuichi	2P-21	Kataoka, Yousuke	3P-22
Ikuma, Naohiko	1P-2, <b>2P-1</b>	Kataura, Hiromichi	1P-6, 1P-17, 3S-8
Imamura, Yutaka	2-9	Kato, Tatsuhisa	1P-2, 2P-8, 2-10,
Imoto, Fumihiko	<b>3P-25</b>		3P-2
Inaba, Takumi	<b>1P-3</b>	Kato, Toshiaki	1P-35
Inoue, Taiki	1-1, 1-3, 2P-14,	Kato, Yuichi	3P-3, 3P-35
	2P-21, 2P-24, 3P-5,	Kato, Yuichiro K.	1-3, 1P-4, 3-1,
	3P-7, 3P-11, 3P-14,		3-2, 3-6, 3P-6
	3P-17, 3P-18, 3P-26	Katsuyama, Shota	3-5
Inoue, Y.	1P-34	Katumoto, S.	1P-34
Irita, Masaru	<b>3-5</b>	Kauppinen, Esko I.	<b>1S-2</b> , 3-7, 3P-14
Isaka, Takuya	1P-24, <b>3P-29</b>	Kawabata, Kosuke	1P-15
Ishi, A.	1P-34	Kawachi, Kazuhiko	2-11
Ishida, Misaki	2-11	Kawahara, Kenji	2P-31, 3P-30
Ishida, Takuya	<b>2P-29</b>	Kawai, Hideki	1P-5
Ishii, Akihiro	1P-4, 3-1, <b>3-2</b> ,	Kawai, Takazumi	1P-19
	3-6, 3P-6	Kawano, Saki	<b>2P-7</b>
Ishikawa, Ryousuke	<b>3P-27</b>	Kawasaki, Kohei	<b>2P-42</b>

Kida, Michio	3P-40	Lee, Dong-Jin	2P-16
Kikuchi, Koichi	2-10, 2P-8, 3P-1, 3P-2	Lee, Kook Jin	1P-40
Kim, Do Hyun	1P-9, 1P-40, 1P-41, <b>2P-16</b>	Li, Jiulong	2P-6
Kim, Gyu-Tae	1P-9, 1P-40, 1P-41, 2P-16	Li, Xinwei	3S-8
Kim, Min-Seok	2P-16	Li, Yan	1P-14, <b>2S-5</b> , 3-3, 3P-18, 3P-19
Kim, Sung-Dae	2P-16	Lim, Hong En	2P-33, <b>3P-38</b>
Kimura, Issei	<b>1-3</b>	Liu, Haihao	1P-42
Kinno, Yasuhiro	<b>3P-21</b>	Liu, Huaping	3S-8
Kinoshita, Hiroki	<b>3P-30</b>	Liu, Kaihui	<b>3S-9</b>
Kiribayashi, Hoshimitsu	2P-20	Liu, Ming	<b>3P-5</b>
Kishimoto, Ken	<b>3P-36</b>	Lu, Fei	3S-10
Kishimoto, Shigeru	1P-10, 3P-9, 3P-12, 3P-13	< M >	
Kitagawa, Sae	<b>2P-19</b>	Machida, Tomoki	2-7
Kitaura, Ryo	1P-19, 2P-9, 2P-35, 3P-21, 3P-28, 3P-39	Machiya, Hidenori	1-3, <b>1P-4</b>
Ko, Jeong Won	<b>2P-6</b>	Maeda, Yutaka	1P-1, <b>3-4</b>
Ko, Weon Bae	2P-6	Maniwa, Yutaka	2P-22, 3P-37
Kobashi, Kazufumi	2-2, 3P-3	Maruyama, Mina	1P-28, 1P-38, <b>2-12</b> , 3P-30
Kobayashi, Kazuhiro	<b>3P-1</b> , 3P-2	Maruyama, S.	1P-34
Kobayashi, Shunji	<b>3P-8</b>	Maruyama, Shigeo	1-1, 1-3, 1S-2, 2P-14, 2P-21, 2P-24, 3-7, 3P-5, 3P-7, 3P-11, 3P-14, 3P-17, 3P-18, 3P-20, 3P-26
Kochi, Taketo	<b>1-2</b>	Maruyama, Takahiro	1P-21, 2P-20
Kodama, Takeshi	2-9, 2-10, 2-13, 2P-8, 2P-12, 3P-1, 3P-2	Masubuchi, Satoru	2-7
Koinuma, Michio	1P-7	Matsubara, Manaho	<b>2P-26</b>
Kokubo, Ken	1P-2, 2P-1	Matsuda, Iwao	1P-29
Komuro, Tomohiko	1P-13	Matsuda, Kazunari	1P-36, 2P-33, 3P-38, 3P-39
Konabe, Satoru	1P-3, <b>2P-34</b> , 3P-4	Matsue, Tomokazu	2-5
Kono, Junichiro	1P-8, <b>3S-8</b>	Matsui, Jun	3-4
Kumakura, Makoto	<b>2P-20</b>	Matsumoto, Kazuhiko	<b>1S-4</b>
Kumamoto, Akihito	2P-21	Matsumoto, Rika	3P-30
Kumatani, Akichika	<b>2-5</b>	Matsunaga, Masahiro	3P-40
Kuragane, Natsuki	<b>1P-23</b>	Matsuo, Yoshiaki	1P-24
Kureishi, Yusuke	3P-39	Matsuo, Yutaka	1P-2, <b>2-8</b> , <b>2P-3</b> , 3-7, 3P-11, 3P-14, 3P-30
Kuroiwa, Kiyoko	3P-23	Matsushita, Yu-ichiro	3P-32
Kutana, Alex	3P-39	Matsuura, Tomoki	3P-13
Kuwahara, Yuki	1P-16, <b>3P-10</b>	Matuda, Kazunari	1P-39
Kwon, Eunsang	2-11		
< L >			
Laiho, Patrik	1S-2		

Michiya, Yoshimasa	<b>3P-28</b>	Nihei, Mizuhisa	3P-8
Mieno, Tetsu	<b>3P-42</b>	Nihey, Fumiyuki	<b>1P-16</b> , 3P-10, 3P-24
Minowa, Hiroya	2P-24	Nishi, Hirofumi	<b>3P-32</b>
Mitani, Takuji	2-10, <b>2P-8</b> , 3P-1, 3P-2	Nishida, Tetsuo	1P-12, 2P-18
Mitsuhara, Masatoshi	2P-31	Nishii, Haruki	<b>2P-41</b>
Mitsuichi, Masaya	3-4	Nishimoto, Shinya	<b>3P-2</b>
Miura, Chiho	2-5	Nishina, Yuta	2P-29
Miyabe, Kyosuke	1P-1, 2P-10	Nishino, Akane	3-4
Miyamoto, Yoshiyuki	<b>2P-32</b>	Nishino, Hidekazu	1P-18
Miyata, Yasumitsu	2-6	Nishino, Makiko	<b>2P-9</b>
Miyauchi, Yuhei	1P-36, 1P-39, 2P-33, 3P-38, 3P-39	Noda, Suguru	1P-15, 1P-22, <b>2S-7</b> , 2P-19, 3P-8, 3P-16
Miyaura, Kenshi	<b>1P-18</b>	Noe, II G.Timothy	3S-8
Mizutani, Ken	<b>2P-24</b>	Nomoto, Takahito	3P-27
Mohamed, Nur Baizura	2P-33, 3P-38	Nonomura, Rei	<b>2P-18</b>
Morimoto, Takahiro	2-2, <b>2-4</b> , 3P-3, 3P-17	Nozaki, Junji	<b>3P-37</b>
Morita, Hiroki	<b>1P-27</b> , 2P-39	Nugraha, Ahmad R. T.	<b>2P-15</b> , 2P-17
Moriya, Rai	2-7	< O >	
Motomiya, Kenichi	1P-12, 2P-18	Obori, Masanao	3P-8
Murakoshi, Kei	2-6	Ochiai, Yuichi	2P-5, 3P-40
Murata, Hidekazu	3-5	Ogamoto, Tatsuro	3P-7
Murata, Michihisa	2P-2	Ogata, Hironori	1P-20, 2P-7, 3P-22
Mustonen, Kimmo	1S-2	Ohata, C.	1P-32, 1P-34
< N >		Ohfuchi, Mari	<b>2P-27</b> , 3-9
Na, InYeob	1P-9	Ohiro, Tatsuo	2P-42
Nagai, Reito	<b>1P-35</b>	Ohkubo, Kei	1P-2
Nagai, Yukuya	<b>1P-22</b>	Ohno, Teruaki	3-5
Nagase, Shigeru	1P-1, 3-4	Ohno, Yutaka	1S-2, 1P-10, 1P-13, 3P-9, 3P-12, 3P-13, 3P-28
Nagata, Tomoko	1P-23	Ohta, Hiromichi	1P-12
Nakagawa, Ayano	2P-9	Ohyama, Shinnosuke	<b>3P-18</b>
Nakahara, Hitoshi	3-5	Okada, Susumu	1P-38
Nakamura, Eiichi	2P-4	Okada, Hiroshi	1P-2, 2P-3
Nakamura, Kazushi	<b>1P-30</b>	Okada, Mitsuhiro	<b>3P-39</b>
Nakamura, Maki	<b>3P-23</b>	Okada, Susumu	1-2, 1-4, 1P-19, 1P-28, 1P-31, 2-6, 2-12, 2P-11, <b>2P-13</b> , 2P-25, 2P-26, 2P-40, 3P-30, 3P-31, 3P-33, 3P-34, 3P-36
Nakamura, Masatoshi	<b>1P-5</b>	Okada, Takeru	2-5
Nakamura, T.	1P-34	Okazaki, Toshiya	1P-39, 2-2, 2-4, 3-4, 3P-3, 3P-17
Nakandakari, Sho	<b>2P-31</b>		
Nakanishi, Terunobu	<b>1P-19</b>		
Nakatori, Natsumi	<b>2-10</b> , 2P-8, 3P-1, 3P-2		
Nanba, T.	<b>1P-32</b>		
Naritsuka, Shigeya	1P-21, 2P-20		

Okochi, Kazuki	3P-42	Sasaoka, Kenji	3P-4
Okochi, Takeshi	<b>3P-7</b>	Sato, Hikaru	<b>1P-26</b>
Okudaira, Saki	<b>1P-39</b>	Sato, Shintaro	3-9
Omachi, Haruka	<b>1P-13</b> , 2P-9, 3P-21	Sato, Yoshinori	1P-12, 2P-18, 2P-24
Onodera, Atsushi	<b>1P-11</b>	Sato, Yoshinori (Stella Chemifa Co.)	1P-12, 2P-18
Ootuka, Youiti	1-5	Sato, Yutaka	<b>3P-22</b>
Osaka, Ryo	2-6	Saucier Yamato, Alexander	<b>1P-38</b>
Osawa, Eiji	2-14, <b>2P-36</b> , 3P-41	Sawahata, Hisaki	<b>1P-28</b>
Osawa, Toru	3P-7	Sekido, Masaru	1P-11
Osawa, Toshio	1P-15	Sekiguchi, Syunsuke	3P-42
Oshima, Takumi	2P-1	Seneor, Pierre	1P-32
Oshiyama, Atsushi	3P-25, 3P-32	Seo, Seungju	<b>3P-11</b>
Otani, Chiko	2-11	Shahi, Simran	3S-10
Otsuka, Keigo	<b>1-1</b> , 3P-5, 3P-26	Shigekawa, Hidemi	1P-19
Oya, Tomoya	3P-27	Shiino, Kyohei	2P-39
Ozeki, Sumio	2P-23	Shiku, Hitoshi	2-5
< P >		Shin, Jong Mok	<b>1P-9</b> , 1P-41
Park, Nam-Gyu	3P-14	Shinohara, Hisanori	<b>1S-1</b> , 1P-13, 1P-19, 2P-9, 2P-35, 3P-21, 3P-28, 3P-39, Tutorial
Park, Se Jeong	1P-9		
Pyon, Sunseng	2-7	Shiomi, Junichiro	3P-8
< R >		Shiromaru, Haruo	<b>2-13</b> , 2P-12
Rajashekar, Badam	3-8	Someya, Takashi	<b>1P-29</b>
Ristimäki, Sami	1P-11	Sone, Erika	3-4
Robertson, John	3-10	Sorimachi, Jun-ya	<b>1-4</b>
Roche, S.	1P-34	Sota, Masaki	1-3, <b>3P-26</b>
Rubio, Angel	2P-32	Souma, Satofumi	3P-4
		Suda, Yoshiyuki	2P-37, 2P-41, 2P-42, 2P-43
< S >		Sugai, Toshiki	1P-27, <b>2P-39</b>
Saha, Shyamal K	<b>2S-6</b>	Sugime, Hisashi	2P-19, <b>3-10</b> , 3P-8, 3P-16
Saida, Takahiro	2P-20		
Saito, Riichiro	1P-37, 1P-42, 2P-15, 2P-17	Sugiura, Takeshi	<b>1P-1</b> , 2P-10
Saito, Susumu	1-6	Suko, Hiroki	3P-14
Saito, Takeshi	1P-16, 3P-10	Suzuki, Akira	<b>2P-28</b>
Saito, Yahachi	3-5	Suzuki, Daisuke	<b>1P-33</b>
Sakaguchi, Takahiro	3P-11, <b>3P-14</b>	Suzuki, Hal	<b>2-11</b>
Sakurai, Ryota	1P-23	Suzuki, Haruka	<b>2P-12</b>
Sakurai, Shunsuke	2-1, <b>2-3</b>	Suzuki, Masashi	2P-41
Samukawa, Seiji	2-5	Suzuki, Mitsuaki	3-4
Sanderson, Joseph	2-13	Suzuki, Seiya	<b>3-11</b>
Sano, Masahito	1P-26	Suzuki, Shinzo	<b>3P-15</b>
Sasabe, Akihiro	<b>3P-6</b>	< T >	
Sasaki, Fusako	1P-16, 3P-10	Taguchi, Yuki	2-13, 2P-12

Taira, Remi	<b>2P-25</b>	Uenoyama, Hiroto	<b>2P-5</b>
Tajima, Kentaro	<b>1P-24</b> , 3P-29	Ukai, Hiroyuki	3P-20
Tajima, Naoko	<b>3P-3</b>	Ukhtary, M. Shoufie	<b>1P-42</b>
Takagi, Yukai	3P-20	Umeda, Yoshito	2P-41
Takahashi, Hideyuki	1P-12	Umehara, Takashi	2P-30
Takahashi, Munehito	<b>2P-43</b>	Uratani, Kento	3P-15
Takahashi, Ryosuke	2-6	Ushiyama, Takuya	<b>3P-9</b>
Takahashi, Ryota	<b>2P-37</b>		
Takahashi, Yasufumi	2-5	< V >	
Takai, Kazuyuki	1P-24, 1P-33, 2P-28, <b>2P-30</b> , 3P-29	Velloth, Archana	<b>2-9</b>
Takashima, Kengo	<b>1-7</b>	< W >	
Takashima, Yasumasa	<b>2P-23</b>	Wakabayashi, Tomonari	2-13
Takeuchi, Osamu	1P-19	Wakamiya, Atsushi	2P-2
Takikawa, Hirofumi	2P-37, 2P-41, 2P-42, 2P-43	Wales, Benji	2-13
		Wang, Guowei	1P-6, <b>1P-17</b>
Tamegai, Tsuyoshi	2-7	Wang, Wei-Wei	3-4
Tamura, T.	1P-32	Wang, Xiaofan	<b>2P-33</b>
Tan, Dezhi	2P-33	Wang, Zhiyong	2P-9
Tanaka, Takeshi	1P-6, 1P-17, 3S-8	Watanabe, Kenji	1-5, 2P-35, 3P-39
Tanaka, Toshihiko	<b>2-14</b> , 2P-36, 3P-41	Watanabe, Takayuki	<b>2-2</b>
Tanaka, Yu	2P-5	Weatherup, Robert	3-10
Tanaka, Yuka	2P-38	Wei, Xiaojun	<b>1P-6</b> , 1P-17
Taniguchi, Takashi	1-5, 2P-35, 3P-39	Wu, Cheng	3P-17
Tatsumi, Yuki	<b>1P-37</b>	Wu, Xingyi	3-10
Terada, Natsuki	2P-39		
Terao, Yuri	3P-30	< X >	
Tohji, Kazuyuki	1P-12, 2P-18	Xiang, Rong	2P-14, 2P-21, 3P-5, 3P-11, 3P-14, 3P-17, 3P-18, 3P-26
Tokuda, Takuto	<b>2P-35</b>		
Tomori, Hikari	<b>1-5</b> , 1P-30		
Toyama, Kiyohiko	3P-24		
Tsuboi, Nozomu	3P-27	< Y >	
Tsuji, Takashi	<b>2-1</b>	Yamada, Hiroko	3-9
Tsuzuki, Mayumi	1P-6	Yamada, Jumpei	1P-21
		Yamada, Michio	1P-1, 3-4
< U >		Yamada, Ryohei	2P-24
Uchida, Yuki	2P-31	Yamada, Takeo	2-4, 3P-3
Uchimura, Jin	2P-23	Yamada, Tonan	3P-27
Uda, Takushi	1P-4, <b>3-1</b> , 3-2, 3-6, 3P-6	Yamagishi, Tamon	1P-23
		Yamaguchi, Junichi	3-9
Ue, Hitoshi	2P-42, 2P-43	Yamaguchi, Takahisa	2-10, 2P-8, 3P-2
Ueda, Naomasa	3P-26	Yamamoto, Daichi	1P-21
Ueda, Yuki	<b>1P-21</b>	Yamamoto, Hiroshi	1P-23
Ueno, Hiroshi	<b>1P-2</b> , 2P-3	Yamamoto, Masashi	1P-12, 2P-18
Ueno, Keiji	2-7	Yamamoto, Shun	3P-18

Yamamoto, Susumu	1P-29
Yamamoto, Takahiro	1-7, 2P-34, 3P-4
Yamanaka, Ayaka	1P-31, 2P-25, 3P-31, <b>3P-33</b>
Yamanaka, Masanori	<b>3P-35</b>
Yamanaka, Tomoki	3P-40
Yamanouchi, Shingo	2P-5
Yamasaki, Shigeto	2P-31
Yamasaki, Yuji	<b>2-7</b>
Yamashina, Tomoki	1P-24, 3P-29
Yamashita, Masatsugu	2-11
Yamazaki, Shintarou	3-5
Yanagi, Kazuhiro	1P-5, 2P-22, 3P-37
Yang, Feng	<b>1P-14</b> , 3P-18, 3P-19
Yang, Juan	<b>3-3</b>
Yasuda, Satoshi	<b>2-6</b>
Yasui, Masanori	1P-1
Yasujiro, Murata	2P-2
Yasuma, Airi	<b>3P-31</b>
Yasunishi, Tomohiro	<b>1P-10</b> , 3P-28
Yokoi, Hiroyuki	<b>1P-7</b>
Yokokura, Eita	<b>1P-20</b> , 3P-22
Yokoyama, Koji	<b>1P-12</b>
Yokoyama, Shun	1P-12
Yomogida, Yohei	1P-5, 1P-6, 2P-22, 3P-37
Yoneyama, Kazufumi	<b>1P-31</b>
Yoon, Jungjin	<b>1P-25</b> , 3-7
Yoshida, Masahiro	1-3, <b>3-6</b> , 3P-6
Yoshida, Shoji	1P-19
Yoshikawa, Ryo	<b>3P-20</b>
Yoshimura, Masamichi	3-8, 3-11
Yudasaka, Masako	1P-39, 3P-23, 3P-24
Yuge, Ryota	<b>3P-24</b>
<b>&lt; Z &gt;</b>	
Zhang, Daqi	3-3
Zhang, Hong	2P-32
Zhang, Wenjin	<b>1P-36</b> , 2P-33
Zhao, Xiulan	<b>3P-19</b>
Zhong, Guofang	3-10
Zhou, Xiaosong	3P-8

### 複写をご希望の方へ

フラーレン・ナノチューブ・グラフェン学会は、本誌掲載著作物の複写に関する権利を一般社団法人学術著作権協会に委託しております。

本誌に掲載された著作物の複写をご希望の方は、(社)学術著作権協会より許諾を受けて下さい。但し、企業等法人による社内利用目的の複写については、当該企業等法人が社団法人日本複写権センター((社)学術著作権協会が社内利用目的複写に関する権利を再委託している団体)と包括複写許諾契約を締結している場合にあつては、その必要はございません(社外頒布目的の複写については、許諾が必要です)。

#### 権利委託先：一般社団法人学術著作権協会

〒107-0052 東京都港区赤坂 9-6-41 乃木坂ビル 3階

URL : <http://www.jaacc.jp/> E-Mail : [info@jaacc.jp](mailto:info@jaacc.jp)

電話 : 03-3475-5618 FAX : 03-3475-5619

注意：複写以外の許諾（著作物の引用、転載・翻訳等）に関しては、(社)学術著作権協会に委託致しておりません。直接、フラーレン・ナノチューブ・グラフェン学会へお問い合わせください。

### Reprographic Reproduction outside Japan

- Making a copy of this publication  
Please obtain permission from the following Reproduction Rights Organizations (RROs) to which the copyright holder has consigned the management of the copyright regarding reprographic reproduction.
- Obtaining permission to quote, reproduce; translate, etc.  
Please contact the copyright holder directly.

Users in countries and regions where there is a local RRO under bilateral contract with Japan Academic Association for Copyright Clearance(JAC) are requested to contact the respective PROs directly to obtain permission.

Users in countries or regions in which JAC has no bilateral agreement are requested to apply for the license to JAC.

#### Japan Academic Association for Copyright Clearance (JAC)

Address : 9-6-41 Akasaka, Minato-ku, Tokyo 107-0052 Japan

URL : <http://www.jaacc.jp/> E-mail : [info@jaacc.jp](mailto:info@jaacc.jp)

Phone : +81-3-3475-5618 FAX : +81-3-3475-5619

2017年3月1日発行

## 第52回フラーレン・ナノチューブ・グラフェン総合シンポジウム 講演要旨集

《フラーレン・ナノチューブ・グラフェン学会》

〒113-8656 東京都文京区本郷 7-3-1

東京大学大学院工学系研究科 機械工学専攻  
丸山研究室内

Phone/Fax : 03-3830-4848

E-mail : [fntg@photon.t.u-tokyo.ac.jp](mailto:fntg@photon.t.u-tokyo.ac.jp)

URL : <http://fullerene-jp.org>

印刷 / 製本 (株)創志企画

# 当日出荷対象製品が大幅に増加しました。

ソーラボジャパンでは国内在庫を大幅に増やし、ますます多くの製品がご注文当日あるいは翌営業日に出荷可能になりました\*。

お急ぎの製品は、是非一度当社ウェブサイトでご納期をご確認ください。  
お客様の急なニーズにも迅速に対応いたします。



## 当日出荷が可能な製品の一例です。

出荷予定日はウェブサイトでご確認いただけます。

### ■ パワー&エネルギーメータ



PM400

タッチパネル式パワー&エネルギーメータコンソール (マルチタッチ対応)



S120シリーズ

フォトダイオードパワーセンサ



ES220C



S470C

サーマルセンサ、焦電エネルギーセンサなども当日出荷対象製品を取り揃えています。

「Today」の表示は  
当日出荷の対象製品

+1	数量	資料	型番 - Universal	定価(税抜)	出荷予定日
<input type="checkbox"/>	<input type="checkbox"/>		<b>PM400</b> タッチパネル式パワー&エネルギーメータコンソール、マルチタッチ対応	¥167,700	✓ Today
+1	数量	資料	型番 - Universal	定価(税抜)	出荷予定日
<input type="checkbox"/>	<input type="checkbox"/>		<b>S120VC</b> 標準フォトダイオードパワーセンサ、Si、200~1100 nm、50 mW	¥52,910	✓ Today
<input type="checkbox"/>	<input type="checkbox"/>		<b>S120C</b> 標準フォトダイオードパワーセンサ、Si、400~1100 nm、50 mW	¥38,220	✓ Today
<input type="checkbox"/>	<input type="checkbox"/>		<b>S121C</b> 標準フォトダイオードパワーセンサ、Si、400~1100 nm、500 mW	¥41,470	✓ Today
<input type="checkbox"/>	<input type="checkbox"/>		<b>S122C</b> 標準フォトダイオードパワーセンサ、Ge、700~1800 nm、40 mW	¥76,310	✓ Today

### ■ レーザ保護メガネ



LG9



LG9A



LG9B

+1	数量	資料	型番 - Universal	定価(税抜)	出荷予定日
<input type="checkbox"/>	<input type="checkbox"/>		<b>LG9</b> レーザ保護メガネ、ブラウンレンズ、可視光透過率：25%、ユニバーサルタイプ	¥25,480	✓ Today
<input type="checkbox"/>	<input type="checkbox"/>		<b>LG9A</b> レーザ保護メガネ、ブラウンレンズ、可視光透過率：25%、コンフォートタイプ	¥25,480	✓ Today
<input type="checkbox"/>	<input type="checkbox"/>		<b>LG9B</b> レーザ保護メガネ、ブラウンレンズ、可視光透過率：25%、スポーツタイプ	¥25,480	✓ Today

\*弊社に直接ご注文いただいた場合の出荷予定日です。また、出荷予定日は在庫状況に応じて変わる可能性がありますのでご了承ください(上記は2017年1月現在のウェブサイト上の製品情報です)。

www.thorlabs.co.jp

E-mail: sales@thorlabs.jp

**THORLABS**

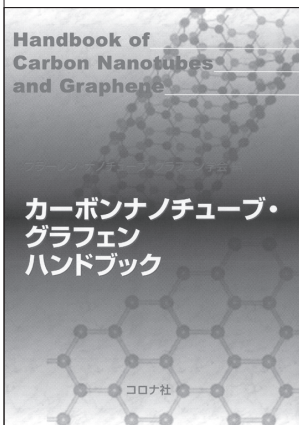
ソーラボジャパン株式会社

〒170-0013 東京都豊島区東池袋2-23-2 TEL : 03-5979-8889 FAX : 03-5979-7285

## 書籍のご案内

◆定価は本体価格+税です。

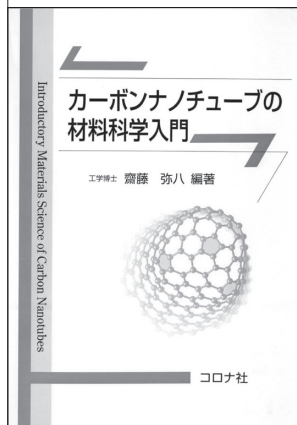
### カーボンナノチューブ・ グラフェンハンドブック



フラーレン・ナノチューブ・  
グラフェン学会 編  
B5判/368頁  
本体10,000円

本ハンドブックでは、カーボンナノチューブの基本的事項を解説しながら、エレクトロニクスへの応用、近赤外発光と吸収によるナノチューブの評価と光通信への応用の可能性を概観。最近囁目のグラフェンやナノリスクについても触れた。

### カーボンナノチューブの 材料科学入門



齋藤弥八 編著  
坂東俊治・中山喜萬・  
春山純志・久保佳実  
共著  
A5判/250頁  
本体3,400円

材料科学に新分野を創出し、エレクトロニクスからエネルギー分野まで広範囲な応用が期待されるナノテクノロジー材料の典型物質「カーボンナノチューブ」について、その製法から物性、実用の可能性までを解説した。

### ドライプロセスによる 表面処理・薄膜形成の応用



表面技術協会 編  
A5判/318頁  
本体4,600円

「ドライプロセスによる表面処理・薄膜形成の基礎」の応用編。第Ⅰ編「ドライプロセスの基礎技術」および第Ⅱ編「ドライプロセスの応用」から構成され、研究現場や製造現場で的確にドライプロセスが実施できるよう工夫し解説した。

### 関連書籍のご案内

#### カーボンナノチューブの基礎

齋藤弥八・坂東俊治 共著/A5判/  
220頁/本体2,800円

#### ドライプロセスによる 表面処理・薄膜形成の基礎

表面技術協会 編/A5判/208頁/本体2,800円

#### エンジニアのための 分子分光学入門

林 茂雄 著/A5判/268頁/本体3,600円

#### 機械屋のための 分析装置ガイドブック

日本塑性加工学会 編/A5判/236頁/本体3,400円

# BRANSON 超音波ホモジナイザー

長くご愛顧いただいておりますBRANSON超音波ホモジナイザーで新たなモデルが誕生しました。

## 主な特長

- 1.電気エネルギーから超音波振動への変換効率が95%以上  
→ 無駄なエネルギーロスが小さく、安定した振幅が得られる。
- 2.通常では、液体の種類によって振幅が安定し難い。  
→ 条件を変えても一定の振幅を保つ機能がついている。
- 3.ジュール (watt/sec) による発振制御が可能  
→ Total何ジュールでこの処理が完了するという情報が論文に掲載できる。

20kHz超音波ホモジナイザー  
BRANSON SONIFIER SFX250,550

40kHz超音波ホモジナイザー  
BRANSON SONIFIER SFX150HH



## 主なアプリケーション

### 分散

カーボンナノチューブ 有機顔料 無機顔料 セラミック セメント 感光体 記録材料  
磁性粉 粉末冶金 酸化鉄 金属酸化物 シリカ アルミナ カーボンブラック  
ポリマー ラテックス 製紙 ファンデーション  
研磨剤 電池 フィラー 光触媒 触媒 ワクチン 体外診断薬 歯磨き粉 シャンプー  
半導体 電子基盤 液晶 貴金属 金属 宝石 タイヤ 発酵菌類 その他

### 乳化

エマルジョン製剤 農薬 トナー ラテックス 界面活性剤 クリーム 乳液 その他

日本国内販売総代理店



株式  
会社

セントラル科学貿易

東京本社: 〒136-0071 東京都江東区亀戸1-28-6 タニビル3F

TEL 03-5627-8150 FAX 03-5627-8151

技術物流センター: 〒272-0146 千葉県市川市広尾2-1-9

TEL 047-701-6100 FAX 047-701-6116

大阪支店: 〒533-0031 大阪府大阪市東淀川区西淡路1-1-36 新大阪ビル

TEL 06-6325-3171 FAX 03-6325-5180

福岡営業所: 〒812-0016 福岡県福岡市博多区博多駅南1-2-15 事務機ビル

TEL 092-482-4000 FAX 092-482-3797

札幌出張所: 〒001-0911 北海道札幌市北区新琴似11条13-7-13-2

TEL 011-764-3611 FAX 011-764-3612

<http://www.cscjp.co.jp>

# 埼玉県ナノカーボンプロジェクト

## 補助率10/10の補助金で

## 応援します！

4月から順次応募開始予定

研究開発費に  
お困りではありませんか？

### 企業様向け補助金① 上限2,000万円（補助率10/10）

- ◆ 対象 単独の企業、複数の企業による共同開発体、大学又は公的研究機関と企業による共同開発体
- ◆ 要件 企業の一つ以上が県内企業であること、若しくは埼玉県先端産業創造プロジェクトにおける各分野の研究会やネットワーク等に参加し、かつ開発の成果が県内中小企業の振興に寄与すること
- ◆ 事例 CNT配合フッ素樹脂製品の開発、フラーレン分散接着剤の開発、フラーレン配合化粧品の開発

### 企業様向け補助金② 上限100万円（補助率10/10）

- ◆ 対象 日本国内に本申請に係る主たる技術開発のための拠点を有する企業
- ◆ 要件 県内企業でない場合は、開発の成果が県内中小企業の振興に寄与すること
- ◆ 要件 CNT発熱ヒーターの開発、グラフェン太陽電池の開発、CNT配合ゴムの開発

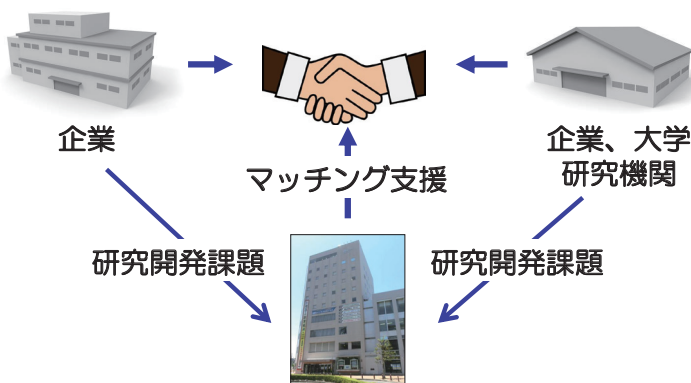
### 大学・研究機関様向け補助金 上限2,500万円（補助率10/10）

- ◆ 対象 大学若しくは公的研究機関又は公的産業支援機関
- ◆ 要件 ①県の先端産業の育成に資する研究開発を行う共同開発体であること  
②共同開発体に大学若しくは公的研究機関を含めること  
③共同開発体に県内中小企業を含むこと
- ◆ 要件 CNT樹脂コンポジットの開発、CNT線材の開発、グラフェン鉛電池の開発

詳細情報についてはHPでご確認ください  
<http://www.saitama-leading-edge-project.jp/>

## 研究開発パートナーを探します

埼玉県産業振興公社ではナノカーボン事業に取り組む企業に対して、専門家による技術相談やマッチング相談等、様々な相談支援メニューで支援しています。



産業振興公社  
問い合わせ先  
公益財団法人 埼玉県産業振興公社  
先端産業支援センター埼玉  
TEL : 048-711-6870  
Mail : sentan@saitama-j.or.jp

## ネットワークを広げます

ナノカーボンに関する情報・人材・技術を埼玉に結集するため、定期的に先端技術交流会を開催しています。ナノカーボンを活用した新たな技術開発に挑戦する大手企業や中小企業の取組などを紹介するとともに、懇親会の開催などを通じて、新たなネットワークづくりにつなげます。



講演



展示

### 問い合わせ先

埼玉県 産業労働部 先端産業課 推進担当  
TEL:048-830-3737  
又は  
MAIL:a3760-03@pref.saitama.lg.jp

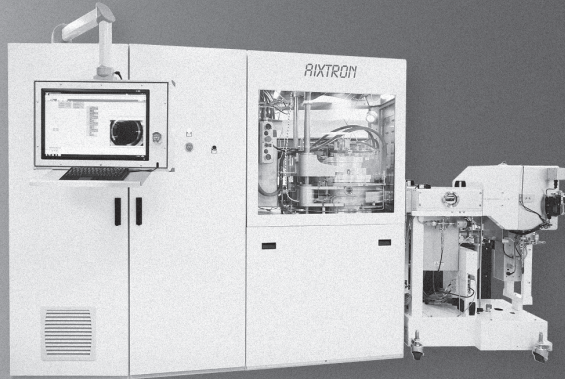
# 研究から量産まで

グラフェン、カーボンナノチューブ & 2Dマテリアル用  
先端成長技術



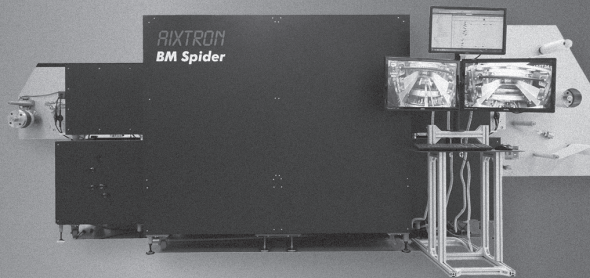
## BM Pro

Your deposition workhorse  
for wafer scale



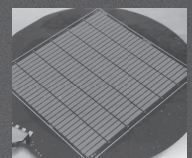
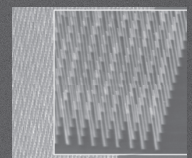
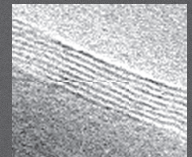
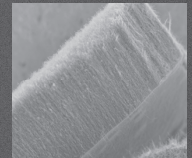
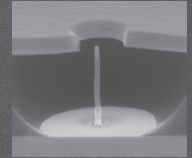
## BM 300T

For your production needs  
at wafer scale



## BM Spider

Your roll-to-roll solution



	BM Pro	BM 300T	BM spider
プロセス	CVD/PECVD Batch	CVD/PECVD Batch	CVD / Roll-to-roll
材料	CNTs, graphene & other 2D	CNTs & graphene	CNTs & graphene
基板サイズ	Up to 8"	8" & 12"	300 mm web width
基板タイプ	wafer & foil	wafer	foil
最高温度	1,050° C (*up to 1,700° C)	1,050° C	1,050° C
シャワーヘッド方式 ガス供給	Yes	Yes	Yes
プラズマ	Yes	Yes	No
ハンドラー/インライン インテグレーション	No	Yes	Yes
両面コーティング	No	No	Yes

アイクストロン株式会社 · [www.aixtron.com](http://www.aixtron.com)  
〒140-0001 東京都品川区北品川1-8-11 Daiwa品川Northビル 9F  
E-mail: [japaninfo@aixtron.com](mailto:japaninfo@aixtron.com) · Phone: 03-5781-0931 · Fax: 03-5781-0940

**AIXTRON**  
Our technology. Your future.



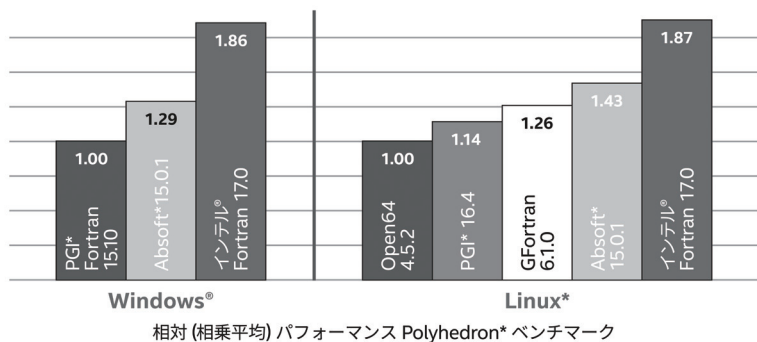
# シミュレーションを高速化 インテル® Parallel Studio XE 2017

第2世代のインテル® Xeon Phi™ プロセッサを含む、最新のインテル® プロセッサ向けに最適化された、高速かつ信頼性の高い C/C++、Fortran、Python\* アプリケーションの開発を支援します。

## インテル® Parallel Studio XE 2017 の主な新機能

- C++14 や C++17、Fortran 2015 暫定版、OpenMP\*4.5 などのサポートを拡張
- インテル® アーキテクチャーにおけるディープラーニングを高速化
- 高速な Python\* 実行環境 "インテル® Distribution for Python\*" を新たに同梱
- ハードウェア・パフォーマンスにとって重要な3つのメトリックを素早くプロファイル

インテル® Fortran コンパイラーによる優れた Fortran アプリケーション・パフォーマンス - Windows®/Linux\*  
(数値が大きいほど高性能)



システム構成：ハードウェア：インテル® Xeon® プロセッサ E3-1245 v5 @ 3.50GHz、ハイバースレディング有効、ターボブースト有効、32GB RAM、ソフトウェア：インテル® Fortran コンパイラー 17.0、Absoft\* 15.0.1、PGI\* Fortran 15.10 (Windows®) / 16.4 (Linux)、Open64 4.5.2、GFortran 6.1.0、Linux OS: Red Hat® Enterprise Linux® Server 7.2、カーネル 3.10.0-327.4.5.el7.x86\_64、Windows OS: Windows® 10 Pro (10.0.10240 N/A Build 10240)、Polyhedron\* Fortran ベンチマーク (www.fortran.uk)。  
Windows® コンパイラー・オプション：Absoft\*-m64-O5-speed\_math=10-fast\_math-march=core-xINTEGGER-stackOx80000000、インテル® Fortran コンパイラー：fast/Qparallel/QxCORE-AVX2/hoststandard-realloc-lhs/link/stack:64000000、PGI\* Fortran -fastsse-Munroll=n4-Mipa=fastinline-Mconcur=numa。  
Linux\* コンパイラー・オプション：Absoft\*-m64-maxv-O5-speed\_math=10-march=core-xINTEGGER、GFortran -Ofast -mfpmath=sse-ftto -march=native -funroll-loops -ftrre-parallelize-loops=4、インテル® Fortran コンパイラー：-fast-parallel-xCORE-AVX2-nostandard-realloc-lhs、PGI\* Fortran -fast-Mipa=fastinline -Msmalloc -Mfprelaxed -Mstack\_arrays -Mconcur=bind、Open64 -march=auto -Ofast -mso -apo。

性能に関するテストに使用されるソフトウェアとワークロードは、性能がインテル® マイクロプロセッサ用に最適化されていることがあります。SYSmark® や MobileMark® などの性能テストは、特定のコンピュータ・システム、コンポーネント、ソフトウェア、操作、機能に基づいて行われたものです。結果はこれらの要因によって異なります。製品の購入を検討される場合は、他の製品と組み合わせられた場合の本製品の性能など、ほかの情報や性能テストも参考にして、パフォーマンスを総合的に評価することをお勧めします。\* その他の社名、製品名などは、一般に各社の表示、商標または登録商標です。  
ベンチマークの出典：インテル コーポレーション

最適化に関する注意事項：インテル® コンパイラーでは、インテル® マイクロプロセッサに限定されない最適化に関して、他社製マイクロプロセッサ用と同様の最適化を行えないことがあります。これには、インテル® ストリーミングSIMD拡張命令2、インテル® ストリーミングSIMD拡張命令3、インテル® ストリーミングSIMD拡張命令3挿入命令などの最適化が該当します。インテルは、他社製マイクロプロセッサに関して、いかなる最適化の利用、機能、または効果も保証いたしません。本製品のマイクロプロセッサ依存の最適化は、インテル® マイクロプロセッサでの使用を前提としています。インテル® マイクロアーキテクチャーに限定されない最適化のなかにも、インテル® マイクロプロセッサ用のものがあります。この注意事項で言及した命令セットの詳細については、該当する製品のユーザー・リファレンス・ガイドを参照してください。注意事項の改訂 #20110804

製品詳細、無料評価版はこちらから  
[www.xlsoft.com/intel/fntg52](http://www.xlsoft.com/intel/fntg52)

~ 最適化、並列化について学べる無料セミナーも開催中! ~



製品の詳細に関するお問い合わせ先： .....



エクセルソフト 株式会社

〒108-0073 東京都港区三田 3-9-9 森伝ビル 6F  
Tel: 03-5440-7875 Fax: 03-5440-7876 E-mail: intel@xlsoft.com  
お問い合わせフォーム：www.xlsoft.com/jp/qa



MERCK



# シグマ アルドリッチの カーボンナノ材料

## 100 種類以上の製品群

### ■ 各種グラフェン

- ・ グラフェンフィルム
- ・ CVD グラフェン
- ・ グラフェンナノプレートレット
- ・ グラフェンナノリボン
- ・ 酸化グラフェン
- ・ 還元型酸化グラフェン
- ・ 金属酸化物 / グラフェン複合材料

### ■ カーボンナノチューブ

- ・ 単層 CNT
- ・ 二層 CNT
- ・ 多層 CNT
- ・ 修飾済み CNT

### ■ プリントドエレクトロニクス用 グラフェンインク

### ■ 透明導電性 CNT インク

### ■ カーボンナノファイバー

### ■ カーボンナノチップ

### ■ 各種フラーレン誘導体

### ■ カーボン ナノホーン

製品の詳細はこちらから [www.aldrich.com/nano-jp](http://www.aldrich.com/nano-jp)

## シグマ アルドリッチ ジャパン

〒153-8927 東京都目黒区下目黒 1-8-1 アルコタワー 5F

[www.sigma-aldrich.com/japan](http://www.sigma-aldrich.com/japan)

製品に関するお問い合わせは、弊社テクニカルサポートへ  
TEL : 03-6756-8245 E-mail : [sialjpts@sial.com](mailto:sialjpts@sial.com)

在庫照会・ご注文方法に関するお問い合わせは、弊社カスタマーサービスへ  
TEL : 03-6756-8275 E-mail : [sialjpcs@sial.com](mailto:sialjpcs@sial.com)

シグマ アルドリッチ ジャパン合同会社はメルクのグループ会社です。



Sigma-Aldrich